A REVISED TWO-EQUATION MODEL OF TURBULENCE

BY

J O ILEGBUSI

MAY 1983

THESIS SUBMITTED FOR THE DEGREE OF

DOCTOR OF PHILOSOPHY

IN THE FACULTY OF ENGINEERING

UNIVERSITY OF LONDON

AND

FOR THE DIPLOMA OF MEMBERSHIP OF

IMPERIAL COLLEGE

COMPUTATIONAL FLUID DYNAMICS UNIT

ROOM 440, MED BUILDING

IMPERIAL COLLEGE OF SCIENCE AND TECHNOLOGY

EXHIBITION ROAD

LONDON SW7 2BX

UK

ABSTRACT

The thesis describes the modifications made to a transport model which characterises turbulence by two properties: K the specific kinetic energy of the fluctuating motion; and W, the time-mean square of the vorticity fluctuations.

Partial differential equations expressing the conservation of these quantities are solved numerically, along with those for the momentum and enthalpy. Emphasis is placed on the correct modelling of the near-wall region to account for the effects of the special features of the flow situations considered. Unlike the practice with the earlier version of this model, the same set of the asymptotic high Reynolds-number values of the model constants is used in all calculations.

Predictions of fluid flow and heat transfer, deduced from the model, are compared with established experimental data and some predictions based on the earlier model. The physical situations considered include:-

turbulent pipe flow;
uniform - and non-uniform pressure flow over a flat plate;
flow over a flat plate with intense heat-transfer and with intense mass-transfer through the surface;
flow and heat transfer downstream of an abrupt pipe-expansion;
flow in a backward-facing step
flow in a plane jet;
flow in a plane mixing-layer; and
flow in a round jet

The new model performs as well as (and in some respects better than) the original version; and since it does not need the inelegant "near-wall fix" of the latter, it is to be preferred. Agreement with experiment is at least as good as that commonly experienced with the more-popular K-ε model in which the dissipation rate (ε) of the turbulence energy is used in place of W.

In addition, an experimental investigation is reported in which a new flow-visualisation technique is developed and used to study the flow in the boundary layer and wake of two-demensional bodies. A qualitative comparison is made between the results for one of the test cases - the backward-facing step - and the predictions based on the new K-W model.

PREFACE

I joined the Computational Fluid Dynamics Unit (CFDU, which until 1982 was the Heat Transfer Section, Department of Mechanical Engineering) of Imperial College in October 1980. The work reported in this thesis is a major part of my research activities between then and December 1982. It is concerned mainly with revision and application of a particular model of turbulence - the K-W model.

During the first three months of the study, I was involved in the studying and application of the STABLEXT Computer code of Spalding as a logical first step towards familiarising myself with the numerical methods employed in the Unit. Some of the work include calculation of turbulent flow in, curved ducts, rotating ducts, diffusers and rectangular channels.

In February 1981, I was included in a group of three involved with predicitons for the 1981 AFOSR-IFP Stanford Conference on Complex turbulent flows. The other members of the Group were Professor S. Y. Goh (then visiting the Unit) and Dr. A. Abdelmeguid. Due to the vast nature of the flows concerned, it was necessary to use the PHOENICS Computer program of Spalding which was then newly released by CHAM (UK) Limited. Despite some obvious initial problems of using such a new general-purpose computer code, it was indeed an opportunity to be one of its first users outside the company. The work lasted about five months at the end of which it was reported and presented to the afore-mentioned conference.

For a brief period of one month (July 1981), I was involved with the prediction of turbulent swirling flows. This involved modification of the K-ε turbulence model in PHOENICS to account for anistropy of flows.

It was after then that Professor Spalding informed me of his intention to revive his old K-W model of turbulence which had then been overshadowed by the K-ε model. Having been involved in turbulent-flow prediction all through the previous ten months, I was more than happy to take up this work which was soon to become the mainstay of my research.

It was realised then that apart from modifying the model, the work would entail replacing the built-in K-ε model in PHOENICS with the new K-W one. However, I did not envisage any essential difficulty in this having earlier successfully introduced a non-isotropic version of the K-ε model.

The research started with the use of the K-W model in its original form for the prediction of simple flows like decay of grid turbulence, flat-plate and pipe-flow. Then it was necessary to modify the model to account for wall effects differently from the earlier practices and subsequently to apply it to varying flow situations. Some of the physical situations considered were made to parallel those already done by Spalding and his co-workers with the old version so as to afford direct comparison. Some of these works have been reported as a series of CFDU reports and in two published papers.

At one stage of the research, we were interested in investigating turbulent flows with small regions of recirculation. For this purpose, a new experimental technique was devised and applied to flow about two-dimensional bodies. This work too has been reported as a CFDU report and included in one of the papers earlier mentioned.

It was after the completion of the experimental investigation in November, 1982 that I started writing up this thesis.

I would now like to acknowledge my debt of gratitude to a number of individuals who have provided valuable assistance during my years at Imperial College. I have mentioned already the important role which my supervisor, Professor Spalding played in initiating the research. His active interest and guidance thereafter are greatly acknowledged. His supervision has always been thorough, and at the same time friendly. Furthermore, he has taught me much on the subject of technical-report writing. If the presentation of this thesis is still inadequate, it would have been worse but for Spalding's constructive criticism. It is indeed a priviledge to have worked with him.

I should also like to thank Drs. A.S.C. Ma and W.M. Pun for the advice which they gave me on technical and non-technical matters. Dr Ma's suggestions on the experimental study and his willingness to help is highly appreciated. I learnt much from Dr. Pun on the basic prediction procedures used in the Unit. I am very grateful.

At the beginning of the study, co-operation and technical discussions with Drs. Adrzej Przekwas, Abdelmeouid and Tatchell and

Professor S.Y. Goh have been invaluable.

The suggestions given by Mr Mike Malin during the course of the research deserves especial mention here. He has shared his time and experience unselfishly with me even at weekends and late evenings. I am greatly indebted.

I am thankful to Dr Martin Guntton for his assistance with the Graphic Plots. Dr W. Al Sanea has been more than helpful in sharing his experience with me. I have also enjoyed the friendship with Christian Languvine and A. Castrejoin. Informal discussions with other research workers - H. Qin, Simon Lo, Paul Shepherd and S. Paramesuaran have been too important to escape mention.

Thanks are due to Miss Frith Oliver for her assistance in various administrative matters. The help of Mr Bob King in setting up the experimental rig and his endeavour at creating a lively and relaxing atmosphere in the laboratory are highly appreciated. I am also grateful to Mr Peter Dale for helping with computing problems.

Many thanks to Miss Adwoa Ackom-Mensah for her excellent typing of the thesis and for her patience in going through every detail of my often-not-too-clear handwriting.

I would also like to extend my gratitude to my parents and friends who offered all possible support and encouragement throughout my studies.

Space does not permit me to list the names of all individuals and organisations who contributed to my work. However, I cannot fail to acknowledge the generous financial supports provided for the study first by the University of Ibadan, Nigeria and later by the Commonwealth Scholarships Commission in the United Kingdom.

London

May, 1983

J.O. Ilegbusi

CONTENTS

LIST OF FIGURES

LIST OF FIGURES

LIST OF FIGURES

LIST OF FIGURES

LIST OF FIGURES

LIST OF FIGURES

LIST OF FIGURES

LIST OF FIGURES

LIST OF TABLES

LIST OF TABLES

LIST OF TABLES

CHAPTER 1

INTRODUCTION

1.1 Background and Objectives Of The Investigation

1.11 The Problem Considered

Turbulent flows, which are of great practical importance, are three-dimensional, time-dependent, and stochastic in nature. They are governed by the well-known Navier-Stokes equations. Procedures exist to solve these equations numerically; however, because the energy-dissipating eddies are very small, the computer mesh required is so fine that the necessary computer storage exceeds by many orders of magnitude what is currently available, to say nothing of the computer time.

Yet the practical need for computation of turbulent flows is pressing; to meet it, consideration is given to only the statistical properties of the turbulence. These properties are governed by an infinite number of correlation equations which are closed by "turbulence modelling". The latter involves approximating the turbulence correlations in terms of knowable quantities. The solution of the resulting set of differential equations, and associated algebraic equations and constants, in conjunction with those of the Navier-Stokes equations, closely simulate the behaviour of the real turbulent fluids.

A good turbulence model must be extensively universal, and not too complex to develop or use. Universality implies that a single set of empirical contants or functions, inserted into the equations, provides close simulation of a large variety of types of flow. Complexity is measured by the number of differential equations which the model contains, and the number

of empirical constants and functions which are required to complete them; increase in the first complicates the task of using the model, increase in the second that of developing it.

Satisfactory calculation procedures and computers are now available for solving differential equations, on the scale of the mean motion, for quite large numbers of simultaneous equations. The main obstacles to model development and use are therefore the difficulty of selecting which set of differential equations is most capable of providing universality and the difficulty of providing the required constants and functions.

1.12 Previous Work

Various turbulence models have been developed or proposed. Some of these have been reviewed by Launder and Spalding (1972a, 1972b), Harlow (1973) and Mellor and Herring (1973).

Among such models are:- Prandtl's (1925) mixing length model; the one-differential-equation models of Prandtl (1945), Bradshaw et al (1967), and Nee and Kovasznay (1968); the two-differential-equations models of Kolmogorov (1942), Harlow and Nakayama (1968), Spalding (1969), Saffman (1970), and Jones and Launder (1972); and the more complex models of Chou (1945), Rota (1951), Davidov (1961), Kolovandin and Vatutin (1969), Hanjalic (1970), and Hanjalic and Launder (1972).

Because partial differential equations were so difficult to solve, engineers even took recourse to integral methods.

These methods involve assumptions about the shape of the mean-velocity profile and about the global behaviour of turbulence as reviewed by Rodi (1972). The introduction of these assumptions allows the partial differential equations to be reduced to ordinary ones, which are relatively easy to solve. However, integral methods lack flexibility. For example, they are cumbersome to use when the mean velocity profile changes shape. In addition, they are very difficult to extend to high Mach number flows, and to flows with non-uniform temperatures and species concentration.

Recent advances in numerical methods (e.g. Patankar and Spalding (1972) and Gosman et al (1969)) have overcome the mathematical difficulties of solving partial differential equations. Thus engineers need no longer be content with integral methods. However, they still lack an adequate physical model to describe turbulent flows.

This thesis describes the revision of a particular two-equation turbulence model, the dependent variables of which are the turbulence energy, K and the time-mean-square of the vorticity fluctuation, W. This model was one of three different two-equation models in prominent use in about a decade ago. The others were the K-ε and the K-Kl models in which ε is the rate of dissipation of turbulence energy and l is the length representing the macroscale of turbulence.

The K-Kl model has been applied to a large number of turbulent flows, both with and without the presence of solid

walls by Rodi and Spalding (1970) and Ng and Spalding (1970, 1972). The K-ε model on the other hand has been applied by many workers among which are Jones and Launder (1972) and Tatchell (1972).

The development of the K-W model (Spalding, 1969) stemmed from a suggestion by Kolmogorov (1942) that the effective viscosity in a turbulent flow might be expressed as a function of the local energy K, and local frequency of the turbulent motion, and that these quantities might be expressed as dependent variables of partial-differential equations. Spalding (1969) subsequently found it more convenient to replace Kolmogorov's fluctuation frequency by a new variable, W, having the dimensions of (frequency)^2, which may be thought of as a measure of the time-mean square of the vorticity fluctuations.

The K-W model in its original form has been described and demonstrated to give fairly satisfactory predictions of turbulent flows in various circumstances (Spalding, 1969, 1971, 1972a, 1972b; Gibson and Spalding, 1972 and Roberts, 1972). A version of the model, the K-W-g model in which g represents the mean-square fluctuations of a scalar, was used by Jensen and Wilson (1975) for flows with chemical reaction.

A similar model was proposed independently by Saffman (1970) in which K and W were interpreted as respectively the "energy density" and "vorticity density". This model shared the same fundamental idea with that of Spalding but the approach differed in detail and spirit.

Whereas Spalding's model was based on the idea that K and W obey conventional "transport" equations, Saffman assumed that these characteristic variables obey non-linear diffusion laws. The diffusion equations (like the transport ones) contain terms to describe the convections by the mean flow, the amplification due to interaction with a mean velocity gradient, the dissipation due to the interaction of the turbulence with itself and the diffusion also due to the self interaction; the latter being related to a turbulent (eddy) diffusivity.

Furthermore, unlike Spalding, K and $W^{1/2}$ were not regarded by Saffman as necessarily having physical significance; they were simply subsidiary variables introduced by analogy with energy and vorticity in order to calculate the mean velocity field and turbulent stresses.

The third essential difference between the models was in the formulation of the production terms in the transport equations. Saffman took the production term in the K equation as simply proportional to the kinetic energy times the absolute value of the rate of strain while Spalding assumes the product of the eddy diffusivity, the mean rate of strain and the appropriate velocity gradient. The production term of the W equation of Saffman is proportional to the product of W and the absolute value of the velocity gradient while Spalding used a term proportional to the product of W/K and the production term in the K-equation.

Saffman's model was applied to inhomogeneous boundary layer flows (Couette flow and two-dimensional wake-and jet-flows) with a measure of success (Saffman, 1970). Further extension and application of the model have been done by Wilcox and co-workers (Wilcox and Alber, 1972, Saffman and Wilcox, 1974, Wilcox and Traci, 1976 and Wilcox and Rubesin, 1980). In the Wilcox-Traci and Wilcox-Rubesin versions, effects of compressibility were accounted for through use of mass-weighted averaged dependent variables and some hypotheses regarding terms in which the compressibility effects are isolated.

Modelling coefficients were made to depend on turbulence Reynolds number and this, coupled with the introduction of molecular diffusivity as a parallel transport mechanism to the turbulence, permitted integration of the transport equation directly to the boundaries. Thus, for example the commonly used "law of the wall" for defining boundary conditions near walls are avoided. Furthermore, the "vorticity density" was interpreted as the dissipation rate per unit energy.

Wilcox and Rubesin also employed a different formulation of the production terms in the equations for the two characteristic variables. The Saffman-type production terms were demonstrated to contain the potential for introducing errors when more general flow fields other than attached boundary layers are considered. An example is the expanding supersonic nozzle in which the kinetic energy along the centreline of the nozzle actually decreases. An increase of energy is indicated by the Saffman production term in the energy

equation as both the energy and the absolute rate of strain tensor are positive.

Thus for the production term in the energy equation, Wilcox and Rubesin used the sum of the products of the local Reynolds stress times the appropriate mean velocity gradient. The analogous term of the specific dissipation rate equation is modelled (like in the Spalding's model) as the product of the production term of the kinetic energy equation, the ratio W/K and a new modelling coefficient.

The K-W model of Spalding was found to require adjustment for the near-wall region. This was regarded by its originator as a sufficient reason for allowing it to be overshadowed by the K-ε model of Harlow and Nakayama (1967), which was then being revived by Jones and Launder (1972) and Launder et al (1972), for the K-ε model appeared to require no such modification.

During the subsequent decade, experience with the K-ε model has not been universally favourable; and it has come to light that some early users of the K-W model who transferred to K-ε have preferred to return, in the interests of agreement with experimental data.

An additional reason for returning is that it is vorticity fluctuations, resulting from the breakdown of vorticity sheets into less regular structures, which give turbulent flows their characteristic properties. Any turbulence model which concerns itself with the fluctuations directly can

draw more direct support from experimental observations than can one involving less accessible concepts.

Indeed, generations of fluid dynamicists have recognized the importance of vorticity. It has provided a powerful qualitative description for many of the important phenomena of fluid mechanics e.g. the formation and separation of boundary layers have been so described in terms of the production, convection and diffusion of vorticity; the dissipation of energy at a rate practically independent of the viscosity in turbulent flows is explained by the amplification of vorticity by the stretching of vortex lines; the lift on a wing is explained by the bound vorticity and trailing vortex structure; and most recently, the concept of the coherent structure in turbulent shear flows has led to the picture of such flows as a superposition of organized, 'deterministic' vortices whose evolution and interaction is the turbulence.

1.13 Objectives of the Investigation

The advances in numerical methods have made it possible to apply nearly any turbulence model to a wide range of flows. Thus, turbulence models can now be tested efficiently. The objectives of this investigation are therefore:

(a) To develop a new version of the K-W model of turbulence

(b) To find the constants and functions of the new model which will give good agreement with experimental data for turbulent flows in varying circumstances.

(c) To prescribe near-wall boundary conditions (where applicable) for the new model appropriate to the various physical situations considered.

(d) To incorporate this new model into a suitable computer code.

(e) To establish whether or not the new model indeed gives good agreement with less arbitrariness of the model 'constants' than before

(f) To conduct a simple and economical experimental investigation of turbulent flows with small regions of recirculation, such as occur near blunt trailing-edges of two-dimensional bodies.

(g) To predict the qualitative structure of the flow observed with the new experimental technique.

1.2 PRESENT CONTRIBUTION

1.21 Outline of the Study

The task of revising a model for turbulent-flow calculation can be thought of as involving four phases of work. First, a new version of the model must be developed. Secondly, the new model must be incorporated into a suitable computer code. Thirdly, predictions with this model must be compared with experimental data. Lastly, an experimental investigation may be carried out to supply additional data and/or to further validate the predictions with the model.

The present study has involved all four phases of the work.

(a) Development of a New Version of the K-W Model of Turbulence

The objectional feature of the earlier version of the K-W model was its inclusion of a term $KW^{-1}y^{-2}$, which became very important when the distance, Y from a boundary wall was small. How, one was inclined to ask, should the fluid "know about" its distance from a wall? And the inclusion of the wall-distance calculation in the equation-solution scheme was troublesome.

The present modification involves instead addition of an extra source term to the W equation equal to:

$$\text{constant} \times \rho W^{3/2} \left[\left| \text{grad} \, (KW^{-1})^{1/2} \right| \right]^2,$$

which would be free from the wall-distance probelm, Spalding (1982a). Since $(KW^{-1})^{1/2}$ is proportional to the length scale of turbulence, the term in brackets attains a fixed value near a wall, which is just what is required to ensure that the logarithmic velocity profile is fitted; elsewhere, the term may have less importance, although it is also significant in shear layers embedded in larger turbulent flows.

The constant in the additional term was obtained directly from a knowledge of the well-known logarithmic velocity profile. Near-wall boundary conditions were prescribed for the new model by devising formulae which fitted exactly some well-known experimental conditions, and varied smoothly in

between. It should be mentioned here, that a similar term was employed by Wilcox and Traci (1976). However, apart from the differences already mentioned between their model and the present one, their modelling constant was not optimized. In addition, the present work provides a wider demonstration of the plausibility of the new term.

(b) Incorporation of the New Model into a Computer Program

The version of the computer code adopted, PHOENICS, was equipped with the K-ε turbulence model but not the K-W one. It was therefore necessary to make use of the facilities provided by PHOENICS for the attachment of user-generated coding sequences. These facilities proved to be satisfactory.

(c) Testing of The New Model

Predictions of fluid flow and heat transfer, deduced from the model, have been compared with established experimental data and some predictions based on the earlier model (Ilegbusi and Spalding, 1982b, 1982c, 1983a, 1983b). The physical situations considered include:- turbulent pipe-flow; uniform and non-uniform pressure flow over a flat plate; flow over a flat plate with intense heat transfer and with intense mass-transfer through the surface; flow and heat transfer downstream of on abrupt pipe-expansion; flow in a backward-facing step; flow in a plane jet; flow in a plane mixing-layer; and flow in a round jet.

In addition, the qualitative structure of one of the flows investigated experimentally in this study has been predicted with the new model coupled with a "particle-tracking" technique.

The predictions have been shown to be satisfactory provided the constant in the additional source term of the W equation is set equal to 2.97.

(d) Experimental Study

An experimental investigation of flow in the boundary layer and wake of two-dimensional bodies has been carried out. A new steady-unsteady flow visualisation techniqoe (Ilegbusi and Spalding, 1982a) has been devised for the purpose. Photographs have been taken of the flow structure created by the body drawn vertically from a coloured fluid into a clear one.

1.22 Outline of the Thesis

The thesis is divided into nine chapters of which this introduction is the first.

In Chapter two, the equations for conservation of mass, momentum and species are given. A statement is given of the auxiliary information and boundary conditions required to close the equation set.

Chapter three is concerned with the development of the improved K-W model. First, the reason for the choice of this particualr model for investigation is given and the original version of it is described in terms of the transport equations for K and W. The modifications made are then outlined and the new model is presented. The method of determining the additional constants of the latter and the boundary conditions are also given.

Before the application of the revised model, the solution procedure employed is briefly described in Chapter four. This includes a statement of the finite-domain equations, outline of

the solution procedure and the incorporation of auxiliary information into the procedure. In addition, the details of the introduction of the new model into the computer code adopted are also given.

In Chapters five to seven, the revised model is applied respectively to turbulent external boundary layers, turbulent internal flows and turbulent free flows. In each chapter, the various flow situations considered are outlined, the available experimental data are briefly reviewed, the computational details are given and the results presented and subsequently discussed.

Chapter eight details the experimental study. The steady-unsteady flow visualisation technique devised for the purpose is described and its application to flow in the boundary layers and wakes of two-dimensional bodies of different geometries are presented.

The last chapter, chapter nine, summarises the main conclusions of the thesis and presents some suggestions for future research.

Following chapter nine are the lists of references and nomenclature, and the appendices.

CHAPTER 2

THE MATHEMATICAL PROBLEM

2.1 Introduction

The first step in the analysis of any flow situation is to consider the general physical laws that describe the fluid dynamics of the flow. The purpose of this chapter is to present the basic equations that govern turbulent flows and to introduce the problems which their solution poses. Also included are the sets of boundary conditions which are required to adequately define the problem.

The equations are first given in their most general form applicable to the flows usually described as "elliptic", by which is meant that perturbation of conditions at any point in the flow can influence conditions at any other point. Included in this group are the recirculating flows considered in chapter six. The assumptions required to reduce the equations to their boundary-layer forms suitable to the flows in which influences travel in one predominant (usually downstream) direction are then given. Examples of this class of flows are considered in chapters 5, 6 and 7.

The remainder of the chapter comprises of six sections. In section 2.2 is presented the conservation equations which govern the transport of mass and momentum while section 2.3 provides the equation for a generic fluid property, ϕ, which, in this context, stands for any of the following; species concentration, stagnation enthalpy, turbulence kinetic energy, turbulence dissipation rate etc. These equations have been

derived from the general form of the Navier-Stokes equations by the neglect of terms of small orders of magnitude. The assumptions made to reduce the equations to their boundary-layer forms are presented in section 2.4.

The above equations do not by themselves constitute a closed set. The need for additional physical hypothesis to bring about closure is discussed in section 2.5. Section 2.6 provides a statement of the boundary conditions for the equations and finally, the closing remarks are presented in section 2.7.

2.2 The Mean Flow Equations and Reynolds Time Averaging

The equations of motion in the absence of external force fields take the following tensorial form for Newtonian fluids:

Continuity:

$$\frac{\partial \rho}{\partial t} + \frac{\partial \rho U_i}{\partial x_i} = 0 \qquad ,(2.2\text{-}1)$$

Momentum:

$$\frac{\partial \rho U_i}{\partial t} + \frac{\partial}{\partial x_j}(\rho \tilde{U}_i \tilde{U}_j) = -\frac{\partial P}{\partial x_i} + \frac{\partial}{\partial x_j}\left[\mu\left(\frac{\partial U_i}{\partial x_j} + \frac{\partial U_j}{\partial x_i}\right)\right] \qquad ,(2.2\text{-}2)$$

where $\tilde{U}_i$ and $\tilde{P}$ represent respectively the instantaneous velocities and static pressure, and ρ and μ are the fluid

density and dynamic viscosity respectively.

The above equations form the Navier-Stokes equations that predict the dynamic behaviour of turbulent as well as laminar flows. However, practical turbulent flows contain a cascade of eddy sizes that represent a wide range of time and length scales. Hence any numerical scheme using equations (2.2-1) and (2.2-2) for turbulent-flow simulations would require a grid fine enough to resolve even the smallest turbulent motions. This is not possible for the solution of practical problems as it is beyond the present computing capability.

The "statistical" representation of the turbulent flow by time-averaging is a useful approach, whereby the time-dependent flow is represented by a mean velocity U_i and a fluctuating velocity field u_i superimposed upon it (Hinze, 1959). The instantaneous velocity ($\tilde{U}_i$) and pressure ($\tilde{P}$) therefore obey the relations:

$$\tilde{U}_i = U_i + u_i \qquad ,(2.2\text{-}3)$$

$$U_i = \frac{1}{2t_o} \int_{-t_o}^{t_o} \tilde{U}_i \, dt \qquad ,(2.2\text{-}4)$$

$$\frac{1}{2t_o} \int_{-t_o}^{t_o} u_i dt = 0 \qquad ,(2.2\text{-}5)$$

$$\tilde{P} = P + p \qquad ,(2.2\text{-}6)$$

$$P = \frac{1}{2t_o} \int_{-t_o}^{t_o} \tilde{P} dt \qquad ,(2.2\text{-}7)$$

$$\frac{1}{2t_o}\int_{-t_o}^{t_o} p\,dt \doteq 0 \qquad ,(2.2\text{-}8)$$

where t_o is a time interval which is long compared with the largest turbulence time scales, but shorter than the period over which the averaged flow quantities may vary.

Substituting definitions (2.2-3) and (2.2-6) into the instantaneous flow equations (2.2-1) and (2.2-2) leads to the following equations governing the mean motion of a steady turbulent flow:

Continuity:

$$\frac{\partial}{\partial x_j}(\rho U_i) = 0 \qquad ,(2.2\text{-}9)$$

Momentum:

$$\frac{\partial}{\partial x_j}(\rho U_i U_j) = -\frac{\partial P}{\partial x_i} + \frac{\partial}{\partial x_j}\left[\mu\left(\frac{\partial U_i}{\partial x_j} + \frac{\partial U_j}{\partial x_i}\right) - \rho\overline{u_i u_j}\right] \qquad ,(2.2\text{-}10)$$

in which the fluctuating velocity correlation tensor, $\overline{u_i u_j}$, known as the Reynolds stress, is defined as:

$$\overline{u_i u_j} = \frac{1}{2t_o}\int_{-t_o}^{t_o} u_i u_j\,dt \qquad .(2.2\text{-}11)$$

This term physically represents the transfer of momentum by the turbulent motion. Due to its presence, the set of equations of motion presented above is not "closed". Thus

additional relationships need to be developed to express $u_i u_j$ in terms of known or calculable variables. These efforts constitute the subject of turbulence modelling introduced in section 2.5 and described in chapter 3.

2.3 The Scalar Property Equation

The conservation equations for a generic fluid property such as the momenta per unit mass of fluid in the different coordinate directions, the specific stagnation enthalpy, species concentration, turbulence energy etc., though are deduced from differing physical principles, they all exhibit a similarity of form. Thus, they can be represented by the single equation for a general scalar property, ϕ as follows.

It is similarly possible to define the time-mean (ϕ) and fluctuating components (ϕ') of Φ such that:

$$\Phi = \phi + \phi' \qquad ,(2.3\text{-}1)$$

$$\phi = \frac{1}{2t_o} \int_{-t_o}^{t_o} \Phi dt \qquad ,(2.3\text{-}2)$$

$$\frac{1}{2t_o} \int_{-t_o}^{t_o} \phi' dt = 0 \qquad ,(2.3\text{-}3)$$

which gives rise, after substitution into and time-averaging the equation for the instantaneous Φ to:

$$\frac{\partial}{\partial x_j}(\rho U_j \phi) = \frac{\partial}{\partial x_j}\left(\frac{\mu}{\sigma_\phi}\frac{\partial \phi}{\partial x_j} - \overline{\rho u_j \phi'}\right) + S_\phi \qquad .(2.3\text{-}4)$$

Here, S_ϕ is the time-smoothed source/sink of ϕ, and $\overline{\rho u_j \phi'}$ is the turbulent transport term, which also requires modelling. In the equation, also, the viscous source which results from the non-constancy of the properties ρ and μ, have been omitted for simplicity.

2.4 Formulation of the Boundary-layer Forms of the Equations

The equations for parabolic flow situations are obtained from the general forms given in (2.2-10) by omitting the terms representing the mechanisms that are weak enough to be ignored. This involves making the following simplifying assumptions for a two-dimensional flow that is predominant along the x-direction, say;

(i) Diffusion fluxes along x-direction are neglected.

(ii) The absence of pressure transmission (by definition of parabolic flows) implies that there are no sharp curvatures of the streamlines and thus the streamwise pressure gradient, $\partial P/\partial x$ is nearly uniform over the cross stream; therefore $\partial P/\partial x$ can be calculated without reference to the momentum balance in the y-direction.

The independence of $\partial P/\partial x$ from $\partial P/\partial y$ results in the decoupling of the x-direction momentum equation from the y-momentum equation. Thus, the pressure term in the x-direction can be written as the gradient in spatial-mean pressure $\bar{p}$ across

the stream.

If this approach is not followed, the equation derived for the pressure (which is a Poisson equation) is elliptic in the main direction, and therefore destroys the parabolic nature of the equation set.

2.5 Auxiliary Relations

Before the equations above could be solved, the boundary conditions, (which will be given in section 2.6) and, auxiliary relations to evaluate the mean pressure p, the density and viscosity, and the Reynolds stresses and fluxes, are required. Each of these latter topics are discussed separately below.

Mean Pressure

The mean pressure will be calculated from the requirement of overall conservation of mass; this process is discussed by reference to the finite-domain forms of the equations in chapter 4.

Density and Laminar Viscosity

In general, these properties may depend upon the local state of the flow (e.g. on the pressure, temperature or composition). The form of the density relations employed for some of the calculations where it is non-uniform, are presented in the appropriate chapters in which the problems are considered. For all the calculations described in this thesis, uniform laminar viscosity is assumed.

Reynolds-Stress and Turbulent-flux Terms

Many of the turbulence models reviewed in chapter 1 (e.g. Harlow and Nakayama (1967), Spalding (1972)) and the one employed in this thesis have in common the use of a gradient-diffusion formulation of the turbulent stresses i.e. the Reynolds stresses are related to the mean strain rate through the Boussineso approximation thus:

$$-\rho\overline{u_i u_j} = \mu_t \left(\frac{\partial U_i}{\partial x_j} + \frac{\partial U_j}{\partial x_i}\right) - \frac{2}{3}\delta_{ij}\rho K \qquad .(2.5\text{-}1)$$

Similarly, the turbulent transport term $\rho\overline{u_i\phi'}$ is expressed thus:

$$-\rho\overline{u_i\phi'} = \frac{\mu_t}{\sigma_{\phi,t}}\frac{\partial \phi}{\partial x_j} \qquad .(2.5\text{-}2)$$

In the above, μ_t is defined as the turbulent (or eddy) viscosity, δ_{ij} is the Kronecker delta, $\sigma_{\phi,t}$ is a turbulent Prandtl/Schmidt number, which is usually assumed to be invariant with direction and taken as a constant, and K, the time-averaged energy of the turbulent motions, is defined as:

$$K = \frac{\overline{u_i^2}}{2} \qquad .(2.5\text{-}3)$$

By so doing, attention has merely been shifted from the Reynolds stresses and fluxes to the eddy viscosity or diffusivity. This latter property is defined in terms of a characteristic length and velocity (an idea apparently borrowed from the kinetic theory of gases). In the present study, these

length and velocity scales are evaluated from two local, time-averaged properties of turbulence, namely; K, the kinetic energy and W, the time mean souare of the vorticity fluctuations as described in chapter three.

Due to the similarity of form of the laminar and turbulent stress relations, it is convenient to combine them, and to work with an effective viscosity (μ_{eff}) defined as the sum of the laminar and turbulent components, thus:

$$\mu_{eff} = \mu + \mu_t \qquad .(2.5\text{-}4)$$

In the next section, the boundary and initial conditions necessary to complete the definition of the problem are presented.

2.6 Boundary and Initial Conditions

In addition to the sets of equations presented above, the mathematical specifications of the problem also requires information about the boundary and initial conditions. The former refers to specification of values of the dependent variables at the edges of the flow while the latter refers to their values at the location where the solutions to the set of equations are begun.

The following types of physical boundary will be encountered in the present study: walls (porous and impervious); planes of symmetry; and the far downstream boundary. For the

parabolic calculations, conditions at the last-mentioned - the downstream boundary need not (and indeed cannot) be specified; they are an outcome of the calculation. The treatment of the remainder is as follows.

At a wall which is stationary and impervious, all components of velocity are zero, and the flux of species through the wall is also zero. For turbulence quantities and cases with porous walls, wall conditions are deduced from experimental knowledge of near-wall turbulent flows in such circumstances as described in chapter three. Finally, at a plane of symmetry the normal velocity is zero, and the normal gradient of all other quantities is zero.

The initial conditions at an inflow boundary are specified from known experimental or theoretical data for the variables.

In order to simplify the later description of the incorporation of these conditions into the finite-difference scheme, it is useful to observe that they can be classified as: either, those at which the value is specified; or, those at which the normal flux, and hence the normal gradient, is zero.

2.7 Closure

The contributions of the present chapter may be summarised as follows:

(a) The equations which describe two-dimensional elliptic and parabolic flows as deduced from the Navier-Stokes equations are presented.

(b) The equations are "closed" through appropriate expressions for the Reynolds Stresses and fluxes.

(c) A standard form of the equations applicable to any generic fluid variable is presented.

(d) The auxiliary information necessary to complete the mathematical specification is outlined.

The turbulence model employed for specifying the turbulent viscosity, μ_t is described in the following chapter.

CHAPTER 3

THE TURBULENCE MODEL

3.1 Introduction

In the equations for conservation of momentum, and the general scalar property ϕ, given in chapter two, there appeared terms involving time-averaged products of velocity fluctations, and fluctuations of ϕ. These were there interpreted as respectively turbulent (or Reynolds) stresses and turbulent fluxes. A turbulence model comprises a set of additional equations, either differential or algebraic, which enables these quantities to be calculated.

In this study, the turbulent stresses or fluxes are related to the gradients of the corresponding flow property through an eddy viscosity as described in chapter two. This viscosity is allowed to vary from one location in the flow domain to the other; but at any point it is assumed to be isotropic. The distribution of the eddy viscosity is calculated from two local, time-averaged properties of turbulence, namely, K, the kinetic energy of turbulence, and W, the time-mean square of the vorticity fluctuations.

This chapter describes this K-W model of turbulence and the modifications made to it for the present study. The remainder of the chapter is divided into five sections as follows.

In section 3.2, the reason for the choice of this model for the present investigation is outlined. This entails a brief review of models of various levels of complexity. A criticism of the old version of the model is contained in section 3.3. The new version of the K-W model is presented in section 3.4. This includes a statement on the need for a review of the KW model, the new idea, the differential equations governing the transport of K and W, and the constants of the new model. Details of the near-wall boundary conditions for the new model are presented in section 3.5. Finally, the achievements of the chapter are summarised in section 3.6.

3.2 Choice of Model Type

3.21 Preamble

Turbulence models of varying complexities have been proposed. These range from Prandtl's (1925) mixing length hypothesis which relates the shear stress directly to the mean velocity gradient, to Daly and Harlow's (1970) model which employs differential transport equations for all the Reynolds stresses. In order to enable a choice of a suitable level of complexity for the present study, the performance of various classes is reviewed briefly. The classes are distinguished by the number of turbulence quantities which appear as dependent variables of differential equations.

3.22 The Performance of Various Model Classes

The Eddy-viscosity Concept

Before discussing the individual classes, it is

pertinent to introduce the eddy-viscosity concept; for it is an essential component of the majority of the models which do not solve a shear-stress equation. This concept has been introduced in chapter two. The relevant equations are contained in section 2.5.

This concept may be vestated simply for a boundary layer as (Boussinesq 1877):

$$\rho\overline{uv} = - \mu_t \frac{\partial U}{\partial y} \qquad ,(3.22\text{-}1)$$

where μ_t is the "eddy viscosity". μ_t is not a fluid property but depends on the state of the turbulence; it can vary considerably from one flow to another and also across the flow.

Equation (3.22-1) expresses the assumption that the shear stress, $-\rho\overline{uv}$, has the same sign as the velocity gradient, $\frac{\partial U}{\partial y}$. Experiments have shown that this appears to be a valid assumption for many flow situations.

(a) Zero-equation Models

This group of models does not employ equations for turbulence quantities. They relate the shear stress uniquely to the local mean flow conditions. A most prominent example is Prandtl's (1925) mixing-length hypotheses which reads:

$$\mu_t = \rho l_m^2 \left|\frac{\partial U}{\partial y}\right| \qquad ,(3.22\text{-}2)$$

the mixing length, l_m, being normally assumed to be proportional to the width of the shear layer or to distance from a wall.

This model, like the other zero-equation models, is economical to use. They work well for boundary layers where the turbulence structure changes but slowly in the main flow direction. However, the empirical constants involved have to be changed for each new flow situation and are thus valid for restricted flow regions only.

(b) One-equation Models

The models in this group employ either a transport equation for the kinetic energy of turbulence, K, or an equation for the viscosity μ_t. Those which employ an equation for K assume either that (Kolmogorov 1942, Prandtl, 1945)

$$\mu_t \propto \rho\sqrt{K}\, l \qquad ,(3.22\text{-}3)$$

where l is the length scale of turbulence, or that $\overline{uv}$ is proportional to K (Bradshaw et al 1967). All the models require empirical specification of the length scale l.

One-equation models take better account of changes in turbulence structure than do zero-equation models. However, because they require empirical length-scale specifications, they still lack universality. They cannot be applied to complex flows; for it is only for well-documented boundary layers that

these distributions are known.

(c) Two-equation Models

The models in this group determine both the intensity (K) and the scale (l) of turbulence from transport equations. Those proposed so far employ the eddy viscosity concept and the relation (3.22-3). All the length-scale equations have $Z = K^a l^b$ as dependent variables, where a and b vary from one author to another as discussed by Launder and Spalding (1972).

Two-equation models have been applied to the calculation of a wide range of boundary layer and recirculating flows by, among others, Rodi and Spalding (1970), Ng (1971), Gibson and Spalding (1972), Spalding (1972a), Jones and Launder (1972), Lefeuvre (1973), Roberts (1972), Matthews and Whitelaw (1971), Date (1973), Chieng and Launder (1980) and Abdelmeguid et al (1981). These studies include such diverse flow situations as; wall flows and free-shear flows, crossflow in a tube bank, confined swirling flow with separation, flow over abrupt pipe-expansion, flow over a plane backward-facing step, flow in a diffuser and flow and heat transfer in a twisted-type heat exchanger.

In general, the performance of the model is good. Mean flow quantities such as surface shear-stress, velocity profiles, pressure drop and heat transfer rates are, in most cases, well predicted. Turbulence quantities, such as K and ε show fairly good agreement with measurements.

While two-equation models have enjoyed a certain amount of success, a number of important defects can be identified. Many of these have been discussed by Launder and Spalding (1972a) among which are the non-universality of the constants for some of the models, the poor performance for flow in a round jet and flows in non-equilibrium shear-layers. Despite these short-comings, however, two-equation models have proved to offer the best compromise between time and cost of computing a particular flow situation and they appear to be the simplest models which promise success in more complex flows.

(d) Three-equation Models

These models do not employ the eddy-viscosity concept. Instead, a transport equation for the shear stress is solved, in addition to equations for the kinetic energy and length scale (Rotta 1969, 1971; Hanjalic and Launder, 1972). Employment of such models seem necessary for the calculation of boundary layers with significant regions in which shear stress and velocity gradients have opposite signs. For other boundary layers, the existing three equation models have not proved superior to two-equation ones (see for example Rodi, 1972).

(e) Reynolds-Stress Models

In flows for which the Reynolds stresses need to be calculated, and which are highly anisotropic as occur in strongly-swirling jets and flows with sharp corners, the models reviewed so far will perform poorly. Models employing transport equations for all the Reynolds stresses are needed. However, these models have not so far, proved superior to two-equation

models for boundary layer flows (Rodi, 1972).

(f) Higher-level Models

More complex models employing differential equations for up to 16 correlations have been proposed (e.g. Kolovandin and Vatutin, 1969). These models have however, not yet been applied.

Deardroff (1970) proposed a large-eddy simulation model that does not seem to fit into the present scheme of classification. He solved numerically the time-dependent Navier-Stokes equations for the three-dimensional large scale motion in a plane channel. In otherwords, he modelled the motion of a scale smaller than his computational mesh with a "turbulent viscosity" assumption. This approach is very expensive in terms of computer storage and time; and it does not seem to predict the mean flow features any better than the simpler methods.

Other models have been proposed. These include the six-equation model of Spalding (1982) in which algebraic equations are solved for three components each of the length scale and of vorticity; and the multi-scale model of Hanjalic et al (1979) which takes account of the fact that the production and dissipation of turbulence energy occur at different spectral regions of the flow.

Economy

All turbulence-model uses involve a compromise, time and cost playing a large part. The computation time increases with

the number of equations to be solved. In addition, multi-equation models need more experiments and computer optimisation to determine the empirical constants than simpler models.

3.23 The Choice

It may be concluded in view of the foregoing considerations that a two-equation model will meet best the requirements of economy, universality, extensibility and realism. In this study, therefore, a two-equation model which employs K, the turbulence energy, and W, the time-mean square vorticity fluctuations as the charateristic properties has been chosen.

The next section critisizes briefly this K-W model in its basic form and outlines the reasons for its revision in the present study.

3.3 A Critique of the Basic K-W Model of Turbulence

The K-W model was devised in about a decade ago (Spalding, 1969). It was shown by Spalding (1972) and Gibson and Spalding (1972) to yield predictions of two-dimensional turbulent flows which were in good agreement with the experimental data. However, it possessed the defect (shared incidentally with the contemporaneously investigated K-Kl model of Rodi and Spalding (1970), and Ng and Spalding (1970, 1972) of requiring a modification of one of its constants for near-wall flows. This defect was usually corrected by inclusion of a term $KW^{-1}y^{-2}$, which became very important when its distance, y, from a

bounding wall was small. However, the question arises as to how the fluid would be aware of its distance from a wall. And it was a relatively difficult task to include this wall-distance calculation in the solution scheme.

In the following section, a new version of the model which corrects the defect mentioned above in a different and universal way is described.

3.4 The New K-W Model

3.41 The Need for the New Model

The inelegant "near-wall fitting" of constants for the earlier version of the K-W model was regarded as a sufficient reason for discarding it in favour of the K-ε model of Harlow and Nakayama (1968), for the latter model appeared to require no near-wall adjustment.

However, experience with the K-ε model has not proved universally favourable. It has therefore been found necessary to return to the K-W model for the sake of agreement with established experimental data.

An additional reason for reverting to the K-W model is its strong physical appeal. W measures the vorticiy fluctuations of the turbulence, and it is becoming clear that it is the breakdown of vorticity sheets into less regular structures that gives turbulence its characteristic sturcture. Vorticity is a property of turbulent flow field of crucial import and indeed, all the problems of homogeneous

incompressible fluids can be posed as questions about the strength and location of the vorticity. The distribution of vorticity is often compact, even though the velocity and pressure fields extend everywhere, and remains so by virtue of the Helmholtz laws of vortex motion, apart from viscous diffusion. Thus the specification of the vorticity field (or its fluctuations) may even be far more economical than that of the velocity.

3.42 Choice of Modification

The objective is to seek an appropriate function S that could be added to the W equation source term to correct for the wall effect.

Different expressions for S can be got by dimensional analysis from the flow parameters. Those considered are:

(a) $$S = \rho W^{\frac{1}{2}} W \cdot f(l/y) \qquad ,(3.42\text{-}1)$$

(b) $$S = -\rho W^{\frac{1}{2}} W \cdot f(\text{grad}l) \qquad ,(3.42\text{-}2)$$

(c) $$S = \rho W^{\frac{1}{2}} \left(\frac{\partial U}{\partial y}\right)^2 \cdot f(l/y) \qquad ,(3.42\text{-}3)$$

(d) $$S = -\rho W^{\frac{1}{2}} \left(\frac{\partial U}{\partial y}\right)^2 \cdot f(\text{grad}l) \qquad ,(3.42\text{-}4)$$

in which f() denotes 'function of' the argument, and l, the length scale is defined as:

$$l = K^{\frac{1}{2}}/W^{\frac{1}{2}} \qquad .(3.42\text{-}5)$$

It is obvious that only options (b) and (d) are free from the wall-distance probelm discussed earlier. In addition, grad l attains a fixed value near a wall, which will be that required to ensure that the logarithmic velocity profile is fitted; elsewhere, it may have less importance (e.g. in free flows) although it may be significant in shear layers embedded in larger turbulent flows.

From the points of view of computational convenience and numerical stability, option (b) will be selected. The simplest form for the function is:

$$f(\text{grad } l) = C_4 \, [|\text{grad } l|]^{C_5} \qquad ,(3.42\text{-}6)$$

in which C_4 and C_5 are constants to be determined.

3.43 Differential Equations for K and W

The turbulence energy K and the vorticity fluctuations W are supposed, as in the original version, to be governed by conventional "transport" equations thus:

$$\frac{DK}{Dt} = \rho^{-1} \left[\text{div} \left(\frac{\mu_t}{\sigma_K} \text{grad} K\right) + S_K\right] \qquad ,(3.42\text{-}1)$$

$$\frac{DW}{Dt} = \rho^{-1}\left[\text{div}\left(\frac{\mu_t}{\sigma_W}\,\text{grad}W\right) + S_W\right] \qquad ,(3.43\text{-}2)$$

wherein the left-hand sides represent time-dependence and bulk-transport terms and the right-hand sides represent firstly the turbulent-diffusion transport and secondly the "source" (i.e. creation and destruction) terms. (Notes on the derivation of these equations are given in appendix A).

The source term for turbulence energy, K, is expressed as:

$$S_k = G_k - C_D\rho KW^{1/2} \qquad ,(3.43\text{-}3)$$

wherein the "generation" term on the right is expressible in Cartesian-tensor form through velocity gradients as:

$$G_K = \mu_t\left(\frac{\partial U_i}{\partial x_j} + \frac{\partial U_j}{\partial x_i}\right)\frac{\partial U_i}{\partial x_j} \qquad ,(3.43\text{-}4)$$

where μ_t, the "turbulent viscosity", is related to K and W by:

$$\mu_t = C_\mu\rho\, KW^{-1/2} \qquad ,(3.43\text{-}5)$$

The source term for vorticity fluctuations, W, is expressed as:

$$S_W = K^{-1}W(C_3G_K - C_2\rho KW^{-\frac{1}{2}}) + C_1\mu_t(|\text{grad}\Omega|)^2 - C_4\rho W^{3/2}(|\text{grad}(KW^{-1})^{\frac{1}{2}}|)^{C_5} \qquad ,(3.43\text{-}6)$$

wherein Ω is the major component of the vorticity of the mean motion.

Of the three terms on the right of this equation, the first parallels S_k, the second is a comparatively small term, and the last is the novelty on which the new K-W model is founded.

The differential equations (3.43-1) and (3.43-2), along with the auxiliary term and constant-defining equations, constitute the turbulence model which is here investigated.

3.44 The Values of the Model Constants

Nine constants appear in the above equations, namely; σ_k, σ_w, C_D, C_μ, C_1, C_2, C_3, C_4, C_5. Of these, the first seven have been established by earlier work (Spalding, 1972), and have been adopted without change. Their values are given in Table 3.44-1.

Constant	σ_k	σ_w	C_D	C_μ	C_1	C_2	C_3
Value	1.0	1.0	0.09	1.0	3.5	0.17	1.04

Table 3.44-1: Previously-established Turbulence-model Constants

Of the two remaining, C_5 was guessed to equal 2.0, implying that the new term is proportional to the square of the gradient of the turbulence length scale and therefore independent

of its sign. The constant C_4 could then be determined by reference to the as-yet-unused Von Karman constant κ (taken as 0.435) in the "logarithmic law of the wall", through the relation (Spalding, 1972)

$$(4\sigma_W^{-1}+C_1C_D-C_\mu C_4)\,\kappa^2 - C_2C_\mu C_D^{-\frac{1}{2}} + C_3C_D^{\frac{1}{2}}C_\mu^{-\frac{1}{2}} = 0 \qquad ,(3.44\text{-}1)$$

This relation is the result of assuming that, in the fully turbulent region close to a wall, the energy generation and decay are approximately equal, and that the convection terms in the W equation are negligble (Details of this are given in appendix B). From this relation, C_4 is deduced to equal 2.97; and it is this value which has been employed in the computations which are to be described.

3.5 Boundary Conditions at a Wall

3.51 The Problem

As explained in the literature (see, for example, Launder and Spalding, 1972a; Spalding 1972a), to use the true wall conditions (K = 0; W = 0) as boundary conditions for K and W would necessitate the solution of the equations through the thin semi-laminar region immediately adjacent to the walls. This would be expensive even if a low-Reynolds-number version of the model were available; and it is not available. Consequently, the practice adopted in the present study is to insert boundary conditions at the computational-grid point lying nearest to the wall, not that at the wall. This involves use of one-dimensional

empirical wall functions to evaluate the shear stress at the wall, and K and W near to the wall.

Various analytical forms have been proposed for the universal velocity profile as reviewed by Kestin and Richardson (1963). These are summarised in Table 3.51.

For simple flows along smooth walls it is adequate to presume that at such points:

(a) the velocity profile obeys the logarithmic law (Schlichting, 1968)

(b) the turbulence energy is proportional to the shear stress, and

(c) the length scale is proportional to the distance from the wall.

These three presumptions respectively entail the relations:

$$\text{(a)} \qquad \frac{U}{\sqrt{\tau/\rho}} = \frac{1}{\kappa} \ln \left| E\left(\frac{y\sqrt{\tau\rho}}{\mu}\right) \right| \qquad ,(3.51\text{-}1)$$

from which the shear stress can be determined from the velocity U;

$$\text{(b)} \qquad K = (C_\mu C_D)^{-\frac{1}{2}} (\tau/\rho) \qquad ,(3.51\text{-}2)$$

TABLE 3.5-1: Various Analytical Forms for the Universal Velocity Profile

Formula for u^+ (y^+)	$n^+ = dy^+/du^+$	Range	Author
$u^+ = y^+$ $u^+ = 2.5\ln y^+ + 5.5$	$n^+ = 1$ $n^+ = 0.4y^+$	$0 \leq y^+ \leq 11.5$ $y^+ > 11.5$	Prandtl & Taylor (see Schlichting 1968)
$u^+ = y^+$ $u^+ = 5\ln y^+ - 3.05$ $u^+ = 2.5\ln y^+ + 5.05$	$n^+ = 1$ $n^+ = 0.2y^+$ $n^+ = 0.4y^+$	$0 \leq y^+ \leq 5$ $5 \leq y^+ \leq 30$ $y^+ > 30$	Von Karman (1939)
$u^+ = 14.53\tanh(y^+/14.53)$ $u^+ = 2.5\ln y^+ + 5.5$	$n^+ = 1+\sinh(y^+/14.53)$ $n^+ = 0.4y^+$	$0 \leq y^+ \leq 27.5$ $y^+ > 27.5$	Rannie (1956)
$u^+ = 2.5\ln(1+0.4y^+) + 7.8(1 - \exp(-y^+/11) - y^+/11)\exp(-0.33y^+)$	$\frac{1}{n^+} = \frac{1}{1+0.4y^+} + 7.8\lvert(1/11)\exp(-y^+/11) - (1/11)\exp(-0.33y^+) + .03y^+\exp(-0.33y^+)\rvert$	all y^+	Reichardt (1951)
$\frac{dy^+}{du^+} = \frac{2}{1+\{1+4\kappa^2 y^{+2}\lvert 1-\exp(-y^+/A^+)\rvert^2\}^{\frac{1}{2}}}$ $\kappa=0.4,\ A^+=26$	$n^+ = 1+\{1+4\kappa^2 y^{+2}\lvert 1-\exp(-y^+/A^+)\rvert^2\}^{\frac{1}{2}}$	all y^+	Van Driest (1956)
$\frac{du^+}{dy^+} = \frac{1}{1+n^2 u^+ y^+\lvert 1-\exp(-n^2 u^+ y^+)\rvert}$ $n=0.124$ $u^+=2.78\ln y^+ + 3.8$	$n^+ = 1+n^2 u^+ y^+\lvert 1-\exp(-n^2 u^+ y^+)\rvert$ $n^+ = y/2.78$	$0 \leq y^+ < 26$	Deissler (1955)
$y^+ = u^+ + A\lvert \exp Bu^+ - 1 - Bu^+ - \frac{1}{2}(Bu^+)^2 - \frac{1}{6}(Bu^+)^3 - \frac{1}{24}(Bu^+)^4\rvert$ (last term in u^{+4} may be omitted)	$n^+ = 1+AB\lvert \exp Bu^+ - 1 - Bu^+ - \frac{1}{2}(Bu^+)^2 - \frac{1}{6}(Bu^+)^3\rvert$ (last term in u^{+3} may be omitted)	all y^+ $A=0.1108$ $B=0.4$	Spalding (1961)

which enables the energy K to be deduced from τ ; and

$$(c) \qquad W = \kappa^{-2} C_D^{-1/2} K/y^2 \qquad ,(3.51\text{-}3)$$

which serves as the third boundary condition, viz. that for W.

More elaborate expressions are needed when the wall is not smooth, when heat and mass transfer are effective, when pressure gradients are present, and when turbulence diffusion from the bulk of the fluid is more important than that generated by wall shear. Some of these will be considered below.

3.52 Effect of Heat Transfer

The present investigation includes heat-transfer predictions for comparison with experimental data. The smooth-wall boundary-condition formula employed, which is based on the work of Jayatillaka (1966) is:

$$(T - T_s) = (\frac{\dot{q}}{c_p})(\frac{U}{\sqrt{\tau\ \rho}} + P_J) \ / \ \sqrt{\tau\rho} \qquad ,(3.52\text{-}1)$$

wherein the function P_J depends upon the laminar Prandtl number σ_{hl} in accordance with the empirical function:

$$P_J = 9.0\ (\frac{\sigma_h}{\sigma_{hl}} - 1)\ (\frac{\sigma_{hl}}{\sigma_h})^{1/4} \qquad ,(3.52\text{-}2)$$

in which σ_h, the turbulent Prandtl number is taken as 0.9.

When heat-transfer rate is intense, as is true in some of the problems considered, the question arises as to how the density ρ and Prandtl number, σ_{hl} should be computed. There have been several conflicting proposals for σ_h also . These proposals include Reynolds' (1874) simple conclusion that σ_h is unity and those of Sleicher (1958), Corcoran et al (1952), Isakof and Drew (1951) and many others. In the present work however, the practice adopted has been to use values of ρ and σ_{hl} appropriate to the temperature at the near-wall grid point.

3.53 Effect of Longitudinal Pressure Gradient

When pressure varies significantly in the direction of flow, the shear stress τ varies significantly between wall and the near-wall grid point. The value inserted on the right hand sides of the above equations has therefore been calculated as a mean, $\bar{\tau}$, in accordance with the practices embodied in the GENMIX computer program (Spalding, 1977). Thus:

$$\bar{\tau} = \tau_s + \left(\frac{y}{2}\right) \frac{\partial P}{\partial x} \qquad ,(3.53\text{-}1)$$

wherein τ_s is the shear stress at the wall, (which appears on the left-hand side of equation (3.51-1).

3.54 Effect of Mass Transfer

The presence of mass transfer poses a similar problem which is solved in a similar way. In this case, the value of $\bar{\tau}$ inserted into the right-hand sides of the equations is given by:

$$\bar{\tau} = \frac{\tau_s + \dot{m} U \kappa \sqrt{\frac{\tau_s}{\rho}}}{(U + \kappa \sqrt{\frac{\tau_s}{\rho}})} \qquad ,(3.54\text{-}1)$$

This, too, is in accordance with the GENMIX practice.

For strong suction, the heat-transfer resistance of the near-wall region is without influence. To account for this, and to accord with physical realism, the practice adopted has been to take as the value of $(T-T_s)/\dot{q}$ the <u>smaller</u> of that given by the above formulae, on the one hand, and $(C_p\dot{m})^{-1}$ on the other.

3.55 <u>Turbulence Diffusion</u>

When diffusion of turbulence from the main flow to the near-wall grid point outweighs the generation of turbulence there from shear effects, as happens in the vicinity of the "reattachment" of a separated flow, equation (3.51-2) gives too low a value of K. In such cases, the practice adopted has been similar to that described in respect of the K-ε model by Launder and Spalding (1974). This is based on the main conclusions of Spalding (1966) on heat transport mechanisms in separated flows. It has two aspects, namely:

(a) the τ appearing on the right-hand sides of the boundary-condition equation is replaced by $(C_\mu C_D)^{1/2}K$; and

(b) K itself is calculated from the balance of turbulence energy generation, dissipation, diffusion and convection in the computaitonal cell surrounding the near-wall grid

point. In the present study, the viscous sublayer has been taken into account in evaluating the generation and dissipation terms. This practice is similar to that employed by Chieng and Launder (1980) with the K-ε model.

When diffusion of turbulence is unimportant, this practice produces the same results as would the direct use of equation (3.51-2).

Details of the above wall functions are contained in appendix C.

3.6 Closure

In this chapter, a new version of the K-W model has been described. First, a term $C_4 \times \rho W^{3/2}[|\text{grad}(K^{1/2}/W^{1/2})|]^{C_5}$ is added to the W-equation source. Then the constants C_4 and C_5 associated with this new term are fixed. Next, the near-wall boundary conditions for the new model have been prescribed for a wide range of flow situations.

CHAPTER 4

THE SOLUTION PROCEDURE AND INCORPORATION OF THE NEW K-W MODEL INTO THE COMPUTER CODE ADOPTED

4.1 Introduction

In the previous two chapters were set out the differential equations which govern two-dimensional turbulent flows, along with the associated boundary conditions and auxiliary relations. These equations are coupled and non-linear and are seldom amenable to analytical solution. The purpose of this chapter is to present a general procedure employed for their solution and to describe the technique used to introduce the new K-W model into the computer code adopted.

The equations have been solved by means of the PHOENICS computer program (Spalding, 1981). This embodies a finite-domain formulation of the equations, and a procedure for solving these, which both derive from the work of Patankar and Spalding (1972). The procedure as in PHOENICS has been described by Spalding (1982) and is outlined briefly here only for the sake of completeness and for the reader's convenience.

However, it should be mentioned that the version of PHOENICS adopted was equipped with the K-ε turbulence model but not the K-W one. It was therefore necessary to make use of the facilities provided by PHOENICS for the attachment of user-generated coding sequences. This has been a development of the present investigation; and is described here for the first time.

The calculation procedure is presented in its most general form well-suited to elliptic flow situations. However, the distinctive features of the parabolic procedure are outlined. These features occur mainly in the treatment of the pressure field. The elliptic procedure employs a single field common to the two momentum equations, whereas the parabolic procedure employs two separate pressure fields - one for the lateral momentum equation and the other for the longitudinal momentum equation. The solution procedure consists of the following major steps:

(i) The flow domain is divided into discrete regions by constructing a staggered finite-domain grid. This yields "control volumes" for each flow variable.

(ii) The integration of the partial-differential equations into algebraic ones (finite-domain equations) for each variable at each cell. This is accomplished by integrating the former equations over the control volumes and using appropriate assumptions for the variation of the variables between grid nodes.

(iii) Solving the resulting set of finite-domain equations by an appropriate algorithm.

(iv) Finite-doman solutions of differential-equation systems are influenced by the number of grid nodes employed, unless this number is large enough for "grid-independent" solutions to have been obtained; and the only way to

determine how large this necessary number is to perform the calculation several times with differing numbers of grid nodes. This practice has been adopted in the present work.

The remainder of this chapter consists of five main parts in which the solution procedure is detailed. In section 4.2, the finite-domain equations are determined and the solution procedure is outlined in section 4.3. Section 4.4 details the incorporation of the new K-W model into PHOENICS, and is the major contribution of the chapter. In this section, the PHOENICS computer code is briefly introduced in order to enhance appreciation of its peculiar features and the problems posed and to assist the reader in understanding the way in which the new turbulence model is introduced. Detailed account of the auxiliary information is contained in section 4.5. The concluding part, (section 4.6), then summarises the main features of the solution procedure and the achievements of the chapter.

4.2 Formulation of the Finite-domain Equations

4.21 The Finite-domain Grid

(a) The set of Control Cells

The whole space of the integration domain is filled by a set of non-overlapping cells which cut orthogonally. Figure 4.21-1 shows a two dimensional cartesian control cell.

The cell-centre points (P, called the grid nodes) are defined within each cell, and are located at its geometrical centre. The neighbour points are defined as points N,S,E,W

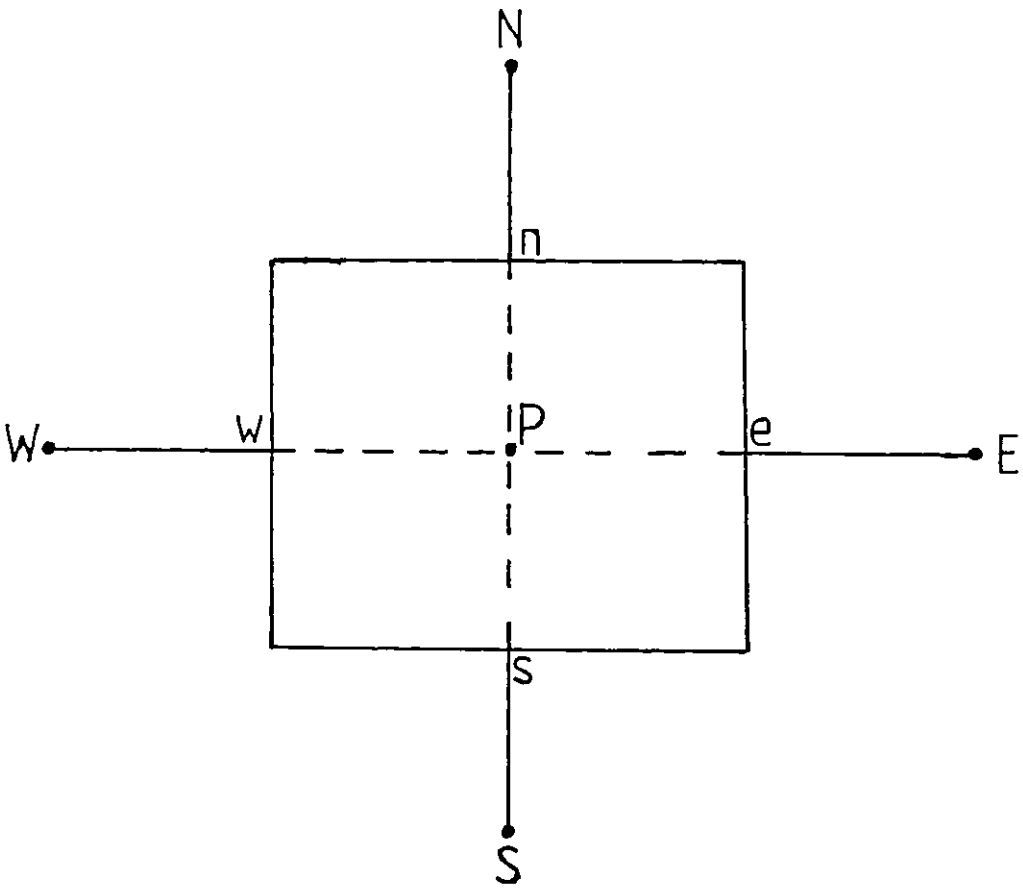

Fig. 4.21-1. A two-dimensional cartesian control cell.

(North, South, East, West). The lines joining P to its neighbours cut the cell faces at n,s,e,w; the values of variables "at" P, N, S, E and W are regarded as representing the values within the whole cell while the values "at: n,s,e,w are regarded as representing values over the whole of the faces of the cell.

The grids may be non-uniform but once the dimensions have been set, they remain fixed during the solution process.

(b) Location of Variables

The pressure, density, exchange coefficient and the scalar properties are stored at the grid nodes while the velocity components are stored at the cell-face locations and are denoted by U_e, U_w, V_n, V_s. The finite-difference equations for P, H, K, W and other scalar properties are obtained by application of the conservation principles to the control cell in which the node is located (e.g. shaded region 1 in figure 4.21-2 below), while those for the velocities are obtained by application of the momentum-conservation principle to the cell formed around the velocity as shown for example by the shaded regions 2 and 3 in figure 4.21-2 for velocities U and V respectively.

This staggered-grid arrangement, like that introduced by Harlow and Welch (1965), has the following advantages:

(i) the velocity components are conveniently located for calculating the convective fluxes of flow properties

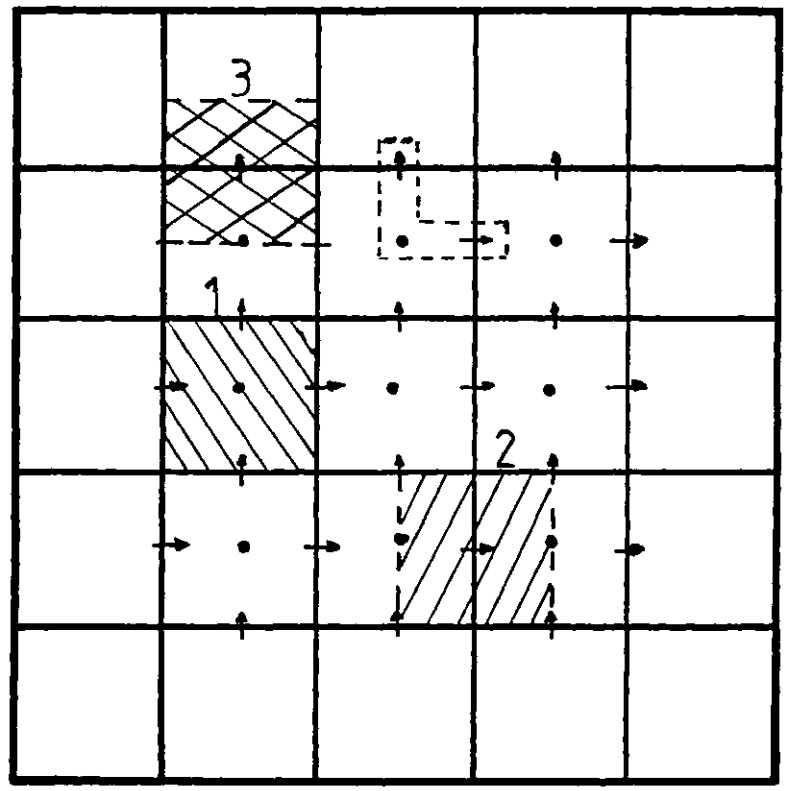

Symbol	Location	Control Volume for:
1	•	P, h, K, W
2	→	U
3	↑	V

Fig. 4.21-2. Grid showing location of variables and their control volumes.

stored at the grid nodes;

(ii) the calculation of mass balance over a region surrounding a grid node is made easy because the velocities normal to the boundaries of this region are located directly on the boundaries;

(iii) the pressures are stored so as to make it easy to calculate the pressure gradients that drive the velocities.

The dotted enclosures shown in Fig. 4.21-2 describe the manner in which the variables have been grouped for the purpose of identification; the variables enclosed by these dotted lines are associated with the same node. It will be noted that this "forward staggering" differs from the "backward staggering" employed by various workers like Tatchell (1972), Pratap (1975) and Al-Sanea (1981).

4.22 Derivation of the Finite-domain Equations

The derivation of the finite domain equations are similar to that of Patankar and Spalding (1972) and have been described by Spalding (1982). Therefore, only a brief outline will be presented here. The equations are derived by integrating the governing differential equations over the control cells. The integrations involve interpolation assumptions which, in the present study, are those corresponding to what are commonly called the "fully-implicit" and "upwind" formulations.

Integration of the general conservation equation 2.3-4 over the control cell P gives:

$$\iint_A (\rho U\phi + J_\phi) \cdot dA = \iiint_{V_o} S_\phi dV_o \qquad ,(4.22\text{-}1)$$

wherein V_o denotes the cell volume, A its surface area and J_ϕ the diffusion flux defined thus:

$$J_\phi = - \Gamma_\phi \text{grad}\phi \qquad .(4.22\text{-}2)$$

In the source term, ϕ is presumed uniform throughout the control cell, thus:

$$\iiint_{V_o} S_\phi dV_o = V_o S_\phi \qquad .(4.22\text{-}3)$$

In the surface integral, variables are presumed constant over each cell face; thus:

$$\iint_A (\rho U\phi + J_\phi) \cdot dA = \sum_{e,w,n,s} (\rho U\phi + J_\phi) \cdot A \qquad .(4.22\text{-}4)$$

(a) Treatment of the Convection Term

The relation in equation (4.22-3) requires the cell-face values of ϕ. In conformity with physical realism, the necessary interpolations involve ascribing to the fluid which crosses a cell boundary the scalar properties prevailing at the grid-point on the Upstream side of that boundary. The contribution of the

convection term to the left-hand side of the balance equation is thus simply;

$$\left(\sum_{e,n} \text{mass outflows}\right)\phi_P - \sum_{w,n} (\text{mass inflows}) \times (\text{incoming } \phi\text{'s}) \quad ,(4.22\text{-}5)$$

By invoking the following mass-continuity principle,

$$\Sigma \text{ mass outflows} = \Sigma \text{ mass inflows} \quad ,(4.22\text{-}6)$$

the relation in equation (4.22-4) is reduced to:

$$\left[\sum_{i=e,w,n,s} \max(0,\pm C_i)\right]\phi_P - \sum_{i=e,w,n,s} \max(0,\pm C_i)\phi_I \quad ,(4.22\text{-}7)$$

wherein C_i is the mass flux through the cell face i and I stands for the corresponding neighbour nodes E, W, N, S. For othorgonal cells,

$$C_i = \rho_{up} U_i A_i \quad ,(4.22\text{-}8)$$

wherein ρ_{up} is the density of the "upstream" fluid.

(b) Treatment of the Diffusion Term

With the aid of the general flux law, equation (4.22-2), the diffusion-flux contribution to the finite domain equation as

obtained from equation (4.22-4), can be expressed thus:

$$\Sigma J_\phi . A \equiv - \Sigma \Gamma_\phi \text{grad}\phi \, . A \qquad ,(4.22\text{-}9)$$

The evaluation of this term may be illustrated by an example say, the diffusive flux through the east face of the cell. The appropriate term in relation (4.22-9) is approximated as $-D_e(\phi_E - \phi_p)$ with:

$$D_e = A_e \Gamma_e / (X_E - X_p) \qquad .(4.22\text{-}10)$$

The cell face value of Γ_e is computed as the harmonic mean of the nodal values, Γ_p and Γ_E, i.e.

$$\Gamma_e \equiv \frac{2}{(1/\Gamma_p + 1/\Gamma_E)} \qquad .(4.22\text{-}11)$$

The remaining faces of the cell are treated analogously.

4.23 Statement of the Finite-domain Equations

(a) General Form

The equation that results from the above derivation can be written in the following general form:

$$\phi_P = \frac{a_E\phi_E + a_W\phi_W + A_N\phi_N + a_S\phi_S + S_U}{a_E + a_W + a_N + a_S} \qquad ,(4.23\text{-}1)$$

The a's denote the 'coefficient' of the finite-domain equations; they are functions of the C's and D's and are given in

Table 4.23-1 which follows. The source term S_ϕ, which appeared in equation (4.22-3) has been linearised thus:

$$S_\phi = S_u + S_p \phi_p \qquad ,(4.23\text{-}2)$$

before being substituted into the general equation.

Coeff	Formulae for Coefficients	
	Main-cell variable	Velocity Variable
a_E	$\max(D_e, D_e - C_e)$	$\max\{\frac{1}{2}(D_e+D_{eF}), \frac{1}{2}(D_e+D_{eF}) - \frac{1}{2}(C_e+C_{eF})\}$
a_W	$\max(D_w, D_w + C_w)$	$\max\{\frac{1}{2}(D_w+D_{wF}), \frac{1}{2}(D_w+D_{wF}) + \frac{1}{2}(C_w+C_{wF})\}$
a_N	$\max(D_n, D_n - C_n)$	$\max\{\frac{1}{2}(D_n+D_{nF}), \frac{1}{2}(D_n+D_{nF}) - \frac{1}{2}(C_n+C_{nF})\}$
a_S	$\max(D_s, D_s + C_s)$	$\max\{\frac{1}{2}(D_s+D_{sF}), \frac{1}{2}(D_s+D_{sF}) + \frac{1}{2}(C_s+C_{sF})\}$

Table 4.23-1: Formulae for the Coefficients of the Finite-domain Equations

In Table 4.23-1, subscrips denote the edges of the main control cells. The subscript F refers to the next cell face in the direction of the velocity component considered.

The formulae for the convection fluxes (C's) and diffusion coefficient (D's) are presented in Table 4.23-2 below.

Cell face	Convection Fluxes C	Diffusive Coefficient D
e	$\rho_{up}U_eA_e$	$\|2/(1/\Gamma_P+1/\Gamma_E)\|\|A_e/(x_E-x_P)\|$
w	$\rho_{up}U_wA_w$	$\|2/(1/\Gamma_P+1/\Gamma_W)\|\|A_w/(x_P-x_W)\|$
n	$\rho_{up}V_nA_n$	$\|2/(1/\Gamma_P+1/\Gamma_N)\|\|A_n/(y_N-y_P)\|$
s	$\rho_{up}V_sA_s$	$\|2/(1/\Gamma_P+1/\Gamma_S)\|\|A_S/(y_P-y_S)\|$

Table 4.23-2: Formulae for the Convection Fluxes (C's) and Diffusion Coefficients (D's)

In the above table, subscript "up" denotes "upstream" value.

4.24 The Finite-domain equations for the velocities

The finite-domain equations for the velocity components are obtained in a manner similar to that of equation (4.23-1), by integrating each momentum equation over the control volume for the appropriate velocity component. The practice adopted for the fluxes across faces of the velocity cells is to average the fluxes through the nearby faces of the main cells; this ensures that the fluxes used in the momentum balances satisfy local continuity, whenever the fluxes for the main cells satisfy continuity. Thus:

$$C_e - C_w + C_n - C_s = 0 \qquad .(4.24\text{-}1)$$

The final form of the equations are then obtained to be similar to equation (4.23-1) with the appropriate definitions of the coefficients.

4.25 The Pressure-Correction Equation

The pressure-correction equation serves to ensure the satisfaction of the continuity equation and provides a means of calculating the pressure. It is derived in the following manner.

First, a general pressure field is used to obtain the velocities (at the faces of a main cell surrounding a point P) which satisfy the momentum equations. The mass fluxes, (i.e the C's) will not in general satisfy local continuity; so there is a finite continuity error in P, which may be denoted by R_*; and is defined thus:

$$R_* = C_e - C_w + C_n - C_s \qquad .(4.25\text{-}1)$$

It is now necessary to make corrections to the mass fluxes, so as to eliminate the error R_*. This is done by correcting the pressures at P and its surrounding nodes E, W, N and S, so as to alter the velocities at the cell faces, and hence the C's appropriately. To achieve this, the following functional dependences of the C's on the pressures are required:

$$C_e(p_P,p_E),\ C_w(p_W,p_P),\ C_n(p_P,p_N) \text{ and } C_s(p_S,p_P).$$

The pressure correction equation thus reads:

$$\frac{\partial C_e}{\partial p_P} p'_P + \frac{\partial C_e}{\partial p_E} p'_E - \frac{\partial C_w}{\partial p_P} p'_P - \frac{\partial C_w}{\partial p_W} p'_W$$

$$+ \frac{\partial C_n}{\partial p_P} p'_P + \frac{\partial C_n}{\partial p_N} p'_N - \frac{\partial C_s}{\partial p_P} p'_P - \frac{\partial C_s}{\partial p_S} p'_S = -R_* \qquad ,(4.25\text{-}2)$$

wherein the p's stand for the pressure corrections, i.e. for the additions which must be made to the pressures so as when the corresponding C changes are made, to satisfy continuity.

By appropriate definitions of the coefficients a_E, a_W, a_N and a_S, this equation can be rearranged into the form:

$$p'_P = \frac{a_E p'_E + a_W p'_W + a_N p'_N + a_S p'_S - R_*}{a_E + a_W + a_N + a_S} \qquad ,(4.25\text{-}3)$$

which is the equation that is actually solved.

4.3 The Solution of the Finite Domain Equations

4.31 General Features

The equations for the velocities, scalar property ϕ and pressure correction which are expressed in the general form (equation 4.23-1), are non-linear because the coefficients and sources are functions of the appropriate variables. In addition, the momentum equations are coupled through the unknown pressure field. Thus, an iterative, guess-and-correct procedure is required for their solution.

In the present study, the finite-domain equations are solved by a variant of the SIMPLE (Caretto et al, 1973) procedure; the novelty being the order of visitation which is selected when variables at cell centres are updated.

The main features of the present solution procedure are as follows:

(a) Treatment of the Non-linear Features of the Algebraic Equations

The finite-domain equations are solved as linear, with the coefficients and sources fixed; and the non-linearities are dealt with by subsequently recomputing the coefficients from the new ϕ's and then solving the finite-domain equations again. This process is repeated till the solution converges fully.

(b) The Structure and order of the calculation

Attention is focused successively on 'slabs' of cells i.e. collection of cells having the same value of the longitudinal distance variable x. The order chosen involves what may be termed "repeated x-direction sweeps" through the integration domain (except for parabolic flows, for which only one x-direction sweep is required).

At each slab, each ϕ variable is dealt with in turn. Firstly, all the coefficients and sources of the NY finite-domain equations for the ϕ in question are established and stored. Secondly, the NY linear equations for ϕ are solved by appropriate use of standard techniques of matrix inversion. All ϕ's are

attended to before attention moves to the next higher (east) slab; and sometimes, the cycle of ϕ solutions is repeated several times before this move is made.

4.32 Sequence of The Solution Steps

The sequence in which the calculation is carried out is as follows:

(i) The calculation starts at the slab of cells at the lowest x-location (i.e. near the west boundary).

(ii) The convection fluxes, C_e, C_w, C_n, C_s, and all diffusive flux coefficients, the D's, are constructed and stored at each main cell in the slab, from the formulae given in Table (4.23-1). To ensure that the C's actually satisfy local continuity, the convection flux through the east face of each cell is sometimes computed by application of local continuity, viz:

$$C_e = C_w + C_s - C_n \qquad ,(4.32\text{-}1)$$

and stored. For consistency, the velocity, U, at this face is then computed as:

$$U = C_e/\rho_{up}A_e \qquad .(4.32\text{-}1)$$

(iii) The finite-domain equations for U are now set up from the formulae given in Table (4.23-1), with the just-calculated C's and D's.

The pressure level at the next slab is now adjusted so as to secure a section-wise momentum balance. This condition ensures that the sum of the residuals of all the finite-domain equations for U at the section sum to zero.

(iv) Then, the longitudinal velocity, U, is solved for each control cell in the current slab, by the Jacobi point-by-point method or by simultaneous solution over the whole slab.

(v) The finite-domain equations are then set up for V, with the C's and D's evaluated at step (ii); V is then computed for each control cell at the current slab, by the Jacobi point-by-point method.

(vi) The finite-domain equation is set up, for each remaining dependent variable (e.g. k, W, h, $\tilde{m}$), in turn; the NY linear equations are solved by some suitable procedure, e.g. the Alternating Direction Implicit method.

(vii) The convection fluxes are re-calculated, by means of formulae given in Table (4.23-2), followed by the continuity error R_*, (see equation 4.25-1) for each cell. Equation (4.25-3) for the unknown pressure correction p'_P for each P cell in the slab is then set up and solved by a suitable linear equation-solving method. To do this, the off-slab corrections, P'_E and P'_W are taken as zero, and the finite-domain equations are solved

in the usual manner*.

(viii) A uniform correction is applied to the pressure to ensure that:

$$\sum_{y} p'_P A_W = 0 \qquad ,(4.32\text{-}3)$$

so that the subsequent addition of the pressure corrections to the pressures does not introduce any additional net force.

(ix) The next task is to translate the pressure corrections into terms of corrections to the velocities, convections and pressures, which will cause mass-conservation principle to prevail for all cells within the slab. Thus:

(a) $P \rightarrow P + p'$,(4.32-4)

(b) $C_n \rightarrow C_n+(\partial C_n/\partial p)(p'_P-p'_N)$,(4.32-5)

(c) $C_s \rightarrow C_s+(\partial C_s/\partial p)(p'_S-p'_P)$,(4.32-5)

(d) $C_e \rightarrow C_w+ C_s- C_n$.(4.32-6)

It is worth mentioning that C_w is not subject to adjustment, if the A_w coefficient of the P'_P equation has been omitted from it.

The three adjusted cell-face velocities are deduced from their respective convection fluxes as follows:

---

* For elliptic flows, the pressure-correction equation is solved for all slabs simultaneously. Thus, the p'-equation solution procedure is operative only when all slabs have been visited.

$$V_n = C_n/(\rho_{up}A_n) \quad ,(4.32\text{-}7)$$

$$V_s = C_s/(\rho_{up}A_s) \quad ,(4.32\text{-}8)$$

$$U_e = C_e/(\rho_{up}A_e) \quad .(4.32\text{-}9)$$

(x) The finite-domain equations for U are set up again, and the section-wise momentum balance procured at step (iv) is re-established, by augmenting the pressure level at the east slab.

(xi) Iteration may be performed at a slab by returning to step (i) and repeating. In a nearly-parabolic flow, much iteration is desirable, because few sweeps will be needed. In a strongly elliptic flow, few iterations are necessary, because the sweeps are needed to express the elliptic effects.

(xii) Attention then passes to the next slab, and the whole process is repeated. Then the next slab is attended to; and so on, until the adjustment sweep has been completed. For a strongly elliptic flow, many sweeps may be needed to produce the required degree of convergence.

In the next section, the details of the technique used to introduce the new turbulence model into the solution scheme and the computer code are given.

4.4 Incorporation of the K-W model into the Computer Program

4.41 Apprieciation of the Problem

As earlier remarked, the version of PHOENICS computer code

employed was equipped with the K-ε turbulence model but not the K-W one. It was thus necessary to introduce the new K-W model, making use of some facilities provided by PHOENICS.

In addition, due to the modular nature of PHOENICS (as briefly described in Appendix D), the coding had to be done independently of the basic equation solver. Thus, it was also essential to ensure numerical stability of the scheme.

These goals were achieved as described below.

4.42 The Central Ideas

Three main ideas have been made use of in the coding of the new K-W model, namely:

(a) The finite-domain equation governing all generic variables (K and W included) which was written in the standard form (equation 4.23-1) is what is actually solved in PHOENICS. The extra coding thus required is for the peculiarities of the new model which occur only in the source terms of the W-equation.

(b) The K-W model (like the K-ε one in PHOENICS) is based on the eddy-viscosity concept. This viscosity is calculated from the kinetic energy and the length scale of turbulence; the latter is obtainable either from K and W or K and ε, the values being identical.

(c) The dissipation rate of turbulence energy, ε, is needed for the sink term of the K equation. This may be deduced directly from the calculated values of W using the relation:

$$\varepsilon = C_D K W^{1/2} \qquad .(4.42\text{-}1)$$

In view of the foregoing, the coding of the K equation and the calculation of the eddy viscosity in PHOENICS are left intact. The general equation (4.23-1) is solved for W but the source terms are added in a separate subroutine. The values of ε are then deduced from W using the relation expressed in equation (4.42-1). The source term required for the W equation is that expressed in equation (3.43-6) and the essential parameters of the coding are G_k, the generation of turbulence energy (equation 3.43-4), gradΩ , the gradient of the major component of the vorticity of the main flow expressed as:

$$\text{grad } \Omega = \frac{\partial^2 U}{\partial y^2} \qquad ,(4.42\text{-}2)$$

and the gradient of the length scale. The length scale l, is expressed as in equation (3.42-5).

4.43 Organisation of the Coding

The listings of the coding for the new model and the associated subroutines are given in Appendices E and F. The coding of the W-equation-source term is divided into seven main

parts namely:

(a) Calculation of the length Scale

The length scale (l) is first calculated from the existing values of K and W using the relation in equation (3.42-5); l (like K and W) being stored at the cell centres.

(b) Calculation of Cross-stream Gradients $\partial U/\partial y$, $\partial V/\partial y$ and $\partial l/\partial y$

The gradients $\partial U/\partial y$, $\partial V/\partial y$ and $\partial l/\partial y$ are calculated from the existing values of U and the length scale l by a call to subroutine GRAD shown in Appendix F1. The general expressions for these gradients for a grid arrangement shown for example in Fig. 4.43-1 are:

$$\left(\frac{\partial U}{\partial y}\right)_{i,j} = 0.25 \left\{\frac{(U_{i,j+1}+U_{i-1,j+1})-(U_{i-1,j}+U_{i,j})}{y_{j+1}-y_j} + \frac{(U_{i,j}+U_{i-1,j})-(U_{i,j-1}+U_{i-1,j-1})}{y_j-y_{j-1}}\right\} \quad ,(4.43\text{-}1)$$

$$\left(\frac{\partial V}{\partial y}\right)_{i,j} = \frac{V_{i,j}-V_{i,j-1}}{\Delta y_{ij}} \quad ,(4.43\text{-}2)$$

wherein ΔY_{ij} is the cross-stream width of cell i,j, and

$$\left(\frac{\partial l}{\partial y}\right)_{i,j} = 0.5 \left\{\frac{(l_{i,j+1}-l_{i,j})}{y_{i+1}-y_j} + \frac{(l_{i,j}-l_{i,j-1})}{y_j-y_{j-1}}\right\} \quad .(4.43\text{-}3)$$

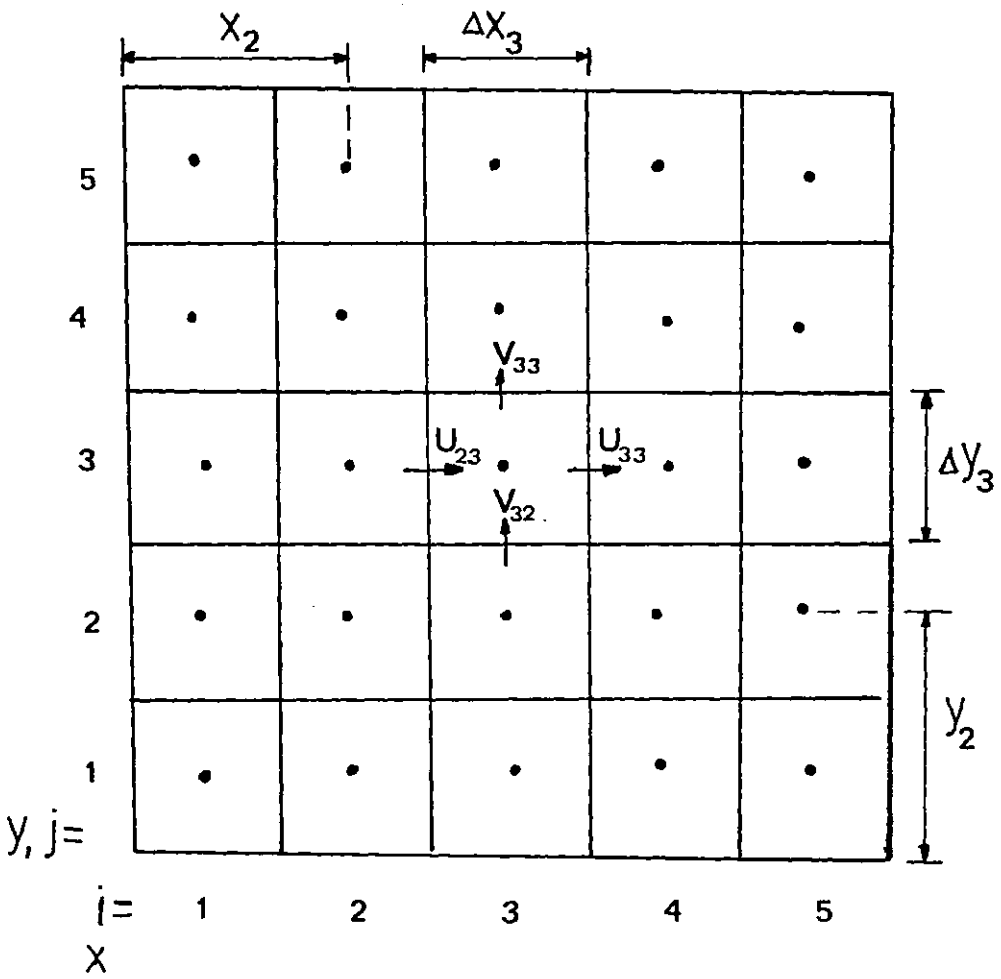

Fig. 4.43-1. Typical grid nomenclature for the coding of the W-equation sources.

In the above equations and figure (4.43-1), i and j refer to the longitudinal and cross-stream locations respectively of the cell considered. It will be noted that the staggered-grid arrangement discussed in section 4.2 in which the velocity corresponding to a particualr cell is stored at the grid line in front of it, has been employed.

The gradient $\partial U/\partial y$ will be required for the calculation of G_k, the generation rate of turbulence energy and also for Ω, the main component of vorticity. $\partial l/\partial y$ is required for the new term introduced into the model (see equation 3.42-6). $\partial V/\partial y$ is usually small and may be neglected.

(c) Calculation of stream-wise Gradients $\partial U/\partial x$ and $\partial l/\partial x$

These gradients are required (and calculated) only for elliptic flows. They are evaluated from the relations:

$$\left(\frac{\partial U}{\partial x}\right)_{i,j} = \frac{U_{i,j}-U_{i-1,j}}{\Delta x_{i,j}} \qquad ,(4.43\text{-}4)$$

in which $X_{i,j}$ is the axial length of the cell ij.

$$\left(\frac{\partial l}{\partial x}\right)_{i,j} = 0.5\left[\frac{(l_{i+1,j}-l_{i,j})}{x_{i+1}-x_i} + \frac{(l_{i,j}-l_{i-1,j})}{x_i-x_{i-1}}\right] \qquad ,(4.43\text{-}5)$$

wherein X_i is the streamwise location of the grid node ij. The two gradients are stored at the cell centres.

(d) Calculation of G_k, the Turbulence-Energy Generation

The generation of turbulence energy is calculated in subroutine PRODK given in appendix F2. From equation (3.43-4), G_k may be expressed in two-dimensional cartesian coordinates as:

$$G_k = \mu_t \{(\frac{\partial U}{\partial y})^2 + 2\left|(\frac{\partial U}{\partial x})^2 + (\frac{\partial V}{\partial y})^2\right|\} \quad ,(4.43\text{-}6)$$

For parabolic flows and a majority of flow situations, only the first term on the right-hand side of the equation is important. However, all the terms are included here for the elliptic flows considered.

The formula adopted for the evaluation of the dominant term $(\partial U/\partial y)^2$ is:

$$(\frac{\partial U}{\partial y})^2_{i,j} = \frac{1}{8}\{\left[\frac{(U_{i,j+1}+U_{i-1,j+1})-(U_{i-1,j}+U_{i,j})}{y_{j+1}-y_j}\right]^2 + \left[\frac{(U_{i,j}+U_{i-1,j})-(U_{i,j-1}+U_{i-1,j-1})}{y_j-y_{j-1}}\right]^2\} \quad .(4.43\text{-}7)$$

This was found to be more accurate than merely squaring the expression for $(\partial U/\partial y)$ as given in equation (4.43-1).

$(\frac{\partial U}{\partial x})^2$ and $(\frac{\partial V}{\partial y})^2$ are obtained by squaring the expressions for $(\partial U/\partial x)$ and $(\partial V/\partial y)$ given respectively in equations (4.42-4) and (4.43-2). The eddy viscosity, μ_t, is obtained from the existing effective viscosity and laminar viscosity using the relation.

$$\mu_t = \mu_{eff} - \mu \quad .(4.43\text{-}8)$$

(e) Calculation of Ω, and $(|\text{grad}\Omega|)^2$

The magnitude of the major component of vorticity, Ω, and the square of its absolute gradient are calculated by a call to subroutine VORTI (appendix F3) using the following relations:

$$\Omega = \left|\frac{\partial U}{\partial y}\right| \qquad ,(4.43\text{-}9)$$

and,

$$(|\text{grad}\Omega|)^2_{i,j} = \tfrac{1}{2}\left|\left(\frac{\Omega_{i,j+1}-\Omega_{i,j}}{y_{j+1}-y_j}\right)^2 + \left(\frac{\Omega_{i,j}-\Omega_{i,j-1}}{y_j-y_{j-1}}\right)^2\right| \qquad ,(4.43\text{-}10)$$

Both are stored at the cell centres.

(f) Calculation and Linearisation of Source Terms

This is the most important part of the coding as it can affect the numerical stability of the scheme. This is particularly important in flow situations where abrupt velocity gradients occur as in the boundary regions of jets issuing into stagnant or slow-moving surroundings.

The source term in the W equation given in equation (3.43-6) is integrated over the control volume and linearised as follows:

$$\iiint_{V_o} S_w = S_u + S_p W \qquad ,(4.43\text{-}11)$$

where:

$$S_u = V_o \left[C_1 \mu_t (|\text{grad}\Omega|)^2 + C_3 \frac{W}{K} G_k \right] \quad ,(4.43\text{-}12)$$

$$S_p = -V_o \left[C_4 \rho W^{\frac{1}{2}} (|\text{grad}1|)^2 \right] \quad ,(4.43\text{-}13)$$

in which V_o is the volume of the cell.

This practice ensures that S_p is always negative and is found to promote numerical stability.

The sources are calculated in subroutine SORCW (Appendix F4) and then added to the W equation in GROUND, S_u being added to the numerator of the equation (4.23-1) while - Sp is added to the denominator.

(g) Boundary Condition at a Wall

In all the calculations involving walls, the grid nodes near the walls are omitted from the above analysis. Instead, the values of W are prescribed specifically from the relation in equation (3.51-3). This is done by linearisation as will be explained in section 4.5 below for a generic fluid variable.

(h) Deduction of Dissipation Rate, ε from W

The dissipation rate ε, of the turbulence energy which will be used both in the sink term of the K equation and in evaluating the eddy viscosity is deduced from the calculated W using the relation in equation (4.42-1).

(i) Miscellaneous Features

The description above has concentrated on the basic features of the coding. Some peculiarities exist for different flow situations. These include treatment of wall boundary-conditions for flows with heat transfer, mass transfer, pressure gradient and significant turbulence diffusion; and the provision of the necessary output for comparison of predicitons with experimental data. These features are handled by way of additional subroutines which are called at appropriate stages of the solution scheme. An example of these subroutines, WALFUN, given in Appendix F5 is used for calculating the wall functions when turbulent diffusion is important.

4.5 Auxiliary Information for the Solution Scheme

4.51 Boundary Conditions

The different boundary conditions that are required to specify the flow situations considered in the present study have been discussed in sections 2.6 and 3.5. The appropriate methods of implementing these in the solution scheme are given below.

The values of the dependent variables must be specified at the boundaries before the set of the finite-domain equations can be solved. These boundary conditions, which determine the uniqueness of the solution for a given flow situation, are usually of two types:

(i) The value of the variable is prescribed at the boundary. This is generally accepted as the most stable of boundary conditions.

(ii) The value of ϕ on the boundary is deduced from the known gradient of ϕ at the boundary.

In the present study, both conditions are handled by way of linearised sources. The details of this approach will be found in Spalding (1982) and only a brief outline will be described here.

The general expression for the boundary-link source term is:

$$S_\phi = (C_\phi + \dot{m}_b)\ (V_\phi - \phi_p) \qquad ,(4.51\text{-}1)$$

where,

C_ϕ = the 'coefficient' of ϕ

V_ϕ = the 'external value" of ϕ

ϕ_p = the value of ϕ in the cell P; and

$\dot{m}_b$ = is the mass flow across the boundary

The latter quantity is computed from:

$$\dot{m}_b = C_m(V_m - P_p) \qquad ,(4.51\text{-}2)$$

where,

C_m = the 'coefficient' for mass flow

V_m = the 'value' for mass flow; and

P_p = the pressure in cell P.

It should be noted that C_m effectively represents the sensitivity of the across-boundary flow to the pressure, P_p, i.e.

$$C_m = \frac{\partial \dot{m}_b}{\partial p_p} \qquad ,(4.51\text{-}3)$$

and as such appears in the denominator of the pressure-correction equation (4.25-3).

This approach allows the convection terms (if present) at boundaries to be handled successfully despite the fact that, for reasons of economy, storage of variables is <u>not</u> provided at boundaries of the integration domain.

In view of equation (4.51-2), the boundary conditions may be reclassified into:

(a) <u>Linear Boundary Conditions</u>

These are the ones for which the 'coefficient' and the 'value' are constants over the boundary region. Examples are inflow or outflow boundaries, free-streams, symmetry planes, boundaries with known diffusive flux and those in which the gradient-diffusion flux are applicable. The necessary boundary conditions are adequately specified by appropriate combination of the 'coefficients' and 'values' occurring in equation (4.51-1).

(b) Non-Linear Boundary Conditions

These are those for which C and/or V are functions of the ϕ's. Examples are boundary conditions at a wall in which 'wall functions' are used as described in section 3.5. They are handled similarly after an appropriate 'linearisation' of the functions. However, iteration may be required because of the implicit formulation of the equations.

4.52 Convergence

A measure of how well the finite-domain equations are satisfied is determined by the degree of convergence of the numerical process. The simplest sign of convergence is the presence of systematic behaviour of the variables between successive sweeps (or iterations), with the differences diminishing.

The convergence is also quantitatively monitored through the use of residuals. A residual of a variable ϕ at a node P, denoted by R_ϕ, is defined as:

$$R_\phi = a_p \phi_p - \Sigma a_i \phi_i - S_u \qquad ,(4.52\text{-}1)$$

where a_p is the denominator of equation (4.23-1). The "simultaneously-existing" residuals are defined as those present for each cell for each variable when the whole variable field has been frozen at the most-recently calculated value. To fascilitate monitoring, the residuals are suitably normalised to the product of a typical ϕ and the mass flow rate, $\dot{m}_b$, through the domain. For many purposes,

$$\sum_x \sum_y \frac{|R_\phi|}{\dot{m}_b \phi_t} \leq 0.05 \qquad ,(4.52\text{-}2)$$

may represent adequate accuracy; here ϕ_t denotes the "typical" ϕ.

Convergence may be promoted in two ways namely by use of:

(i) Intertial Under-relaxation

This adds the following term to the finite-domain equation for the ϕ to which it is applied:

$$S_{\phi r} = \lambda(\phi_p - \phi_{p,old}) \qquad ,(4.52\text{-}3)$$

where λ is a positive number, which may be freely chosen; $S_{\phi r}$ is the term added and $\phi_{p,old}$ is the previously-existing value of ϕ at the cell in question. For large λ, this approach has the effect of keeping ϕ_p close to $\phi_{p,old}$. For velocity variables, this also has the effect of diminishing $\partial(vel)/\partial p$, making it difficult for the pressure corrections to change the velocity.

(ii) "Under-relaxation" of the pressure corrections

This is a means of reducing the magnitude of the pressure corrections before application to the pressures. Thus:

$$P'_{p_{new}} = R_f P'_p \qquad ,(4.52\text{-}4)$$

where $P'_{p_{new}}$ is the new value of the pressure correction and R_f is the under-relaxation factor lying between 0 and 1.

The computational details, provided for some of the test cases considered in chapters 5 to 7, give the values required for the converged solution such as: the number of iterations and/or sweeps performed, the sum of the absolute values of the residuals over the whole field, the net values of the residuals and other relevant information.

4.53 Numerical Stability

Numerical instability or divergence is said to occur when the errors in the solution scheme continue to increase or fluctuate. Instabilities are known to be caused by many factors, see for example Runchal (1971) and Roache (1976). Such factors include:

(i) Truncation Errors - these are induced into the numerical scheme by the finite-domain equations and they depend mainly on the grid size.

(ii) Perturbations - These result from unrealistic values of the initial conditions used to start the calculation. The perturbations are not very critical for the steady flows considered; however, the closer the initial guess is to the solution, the smaller the effect of these perturbations

is on the stability and convergence speed.

(iii) Boundary Conditions - The boundary conditions in which the value of the dependent variables are specified are known to be the most stable of all boundary conditions. Those in which the normal gradients of the variables are specified at the boundary are less so and should be handled with more care.

(iv) Coupling and Non-linearity of the Equations - These may give rise to large changes in the values of the finite-domain coefficients between successive iterations and/or sweeps and may lead to instability or divergence.

These instabilities are in most cases, successfully avoided by careful choice and handling of grid sizes, boundary and initial conditions and if necessary, the relaxation techniques described in section 4.52 above.

4.6 Closure

In this chapter, the finite-domain form of the partial differential equations governing a generic fluid variable and the method of solution have been presented. The method used to introduce the new turbulence model into the computer code employed in the present study has been described. Remarks have also been made on the capabilities and limitations of the numerical solution procedure.

The procedure as presented, is general and flexible, and may be applied to calculate various physical flow situations governed by different boundary conditions.

The results of the computations made using the procedure will be presented in the following three chapters.

CHAPTER 5

PREDICTION OF TURBULENT EXTERNAL BOUNDARY LAYERS

5.1 Introduction

So far, the equations governing the transport of a fluid variable, the turbulence model employed for the closure of the equations and the method and means of their solution have been established. In this chapter, the results of the computations based on these features are presented for turbulent external boundary layer flows.

The term "external" generally refers to flows in which the turbulent region is significantly affected by at most one wall. External boundary layers are indeed the commonest members of the class of "thin shear layers" and provide a convenient framework within which to test a new turbulence model and consider the effects of boundary conditions. For example, if the wall or free stream conditions are changed, the shear layer will 'feel' this change as a more or less strong perturbation. In the present context, however, unperturbed free shear layers e.g. the classical jets and mixing layers will be excluded; their description being deferred until chapter 7.

The physical situations considered here range from the relatively simple uniform-pressure flow over a smooth flat-plate to boundary layers with intense heat-transfer and with intense mass-transfer through the surface. All the flows are "parabolic", by which is meant that influences travel in only one (downstream) direction. This feature substantially reduces the cost of computation as discussed earlier in chapter 4.

These flow situations are of great practical importance in varioius fields of Engineering. The subject of flow on a flat plate with or without pressure gradient is relevant to the calculation of the skin-friction drag on ship hulls, on lifting surfaces and aeroplane bodies in aeronautical engineering, and on the blades of turbines and rotary compressors. It is also important to the understanding of the processes which occur in a diffusser. The structure of turbulent boundary layers with blowing or suction is of some practical importance, particularly with a view to increasing the maximum lifts on aerofoils.

The chapter is divided into six sections of which this introduction is the first. In sections 5.2 to 5.5 are presented respectively the calculations of: flat plate boundary-layer flow with uniform properties (data of Klebanoff, 1954 and of Wieghardt as processed for the AFOSR-IFP Stanford conference by Coles and Hirst, 1969); boundary layers with pressure gradients (data of Bradshaw, 1965); and flow with transpiration cooling (data of Moffat and Kays, 1968). In each of the sections, available experimental data are briefly reviewed, the various cases considered and the computational details are described, the results are presented and subsequently discussed.

Section 5.6 contains the concluding remarks and a summary of the major achievements of the chapter.

5.2 Smooth flat plate with uniform properties

5.21 The problem

In order to test the new K-W turbulence model and to study the influence of the "constants" established on flow

parameters, it is necessary to first apply the model to a simple flow situation. For this purpose, the turbulent boundary layer which forms on a smooth flat-plate, exposed to a uniform fluid stream is considered. The task is to predict the boundary-layer parameters like the shape factor, local skin-friction coefficient, momentum thickness, mean velocity distribution and invariably, the turbulence quantities.

The accuracy and physical realism of the predictions are assessed by comparing with established experimental data. In the following section, a brief review of some available experimental data is undertaken so as to choose the most appropriate for this purpose.

5.22 Review of experimental data

Numerous experimental data are available for this flow situation. These are well-detailed in the literature (see for example, Schlichting, 1968; Hinze 1959). Therefore, only a brief review will be presented here.

The data for the mean-velocity distribution across the turbulent boundary-layer on a smooth flat-plate with zero pressure gradient have been obtained by Klebanoff and Diehl (1951), Klebanoff (1954), Smith and Walker (1959) and those of Wieghardt as processed by Coles and Hirst (1969). Except for Smith and Walker, all the experimenters made their measurements only in the fully-turbulent region of the boundary layer. These measurements have been shown to be consistent and to obey the similarity presumption by Hinze (1959).

Extensive measurements on turbulence quantities have been made by Klebanoff and Diehl (1951), Klebanoff (1954), Corrsin and Kistler (1954), and Wieghardt, (see Coles and Hirst (1969)). These measurements cover a wide range of Reynolds numbers and plate dimensions and include the distributions of turbulence intensities, turbulence energy, shear stress and eddy viscosity.

5.23 The cases considered

In the present study, two of the experimental situations reviewed above have been considered, namely, that of Klebanoff and that of Wieghardt. The details of the computations are described in the following section.

5.24 Computational details

The physical situation considered for the present computations is illustrated in figure 5.24-1. The origin of the boundary layer corresponds to the leading edge of the plate while the exit boundary is located sufficiently downstream of the leading edge to allow the flow to be fully developed. The free-stream boundary represents the locus of the positions where the mean velocity attains a value of about 99% of the mains-stream velocity.

All the flows considered in the present and subsequent sections are parabolic. Thus the boundary-layer forms of the governing differential equations for U and V in addition to the continuity equation as presented in chapter 2 are solved.

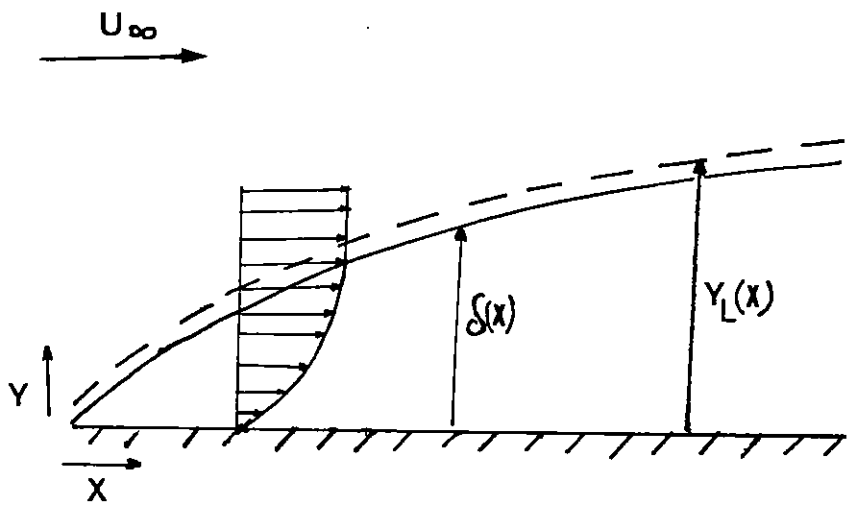

Fig. 5.24-1. Nomenclature for boundary layer on a flat plate.

The grid employed in each of the cases considered in this and the subsequent sections are made to expand with the boundary layer growth. The general relation for the growth of the grid width is:

$$y_L = FX^e \qquad ,(5.24\text{-}1)$$

in which y_L is the vertical height of the free-stream grid line above the plate, X the longitudinal distance; and F and e are constants, taken as 0.02 and 0.8 respectively. The intial grid-width is taken as 0.01m.

It should be noted that y_L merely prescribes the spread of the grid and not that of the boundary layer; the latter being an outcome of the computation.

In order to examine the effects of grid size on the solution, systematic grid-refinements are carried out in both the X - and Y - directions.

Grid No.	Cross-stream Nodes	Shape factor H_{12}
1	10	1.265
2	15	1.29
3	18	1.30
4	24	1.30

Table 5.24-1: Effect of Cross-stream grid nodes on the shape factor for fully-developed flat-plate flow.

Table 5.24-1 shows the different grids employed and their effects on the predicted boundary-layer shape factor for the fully-developed flow. It is seen that the solution obtained with the 18 non-uniform cross-stream grid nodes and a forward-step size of 30% of the grid width can be regarded as sufficently grid-independent. The results presented in section 5.25 below are based on the use of this particular grid.

The boundaries of this flow domain comprise the plate (i.e. smooth wall), the inlet plane at which calculation starts, and the free stream boundary (see fig. 5.24-1). The exit plane need not (and cannot be) specified because of the parabolic nature of the flow. The boundary conditions employed are:

(i) inlet plane

$$\frac{U}{U_G} = \left(\frac{y}{y_G}\right)^{\frac{1}{2}} \qquad ,(5.24\text{-}2)$$

$$V = 0 \qquad .(5.24\text{-}3)$$

The initial turbulence energy profile is calculated from the procedure employed by Ng and Spalding (1970) in which K is represented by the polynominal,

$$k = a + b\eta + c\eta^2 + d\eta^3 \qquad ,(5.24\text{-}4)$$

where:

$$\eta = y/y_G \qquad ,(5.24\text{-}5)$$

$$a = \tau_s/(\rho_s C_D^{\frac{1}{2}}) \qquad ,(5.24\text{-}6)$$

$$b = y_G \frac{dP}{dx} / (\rho_s C_D^{\frac{1}{2}}) \quad ,(5.24\text{-}7)$$

$$c = -3a - 2b \quad ,(5.24\text{-}8)$$

$$d = 2a + b \quad .(5.24\text{-}9)$$

W is related to K by the following relations deduced from the logarithmic law of the wall and equation (3.43-5) for the turbulent viscosity:

$$\eta \leqslant \frac{C_D}{\kappa} \quad : \quad W = \frac{K}{C_D^{\frac{1}{2}} \kappa^2 y^2} \quad ,(5.24\text{-}10)$$

$$\eta > \frac{C_D}{\kappa} \quad : \quad W = \frac{K}{C_D^{5/2} y_G^2} \quad .(5.24\text{-}11)$$

(ii) Free stream:

$$U = U_G \quad .(5.24\text{-}12)$$

In addition, zero values of V,P,K and W are prescribed.

(iii) Wall

Wall functions are employed as described in section 3.5

(e) Initial conditions

The conditions specified at the inlet plane i.e. equations (5.24-2) to (5.24-11) are used as intial guesses for the field values.

Table 5.24-2 summarises some of the above and other details of the computation. The 'Net' volumetric error gives

the slab sum of the volumetric imbalance of each cell; while the 'absolute' error gives the slab sum of the absolute volumetric imbalances of each cell. Of the two, the latter is considered to be more important for the former could be small by cancellation of large positive and negative errors. In Table 5.24-2 below, each of these errors has been non-dimensionalised with the volumetric flux into the domain of calculation.

Variable	Value
Grid	18 along y; $x = 0.3Y_L$
Type of grid spacing	Non uniform, mostly near wall
Number of sweeps	1
Number of iterations on each variable	5
Inertial under-relaxation factor	10^{10} (ineffective)
Non-dimensionalised Net volumetric error	-7.331×10^{-6}
Non-dimensionalised Absolute volumetric error	3.913×10^{-5}

Table 5.24-2: Computational details for smooth flat plate flow with uniform properties

5.25 Results

Predictions are compared in figure 5.25-1 with the data of Wieghardt as processed for the AFOSR-IFP Stanford Conference by Coles and Hirst (1969). The parameters compared are the

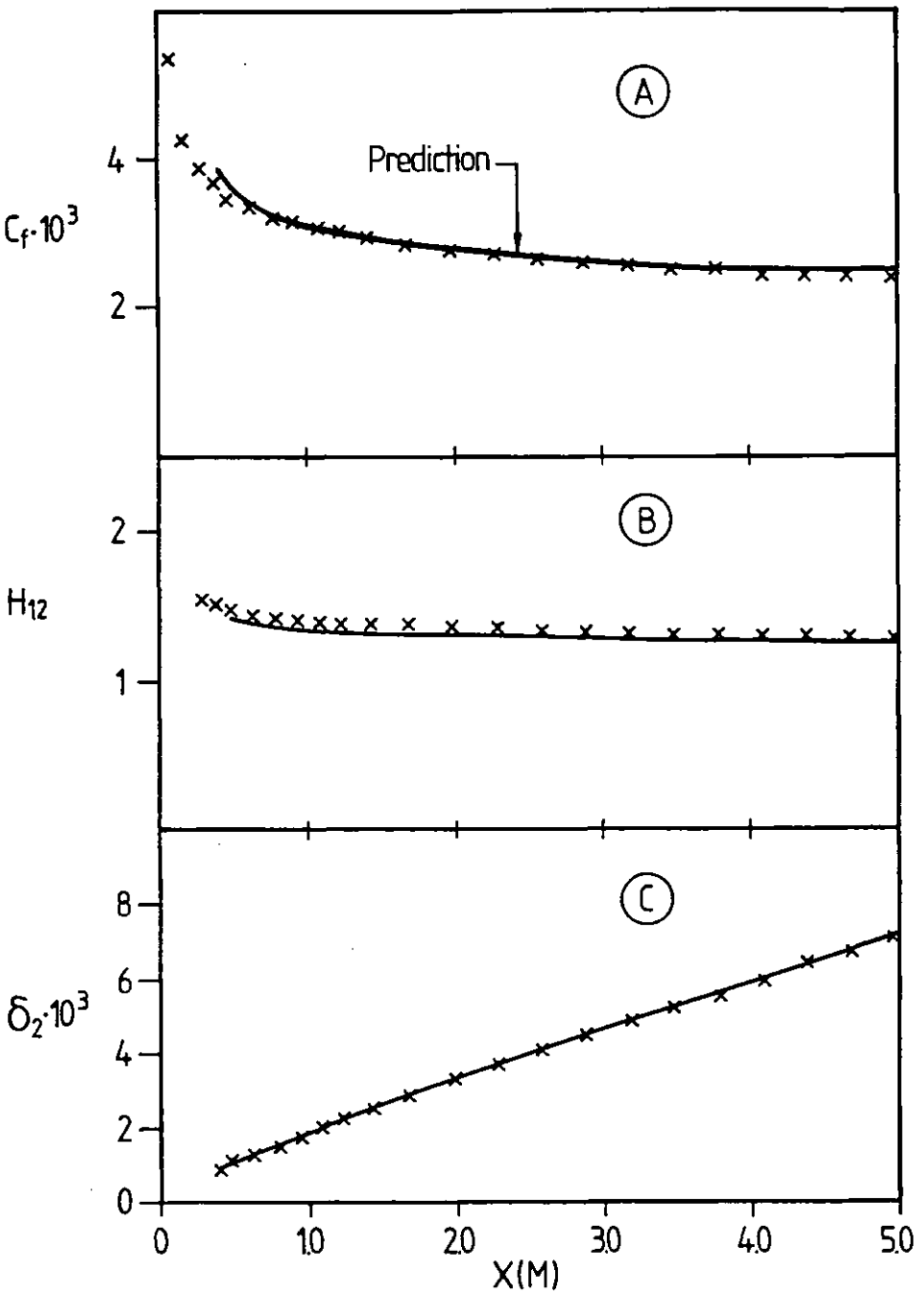

Fig. 5.25-1. Distribution along plate of:
(A) Skin-Friction Coefficient (C_f)
(B) Shape Factor (H_{12})
(C) Momentum Thickness (δ_2)
(Experimental Data of Wieghardt, processed by Coles and Hirst, 1969.)

boundary-layer shape-factor H_{12}, the local skin-friction coefficient, C_f, and the momentum-thickness δ_2. Predicted mean-velocity, turbulence-energy and shear-stress distributions are compared in figures 5.25-2 and 5.25-3 with the data obtained by Klebanoff (1954) at approximately the same values of the momentum-thickness Reynolds number, Re_2 of 7500. It is known from experiment and computations however, that Re_2 has little effect on the profiles.

5.26 Discussion

The agreement between the predicted and experimental results is satisfactory, indeed probably within the margin of experimental error over most of the range. Figure 5.25-3 shows that the ratio $\tau/\rho K$ is approximately equal to 0.3 i.e to $C_D^{\frac{1}{2}}$, as is to be expected for a flow in which generation and dissipation of turbulence energy are nearly in local balance everywhere. It will also be observed from this same figure that in the region $y/y_G < 0.1$, the shear stress approaches a constant value, thus justifying the usual assumption of constant shear-stress in the wall region for this type of flow.

The comparison described above is directly relevant to the novel feature of the new K-W model; for if the C_4-term (equation 3.43-6) were not correctly describing the W-source, good agreement would definitely not have been obtained.

5.3 Smooth flat plate with longitudinal pressure-gradient

5.31 The problem

The next problem to which the new K-W model is applied is

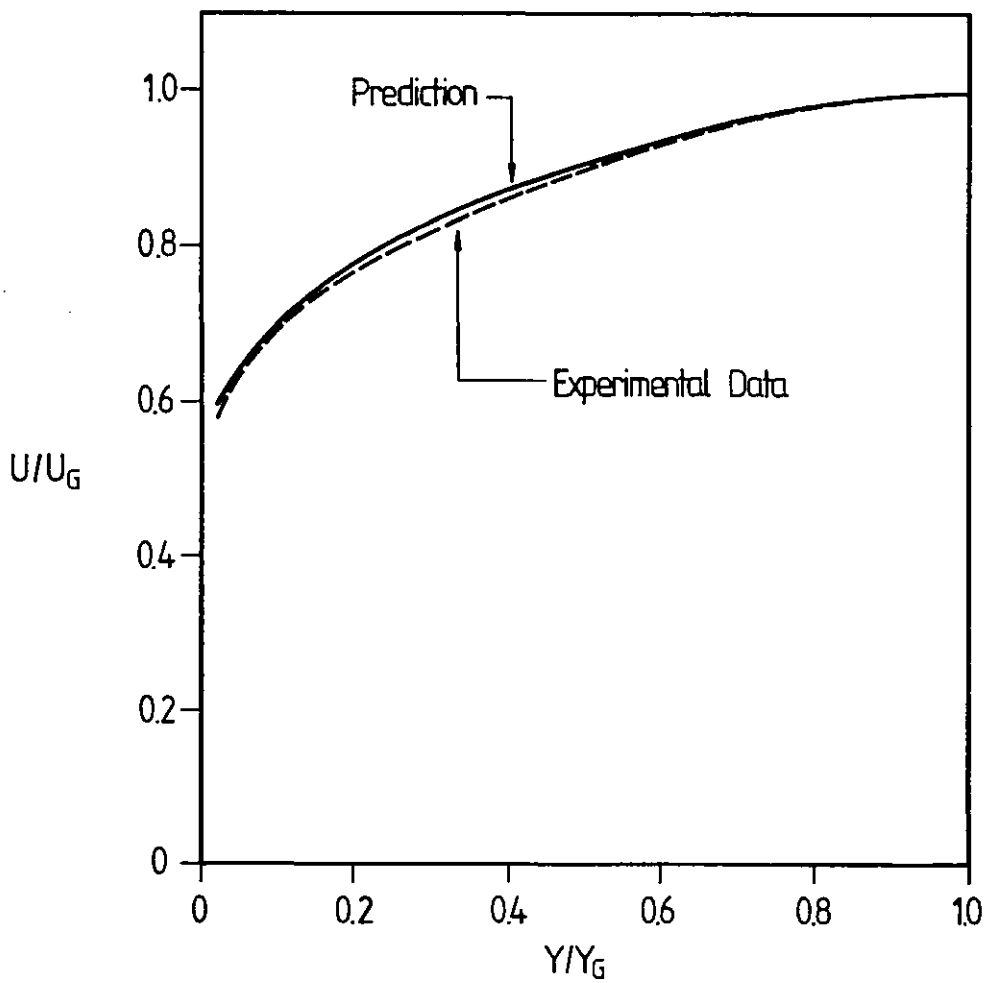

Fig. 5.25-2. Mean Velocity Distribution on flat plate. (Experimental data of Klebanoff P.S, 1954).

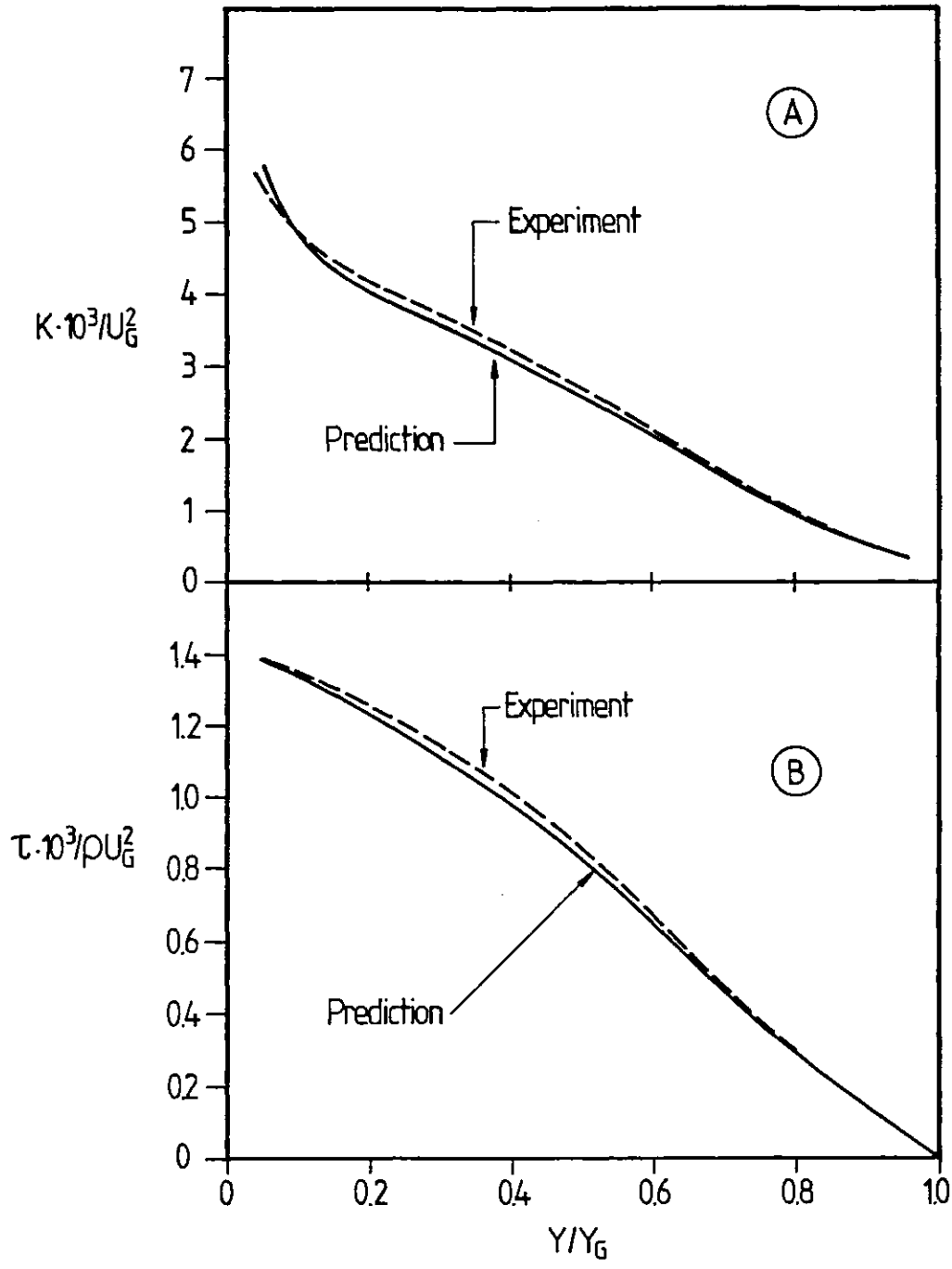

Fig.5.25-3. Distributions on flat plate of:
(A) Turbulence Kinetic Energy.
(B) Reynolds Shear Stress.
(Experimental Data of Klebanoff P.S, 1954).

the equilibrium boundary-layer in mild and severe longitudinal pressure-gradients. The task is to predict the mean-velocity profiles and the integral parameters like distributions of shape factor H_{12}, of drag coefficient (friction factor) C_f, and of momentum-thickness Reynolds number Re_2; given the variation of longitudinal pressure with distance along the plate, and making the assumption that the boundary layer is two-dimensional.

This problem is concerned with the analysis of equilibrium turbulent boundary-layers which, incidentally, are the nearest equivalent of the family of laminar boundary-layers with similar profiles (Falker-Skan flows). A necessary condition for similarity is that the contribution of the pressure gradient to the growth of the momentum deficit $\rho U^2 \delta_2$ shall be a constant multiple of the contribution of the surface shear-stress. Since

$$\frac{d}{dx}(\rho U^2 \delta_2) = \tau_s + \delta_1 \frac{dP}{dx} \qquad ,(5.31\text{-}1)$$

where δ_1 is the displacement thickness, this implies:

$$(\frac{\delta_1}{\tau_s}) \frac{dP}{dx} = \text{constant} \qquad ,(5.31\text{-}2)$$

in compressible or incompressible flow. Townsend (1956, 1961) and Mellor and Gibson (1966) have shown that approximate similarity is obtained (in incompressible flow), if:

$$U \alpha x^a \qquad ,(5.31\text{-}3)$$

in which 'a' is constant, as in laminar flow. This latter nominal definition of similarity is adopted for the flow situations to be considered.

5.32 Review of experimental data

There have been many experimental investigations of hydrodynamic boundary-layers on smooth surfaces submerged in streams in which the pressure varies in direction of flow. A comprehensive review of these is contained in Coles and Hirst, (1969). These studies could be classified into two groups namely:

(i) Those in which the measurements were taken in a decreasingly adverse pressure-gradient, i.e. $dP/dx > 0$, $d^2P/dx^2 < 0$; and

(ii) those with increasingly adverse pressure-distribution i.e. dP/dx and d^2P/dx^2 are both positive.

Included in the first group are the works of Clauser (1954), Stratford (1959), Bradshaw (1965) and Bradshaw and Hellens (1966). Prominent in the second group are the work of Samuel and Joubert (1974) and partly Sandborn and Slogar (1955). This latter group arose out of the recognition that there are many real flow situations (such as on ship hulls, aircraft wings and bodies of revolutions), where part of the streamwise pressure gradient distribution is increasingly adverse (see e.g. Goldstein 1965, where measured pressure distributions on aerofoils and airship hulls are presented). An

increasingly adverse pressure gradient distribution is also observed on many of the wing sections presented by Abbott and Von Doenhoff (1949).

5.33 The Case Considered

The experiment of Bradshaw (1965) includes measurements in two boundary layers with the power-law variations of free-stream velocity (equation 5.31-3), giving 'moderate' (a = -0.15) and 'strong' (a = -0.255) adverse pressure-gradients. These gradients were not particularly severe; they have however been chosen here partly because shear-stress and turbulence-energy measurements were made, and partly because the experiment is considered to be of high enough quality for all practical purposes (see for example, Coles and Hirst, 1969).

5.34 Computational details

The flow configuration, flow type, boundary conditions and grid are similar to those described in section 5.24. However, a forward step-size of 10% of the grid width is employed. The effect of cross-stream grids is shown in Table 5.34-1 overleaf. It is found that the normalized values of K and τ at a chosen location 83 inches from the leading edge of the plate, do not change significantly when grids are increased beyond 36. This is the grid employed for the calculations to be described.

The grid-expansion rates employed (see equation 5.23-1) are deduced from the measured velocity and boundary-layer parameters, δ_1, δ_2 and Y_G at different streamwise

locations to be proportional to $x^{0.8}$ and $x^{0.894}$, for the "mild" and "strong" pressure-gradients respectively.

Grid Number	a = -0.15		a = -0.255	
	$\frac{K}{U_G^2} \times 10^3$	$\frac{\tau}{\rho U_G^2} \times 10^3$	$\frac{K}{U_G^2} \times 10^3$	$\frac{\tau}{\rho U_G^2} \times 10^3$
18	4.812	1.422	10.083	3.168
24	4.840	1.450	10.330	3.240
30	4.850	1.466	10.406	3.278
36	4.857	1.473	10.429	3.309
48	4.859	1.476	10.433	3.309

Table 5.34-1: Effect of cross-stream grids on K and τ at $y/y_G = 0.4$ for location 83 in from leading edge of plate. (Note: $U_G \propto x^a$)

Variable	Value
Grid	36 along Y; $x = 0.1Y_L$
Type of grid spacing	Non uniform; mostly near wall
Iterations on each variable	10
Inertial under-relaxation factor	10^{10}
$\frac{\text{Net volumetric error}}{\text{volume flux}}$	-1.119×10^{-5}
$\frac{\text{Absolute volumetric error}}{\text{volume flux}}$	5.807×10^{-5}
Computer time	99 sec.

Table 5.34-2: Computational details for flat-plate flow with longitudinal pressure-gradient.

At the wall, the wall function described in section 3.53 is employed.

Each calculation requires 5 iterations on the equation for each variable solved for, at the end of which the absolute volumetric error is reduced to order of 10^{-5} of the volumetric flux into the domain. These and other details of the computation are summarized in Table 5.34-2 overleaf:

5.35 Results

Figures 5.35-1 to 5.35-6 show typical predictions of mean velocity, shape factor, skin friction, momentum thickness, turbulence energy and the shear stress. Also shown are the experimental data of Bradshaw (1965), in which the pressure gradients were adjusted so as to make the shape factor H_{12} nearly independent of longitudinal distance. The experiment is that characterised by the identifying number IDENT = 2600 in the compilation of Coles and Hirst (1969). The predictions with the old version of the KW model by Gibson and Spalding (1972) are included in figures 5.35-5 and 5.35-6.

5.36 Discussion

The measure of agreement between predictions and data is considered generally satisfactory. It can be seen from figures 5.35-5 and 5.35-6 that the new model performs better than the old. Figure 5.35-6 shows that the shear-stress distribution is quite adequately predicted, particularly over the inner part of the boundary layer. The maximum shear stress increases, with

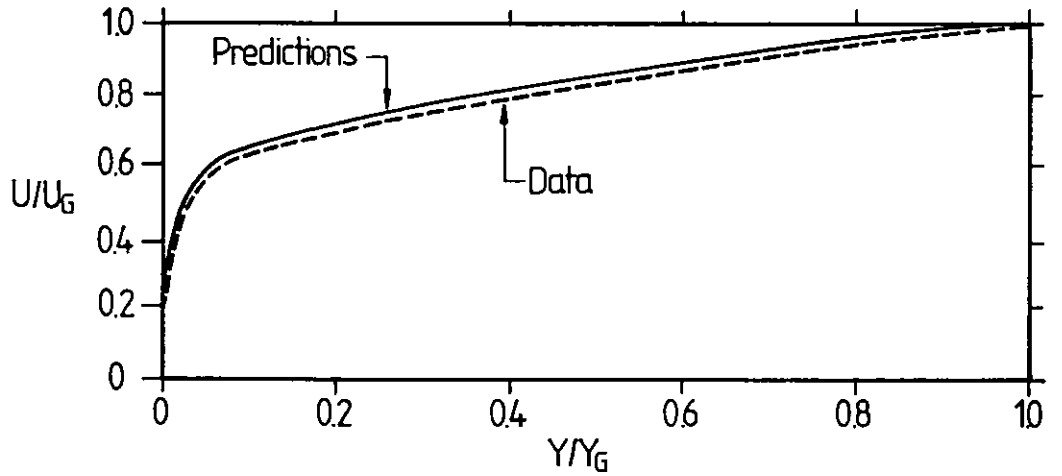

Fig. 5.35-1 Predicted and Measured Mean Axial Velocity for Mild Pressure Gradient along a flat plate. Data of Bradshaw (1965); x=83 in., a=-0.15.

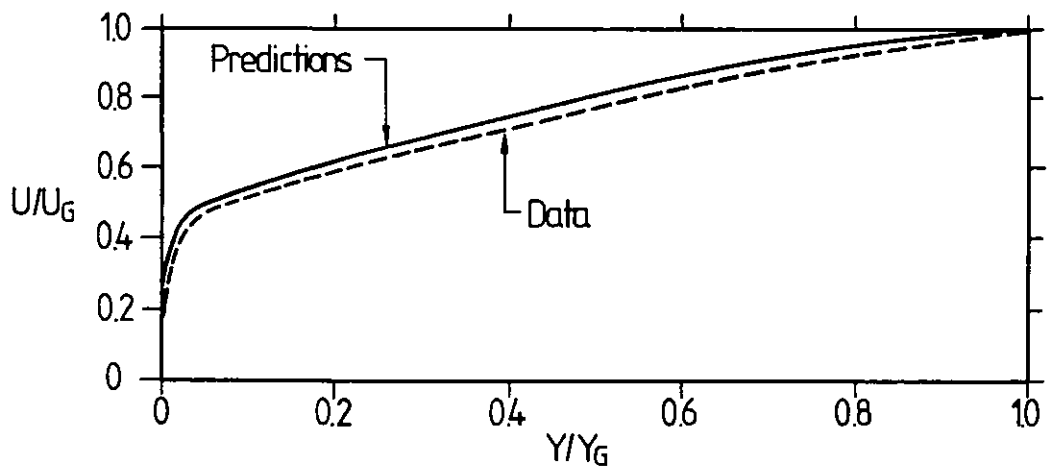

Fig. 5.35-2. Predicted and Measured Mean Axial Velocity for Severe Pressure Gradient along a flat plate. Data of Bradshaw (1965); x=83 in., a=-0.255.

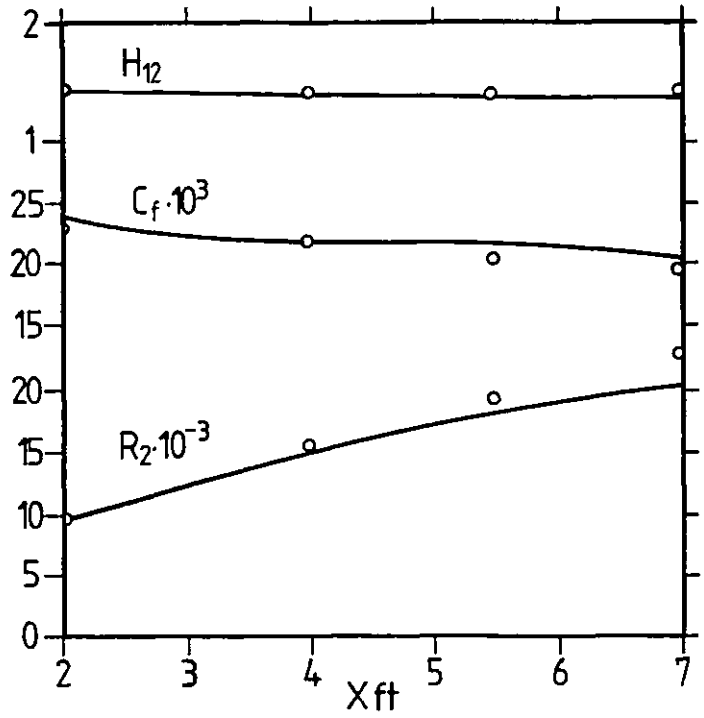

Fig. 5.35-3. Predicted and Measured Shape Factor, Skin Friction and Momentum-Thickness Reynolds Number on a flat plate with mild pressure gradient. Data of Bradshaw (1965).

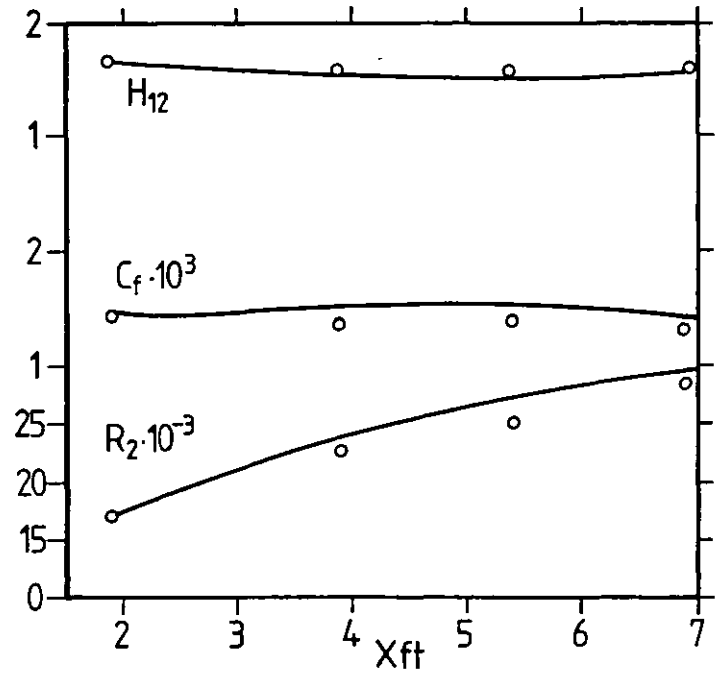

Fig. 5.35-4. Predicted and Measured Shape Factor, Skin Friction and Momentum-Thickness Reynolds Number on a flat plate with severe pressure gradient. Data of Bradshaw (1965).

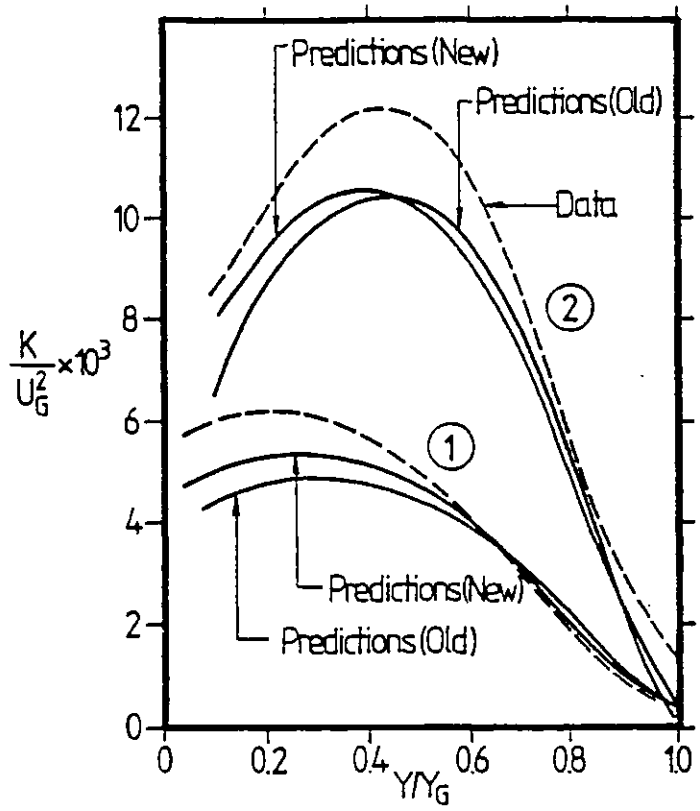

FIGURE 5.35-5: Predicted and measured turbulence energy on a flat plate with mild (1) and severe (2) pressure gradients; data of Bradshaw (1965)

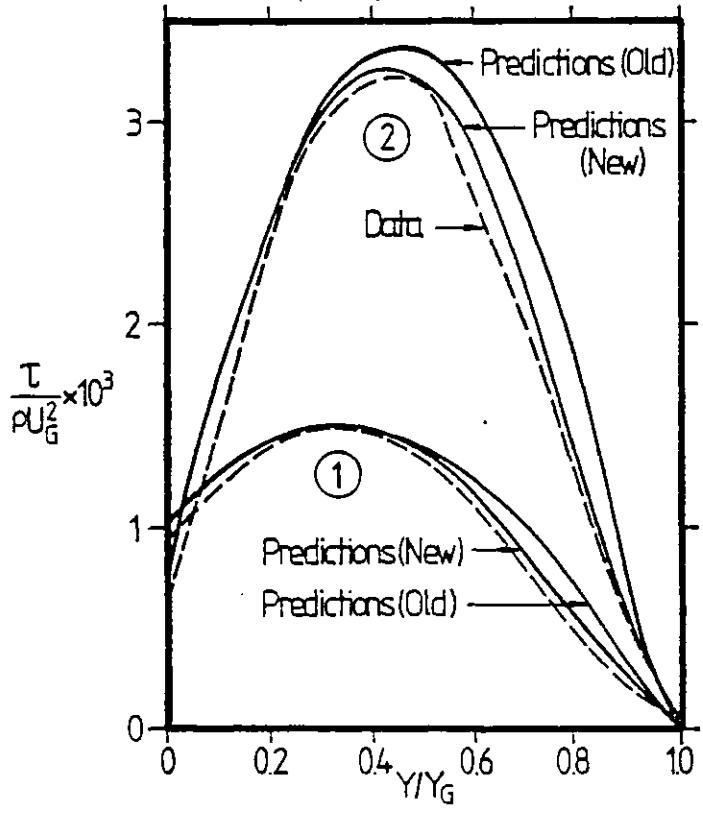

FIGURE 5.35-6: Predicted and measured shear stress on a flat plate with mild (1) and severe (2) pressure gradients; data of Bradshaw (1965)

increasing pressure gradient, as the wall shear-stress decreases. The distribution of the turbulence energy as shown in Fig 5.35-5 is not so satisfactory. There is no obvious reason for this latter discrepancy. However, it should be noted that Bradshaw's measurements show that for the two flows considered, the ratio $\tau/\rho K$ is not constant, as inferred from the energy balance near the wall and substantiated by flat-plate measurements. He attributes the variation of this ratio partly to an "inactive" component of the turbulent motion which does not contribute to the shear stress or to the dissipation rate. The assumption of an "average shear-stress" in the wall region as described in section 3.53 may therefore be considered acceptable as the shear stress is thereby reasonably well predicted.

From the computational standpoint, it seems that the error incurred in specifying the boundary condition for K through equation (3.51-2) is partially balanced in the calculation of effective viscosity by a similar error in W.

5.4 Smooth Flat Plate with Intense Heat Transfer

5.41 The Problem

One of the simplest cases of convective heat-transfer is that of the isothermal smooth flat-plate aligned with and the immersed in a uniform-velocity stream of air having such a velocity that the boundary layer is turbulent. An aspect of this flow that has long drawn the attention of researchers is predicting the influence of the effects of non-uniform fluid properties e.g. density caused by a large temperature difference

between the plate and the stream. This is the problem to which the new K-W model is next applied.

5.42 Review of Experimental Data

A comprehensive review of some available data on this flow situation has been done by Chi and Spalding (1966). They include the data of Reynolds et al (1958), Johnson and Monaghan (1951), Pappas (1954) Brevoort and Arabian (1958), Hill (1959), Winkler (1961) and Chi (1965). These cover a range of Stream-to wall-temperature ratios and Mach numbers. These data were analysed by Chi and Spalding; and a correlation was thereby proposed for the Stanton number distribution along the plate.

5.43 The Case Considered

The experimental situation reported by these latter authors for which the absolute temperature ratios (mainstream to plate) ranged from 1.5 to 2.7 is considered here.

5.44 Computational Details

Chi and Spalding (1966) made no turbulence measurements. Therefore, the initial turbulence energy and W profiles are calculated as described in section 5.24.

The expanding grid system earlier mentioned (section 5.24) is again employed, with the width of the grid taken as proportional to $X^{0.8}$. A forward step-size of 10% of the boundary-layer thickness is used. The effect of cross-stream grid-sizes is shown in Tables 5.44-1 and 5.44-2 overleaf. It can be concluded, by reading down the columns, that 30 cross-

stream grid-nodes provide sufficient "grid-independence".

Re_x / Grid No.	$2x10^5$	$4x10^5$	$6x10^5$	$8x10^5$	10^6	$2x10^6$
	STANTON NUMBER x 10^5					
18	2.997	2.278	1.964	1.780	1.602	1.096
24	3.227	2.456	2.120	1.882	1.702	1.166
30	3.273	2.491	2.145	1.909	1.727	1.182
36	3.278	2.496	2.149	1.913	1.730	1.184

Table 5.44-1: Effect of Cross-stream Grids at T_G/T_S=2.7 for Differenct Reynolds Numbers

T_G/T_S / GRID No.	1.5	2.0	2.7
	Stanton Number x 10^3 at Re_x= 10^6		
18	1.416	1.462	1.602
24	1.474	1.519	1.703
30	1.502	1.545	1.727
36	1.504	1.546	1.730

Table 5.44-2: Effect of Cross-stream Grids at a Particular Reynolds Number for Different T_G/T_S

The effective Prandtl number (σ_h), of the turbulent fluid is taken as equal to 0.9, and the effect of the laminar sub-layer in resisting heat transfer is accounted for as

described in section 3.52.

5.45 Results

Figure 5.45-1 shows the Stanton number compared with some of the data collected by Chi and Spalding (1966). Also shown are the overall-best-fit correlations proposed by those authors and the predictions with the old version of the K-W model reported by Gibson and Spalding (1972). Three absolute temperature ratios, T_G/T_S equal to 1.5, 2.0 and 2.7 are considered.

5.46 Discussion

Figure 5.45-1 shows that the new model can perform as well as the old version in predicting the characteristics of flow with intense heat transfer.

The maximum difference between the present predictions and the correlation is 7%. However, it should be mentioned that some uncertainty still surrounds the value of the correlation especially at temperature ratios higher than 1.5 (Chi and Spalding, 1966). Therefore, the prediction may be considered satisfactory, considering in addition, the scatter in the data.

5.5 Smooth Flat Plate with Intense Mass Transfer Through the Surface

5.51 The Problem

The next problem against which the new K-W model is tested is the prediction of heat transfer from a flat plate with a range of blowing and suction through the surface. This problem has been a subject of intensive investigation because of

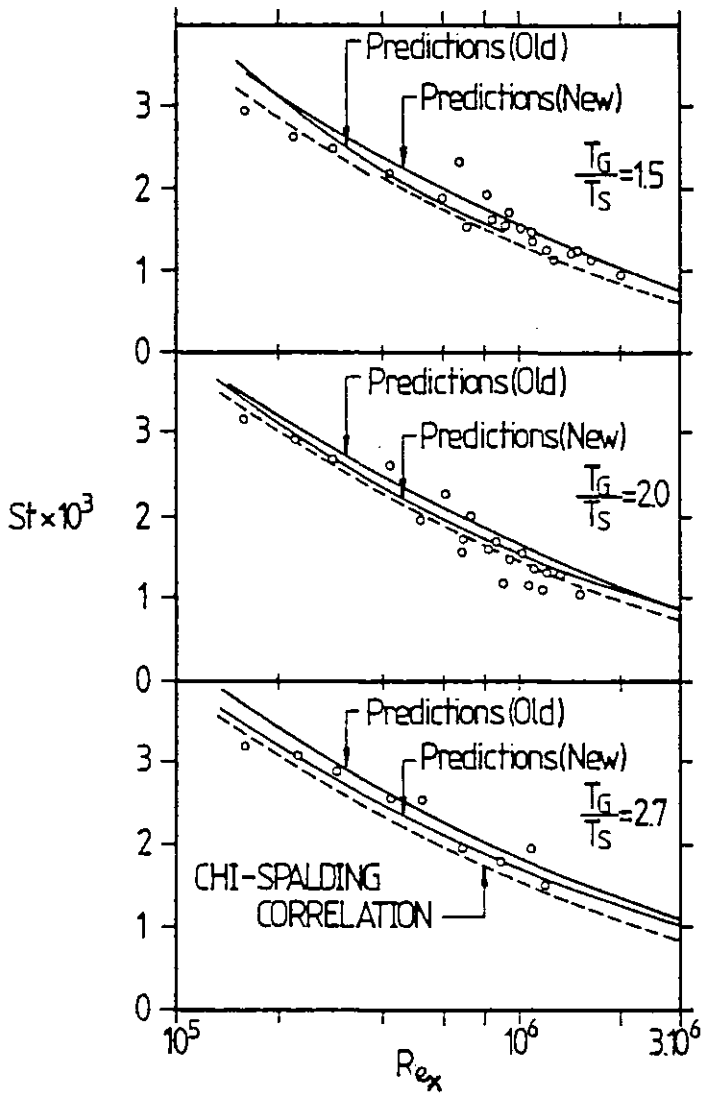

FIGURE 5.45-1: Predicted and measured Stanton number with length Reynolds number on a flat plate with intense heat transfer. Data of Chi and Spalding (1966)

its practical relevance.

5.52 Review of Experimental Data

The experimental investigation of this problem has been well advanced. They include cases with massive blowing, surface catalycity and blowing with reacting boundary-layers. However, only a few investigators have dealt with the basic problem of uniform blowing or suction - the one being investigated here. These experiments include those of Mickley et al (1954), Pappas and Okuno (1964), Torii et al (1966) and Moffat and Kays (1968).

5.53 The Case Considered

The data from all these experiments except for the last (that of Moffat and Kays), considered either separately or together, have been found to display an unsatisfactory amount of scatter, and no definitive statement can be made regarding the variation of Stanton number with blowing. Thus, the data of Moffat and Kays (1968) have been investigated in the present study.

Their data are for a case of uniform blowing and suction, constant free stream velocity and essentially constant properties. The mass transfer rates ($\dot{m}/\rho_G U_G$) range from about -0.0077 (asymptotic suction layer behaviour) to +0.0096 (near "blow off").

5.54 Computational Details

A forward step-size of 10% of the boundary-layer thickness is used. The effect of cross-stream grid sizes is

investigated for one case each of conditions of suction and blowing; the results of which are shown in Tables 5.54-1 and 5.54-2 overleaf. It can be seen by reading down the columns that 30 grid nodes can be considered adequate for flows with suction while 36 nodes are required for flows with blowing. In each case, over 80% of nodes lie within the thermal and momentum boundary-layers. Evidently, the additional six nodes are required to resolve property changes in the fast-expanding boundary-layers with blowing.

5.55 Results

Figure 5.55-1 shows the predicted and measured variation with the length Reynolds number, Re_x, of the Stanton number, St, for the problem considered. Five different blowing rates and four different suction rates are presented. Also shown are the results when there is no mass transfer across the boundary layer.

5.56 Discussion

The results presented in figure 5.55-1 show that agreement is satisfactory for the whole range of mass transfer rates considered,

$$(-0.0077 \leqslant m/\rho_G U_G \leqslant 0.0096) .$$

It is probable that, at the extreme mass-transfer rates, the effects of streamwise convection can no longer be disregarded in deriving wall functions. This is particularly the case for strong suction rates, where an asymptotic limit

Re_x / Grid No.	4×10^5	8×10^5	2×10^6
	STANTON NUMBER $\times 10^3$		
18	3.205	2.985	2.886
24	3.425	3.107	2.991
30	3.465	3.296	3.066
36	3.472	3.299	3.068

Table 5.54-1: Effect of Cross-stream Grids on Stanton Number for a Suction Rate $\dot{m}/\rho_G U_G = -0.0024$ at Three Length Reynolds Numbers

Re_x / Grid No.	4×10^5	8×10^5	2×10^6
	STANTON NUMBER $\times 10^3$		
18	1.024	0.826	0.632
24	1.085	0.858	0.651
30	1.132	0.872	0.665
36	1.157	0.880	0.672
42	1.161	0.885	0.675

Table 5.54-2: Effect of Cross-stream Grids on Stanton Number For a Blowing Rate $\dot{m}/\rho_g U_g = 0.0038$ at Three Length Reynolds Numbers

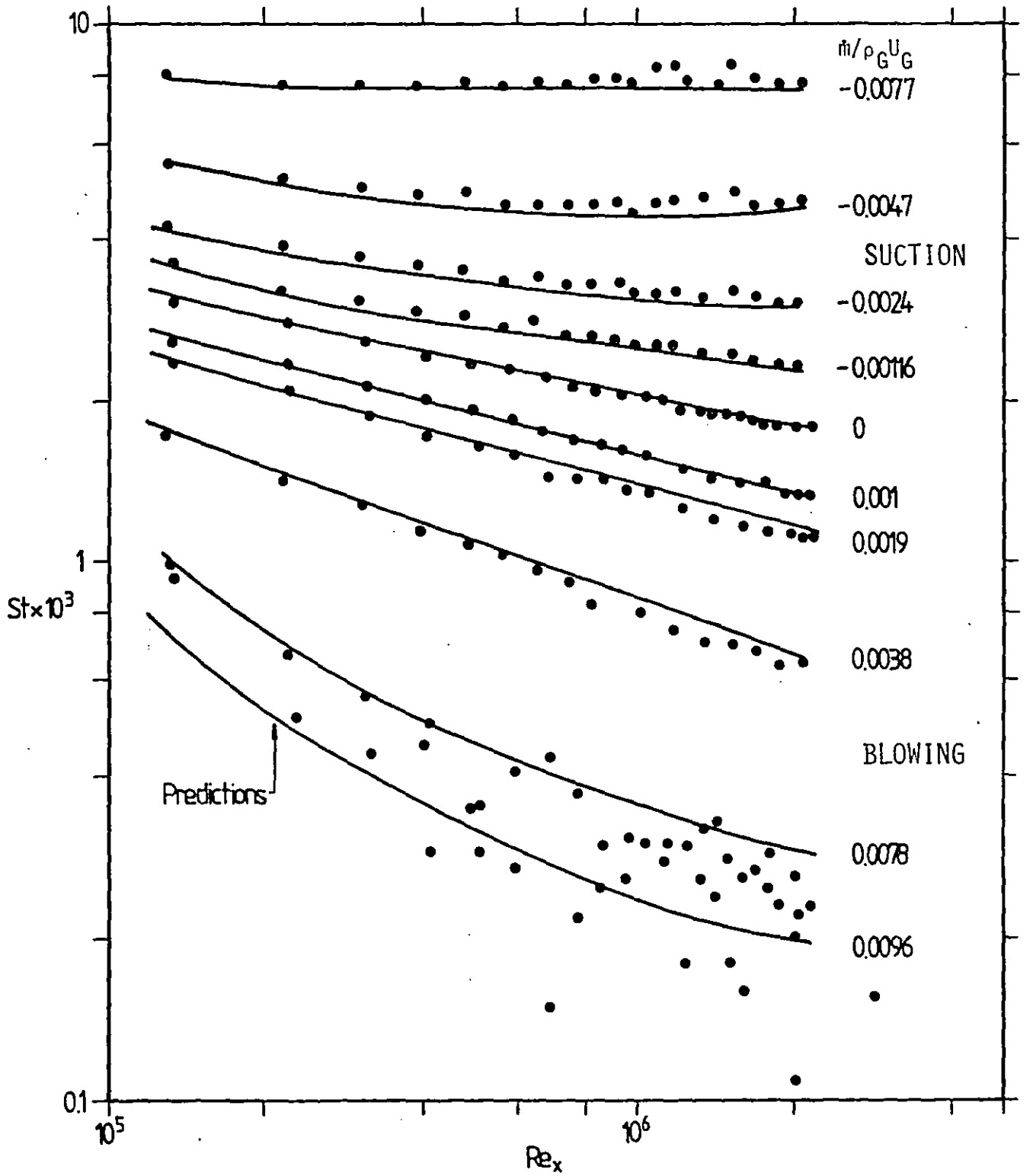

Fig. 5.55-1. Predicted and Measured Variation with the Length Reynolds Number of the Stanton Number for Heat Transfer to a Porous Flat Plate with Low Temperature Ratio and Various Degrees of Suction and Blowing; Data of Moffat and Kays (1968).

(St → $-\dot{m}/\rho_G U_G$) is approached. This limit is almost approached in two of the cases considered ($\dot{m}/\rho_G U_G$ = -0.0077 and -0.046). The predictions for these cases are however satisfactory because of the use of sub-layer resistance factor (as described in section 3.54) that ensures the above limit is approached.

For strong blowing rates, the Stanton-number limit is zero and its behaviour appears from figure 5.55-1 to be quite adequately predicted.

An alternative treatment of the near-wall region might employ a Van-Driest-type formula for the effective viscosity from the sublayer to the turbulent wall-region. This course of action has not been followed here; but it may well be essential for flows which combine some degree of film and transpiration cooling.

5.6 Closure

It has been demonstrated in this chapter that the new K-W model of turbulence can predict satisfactorily equilibrium boundary-layers, with uniform properties, with longitudinal pressure-gradients, with intense heat-transfer and with intense mass-transfer.

Whether or not the constants of the new model could be accepted as adequately simulating the near-wall region will depend on the performance of the model when applied to the second class of "wall-bounded flows" - internal flows. This is

the subject of the next chapter.

CHAPTER 6

PREDICTION OF TURBULENT INTERNAL FLOWS

6.1 Introduction

In the previous chapter, the application of the new K-W model to turbulent external flows was presented. The present chapter describes its further application to the second class of "wall flows" - turbulent internal flows.

An internal flow refers to any flow through a (circular) pipe, (non-circular) duct or (open, liquid-flow) channel where confining walls, or a free surface, guide the flow from an arbitrarily-defined inlet state to an equally arbitrary-outlet state. It includes the relatively simple laminar flow through a pipe (Poiseuille flow) and the more complex turbulent flow in the impeller (rotor) and diffuser (stator) of a centrifugal compressor stage and many others. The practical relevance of its study cannot therefore, be overemphasized.

The physical situations considered here include both boundary-layer and recirculating flows. In each case, the predictions, based on the new K-W model of turbulence, are compared with established experimental data.

The remainder of this chapter is divided into five sections. Section 6.2 describes the prediction of fully-developed turbulent flow in a pipe and its comparison with the data of Laufer (1954). In section 6.3 is presented the prediction of the hydrodynamic and heat-transfer characteristics of turbulent flow downstream of a pipe expansion. The

predictions are compared with the measurements of Zemanick and Dougall (1970). The prediction of turbulent flow in a backward-facing step is presented and compared with the data of Kim et al (1978) in section 6.4. The study here goes beyond the experimental investigation by providing full representation of the two-dimensional distributions of the velocity vectors, streamlines and of K. Typical field values of the velocity components, K, $W^{1/2}$ and the length scale at three locations beyond the step are also provided. These predictions, while being interesting in themselves, also provide a body of material with which future modellers and/or experimenters may wish to compare their result.

Finally, section 6.5 presents the concluding remarks on the major achievements of the chapter.

6.2 Fully-developed Pipe-Flow

6.21 The Problem

Perhaps the most widely investigated of all turbulent flows is the fully-developed flow through a smooth pipe of uniform circular cross-section. A fully-developed flow by definition is one that is independent of inlet or outlet state and one where conditions are statistically identical at each axial position. Because of this simplicity, it has been chosen as the first example of internal flows on which the new K-W model is tested.

The task is to predict both the mean and turbulence characteristics of the flow.

6.22 Review of Experimental Data

Numerous experimental data exist for this flow situation. Summary discussions and interpretations of these data have been too well detailed in Schlichting (1968), Hinze (1959) Goldstein (1938), Townsend (1976), Bradshaw (1978) and many others to warrant any extensive review here. However, it is worth mentioning that the data of Laufer (1954) have remained prominent and in addition to the more recent data of Lawn (1971) and Bremhorst and Walker (1973), are the often-quoted standard for turbulence measurements.

6.23 The Case Considered

For the above reasons Laufer's (1954) data have been chosen for comparison with the predictions in the present study.

6.24 Computational Details

The flow is axisymmetrical (see figure 6.24-1) and the governing equations are thus expressed in polar coordinates. Due to the parabolic nature of the flow, the boundary-layer forms of these equations are solved.

The calculation is performed with 18 non-uniformily-spaced radial grid-nodes and a forward step-size of 30% of the radius. Most of the nodes are placed near the pipe wall.

The mathematical technique paralells the experimental one: integration starts with an arbitrary profile of velocity at the entrance section and proceeds downstream until the profile

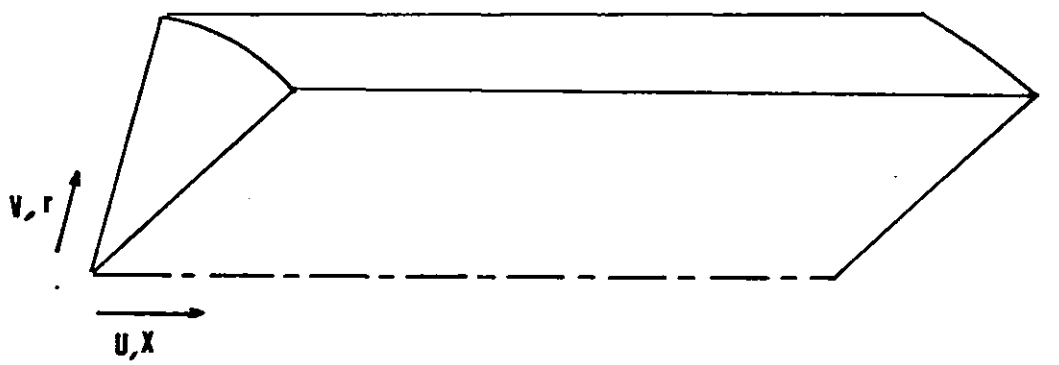

Fig. 6.24-1. Flow configuration in a pipe.

ceases to undergo further change. The initial turbulence energy and W are prescribed using the procedure of Ng and Spalding (1970) as described in section 5.24.

6.25 Results

Figures 6.25-1 to 6.25-4 show respectively the predicted mean velocity, the normalised Reynolds shear-stress, the ratio of shear stress to kinetic energy and the normalised kinetic-energy profiles for the fully-developed flow. Also displayed are the experimental data of Laufer (1954).

6.26 Discussion

The agreements in all cases are generally satisfactory both near to and far from the wall.

An approximately linear profile is predicted for the shear stress in figure 6.25-2. This is in conformity with the analytical result obtained from equilibrium between shear-stress forces and pressure forces. The predicted profiles of the turbulence energy and shear stress are also closely similar to the corresponding profiles obtained in boundary-layer flow on a flat plate after correcting the latter for intermittency (see Hinze, 1959). Thus, the present predictions agree with the generally observed fact that, if the effect of the intemittency of the boundary-layer flow near the outer boundary is taken into account, there is close similarity between the large-scale motions in pipe flow and in the fully-turbulent regions of the boundary layer. These motions are mainly responsible for the turbulence kinetic energy and the turbulence shear stress.

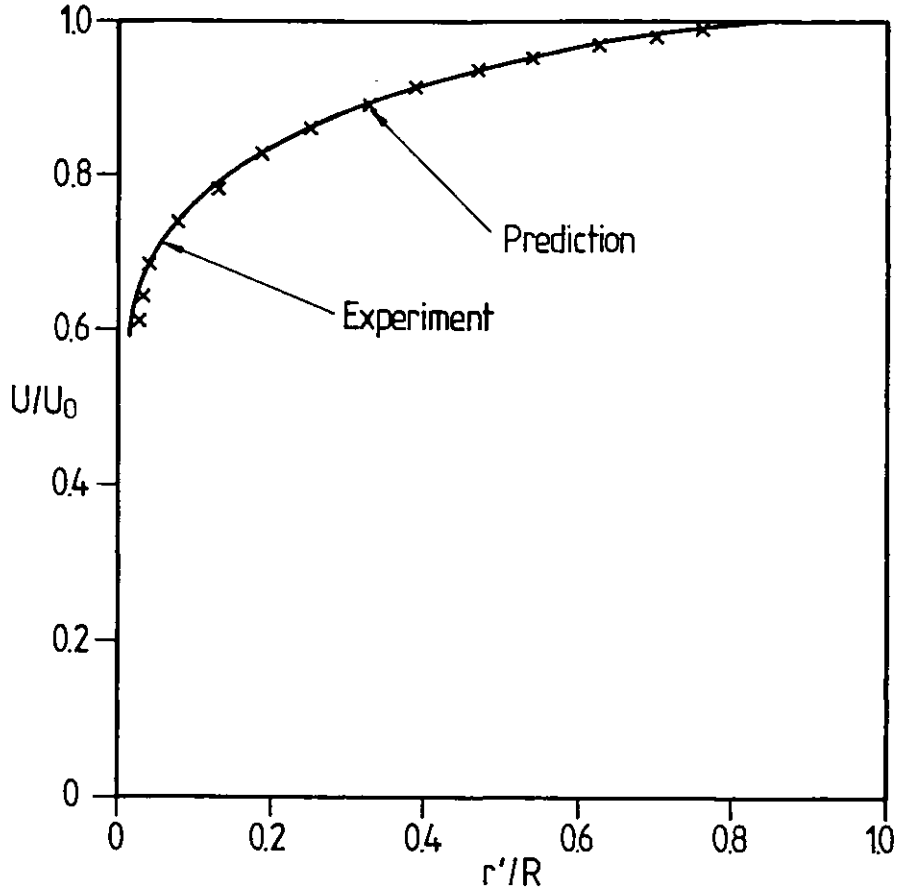

Fig. 6.25-1. Mean Velocity Profile (Re=500,000). Pipe-flow data of Laufer (1954).

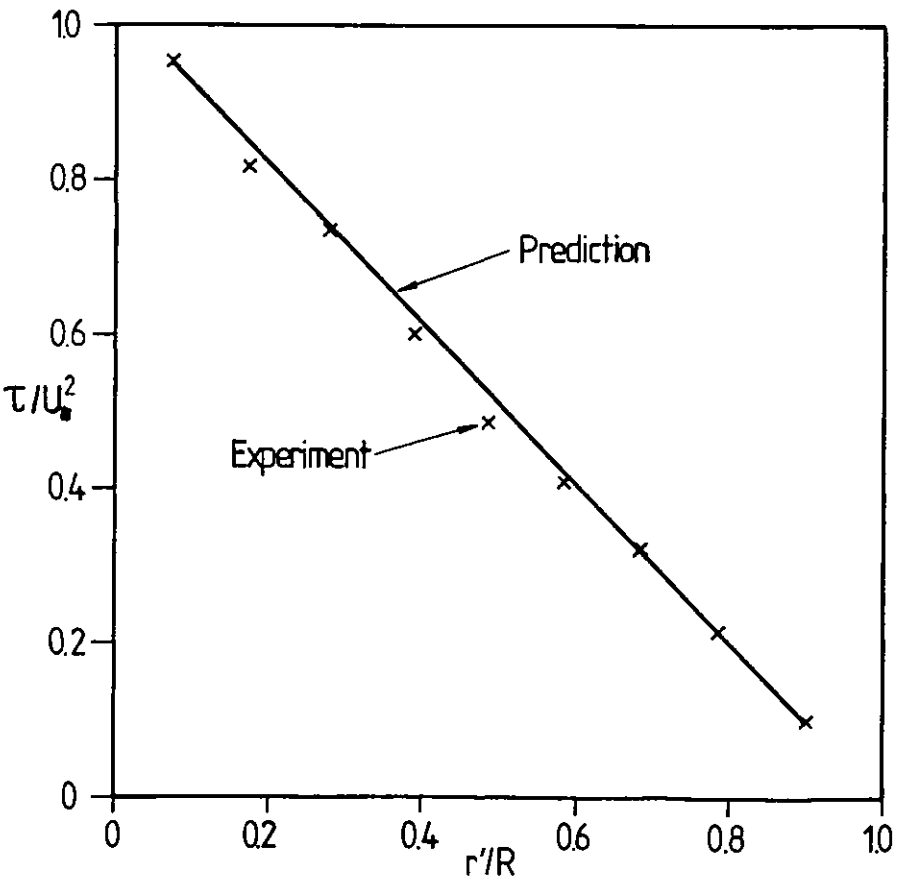

Fig. 6.25-2. Reynolds Shear-Stress Distribution. Pipe-flow data of Laufer (1954).

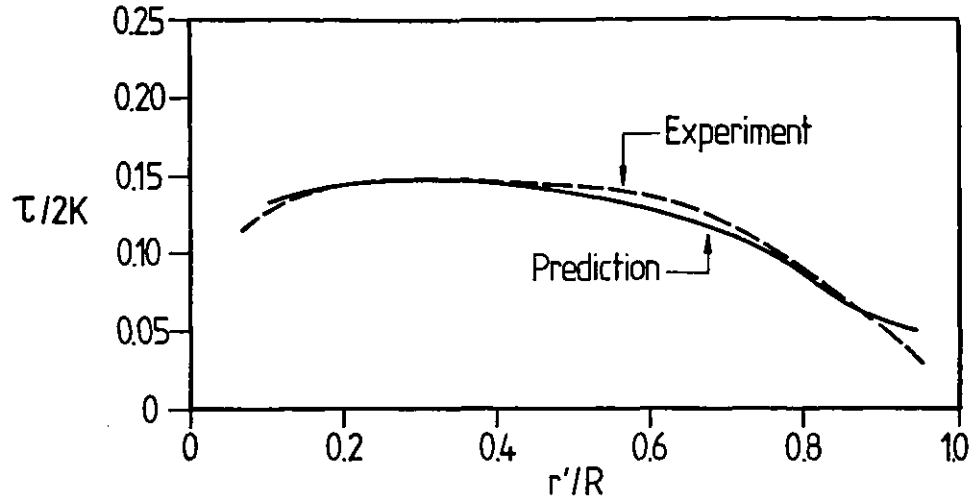

Fig. 6.25-3. Ratio of Shear Stress to Turbulence Kinetic Energy (Re=500,000). Pipe-flow data of Laufer (1954).

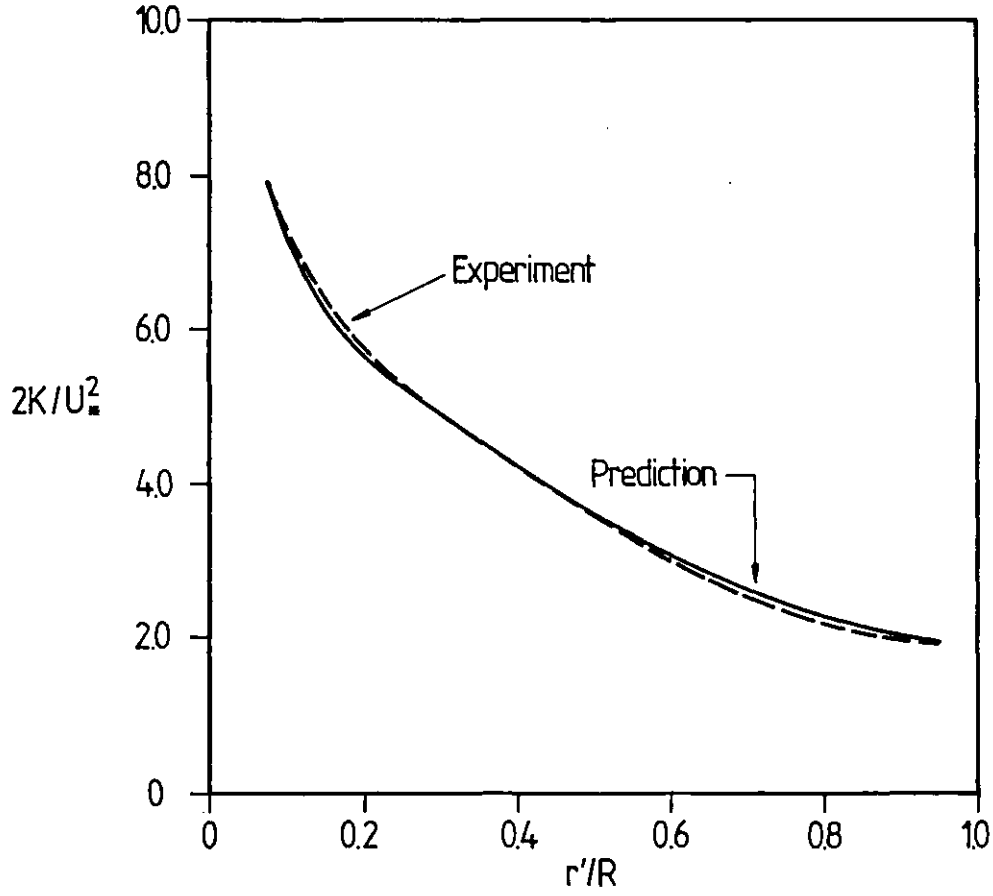

Fig. 6.25-4. Distribution of Turbulence Kinetic Energy (Re=500,000). Pipe-flow data of Laufer (1954).

It will also be noted that the predicted ratio of the maximum shear-stress to the maximum specific-energy is about 0.3 i.e $C_D^{1/2}$ in figure 6.25-3. This is to be expected for a flow that is in local equilibrium.

6.3 Flow and Heat Transfer Downstream of a Pipe Expansion

6.31 The Problem

When fluid flows steadily from a pipe of small diameter into a coaxial one of large diameter, a region of recirculating flow appears immediately downstream of the enlargement section (see Fig. 6.31-1). At high Reynolds numbers, the flow is turbulent. If the flow persists for a long enough axial distance, it reattaches to the wall and subsequently recovers to the fully-developed state. The exact reattachment point is elusive to measure.

This flow, like other separated flows, exhibits some exceedingly complex fields that generally have much higher levels of turbulence energy and stress than do boundary layers. It is however, desirable to be able to calculate such flows, partly in order that the pressure drop may be predicted, and partly because for good or ill, the heat-transfer rate in the vicinity of the recirculation often exhibits a maximum value three or four times as large as that which fully-developed pipe-flow would provoke.

The reason for this heat-transfer augmentation may be attributed to increases in the turbulence energy of the fluid stream. The cruicial feature is that the expansion or blockage

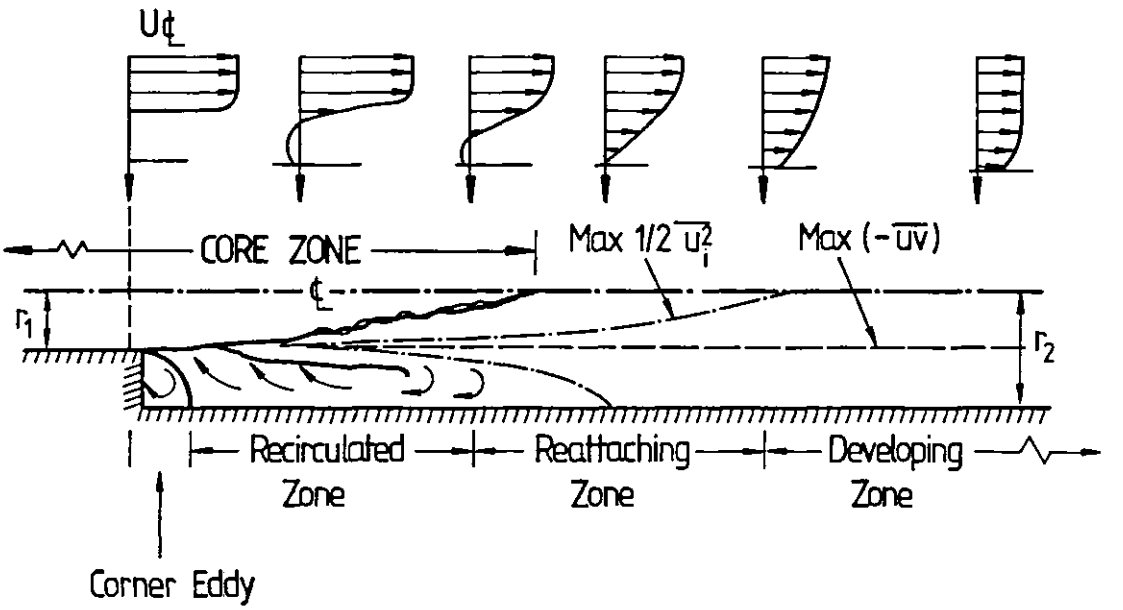

Fig. 6.31-1. Flow in an abrupt pipe-expansion.

generates high shearing-rates in regions removed from the immediate vicinity of the pipe wall. In such regions, turbulence-energy generation rates will be large (due to the high shearing) while dissipation rates will be low because, away from the wall, large-scale motions predominate. (It is usually supposed that, for a given turbulence energy, the dissipation rate varies inversely with length scale). The turbulence energy level thus increases rapidly to magnitudes many times greater than commonly found in pipe flow. These elevated energies in turn lead to higher turbulent-diffusion coefficients in the main (i.e. the turbulent) region of the flow and to a diminuition in the thickness of the near-wall "skin" through which heat must pass largely by molecular diffusion.

Separation is a phenomenon of critical importance for fluid-mechanical devices and systems. "Best" performance often occurs under conditons not far removed from those which produce separation. However, a precipitous drop in performance can take place once separation is actually encountered. Large-scale unsteadiness in the flow leading to unexpected mechnical loads can also result. These deleterious effects are a consequence of the global effect of separation on the flow field. As a result of interactions with the free stream, or the core, the effects of separation are not confined to only the shear layer considered by boundary-layer calculations. The practicing engineer often cannot make competitive fluid-mechanical designs if he avoids separation by too great a margin, nor can he afford to suffer from the consequences of inadvertently trigerring it while attempting to achieve maximum performance.

So far, the new K-W model has been applied to boundary-layer flows. In this and the next section (sections 6.3 and 6.4), it will be tested on flows with regions of separation.

6.32 Review of Experimental Data

Figure 6.32-1 shows the three basic geometries of two-dimensional axisymmetric expansions investigated in the literature. A summary of the various workers is also shown.

A detailed experimental study of the flow behind a sudden expansion in a circular duct of 100mm diameter was made by Moon and Rudinger (1977) using a Laser Doppler velocimeter. The diameter of the inlet tube was 70mm, thus giving an expansion ratio of approximately 2.0, which is representative of typical dump combustors. The inlet tube was long enough (1260mm or 18 tube diameters) to give a fully-developed velocity profile upstream of the step.

The measurements of Roquemore et al (1980) were for an axisymmetric flow behind a disk. The data include mean velocity and turbulence intensities. A detailed mapping of the turbulent flow past a ring (rectangular roughness element) was made by Logan and Phatarphruk (1979) for several ring heights (0.125 to 0.375 inch) and widths (0.131 to 0.655 inch). A circular pipe of 2.44-inch diameter was used with a ring-type roughness attached to the wall. The flow approaching the ring was of fully-developed pipe-flow.

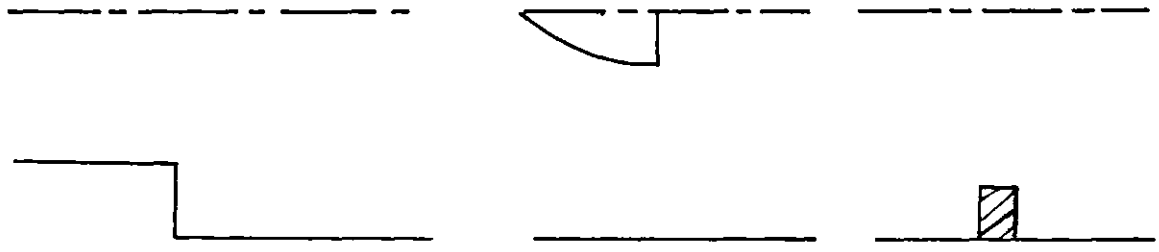

Ede et al (1956).
Ede (1959).
Ede et al (1962).
Charturvedi (1963).
Krall and Sparrow (1966).
Emerson (1966).
Zemanick and Dougall (1970).
Moon and Rudinger (1977).

Roquemore et al (1980).

Logan and Phatarphruk (1979).

Fig. 6.32-1. Two-dimensional asymmetrical expansion geometries investigated experimentally in the literature.

The above studies were concerned mainly with the hydrodynamics. Turbulent heat-transfer in tubes and ducts has been a subject of intensive experimental (and analytical) study for many years. However, only very limited data exist for the flow downstream of a pipe expansion.

Prominent among these latter data are those of Krall and Sparrow (1966), Ede et al (1956), Ede et al (1962), Ede (1959), Emerson (1966) and Zemanick and Dougall (1970). These together cover a wide range of diameter ratios, Reynolds numbers and Mach numbers at separation.

Krall and Sparrow's experiment concerns heat-transfer study for the region downstream of an orifice in a circular channel with water as the working fluid. The ratio of orifice to downstream diameter was varied from 1/4 to 2/3 and the downstream Reynolds number ranged from 10,000 to 130,000. Their curves of local heat transfer show clearly-defined peaks at positions which they believe correspond to the reattachment points. Their results also suggest that the position of the reattachment point is a function only of the expansion ratio, being unchanged for the Reynolds numbers investigated.

6.33 The Case considered

Zemanick and Dougall performed a similar experiment to krall and Sparrow's but without the use of orifices. Therefore, it has been chosen for the present investigation as the results would thereby be free of vena contracta effects. The experiment concerns three expansion geometries, ratio of upstream-to-

downstream diameter of 0.43, 0.54 and 0.82 with air as the working fluid. The data are given for Reynolds numbers from 4000 to 50,000-90,000 depending on geometry.

In this study, the 0.54 diameter ratio is chosen for investigation.

6.34 Computational Details

The flow configuration is shown in Fig 6.34-1. The calculation is started at the expansion and ended 12 diameters (of the larger pipe) downstream of it. Axial symmetry is assumed.

The presence of the recirculation renders inapplicable the boundary-layer procedures used for the earlier calculations; instead the solution of the full elliptic differential equations is necessary.

The entering fluid is assumed to have uniform axial velocity, turbulence intensity (3%) and arbitrary enthalpy (corresponding to the bulk temperature at inlet of test section). W is deduced from the values of K and the distribution of the eddy viscosity, μ_t for a fully-developed pipe-flow.

At the downstream boundary of the integration domain, the fluid is assumed to leave without a radial velocity component. The enthalpy at all walls is precribed by way of constant heat flux. The step wall is always taken as adiabatic. The wall

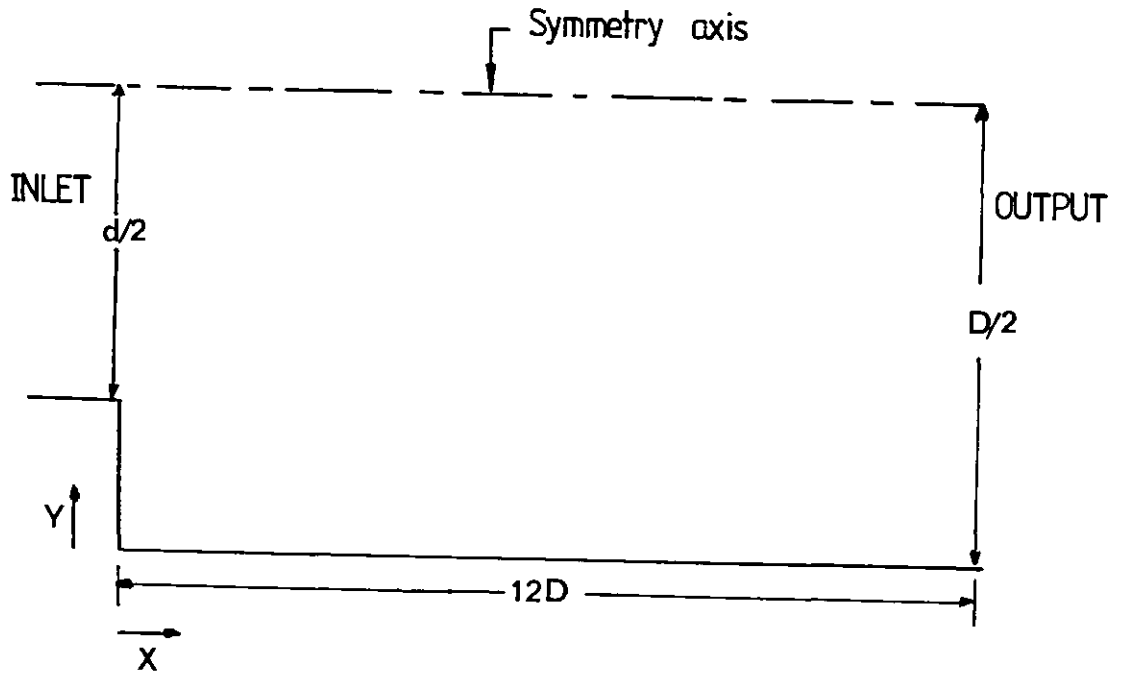

Fig. 6.34-1. Domain of calculation for flow in a pipe expansion.

function described in section 3.55 is used to account for the effect of separation.

The calculation reouires 22 x 22 non-uniformly spaced grids for sufficient accuracy. Most of the nodes are located at the high-shear regions at the pipe junction and near the wall. The computing time is typically 15 minutes on the Perkin Elmer 3220.

The constants of the new K-W model, it should be mentioned, were unchanged from the ones used for the earlier boundary-layer calculations.

6.35 Results

In figure 6.35-1 are shown the predicted variation of the local Nusselt number with axial distance along the duct at two Reynolds numbers of 66,260 and 48,090 for a diameter ratio of 0.54. Also shown are the experimental data of Zemanick and Dougall. Figure 6.35-2 shows the predicted variation of the maximum Nusselt number with Reynolds number compared with the same experimental situation.

6.36 Discussion

It can be seen from figures 6.35-1 and 6.35-2 that agreements between predictions and measurements could be considered fair. The measured locations of the maximum heat-transfer coefficients are approximately reproduced in the calculations. However, figure 6.35-1 shows that the predictions give broader maximum Nusselt numbers than the measurements.

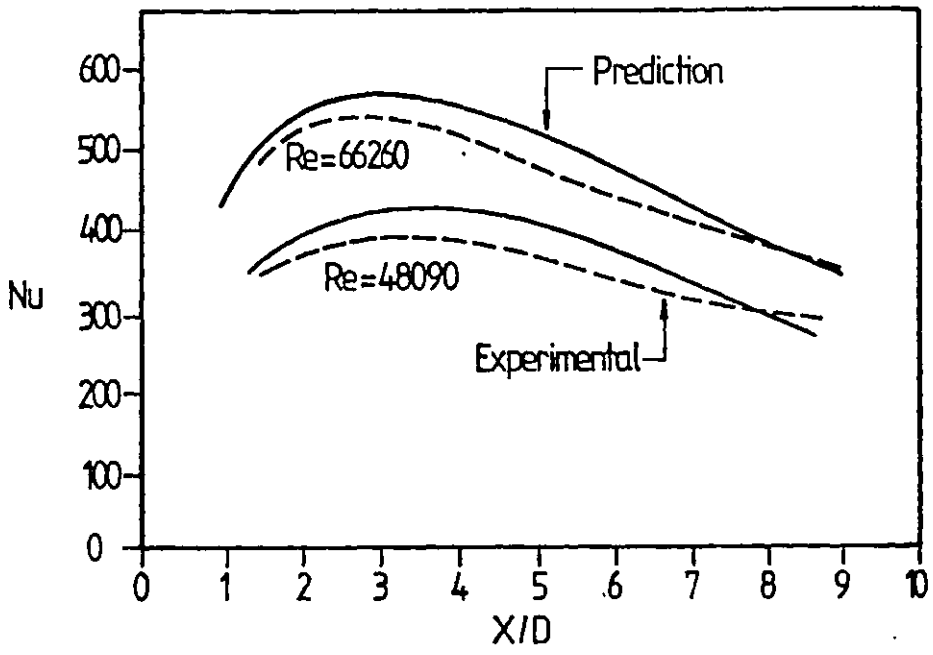

Fig.6.35-1.: Nusselt Number Distribution for d /D=0.54. (Pipe-expansion data of Zemanick and Dougall, 1970).

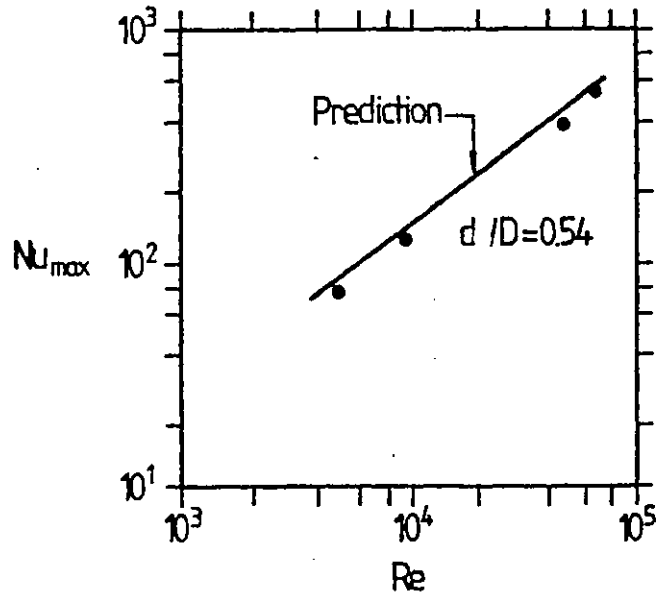

Fig.6.35-2. Variation of Maximum Nusselt Number with Reynolds Number: d /D= =0.54. (Pipe-expansion data of Zemanick and Dougall, 1970).

The variation of the maximum Nusselt number shown in figure 6.35-2 suggests that the predicted behaviour exhibits a slightly smaller sensitivity to Reynolds number than do the measurements.

The above results show that the new KW model, in conjunction with a wall-region treatment that accounts for turbulence diffusion, can satisfactorily predict the heat-transfer characteristics downstream of a pipe expansion.

The next task is to test its performance on a two-dimensional expansion for further validation. This is described in the next section.

6.4 Flow in a backward-facing Step

6.41 The Problem

Much less is known about the details of the flow for two-dimensional step expansions (figure 6.41-1) than for the case of axially symmetric expansions described earlier. It has been observed (see for example Abbott and Kline, 1962) that in the former, the interraction of the core with the unseparated wall boundary-layer can sometimes be significant.

Furthermore, small changes of upstream conditions could cause the stalled-region sizes to change and could cause a shift in location of reattachment point, which indicates, again, the complexity of displacement and shear interactions in purpotedly very simple internal-flow situations.

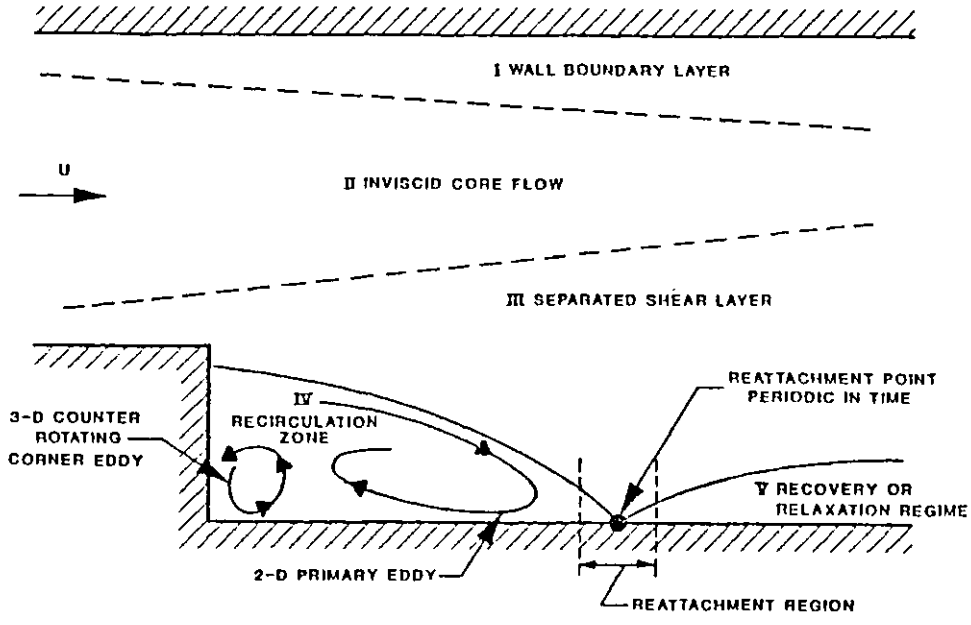

FIGURE 6.41-1: Streamline pattern for separating and reattaching flows in backward-facing step geometries

The task is to predict the flow structure occassioned by the separation and the associated effects mentioned.

6.42 Review of Experimental Data

Very few experimental data exist for the flow in two-dimensional expansions. The various geometries investigated in the literature are shown in Fig. 6.42-1.

A comprehensive mapping in the separated region behind a backward-facing step was made by Kim et al (1978) and Eaton and Johnston (1980). Kim et al used pressure probes for mean velocity measurements and hot wire anemometers for turbulence quantities. The configuration they investigated had a test section inlet height of 3.0 inches with the step height of 1.5 inches, thus giving an expansion ratio of 1.5. The reference velocity was held constant at a value of 18.2m/s at about four step heights upstream of the step. Further measurements in the same set-up were made by Eaton and Johnston (1980) for step heights of 1.0 and 2.0 inches using pulsed-wire anemometers.

The structure of turbulent flow behind a backward-facing step (expansion ratio = 2.0) with and without combustion was investigated by Pitz (1951) using a Laser Doppler Velocimeter. The step height was one inch. Detailed flow mapping behind a two-dimensional fence was made by Durst and Rastogi (1977) using hot-wire anemometers. Subsequently, they reported (see Durst and Rastogi, 1979) results with rectangular fences of different dimensions.

Eaton and Johnston (1980).
Kim et al (1978).

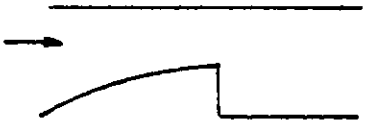

Pitz (1980).

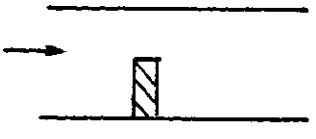

Durst and Rastogi (1979)

Fuji et al (1978).

Fig. 6.42-1. Two-dimensional plane expansions investigated experimentally in the literature.

The flow-field behind a flame stabilizer is more complex because of its shape. The aerodynamic characteristics of separated flow behind a wedge-shaped flame stabilizer were studied experimentally be Fuji et al (1978) with the aid of Laser Doppler Velocimetery. The flame stabilizer was an equilateral triangle in cross section with each side being 25mm.

6.43 The Case Considered

The experimental situation of Kim et al (1978) for flow behind a backward-facing step has been chosen for comparison with the predictions with the new K-W model of turbulence. These authors have reported measurements of the mean velocity, wall static pressure, pressure coefficients and turbulence quantities.

6.44 Computational Details

The calculation domain is shown in Fig. 6.44-1. Also shown is the partial layout of the grid network used. The grid is made to fit the duct and step. The grid lines are distributed non-uniformly over the flow domain with a larger number of nodes in the mixing layer just off the corner. A total of 30 Y-grids are used to span 4.5 inches, out of which 14 nodes are used for the 1.5-inch step, as shown. The first interior node is 0.18 inch (0.12H) from the step-side wall; H denotes step height. The smallest axial grid-spacing is 0.3 inch and a total of 42 axial nodes are used.

That this grid gives sufficient accuracy may be seen from Table 6.44-2 below which displays the predicted recirculation

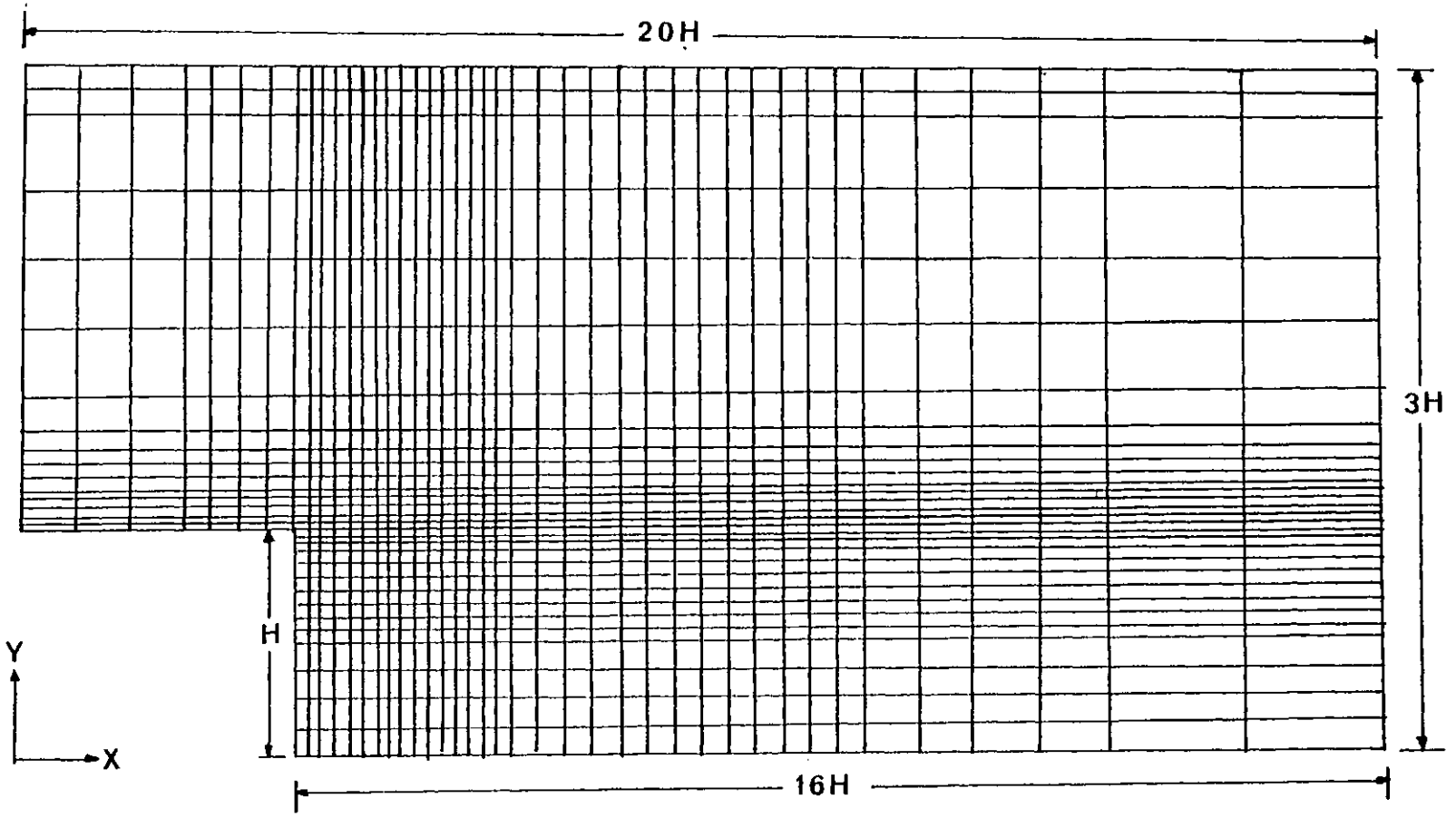

Fig. 6.44-1. Calculation domain and partial layout of the grid network for backward-facing step (Kim et al, 1978).

lengths (L_R) for five selected grids investigated. L_R is here defined as the axial distance beyond the step at which the mean-flow velocity at the step wall changes sign. It can be seen by reading down the column that the recirculation length does not change significantly beyond the 30 x 42 grid-nodes.

GRID NO.	GRID	L_R/H
1	12 x 20	4.8
2	20 x 20	6.0
3	20 x 42	6.8
4	30 x 42	7.2
5	40 x 50	7.2

Table 6.44-1: Effect of Grid Nodes on Recirculation Length for Flow Behind a Backward-facing Step

At the inlet section, the measured velocity and turbulence intensity are prescribed. The boundary-layer thicknesses of the two bounding walls there are assumed equal. At the exit boundary, a constant pressure condition is imposed. This is not expected to affect the flow structure as this boundary is placed far downstream of the expected recirculation region.

The region near the step wall at the separation zone is treated by use of the wall function described in section 3.55 to account for the significance of turbulence diffusion.

6.45 Results

Table 6.45-1 shows the predicted and measured values of the recirculation length normalised the step height. The latter is defined in the present computation as the axial length of the reverse (i.e. stalled) flow beyond the step (i.e to the position where the mean streamline is reanchored to the wall.

Variable	Experimental Value	Present Prediction
L_R/H	7.0	7.2

Table 6.45-1: Measured and Predicted Recirculation Lengths

Figures 6.45-1a and 6.451b show the distributionss of the wall-static pressures along the two bounding walls. The coefficient $C_{p\ wall}$ is defined as:

$$C_{p\ wall} = \frac{P_{wall} - P_o}{\frac{1}{2}\rho U_G^2} \qquad ,(6.45\text{-}1)$$

in which P_o and U_G are respectively the pressure and free-stream velocities at 4 step heights before the step (i.e at inlet of the calculation domain).

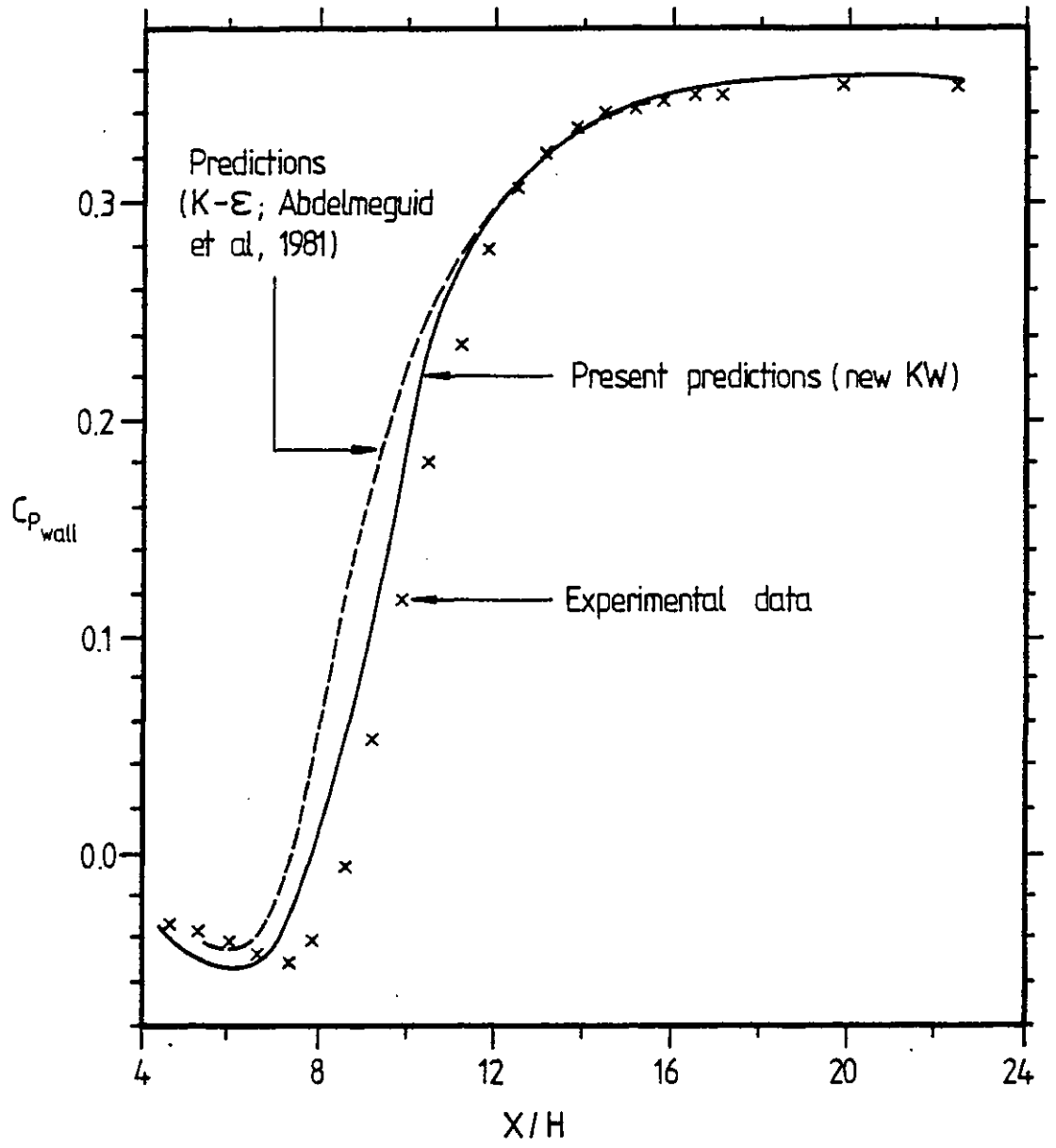

Fig. 6.45-1a. Wall-static pressure distribution along the stepped wall of a backward-facing step.
(Data of Kim et al, 1978).

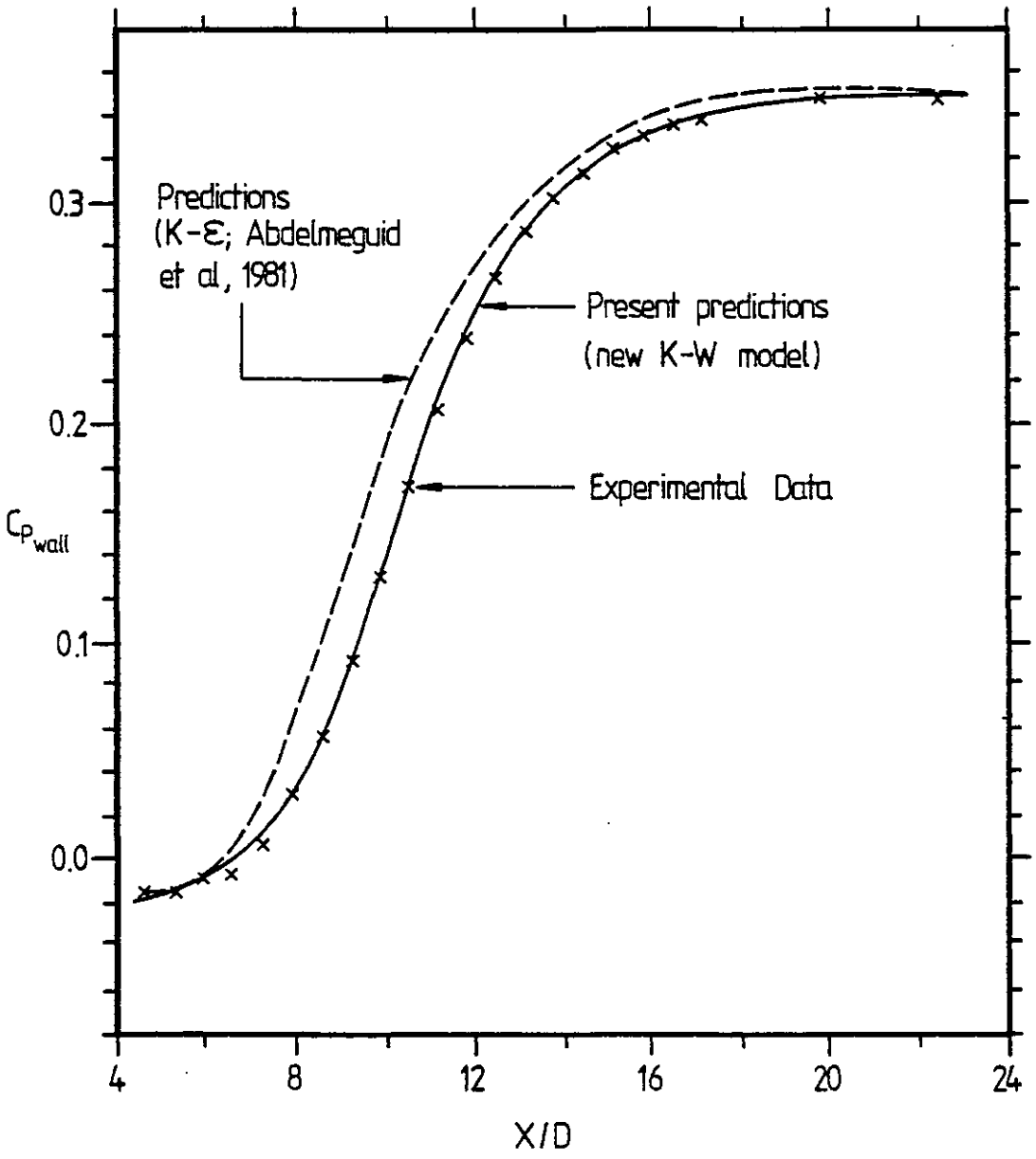

Fig. 6.45-1b. Wall-static pressure distribution along the non-stepped wall of a backward-facing step.
(Data of Kim et al, 1978)

In Figure 6.45-2 are shown the predicted distributions of the mean velocity of the main flow at three streamwise locations beyond the step. The mean velocity at each section is normalised with the reference velocity (U_{ref}) of 18.2m/s. Also shown are the data of Kim et al (1978).

The profiles of the turbulent shear-stress at three streamwise locations beyond the step are shown in figure 6.45-3. The first of these sections (X = 11.66H) lies just outside the recirculation region. In Figures 6.45-4 and 6.45-5 are shown the distributions of the maximum shear-stress along the channel. In Fig. 6.45-5 are also included the data of Tropea and Durst (1980) (see Eaton and Johnston, 1981). In the latter figure in addition, the axial distance has been written in terms of the recirculation length, X_R. The shear stress in each of the figures has been normalised with the souare of the free-stream velocity at inlet of the calculation domain.

Figures 6.45-6 and 6.45-7 show respectively the velocity vectors and streamline plots while in Figure 6.45-8 is shown the contour plot of the the non-dimensional turbulence energy in the flowfield. Figure 6.45-9 shows the contour plots of the length scale normalised with the width of the wider channel (3H).

Tables 6.45-2 to 6.45-4 show the predicted non-dimensional values of the mean velocity, cross-stream velocity, turbulence energy, freouency ($W^{1/2}$) and the length scale across the duct at three axial positions 5.33H, 8.0H and 13.33H respectively beyond the step.

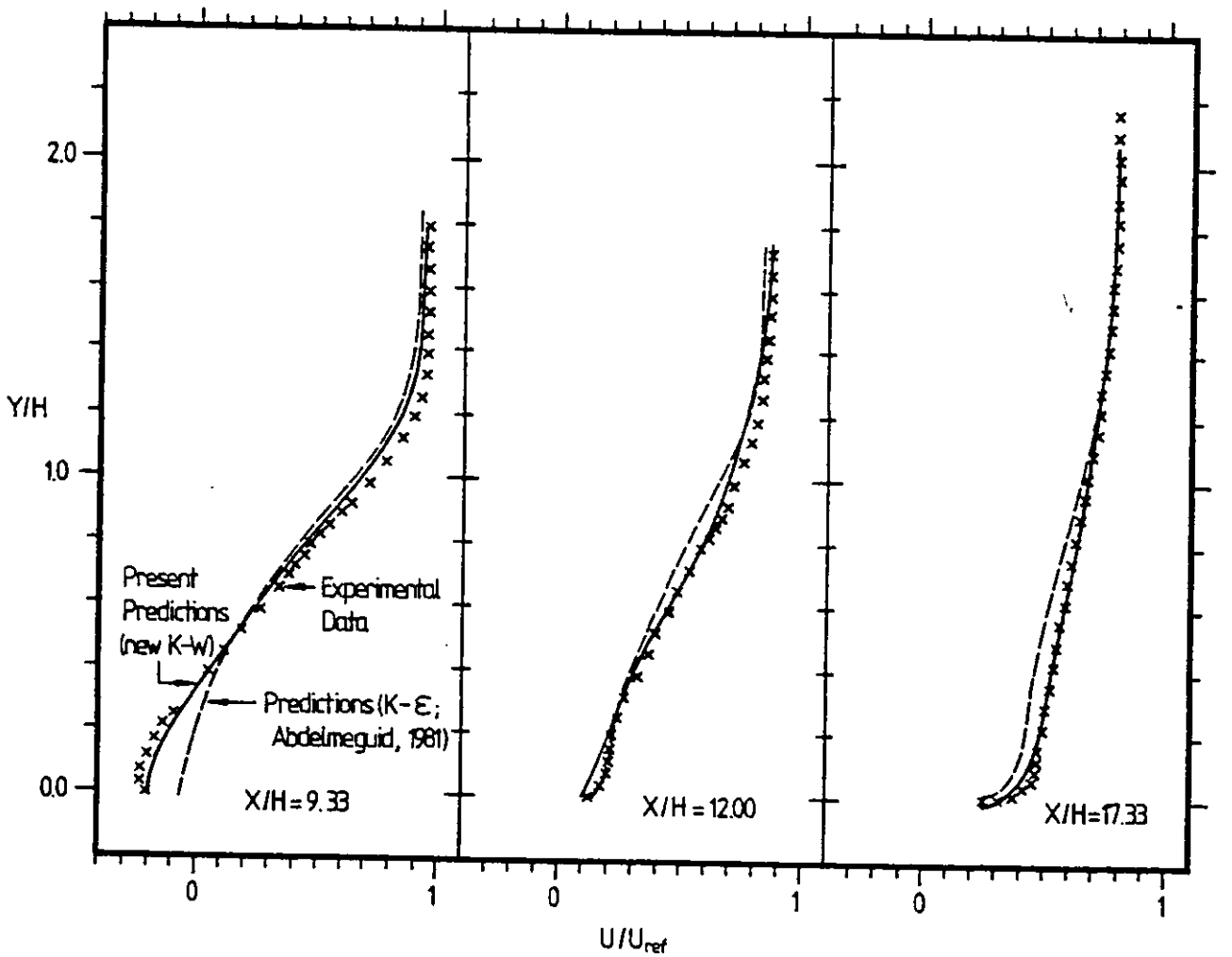

Fig. 6.45-2. Mean-velocity distribution at three streamwise locations for flow in a backward-facing step. (Data of Kim et al, 1978).

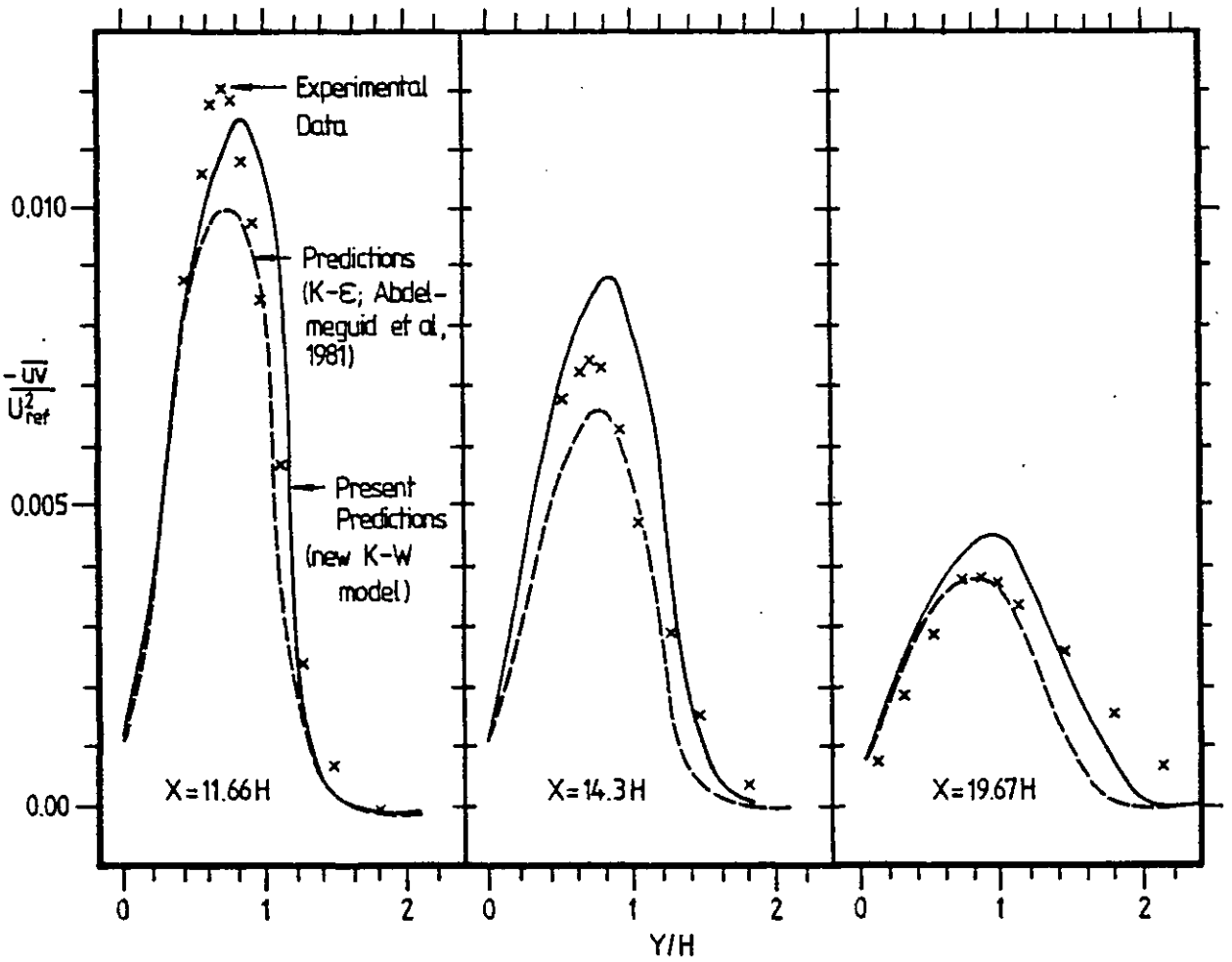

Fig. 6.45-3. Turbulence shear-stress distribution at three streamwise locations in a backward facing step; (Data of Kim et al, 1978).

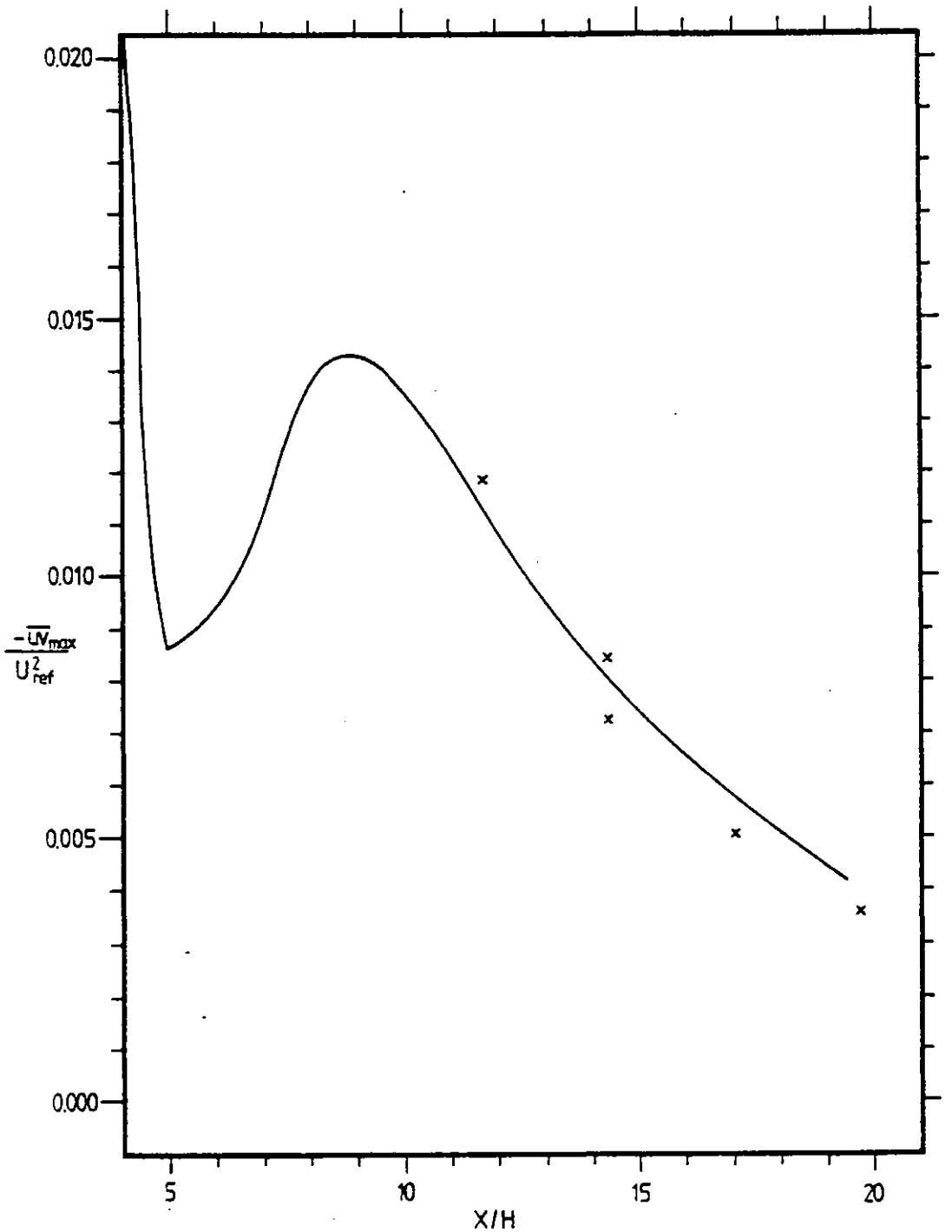

Fig. 6.45-4. Streamwise distribution of maximum shear stress in a backward-facing step; (Data of Kim et al, 1978).

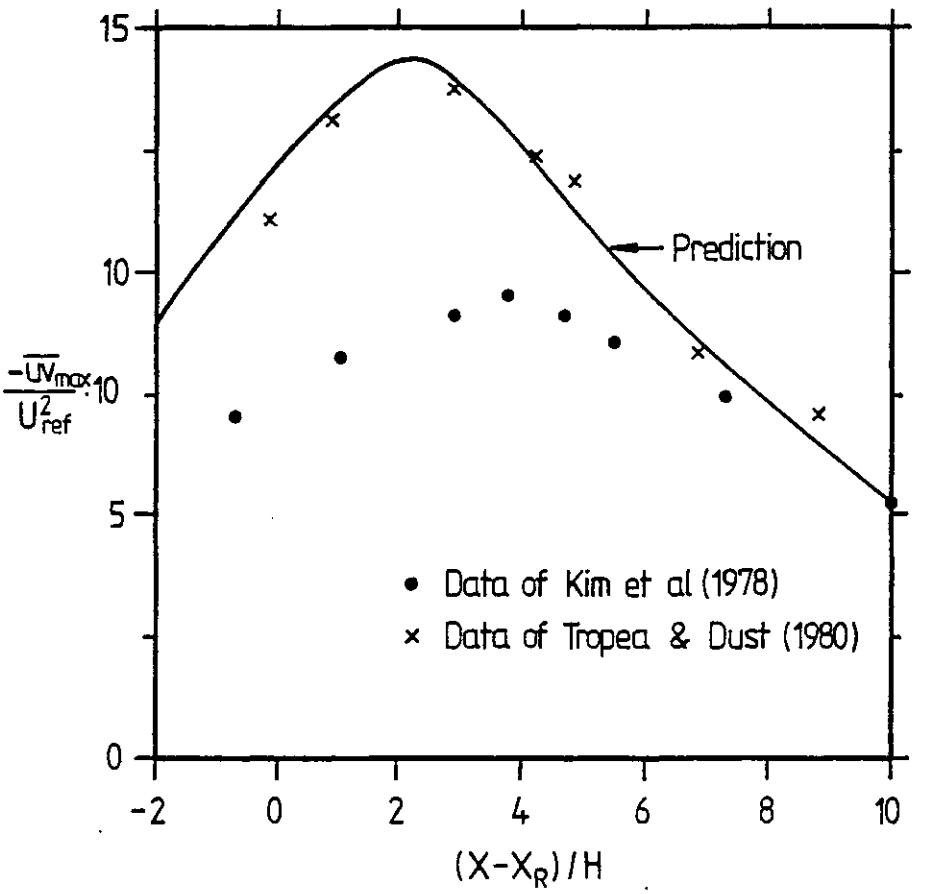

Fig. 6.45-5. Streamwise distribution of maximum shear stress in a backward facing step.

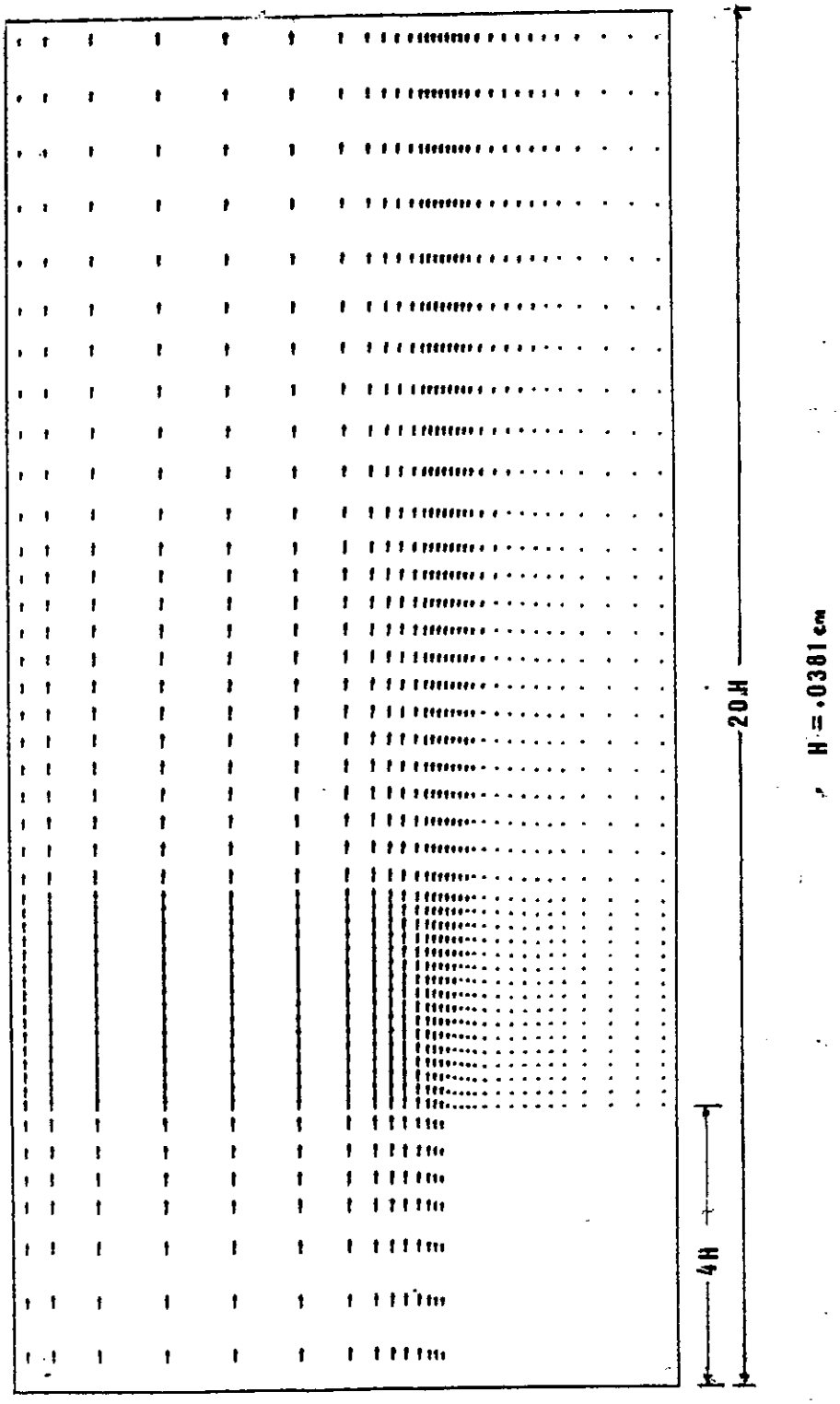

FIGURE 6.45-6a: Predicted velocity vectors showing magnitude and direction for flow in a backward-facing step

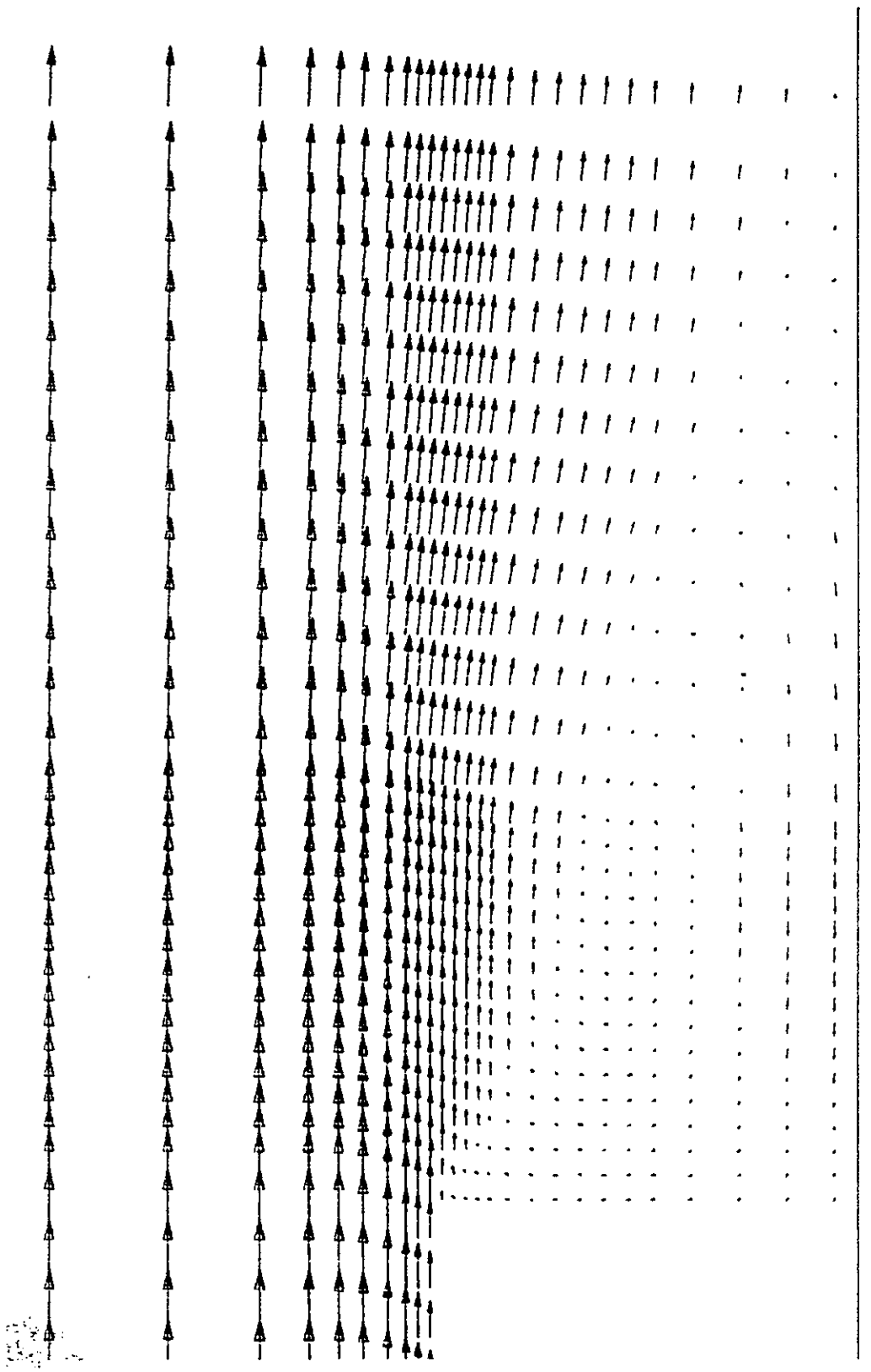

FIGURE 6.45-6b: Predicted velocity vectors near the step for flow in a backward-facing step

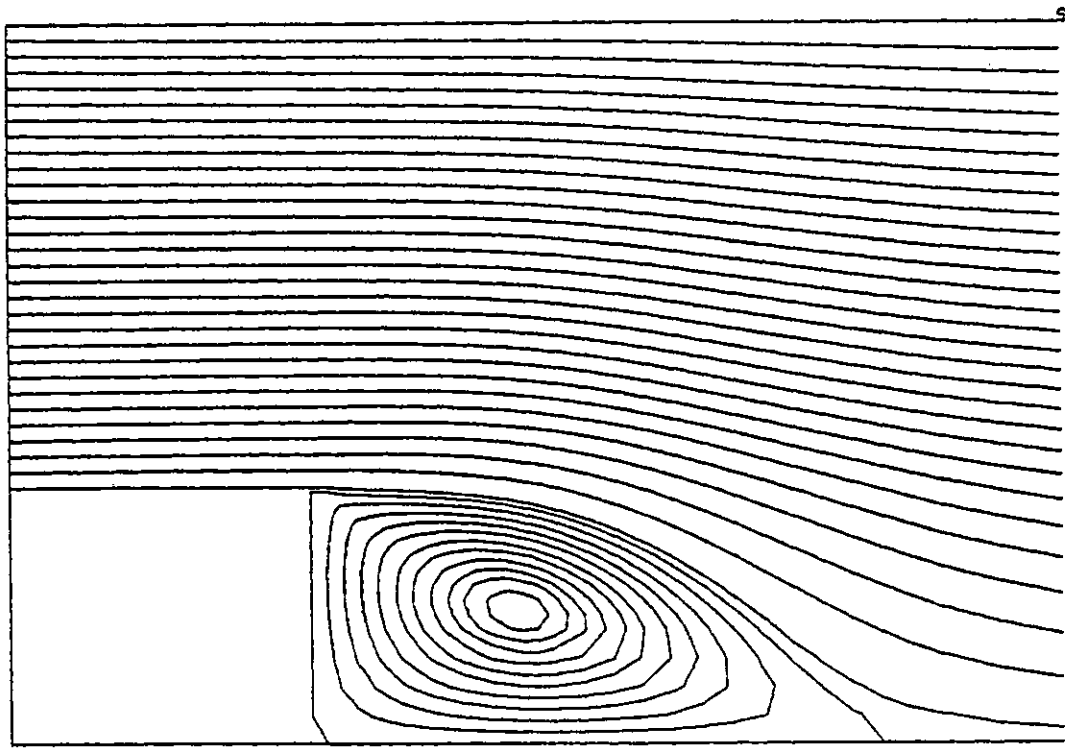

FIGURE 6.45-7: Predicted streamline plots near the step for flow in a backward-facing step

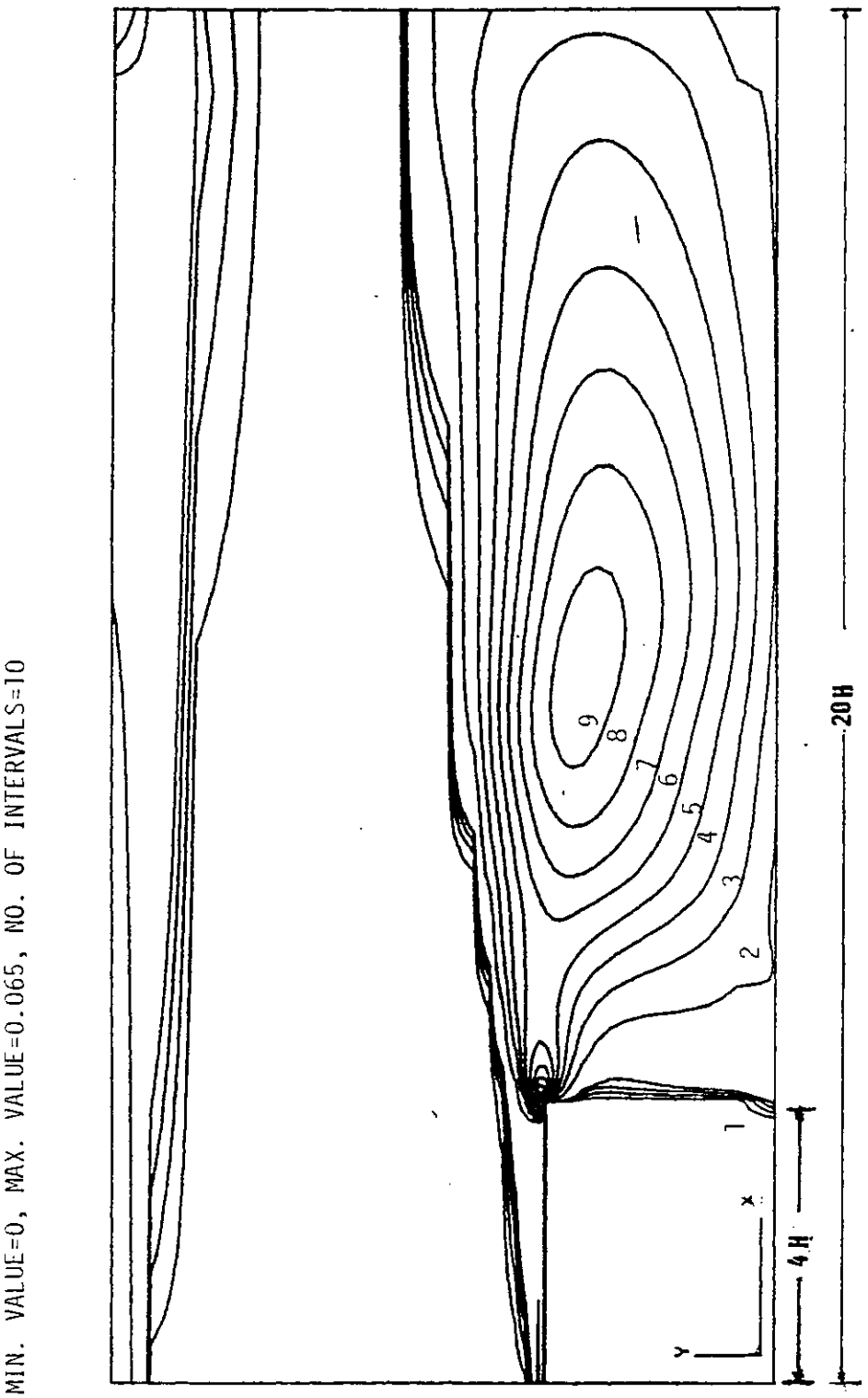

FIGURE 6.45-8: Predicted turbulence energy (K/U_{ref}^2) contours for flow in a backward-facing step

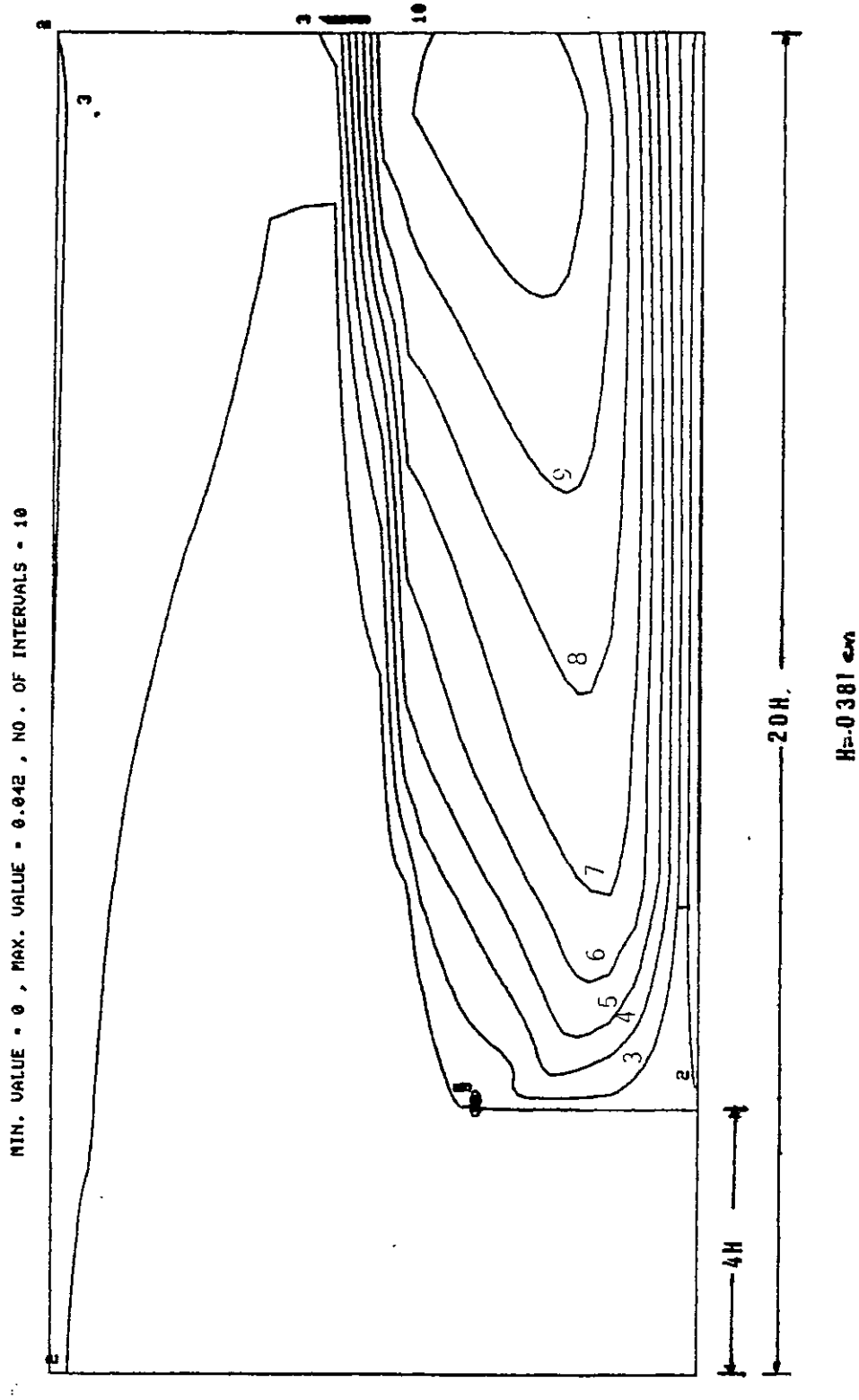

FIGURE 6.45-9: Predicted length-scale (1/3H) contours for flow in a backward-facing step

Y/H	U/U_{ref}	V/U_{ref} x 10^2	K/U^2_{ref} x 10^2	$\frac{w^{1/2}}{\lvert \partial u/\partial y \rvert}$	$l/3H$ x 10^2
0.18	-0.056	-1.400	2.244	5.058	1.590
0.30	0.0096	-2.300	2.860	4.192	2.410
0.51	0.138	-3.967	3.669	3.265	2.788
0.63	0.226	-4.796	3.961	3.053	2.724
0.75	0.327	-5.529	4.055	2.898	2.560
0.87	0.439	-6.129	3.898	2.723	2.345
0.945	0.518	-6.415	3.602	2.586	2.190
1.005	0.584	-6.571	3.235	2.540	2.061
1.065	0.651	-6.668	2.744	2.476	1.924
1.125	0.718	-6.669	2.139	2.489	1.779
1.230	0.819	-6.547	1.090	2.526	1.527

Table 6.45-2: Predicted Normalised Values of Flow Variables Across Duct at Axial Location of X = 9.33H

Y/H	U/U_{ref}	V/U_{ref} x 10^2	K/U^2_{ref} x 10^2	$\frac{w^{1/2}}{\lvert \partial u/\partial y \rvert}$	$l/3H$ 10^2
0.18	-0.135	-1.304	2.008	5.288	1.562
0.30	0.190	-2.126	2.537	4.536	2.521
0.51	0.291	-3.416	3.188	3.492	3.144
0.63	0.357	-4.016	3.394	3.236	3.185
0.75	0.430	-4.493	3.425	3.043	3.107
0.87	0.508	-4.823	3.244	2.850	2.958
0.945	0.562	-4.948	2.987	2.708	2.837
1.005	0.605	-4.990	2.700	2.652	2.729
1.065	0.649	-4.985	2.339	2.589	2.609
1.125	0.693	-4.931	1.914	2.575	2.476
1.230	0.761	-4.734	1.139	2.577	2.218
1.365	0.832	-4.359	0.254	3.044	1.664

Table 6.45-3: Predicted Normalised Values of Flow Variabeles Across Duct at Axial Location of X = 12.00H

Y/H	U/U_{ref}	V/U_{ref} x 10^2	K/U^2_{ref} x 10^2	$\frac{w^{1/2}}{\lvert\partial u/\partial y\rvert}$	$l/3H$ x 10^2
0.18	-0.342	-0.352	1.139	5.110	1.317
0.30	0.389	-0.583	1.418	4.596	2.429
0.51	0.452	-0.949	1.751	3.935	3.555
0.63	0.487	-1.114	1.871	3.650	3.855
0.75	0.523	-1.241	1.931	3.413	3.997
0.87	0.561	-1.323	1.919	3.218	4.035
0.945	0.585	-1.352	1.867	3.103	4.020
1.005	0.605	-1.359	1.803	3.043	3.993
1.065	0.625	-1.352	1.715	2.992	3.953
1.125	0.645	-1.332	1.605	2.960	3.903
1.230	0.679	-1.265	1.370	2.952	3.796
1.365	0.720	-1.124	1.008	2.928	3.625

Table 6.45-4: Predicted Normalised Values of Flow Variables Across Duct at Axial Location of X = 17.33H

6.46 Discussion

The predicted recirculation length shown in Table 6.45-1 may be considered satisfactory considering the reported uncertainity of $\pm$0.5 step height in the measurement. In addition, the present prediction appears better than a value of 6 step heights obtained with the K-ε model (e.g Abdelmeguid et al 1981).

The predicted outer-wall static-pressure variation shown in Figure 6.45-1a agrees well with the measurements. This is expected because of the little or no complication of the flow structure there. The predictions for the stepped wall in Figure 6.45-1b show some discrepancy with the data in the recirculation region. This discrepancy however dies off beyond the reattachment region. The predicted location of the minimum wall pressure in the stepped wall is about 2.2 step heights compared

with the value of about 3.4 step heights deduced from the reported data. Except in the immediate neighbourhood of the reattachment however, the difference between prediction and measurement is within the limit of the experimental uncertainity of 0.01.

It is also obvious from both figures that the predictions with the new K-W model are generally better than those with the K-ε especially for the stepped wall.

Figure 6.45-2 shows that the mean velocity distribution is generally well predicted with the new K-W model at the three axial locations considered (the first of which lies within the recirculation region). In the latter case, the magnitude of the predicted reverse flow velocity is slightly less than the measured value. However, the discrepancy is within the experimental uncertainty. The reverse flow is more adequately predicted than the K-ε model in this region. In addition, the recovery of the flow structure beyond the recirculation zone seems to be slightly better simulated with the new K-W model as shown in the velocity profiles at X = 12.00H and X = 17.33H in Fig. 6.45-2. The relative performance of the two models in the recirculation zone is to be expected since in this region, the mean axial velocities are closely correlated with the reattachment length.

Figure 6.45-3 shows that the predictions with both models and the measurements display similar trends. The profiles first increase monotonically to their peaks (at about y/H = 0.9 for

the data and the K-ε model, and y/H = 0.94 for the K-W model) before descending to their flat free-stream values. This behaviour becomes more gradual across the flow with streamwise distance. In all cases also, the K-W model seems to display a more gradual return to the free-stream levels than the K-ε model.

Agreement between predictions and measurements may be considered generally satisfactory. The predicted maximum shear-stress with the K-W model in the first section (just beyond the recirculation zone at $X-X_{step}$= 7.66H) is about 4% less than the measured value. This result is within the experimental uncertainty. The maximum shear-stress is underpredicted by about 17.5% with the K-ε model in this same location.

Further downstream, the shear stresses are overpredicted with the K-W model over most of the range; the maximum differences being about 21% at 10.3H and 18% at 15.67H beyond the step. The K-ε model underpredicts the shear stress at the former section; the maximum difference in this case being about 11%. At the last section, the K-W model appears to perform better in the free-stream region.

The overall superiority of the K-W model in Figures 6.45-1 to 6.45-3 may be due to its better prediction of the size of the recirculation region.

The maximum shear-stress along the channel shown in Figures 6.45-4 and 6.45-5 are fairly well predicted beyond the

recirculation region in consistency with the observed features in Figure 6.45-3. The maximum shear-stress drops sharply from a maximum value just beyond the step, exhibits a slight kink at about 1.3 step-heights and rises to a second maximum at about 5 step heights beyond the step.

The prediction may be considered fair however in view of the considerable scatter of the available data for the shear stress in the literature for the separation region (see for example, Eaton and Johnston, 1981). The predictions agree fairly well with one of these sets of data, namely, that of Tropea and Durst as shown in Figure 6.45-5. It should also be noted that the shear-stress data of Kim et al in the separation region has been observed by Eaton and Johnston to be too low due to the X-array hot wire used in their measurements.

The various flow regimes beyond the step are clearly reproduced in the velocity vector plots of Figures 6.45-6a and 6.45-6b and in the streamline plot of Figure 6.45-7. These regimes include the recirculation zone, the recovery region and the inviscid core.

Figure 6.45-8 and Tables 6.45-2 to 6.45-4 show that the maximum turbulence energy occurs in the high-shear regions away from the walls. The tables also show the expected flow towards the stepped wall as all the cross-stream velocities, V are negative. This is partly responsible for the curvature of the streamlines as observed in Figure 6.45-7.

The normalised freouency $W^{1/2}/|\partial U/\partial y|$ shown in the three tables exhibits a maximum near the stepped wall and decreases progressively towards the core. The normalised length-scale l/3H on the other hand rises gradually from the stepped wall, reaches a maximum and then descreases towards the core as shown in Figure 6.45-9. The overall maximum value occurs towards the exit of the domain where turbulence energy is low.

6.5 Closure

In this chapter, the new K-W model has been applied to three kinds of internal flows namely; Fully-developed flow in a pipe, flow and heat transfer in a pipe expansion and flow behind a backward-facing step. The predictions have been compared with established experimental data and agreements have been found to be generally fair.

In the case of the backward-facing step, the results have been compared with predictions based on the K-ε model. The new K-W model has been found to perform better than the K-ε model. Furthermore, the predictions with the new model in this particular case has been carried beyond the experimental information. Flowfield values and contour plots of some flow variables have been provided.

This now concludes the application of the new K-W model to wall-bounded flows. The next task, which is a test of its performance on turbulent free-flows is described in the following chapter.

CHAPTER 7

PREDICTION OF FREE TURBULENT BOUNDARY-LAYERS

7.1 Introduction

The Flows Considered

This Chapter is concerned with the application of the new K-W model to a class of flows called "free turbulent boundary-layers". Free turbulence is encountered in a flow field where there is no direct effect of any fixed boundary on the turbulence in the flow. There may be indirect influence, because a fixed boundary may create the conditions for the existence of a free turbulence; for example, walls (splitter plate, nozzle lips or wake body) usually create the free boundary-layer; and in case of the jet, walls govern the free stream.

The label "boundary layer", it will be recalled, is applied to flow regions in which there is a single predominant direction of flow, and in which shear stresses, heat fluxes and diffusion fluxes are significant only in directions perpendicular to the predominant direction.

Two typical examples of free flows are considered namely, jets and mixing layer (Figs 7.1-1 and 7.1-2). For the jets, both plane and axisymmetric cases are included.

The shaded areas in Figure 7.1-1 define the free turbulent-boundary-layer regions. The flow outside these regions is called free stream. Normally, this flow can be considered as uniform and non-turbulent.

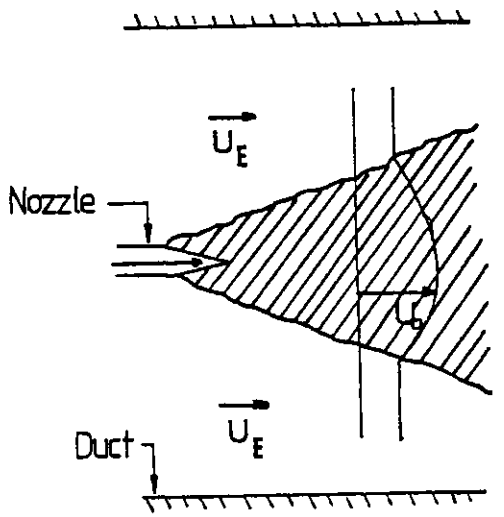

Fig. 7.1-1. A free turbulent boundary-layer (The Jet).

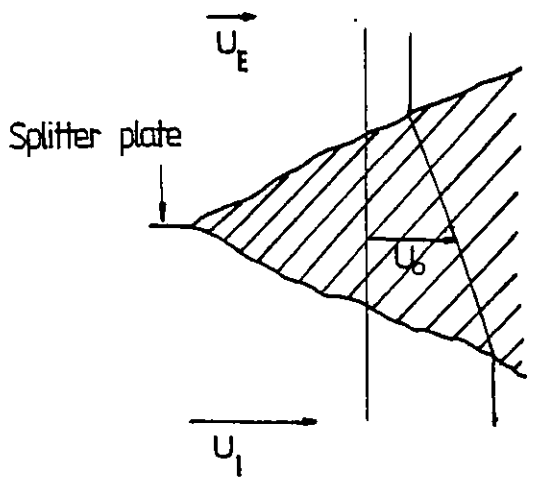

Fig. 7.1-2. A free turbulent boundary layer (The Mixing Layer).

Practical importance

Free turbulent boundary-layers are of great practical relevance in many kinds of engineering equipment, in the atmosphere and in rivers. Jet engines, jet ejectors, wakes behind aeroplanes and submarines, cooling-water dispersal in rivers, chimney plumes, and jet streams in the atmosphere are a few examples.

In practice, flows may not always be purely "free" and of the plane or axisymmetric boundary-layer type. However, the process of free mixing is prominent in all these flows, whether it is a mixing of fast and slow moving streams, of hot and cold fluid, or of fuel and oxidiser. In order to study the real problem, Engineers often recourse to the study of the idealised situation namely, the free boundary-layer. For example, researchers concerned with the combustion process in a furnace often investigate this process with the walls absent; that is they consider the furnace flame as a free boundary-layer.

Similarity consideration

An important feature of free turbulent boundary layers is their tendency to become self-similar after a certain development region. A self-similar flow is one in which one velocity and one length scale are sufficient to render its time-averaged quantities dimensionless functions of one geometrical variable only.

The velocity and length scales usually chosen in similarity theory are respectively the maximum excess (or

deficit) velocity, U_o (defined e.g in Fig 7.1-2) and the characteristic width δ_o. This width may be defined in various ways; for example, it could be taken as the half width, $y_{1/2}$ of a jet or the half radius of a round jet etc.

The necessary conditions for self-similarity are (Rodi, 1972; Townsend, 1956):

$$\frac{d\delta_o}{dx} = \text{const} \qquad ,(7.1\text{-}1)$$

$$\frac{U_E}{U_o} = \text{const} \qquad ,(7.1\text{-}2)$$

$$\frac{\delta_o}{U_o}\frac{dU_o}{dx} = \text{const} \qquad .(7.1\text{-}3)$$

The implications of these conditions are as follows. U_E must either be zero or vary in the same way as U_o. This variation may be expressed as:

$$U_o \alpha \; X^m \qquad ,(7.1\text{-}4)$$

where m is a constant. Furthermore,

$$\delta_o \alpha \; X \qquad ,(7.1\text{-}5)$$

and

$$Re = \text{const} \qquad ,(7.1\text{-}6)$$

where Re is the Reynolds number defined thus:

$$Re = \frac{U_o \delta_o}{\nu} \qquad .(7.1\text{-}7)$$

These conditions are exactly satisfied in two of the cases to be considered - the round jet and plane mixing layer. In both cases, the surrounding fluid is stagnant; thus U_E = const = 0. Since the local Reynolds number as defined in (7.1-7) will also be constant, the similarity region is unlimited.

The plane jet to be considered in which $|U_E/U_o| \gg 1$ is approximately self-similar (Rodi, 1972).

Outline of the chapter

The remainder of this chapter comprises of four sections. In section 7.2, the prediction of flow in a plane jet is presented and compared with the data of Bradbury (1965). Section 7.3 describes the prediction of flow in a plane mixing-layer and its comparison with the data of Wygnanski and Fiedler (1970). The prediction of flow in a round jet and its comparison with the data of Wygnanski and Fidler (1969) are presented in setion 7.4. Section 7.5 contains the concluding remarks on the achievements of the chapter.

7.2 The Plane Jet

7.21 The Problem

When a fluid emerges steadily from a wide slot, with

straight parallel edges, into a slow-moving parallel stream of the same fluid or into a stagnant surrounding, it may form a turbulent jet (see fig. 7.1-2). At the upstream end of the jet, there are two plane mixing-layers - the wedge-shaped regions springing from the two edges of the slot. These mixing layers coalesce a few slot widths from their starting points; downstream of a further flow-readjustment region, a wedge-shaped jet is formed (see Fig 7.21-1). As already described in section 7.1 above, for the case of stagnant surrounding or very nearly for the case with very slow-moving surroundings, the cross-stream profiles of velocity and composition vary in scale, with increasing longitudinal distance, but not in shape i.e. the flow is self-similar.

In this section, attention is focused on the jet; the mixing layer being deferred till the next section. The problem is to predict, with the aid of the new K-W model of turbulence, the rate of spread of the jet and the similarity profiles of the velocity, turbulence energy and shear stress.

7.22 Review of Experimental Data

Rodi (1972) has given a comprehensive review of data on the plane jet. These are summarised in Table 7.22-1 overleaf.

Bradbury's jet could not have been exactly self-similar because U_E/U_o was not constant. As described in section 7.1, approximate self-similarity may exist if $U_E/U_o \gg 1$ which would occur far downstream as an asymptotic condition. Bradbury's measurements did not extend far downstream to satisfy

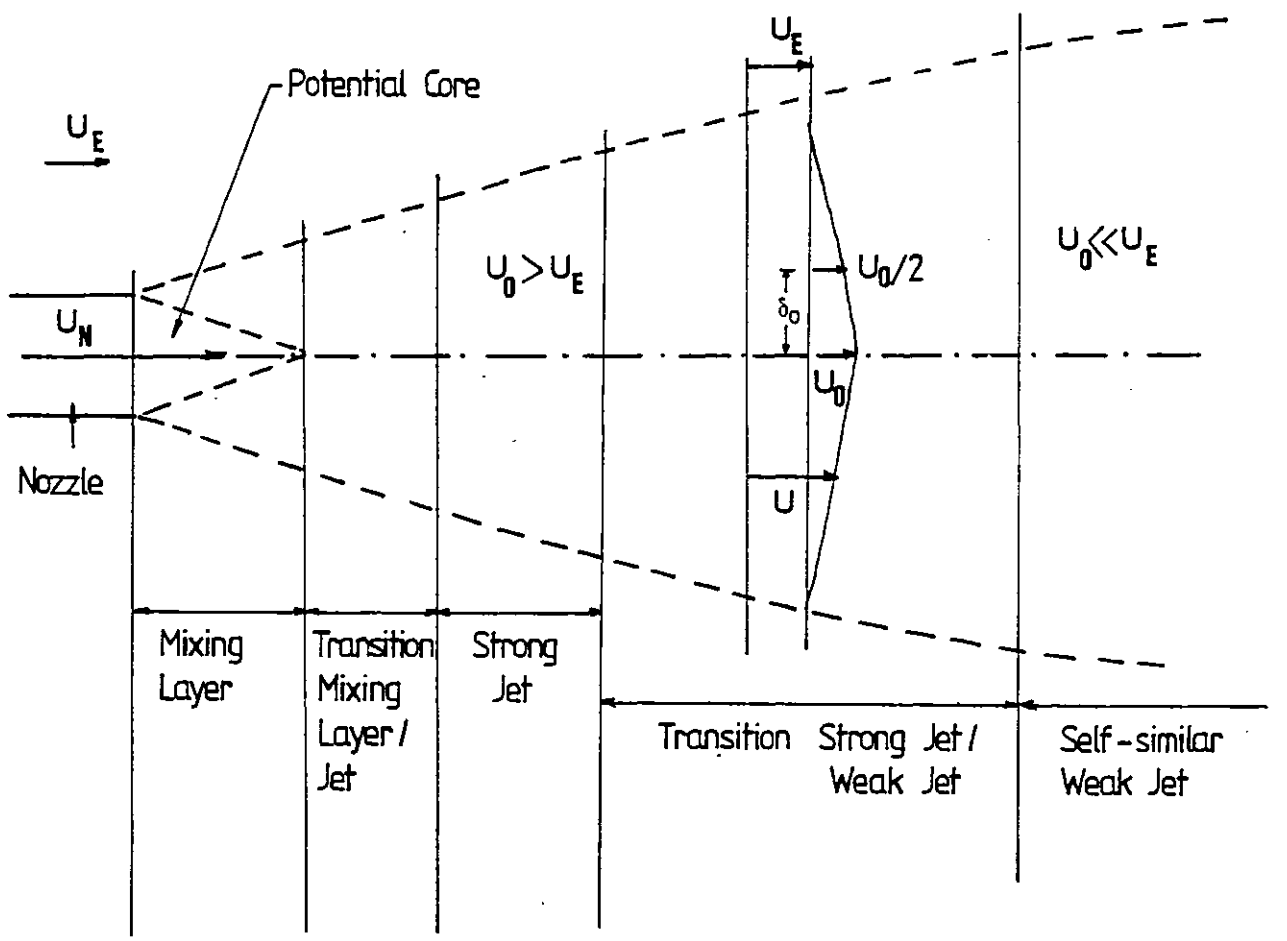

Fig. 7.21-1. Jet-flow regions and nomenclature.

TABLE 7.22-1: Experimental data on plane jets

Experimenter	Nozzle dimensions (h x B) cm	Range (x/h)	Re_h	Start of self-similar region (x/h ≈)	$\frac{dy_{\frac{1}{2}}}{dx}$	Measured $\frac{uv_{max}}{U_o^2}$	$\frac{K_c}{U_o^2}$	Remarks
Bradbury (1965)	.95 x 46	14 - 70	3×10^4	30	not constant	.0242	.067	$U_E/U_J = .16$
Heskestad (1965)	1.25 x 150	47 - 155	$.47 \times 10^4$ -3.7×10^4	65 but $\overline{u_c^2}/U_o^2$ keeps rising	.11	.021	.07	Strong influence of Re_h on $\frac{\overline{u_c^2}^{\frac{1}{2}}}{U_o}$
Patel (1970)	.7 x 80	12 - 152	3.5×10^4	30 for U and $\overline{u^2}$	.103	.021	0.64	-
Gutmark (1970)	1.3 x 50	10 - 150	3×10^4	120	.102	.024	.077	-
Robins (1971)	Aspect Ratios 21-138	5 - 100	1×10^4 6×10^4	60	.103	.02	.064	-

this condition.

However, the departures from self-similarity were insignificant in the region of interest. Also, reducing U_E/U_J from 0.16 to 0.07 had no effect on the results where U_J is the jet velocity at the nozzle exit, nor had halving the Reynolds number. Thus, Bradbury's flow may be considered representative of a truly self-preserving jet.

7.23 The Case Considered

The experimental situation chosen for comparison with predictions is that of Bradbury (1965). The flow is defined by the parameters in Table 7.22-1 and Fig. 7.21-1.

The measurements include decay of centre-line velocity, spread of jet half-width, δ_o which is defined in Fig. 7.21-1, axial mean velocity profiles ($14 \leq x/h \leq 70$), turbulent shear stress profiles ($x/h = 51$ and 70) and turbulent intensity profiles at $x/h = 51$ and 70 from which a turbulent kinetic-energy profile was constructed. Lateral mean-velocity profiles ($x/h = 20$ and 60) were deduced from the measurements by Bradbury using continuity.

The mean-velocity profiles were measured with separate pitot and static tubes, while constant-current hot-wire anemometers were used for the turbulence measurements.

7.24 Computational Details

Plane symmetry is assumed, so the calculation is

performed only over one half of the jet.

The inlet plane is located at the jet exit. At inlet, the outer boundary of the domain is located in the free-stream at y/h = 1 where h is the slot height of the nozzle.

The height of the outer boundary, y_L, is made to change with downstream distance so that the flow domain covers only that region where jet properties vary. The location of y_L is defined thus:

$$y_L = y_o + fX \qquad ,(7.24\text{-}1)$$

in which y_o is the value of y_L at inlet and f is the rate of spread of the outer boundary taken as 0.145. This value is deduced from the half-width spreading rate of the plane jet as presented by Rodi (1972). It should be noted that f merely prescribes the spread of the grid and not the jet itself. The latter is an outcome of the calculation.

In Table 7.24-1 overleaf is presented a summary of the grids used.

In each case, the grid is distributed uniformly in the lateral direction.

Figures 7.24-1 and 7.24-2 respectively show the effects of forward-step size and lateral-grid refinements on the turbulent-kinetic-energy similarity profiles. It is obvious

Run No.	No of Lateral Grid cells	Forward Step Size x/y_L	No of Forward Step
1	20	0.3	60
2	20	0.2	85
3	20	0.1	170
4	25	0.1	170
5	30	0.1	170
6	40	0.1	170

Table 7.24-1: Summary of Grids Used for Plane-jet Calculation

that sufficient accuracy will be obtained with 30 lateral grid nodes and a forward step-size of 10% of the grid width. This grid is used for the calculations to be described.

The jet axis is a plane of symmetry, consequently, it is a zero flux boundary.

At the outer boundary of the calculation domain, the following conditions are applied:

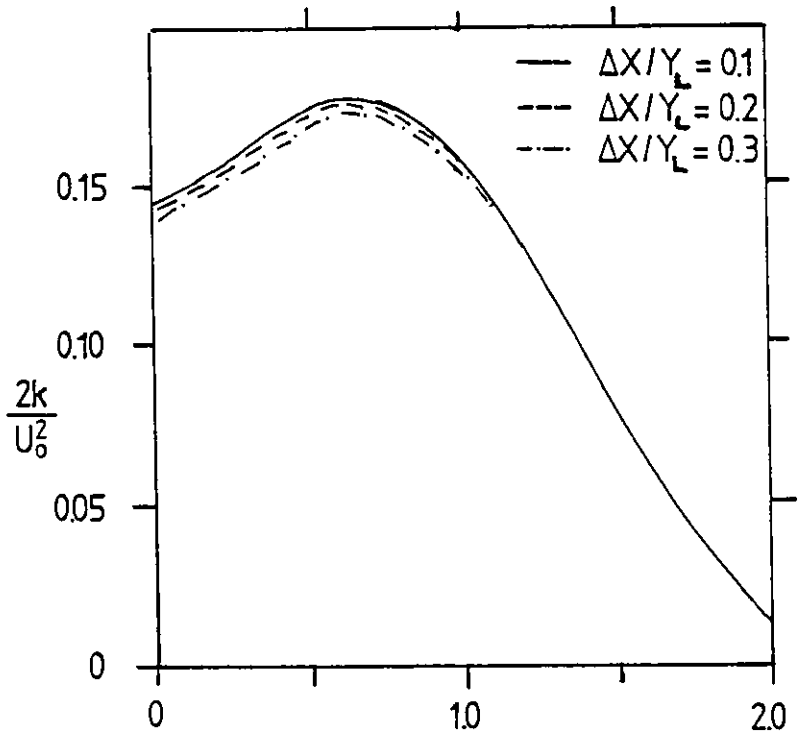

Fig. 7.24-1. Effect of forward-step size on turbulent energy similarity profile of a plane jet.

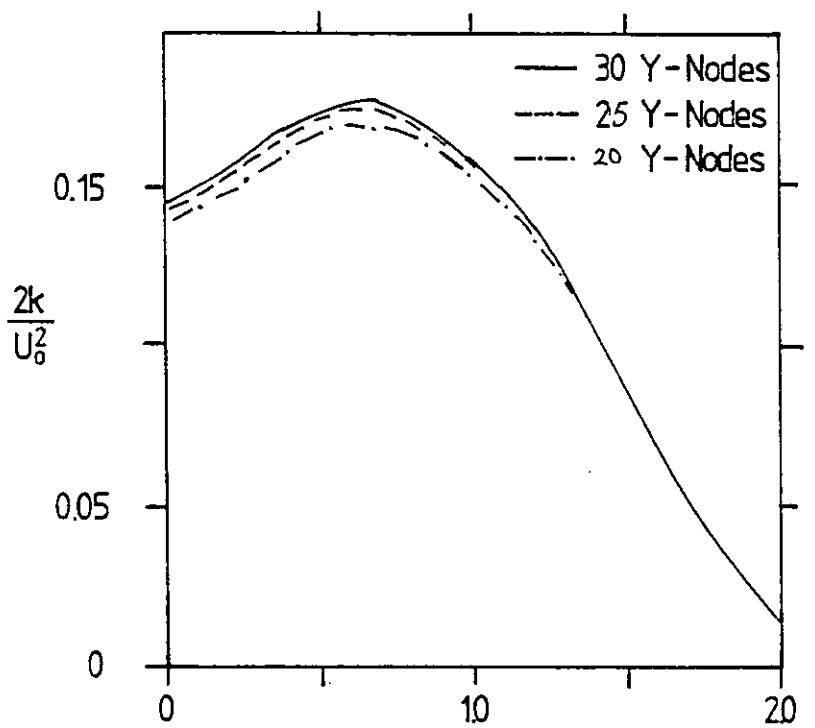

Fig. 7.24-2. Effect of lateral-grid size on turbulent energy similarity profile of a plane jet.

(i) Fixed pressure, thus the mass flow across the boundary is calculated from continuity.

(ii) The external free stream velocity is U_E= 4.8m/s.

(iii) A small amount of turbulence level ($K = 0.001\ U_E^2$) is assumed. The length scale is taken as 10% of the grid width. This turbulence level it will be noted, is virtually negligible.

Due to the parabolic nature of the flow, the downstream boundary condition is of no consequence.

The calculation starts at the jet exit plane where the inlet distributions of all flow variables are not reported by Bradbury. Thus, these conditions must be estimated.

It should be mentioned that for self-similar flows, the similarity solution will be independent of the initial profiles. However, the downstream development of most non-similar flows and the near field of self-similar flows is influenced by the initial conditions.

In the present calculation, the following conditions are imposed at inlet:

(i) A mean-axial-velocity profile that accounts for the momentum loss in the nozzle-wall boundary-layers is used. From Bradbury's measured excess momentum flux, the

estimated nozzle-wall boundary-layer thickness is 0.15h. The axial velocities within the boundary layer are then calculated from a 1/7th power-law distribution. Within the boundary layer, the grid axial-velocities are then scaled to match the experimental momentum-flux. The details of the calculation are given in Appendix G.

The lateral velocity is assumed to be zero.

(ii) Within the jet, uniform value of 0.01 U_J^2 is used for K. In the free stream, a small amount of turbulence as described earlier is assumed but this is negligible in comparison. The length scale from which W is estimated is taken to be about 10% of nozzle-slot height.

7.25 Results

Figure 7.25-1 shows the predicted decay of jet centre-line axial velocity compared with the measurements of Bradbury (1965). In Figures 7.25-2 are shown the predicted rate of jet spread (defined as $y_{1/2}/h$, where $y_{1/2}$ is the jet half-width and h is the nozzle-slot height). Also shown are the experimental and analytical results of Bradbury.

Figures 7.25-3 and 7.25-4 show respectively the axial and lateral mean-velocity profiles compared with Bradbury's measurements. The predicted and measured similarity profiles of the shear stress and turbulence energy are shown respectively in figures 7.25-5 and 7.25-6.

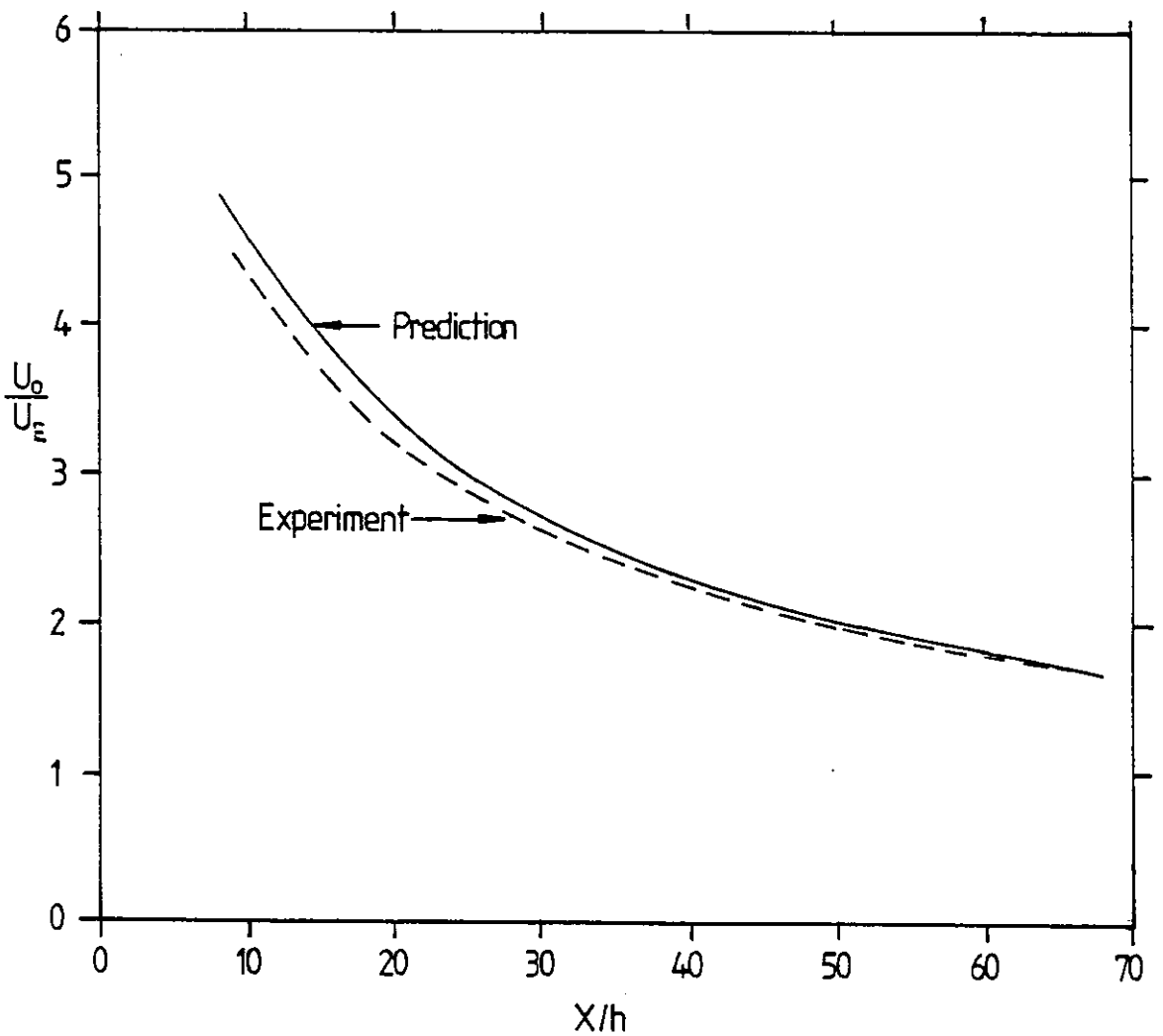

Fig. 7.25-1. Decay of centre-line axial velocity of a plane jet. (Experiment of Bradbury, 1965).

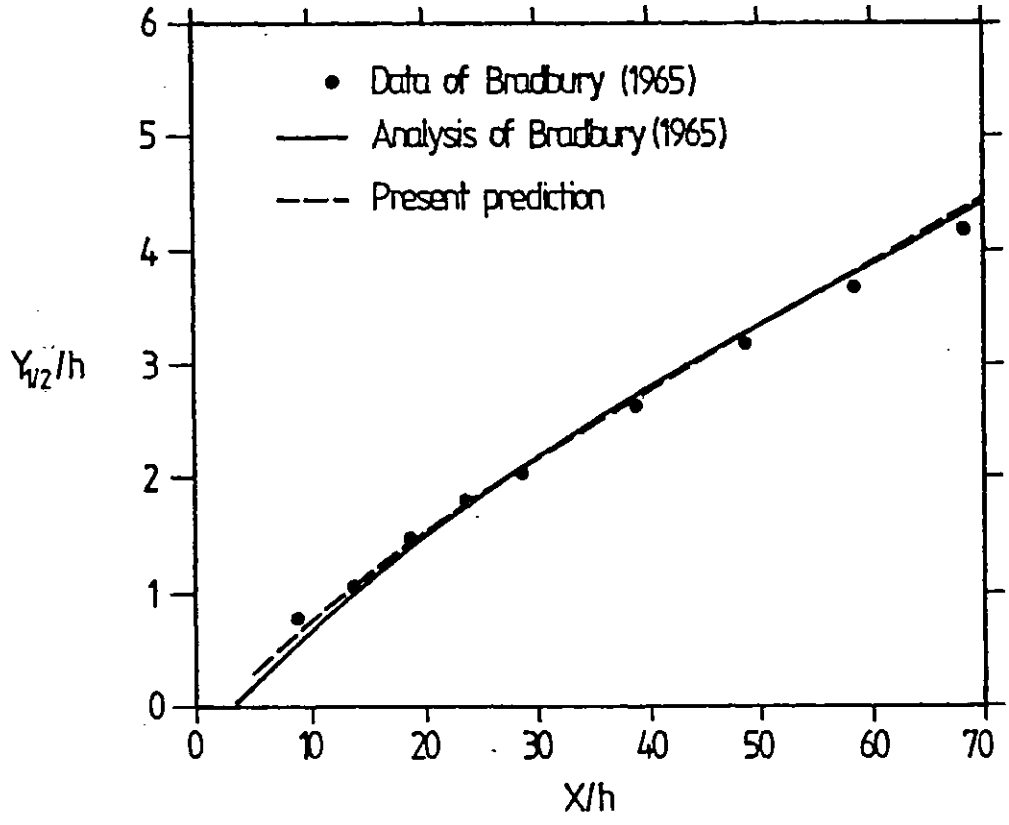

Fig. 7.25-2. Variation of Plane-Jet Width (Data of Bradbury, 1965)

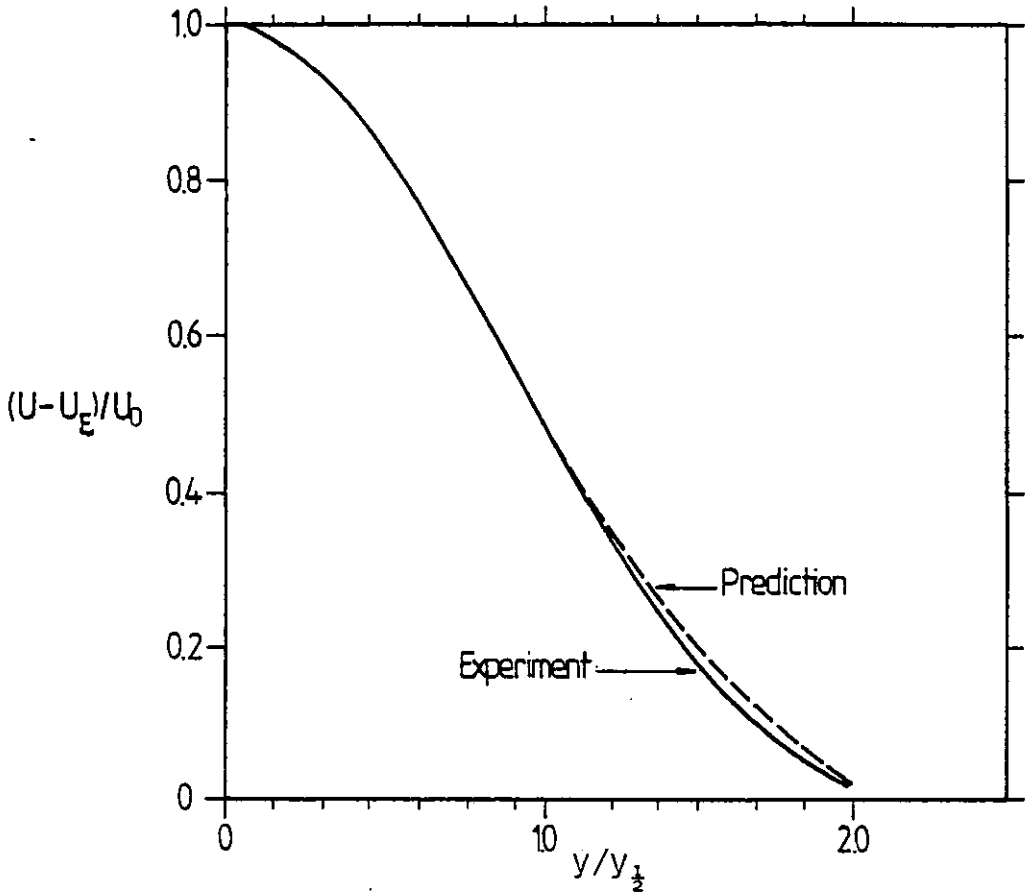

Fig. 7.25-3. Axial Mean Velocity (X/h=70); Plane-Jet data of Bradbury (1965).

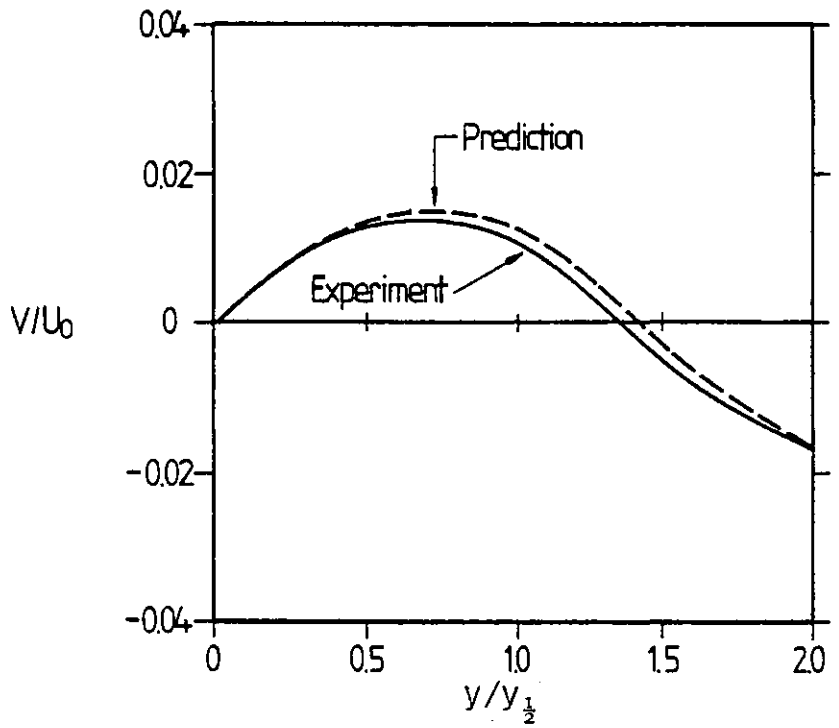

Fig. 7.25-4. Lateral Mean Velocity (X/h=60); Plane-Jet data of Bradbury (1965).

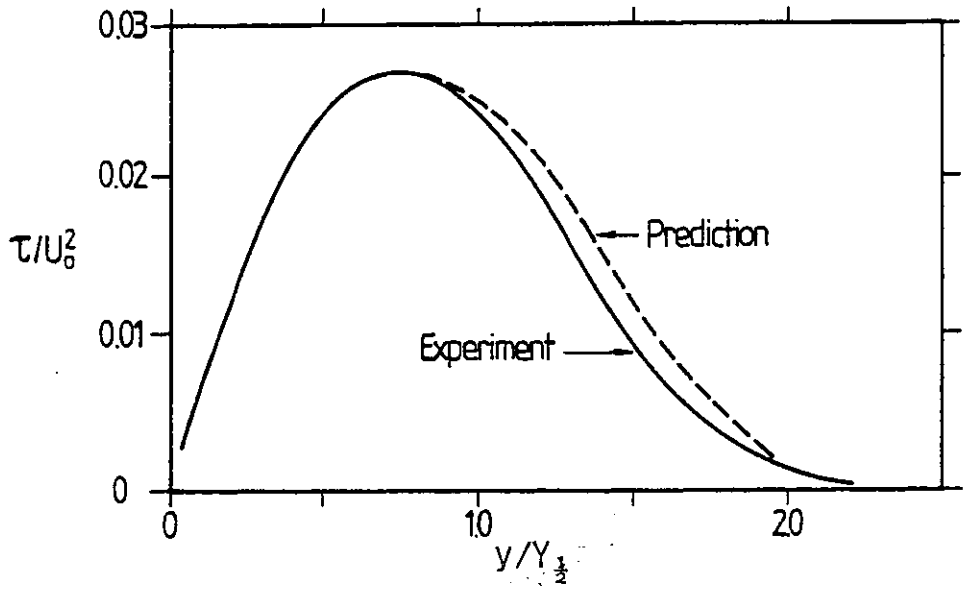

Fig. 7.25-5. Shear Stress (X/h=70); Plane-Jet data of Bradbury (1965).

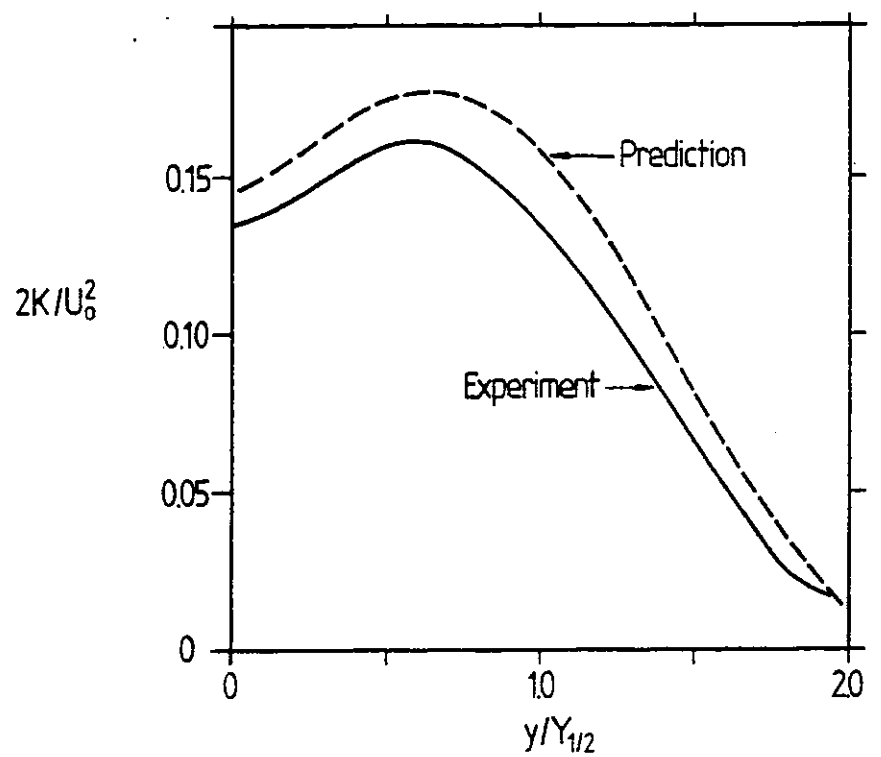

Fig. 7.25-6. Turbulence Kinetic Energy (X/h=70); Plane-Jet data of Bradbury (1965).

7.26 Discussion

The predictions seem to be in fair agreement with the measurements. Fig 7.25-2 shows that the predicted rate of jet spread is not constant. This behaviour is expected in view of the fact that Bradbury's flow is not exactly self-similar.

Beyond x/h = 50, the predicted profiles of both mean flow and turbulence quantities are substantially self-similar, which is consistent with Bradbury's experimental observation.

The predicted mean velocity profiles shown in figures 7.25-3 and 7.25-4 agree well with measurements. Figure 7.25-5 shows that the shear stress is satisfactorily predicted especially near the jet axis. However, the prediction at the outer region compares well with the profile calculated from mean velocity results for U_E/U_J = 0.16, the condition at which most measurements were made.

The result for the turbulent kinetic-energy shown in Figure 7.25-6 is not so satisfactory. The maximum predicted energy is some 7% above Bradbury's measurements. However, the prediction is in the consensus of the data as the predicted energy exhibits a maximum near the position of maximum shear.

7.3 Plane Mixing Layer

7.31 The Problem

The ideal mixing layer is formed by the mixing between two semi-infinite streams (see Fig 7.1-2). This ideal flow can only be approximated by experiments. The best approximations

are the mixing between two-dimensional half-jets, and the initial regions of plane and round jets. However, in the latter case the extent of the mixing layer is rather limited.

The task is to use the new K-W model to predict the angle of the wedge-shaped mixing-layer (i.e. the rate of spread) and the profiles of fluid variables across this layer.

7.32 Review of Experimental Data

An extensive review of available experimental data on the plane mixing-layer has been carried out by Rodi (1972). A summary of the findings is contained in Tables 7.32-1 and 7.32-2 overleaf.

7.33 The Case Considered

Rodi (1972) has found that there is no general agreement between the various experimental situations reviewed in section 7.32 (see Tables 7.32-1 and 7.32-2). However, the data of Wygnanski and Fiedler (1970) may be considered substantially acceptable and so will be used for comparison with the predictions.

7.34 Computational Details

The domain of calculation is made to cover essentially the mixing region.

The inlet plane is placed near the nozzle exit where the inner and outer boundaries are located respectively in the fast-moving and the quiescent fluids at $y = \pm 0.06$m from the

Experimenter	Dimensions of nozzle (h x b) cm	Range cm	Max $Re_x \times 10^{-5}$	$\frac{\sqrt{u'^2}}{U}$ at exit	$\frac{U_E}{U_1}$	$\frac{d(y_{.1} - y_{.9})}{dx}$	Means $\frac{\delta W_{max}}{U_0^2}$	Calc $\frac{\delta W_{max}}{U_0^2}$	$\frac{K_{max}}{U_0^2}$	Remarks
Zhestkov et al (see	4 x 12.5 4 x 12.5	<10	7.1	?	0 -.64					
Miles Miles and Shir (1968)	?	<105	26	3%	.14 .22 .36 .46 .55 .65 .76 .83					
Mills (1968)	5 x 15 5 x 15	<20	1.8	?	0 .3 .6	.178 .098 .07				
Sabin and Mark (1962)	.64 x 30 11.5 x 30	< 6	1.1	?	.2 .36 .6					Influence of walls noticeable
Sabin (1965)	?	50 <x <115	1.8	?	.35 .46 .61					Water tunnel experiments
Spencer (1970)	19 x 38 19 x 38	<127	26	.1%	.15 .22 .305 .54 .61 .76	.078 .0328	.0132 .011	.011 .0104	.035 .032	Detailed information only for U_E = .3, .6
Brown and Roshko (1971)	2.5 x 10 2.5 x 10	< 10	5	.1% .5%	.143 .378					Nitrogen 7 atm.

TABLE 7.32-1: Data for mixing layer between two moving streams

TABLE 7.32-2: Experiments on mixing layers with $U_E=0$

Flow Situation	Experimenter	Half jet dimensions (cm)	Range cm	Max Re_x x 10^{-5}	$\overline{u^2}^{1/2}/U$ at exit	$\frac{d(y_{.1}-y_{.9})}{dx}$	Means $\frac{\overline{uv}_{max}}{U_I^2}$	Calc $\frac{\overline{uv}_{max}}{U_I^2}$	$\frac{K_{max}}{U_I^2}$	Remarks
Two-dimensional half-jet with solid three boundaries	Reichardt (1942)	32 x 32	<160	32	?	.131				most runs
						.15				one run
	Liepmann & Laufer (1947)	152 x 19	< 90	11	1%	.16	.008	.0106	.021	$\overline{w^2} \approx \overline{v^2}$ assumed
	Wygnanski & Fiedler (1970)	51 x 18	< 58	4.65	.1%	.2	.0091	.0138	.035	wall at x = 0, trip wire used
	Patel (1970)	76 x 43	<100	18	.5%	.165	.0103	.0112	.0275	
Initial region of a plane jet	Albertson et al (1948)		$1 < \frac{x}{\bar{h}} < 4$	?	?	.155				data obtained from Abramorich
	Mills (1968)	5 x 15	$2 < \frac{x}{\bar{h}} < 4$	1.8	?	.178				
	Sunyach & Mathieu (1970)	4 x 48	$1.5 < \frac{x}{\bar{h}} < 3$	1.6	.25%	.18	.0137	.0125	.05	
Initial region of a round jet	Maydew & Reed (1963)		$.5 < \frac{x}{D} < 3.9$			.16				Exit Mach number = 0.7
	Bradshaw et al (1964	D = 5	$x/D = 2$ $2.3 < \frac{2x}{D} < 7$	7.0	0 1% at x/ = 2	.165	.010	.011	.027	
	Sami et al (1967)	D = 30	x/ = 3 3 2x 15		.5%	.163	.0109	.0108		

nozzle lip.

The cross-stream width of the grid, y_L, is expanded with downstream distance, x, using the relation in equation (7.23-1). The constant of proportionality f, is taken as 0.33. This ensures that the grid covers the mixing layer for the axial length required for self-similarity.

A grid having 50 cross-stream nodes and forward-step size of 1% of the grid width is employed. Most of the nodes are placed within the high-shear region where the velocity gradient is steep.

At inlet, uniform turbulence intensity of 0.09% and length scale of $0.2y_L$ are specified within the layer while essentially zero values of variables are prescribed in the stagnant fluid outside. An arbitrary velocity profile similar to that of Tollmien (1926) is specified within the mixing layer (see Fig. 7.31-1) thus:

$$\frac{U}{U_I} = \frac{5}{3}\eta^2 - \frac{2}{3}\eta^5 \qquad ,(7.34\text{-}1)$$

in which

$$\eta = 1 - \frac{y}{y_E} \qquad .(7.34\text{-}2)$$

At the free-stream boundaries, the imposed conditions are: constant pressure, zero K and W; and the velocities corresponding to the stream values.

7.35 Results

In Table 7.35-1 are shown the predicted rate of spread, the maximum shear stress τ_{max}, and the maximum specific turbulence energy K_{max} for the fully-developed plane mixing-layer. Also shown are the experimental values representing averages of the data of Wygnanski and Fiedler (1970).

Quantity	Rate of Spread $(y_{0.9}-y_{0.1})/X$	Relative Maximum Shear-stress	Relative Maximum Specific Energy K_{max}/U^2_{max}
Present Prediction	0.16	0.0109	0.0335
Experimental Value (Wygnanski & Fiedler, 1970)	0.16	0.0091	0.034

Table 7.35-1: Results For the Turbulent Mixing Layer of a Plane Jet

The rate of spread is defined by $(Y_{0.9} - Y_{0.1})/X$, where $(y_{0.9} - y_{0.1})$ represents the cross-stream distance between points where the fluid velocity has values equal to 0.9 times and 0.1 times the velocity at the edge of the layer, and x is the distance from the virtual origin of the mixing layer.

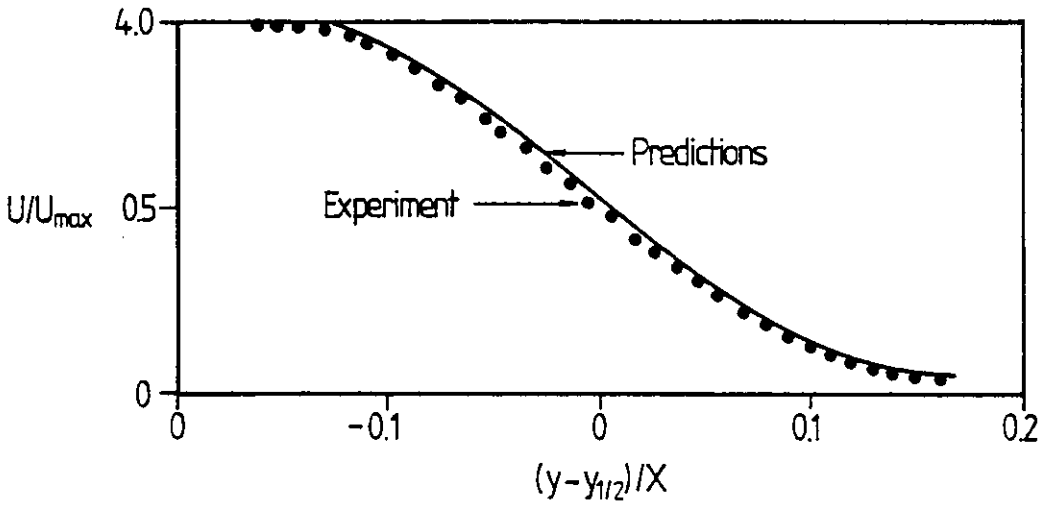

Fig. 7.35-1. The Mean Velocity Profile for the fully-developed mixing layer. Data of Wygnanski and Fiedler (1970).

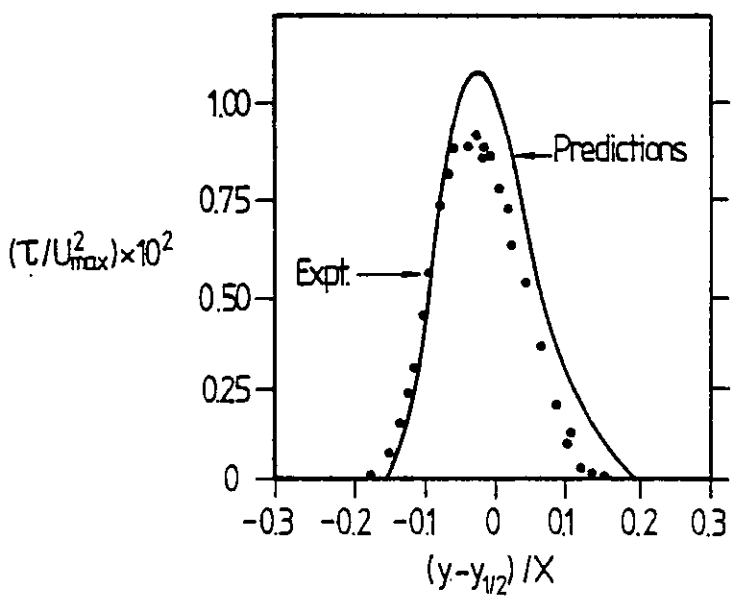

Fig. 7.35-2. The Average Shear-Stress Profile for the fully developed mixing layer. Data of Wygnanski and Fiedler (1970).

The shear stress and energy are normalised by reference to the square of the maximum velocity.

Figures 7.35-1 and 7.35-2 show respectively the predicted normalised similarity profiles of the mean velocity and shear stress across the mixing-layer compared with the data of Wygnanski and Fiedler (1970). The origin of the lateral coordinate ($y_{1/2}$) is chosen at a point at which the mean velocity is equal to one half of its free stream value and rendered dimensionless by having been divided by x, the distance from the virtual origin of the flow.

7.36 Discussion

It can be seen from Table 7.36-1 that the predictions agree fairly well with the measured values. It should be noted that the ratio of τ_{max} to K_{max} is equal approximately to 0.3; i.e. to $C_D^{1/2}$. This is to be expected for a flow that is in local equilibrium.

The mean-velocity profiles (Fig. 7.36-1) agree within the experimental accuracy of the measurements. The maximum shear stress (Fig. 7.36-2) is overpredicted by about 20%. However, since the computations certainly satisfy the conservation-of-momentum equation exactly, some doubt may be expressed about whether this can be true of the measurements of shear stress. The latter assertion is confirmed by Rodi (1972) who found that the maximum shear stress calculated from the data of Wygnanski and FIedler (1970) is 0.0138 compared with the measured value of 0.0091 (see Table 7.32-1).

7.4 The Round Jet

7.41 The Problem

The flow under consideration is that which ensues when fluid emerges into a stagnant reservoir from a nozzle of circular cross-section (see Fig. 7.21-1). After a short flow-adjustment region, the flow takes the form of a conical jet with velocity profile along a radius which differ from one another in scale, but not in shape (i.e. the flow becomes self-similar); the maximum velocity of a section is found on the jet axis and it varies as X^{-1}, where X is again the distance from the nozzle.

The case investigated here is that in which the issuing fluid has the same density as that of the fluid, and is chemically inert.

It is desirable to predict the jet spreading-rate and the similarity profiles of velocity, kinetic energy and shear stress.

7.42 Review of Experimental Data

The mean flow-field of round jets was studied by numerous experimenters, but the turbulence field in the truly self-similar region only by few. These have been extensively reviewed by Rodi (1972), a summary of which is contained in Table 7.42-1 overleaf.

7.43 The Case(s) Considered

Comparison of predictions with the new K-W model will be made principally with the data of Wygnanski and Fiedler (1969).

However, the data of Rodi (1972) are also considered in the comparison of the predicted and measured turbulence energy.

Experimenter	Nozzle dimen. (cm)	Range x/D	Re_D	Start of self-preserved region	$\frac{d\delta_o}{dx}$	Meas $\frac{\overline{uv}_{max}}{U_o^2}$	$\frac{K_c}{U_o^2}$	Remarks
Wygnanski & Fiedler (1969)	D=2.6	20-98	10^5	$x/D \simeq 70$	.086	.0165	.101	Strange change in slope of U_J/U_o versus x/D at x/D=57
Rodi (1972)	D=1.29	62-75	8.7×10^4	$\frac{x}{D} < 62$	.086	.0186		

Table 7.42-1: Experimental Data on Round Jet Issuing into Still Air

The data of Wygnanski and Fiedler include: the axial variation of centre-line mean-velocity and centre-line turbulent-intensities; mean axial-velocity profiles at X/D = 40, 50, 60, 75 and 97.5; turbulent-intensity profiles at X/D = 20, 50, 60, 75 and 97.5; and the turbulent-shear-stress profiles at x/D = 50, 60 and 75. The measurements show that the mean-flow is already self-similar at some 20 nozzle diameters downstream while the turbulence does not attain true similarity until some

70 diameters downstream. Using Wygnanski and Fiedler's data Rodi (1972) has constructed the self-similar turbulent-kinetic-energy profile from the measured turbulent-intensity profiles and also deduced a rate of spread $d\delta_o/dx = 0.086$ from the measured mean-velocity profile. These derived quantities are chosen for comparison with the predictions in the present study.

7.44 Computational Details

(a) The Flow Configuration

Since the flow is axisymmetric, a polar coordinate system is used. The inlet plane is located at the nozzle exit and the outer boundary there is placed one nozzle diameter from the axis.

The outer-boundary width (r_o) is expanded with downstream distance according to:

$$r_o = r_{o,in} + fx \qquad ,(7.44\text{-}1)$$

in which $r_{o,in}$ is the value of r_o at inlet and f, the spreading rate of the outer boundary, is taken as 0.225 and deduced from the half-radius spreading-rate of the round jet presented by Rodi (1972). It should, once again, be emphasised that f here prescribes the spread of the grid and not the jet itself, the latter being an outcome of the prediction.

(b) The Grid

Figs. 7.44-1 and 7.44-2 show respectively the effect of successive forward-step-size refinements on the reciprocal of

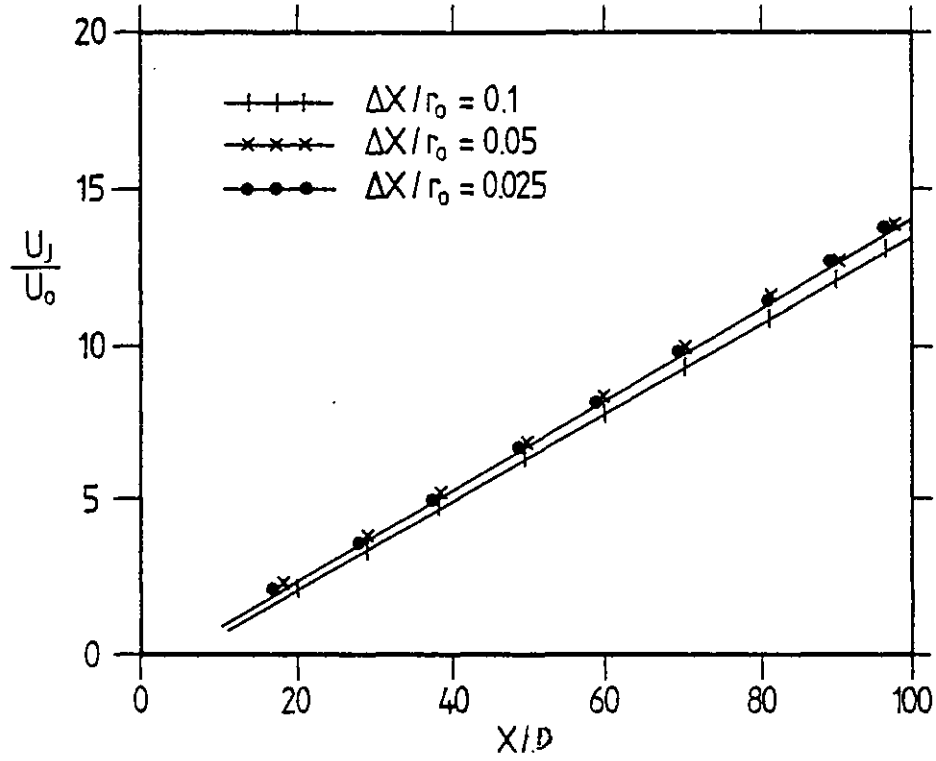

Fig. 7.44-1. Effect of forward step-size on axial variation of centre-line mean velocity of a round jet.

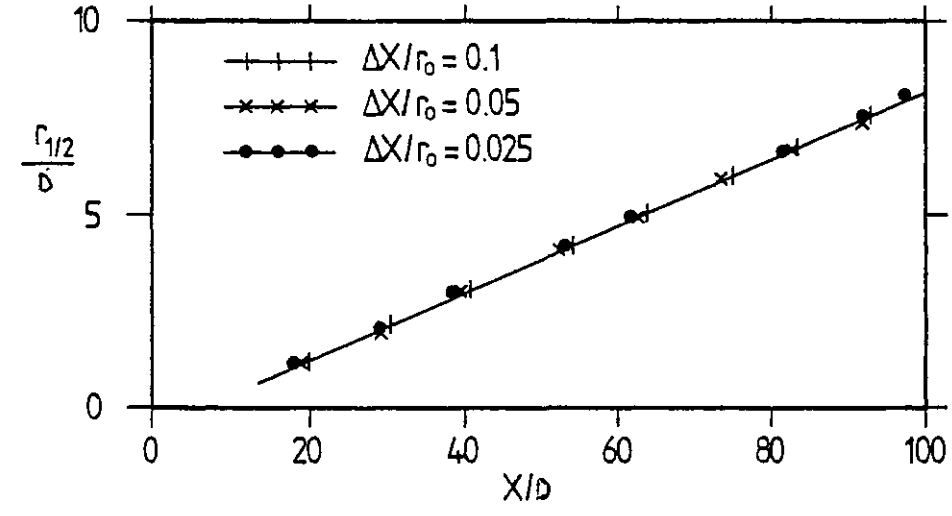

Fig. 7.44-2. Effect of forward step-size on spread of round jet half-radius.

the centreline velocity and jet half-radius. Figures 7.44-3 and 7.44-4 respectively show the effect of forward-step size on the mean velocity and turbulent-kinetic-energy similarity-profiles.

The similarity profiles correspond to a location X/D = 85, where it is expected that both the mean flow and turbulence are self-similar.

It can be seen from the above figures that the mean flow is sufficiently grid-independent at a forward-step size of $X/r_o = 0.05$. However, the turbulence predictions require a step size of $X/r_o = 0.025$ for sufficient accuracy.

It is interesting that this round jet requires a much smaller relative step-size than the plane jet (see section 7.2). Presumably, this can be attributed to the necessity of resolving the more rapid decay of velocities in the round jet.

Figures 7.44-5 and 7.44-6 respectively show the effect of successive radial-grid refinements on the reciprocal of the centre-line velocity and jet spread. Figures 7.44-7 and 7.44-8 respectively show the effect of radial-grid size on the mean velocity and turbulent-kinetic-energy similarity-profiles at x/D = 85.

The spread of the jet and the mean flow seem to be insensitive over the range of radial grid-nodes considered. Fig. 7.44-8 shows that 40 radial grid-nodes could be considered to give sufficient accuracy of the turbulence-energy profile.

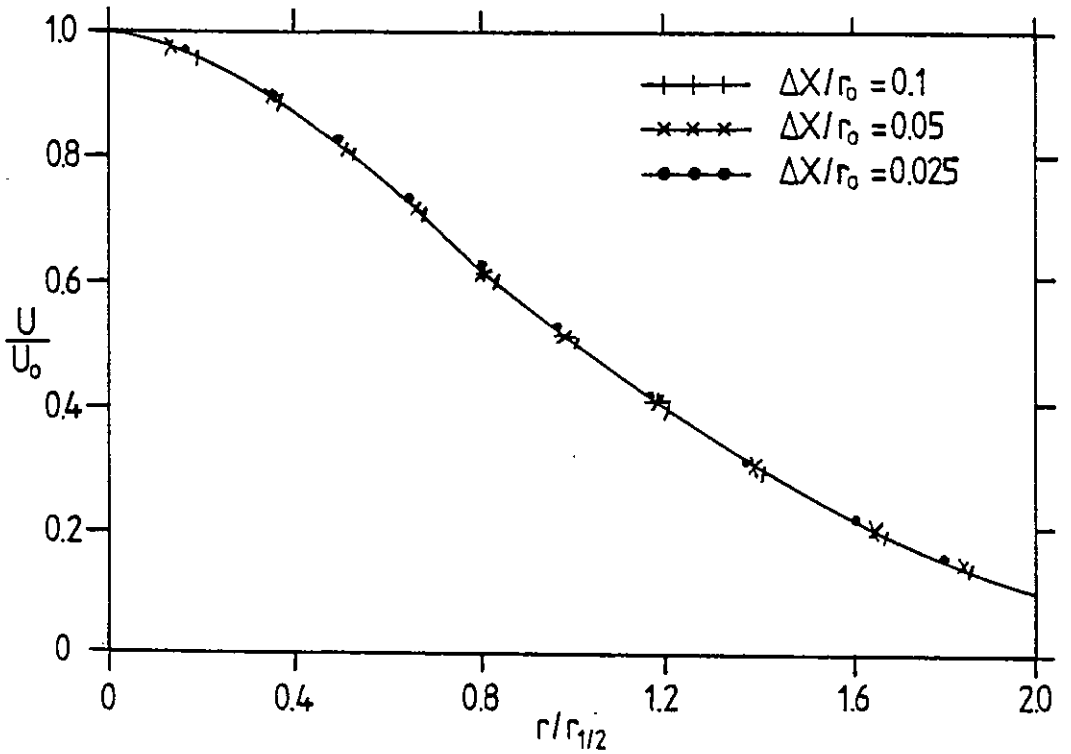

Fig. 7.44-3. Effect of forward-step size on mean axial-velocity similarity profile of a round jet.

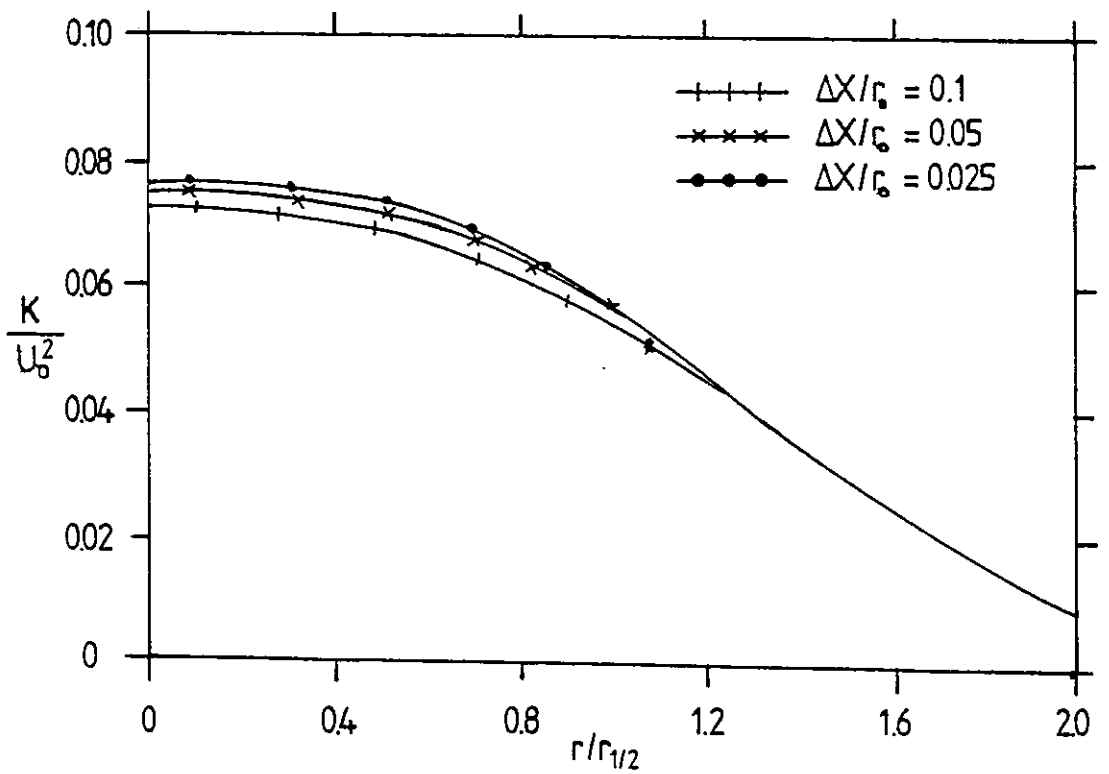

Fig. 7.44-4. Effect of forward-step size on turbulence kinetic energy similarity profile of a round jet.

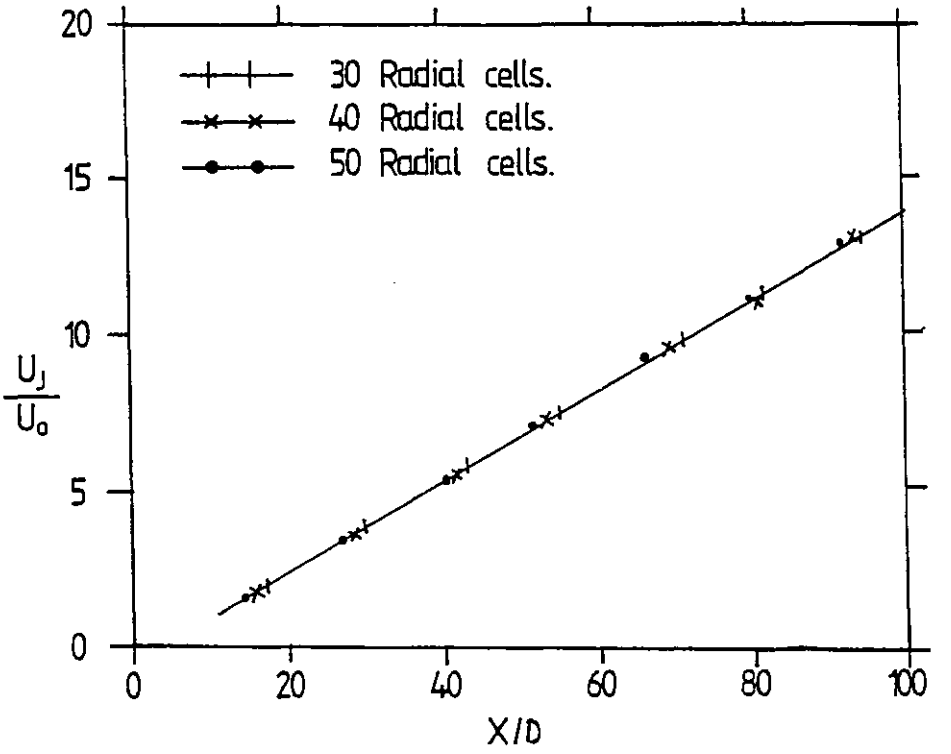

Fig. 7.44-5. Effect of radial-grid size on axial variation of centre-line mean velocity in a round jet.

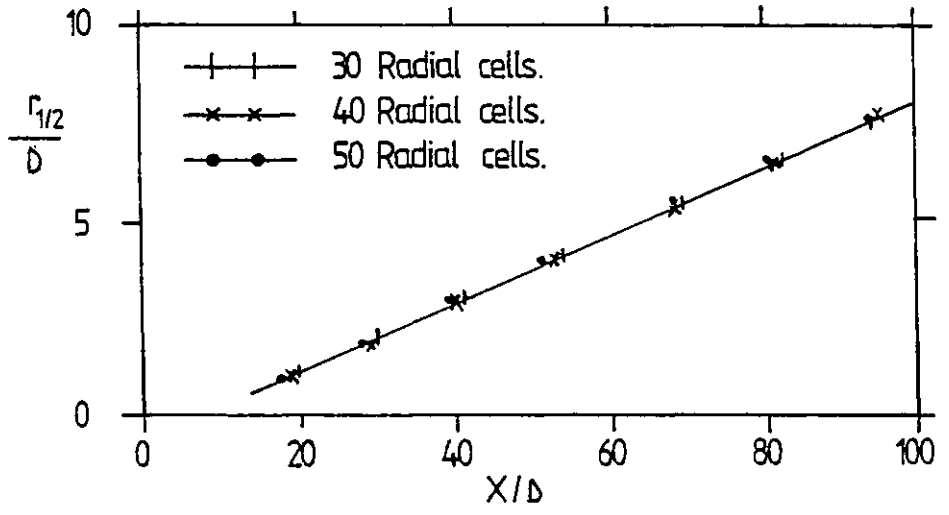

Fig. 7.44-6. Effect of radial grid size on spread of round jet half-radius.

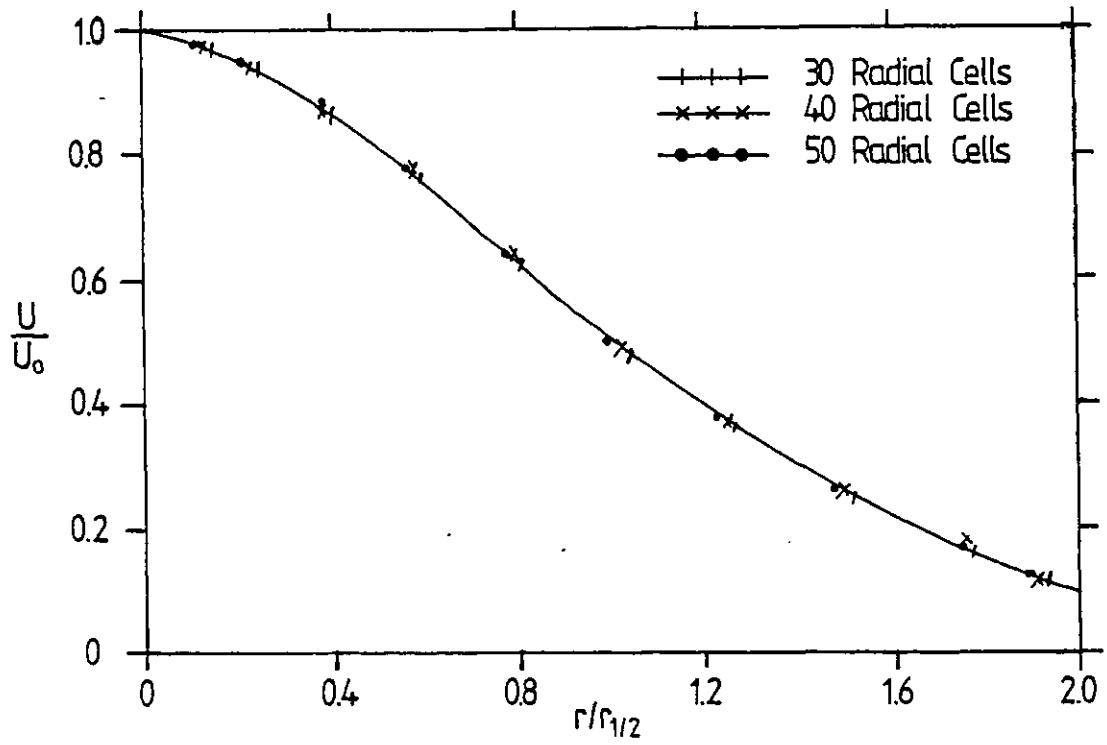

Fig. 7.44-7. Effect of radial-grid size on mean velocity similarity profiles of a round jet.

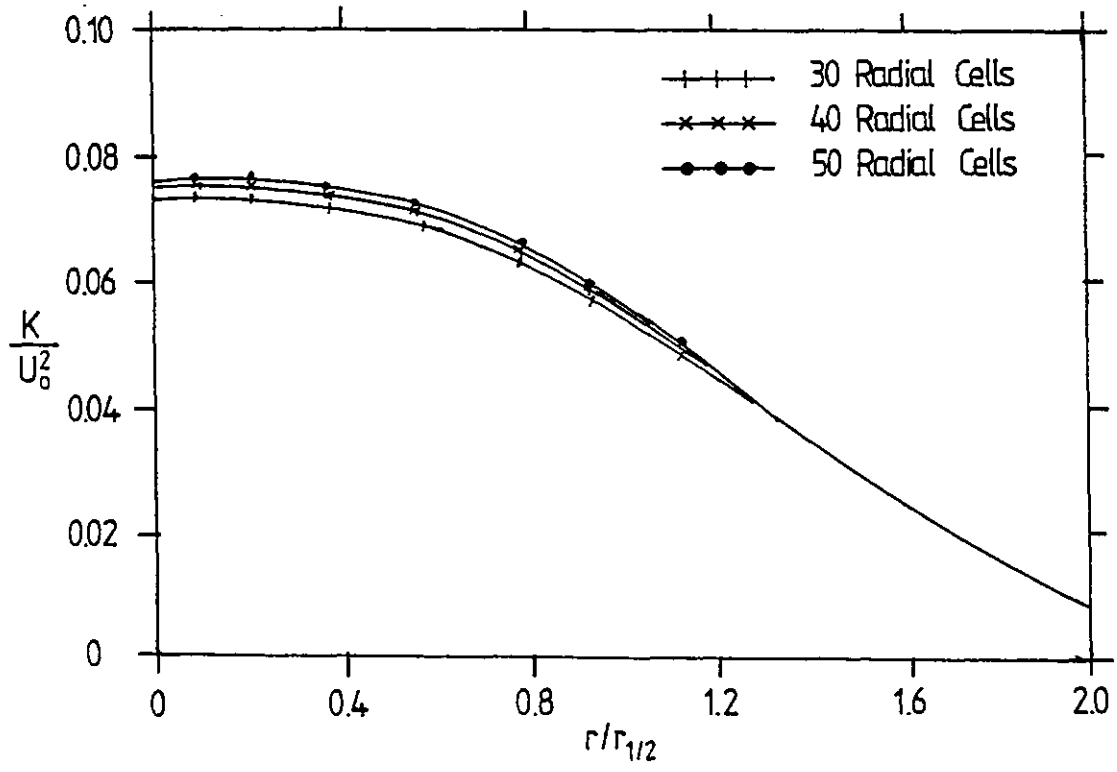

Fig. 7.44-8. Effect of radial-grid size on turbulence kinetic energy similarity profiles of a round jet.

It would be noted that the round jet here requires 10 more cross stream nodes than the plane jet to resolve the flow. This is expected because the round jet is relatively wider than the plane-jet-in-moving surroundings.

In view of the foregoing, 40 radial nodes and a forward step of 2.5% of radial width are employed for the calculations.

(c) Boundary Conditions

At the inlet, a uniform velocity is assumed within the nozzle. The turbulence energy is prescribed from the measured turbulence intensity of 0.1% and the length scale (from which W is deduced) is assumed to be proportional to the grid width.

The other boundaries are treated similarly to the plane jet described in section 7.2

(d) Similarity Consideration

A test is also made for the similarity behaviour of the predictions. Figures 7.44-9 and 7.44-10 show respectively the predicted mean axial-velocity and turbulent-kinetic-energy profiles at X/D = 40, 60 and 80. It can be seen that the mean flow is already self-similar some 40 nozzle diameters downstream while the turbulence field requires a further 20 diameters.

It can also be seen from figures 7.44-5 and 7.44-6 that the axial variation of U_o and $r_{1/2}$ are fairly in accordance with the similarity power-laws described in section 7.1 above.

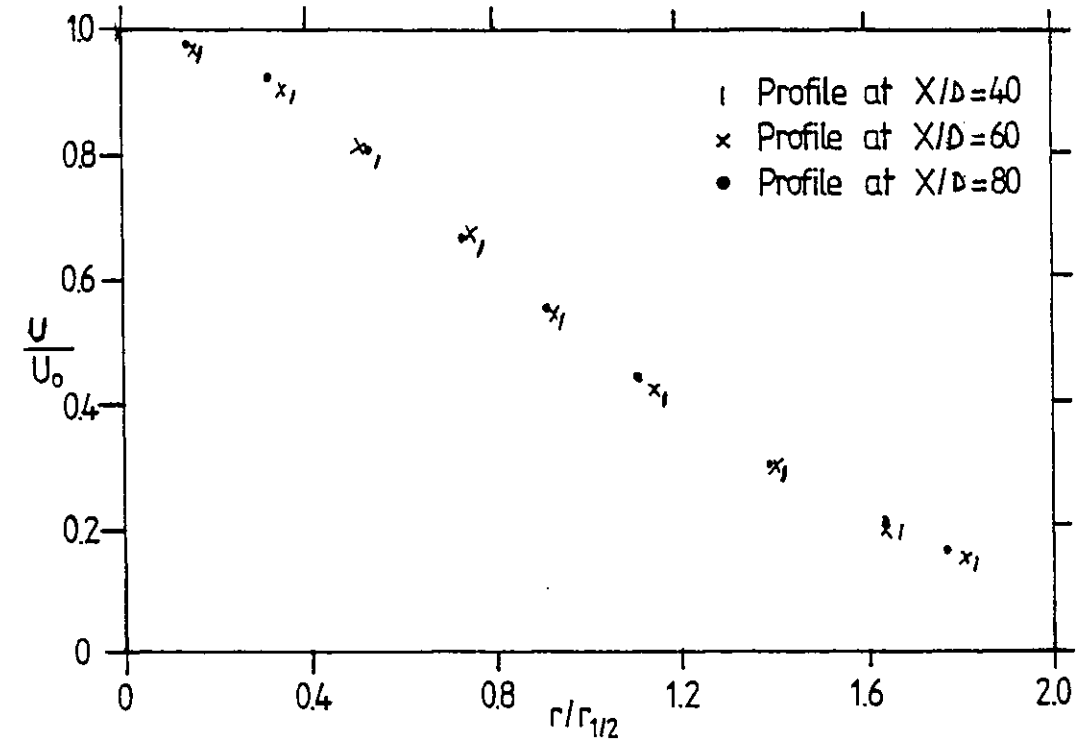

Fig. 7.44-9. Test for similarity on mean axial velocity in a round jet.

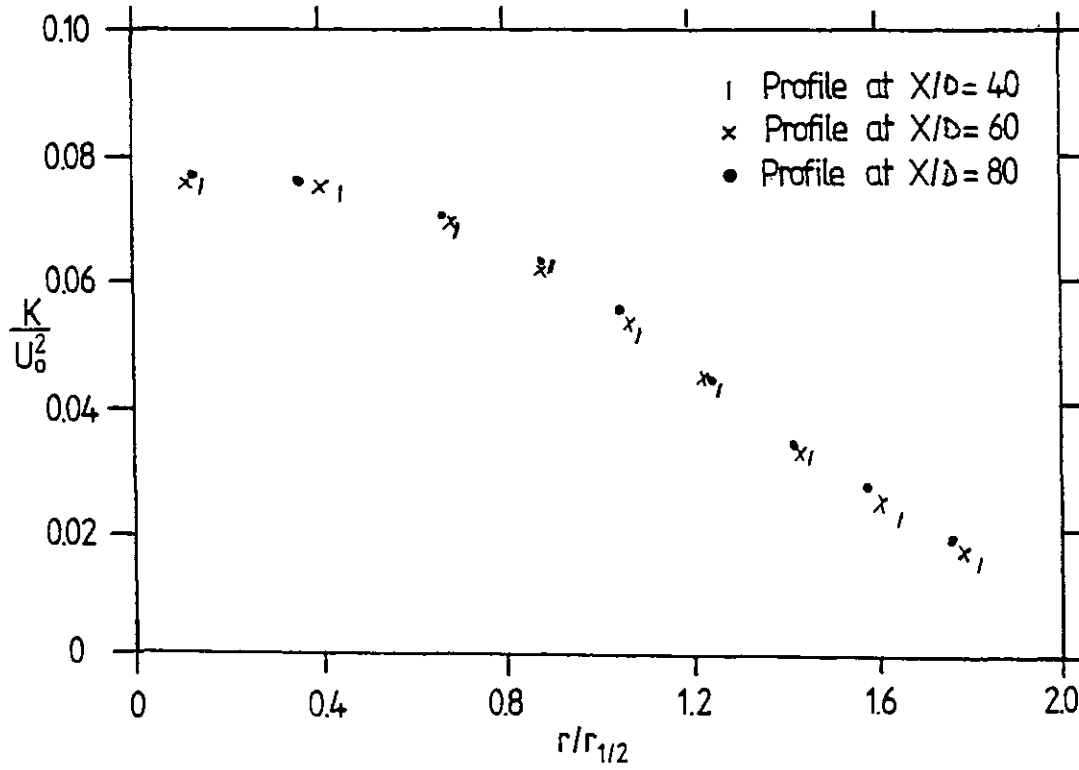

Fig. 7.44-10. Test for similarity on turbulence kinetic energy in a round jet.

(e) Turbulence Model "Constants"

As is true of all other two-equation turbulence models, it has been found that one of the "constants" of the turbulence model has to be changed to give realistic results. In the present case, C_3 (see equation 3.42-6 and Table 3.43-1) has been changed to 1.42. It will however be noted that this practice is much simpler than employing a functional relation for the "constants" as is usually done (see for example, Rodi, 1972).

7.45 Results

Figure 7.45-1 compares the predicted and measured reciprocals of the mean velocity along the jet axis. Figure 7.45-2 compares the predicted and experimental variations of the jet half-radius, δ_o, normalised with the nozzle diameter.

Figure 7.45-3 shows the predicted and measured mean axial-velocity similarly profile. In Figure 7.45-4, the predicted self-similar profiles of turbulence energy is compared with the experimental profiles of Wygnanski and Fiedler (1969) and of Rodi (1972).

Fig 7.45-5 compares the predicted shear-stress similarity profile with the measurement of Rodi. The measured values of Wygnanski and Fiedler are believed to be too low because of their measurement technique.

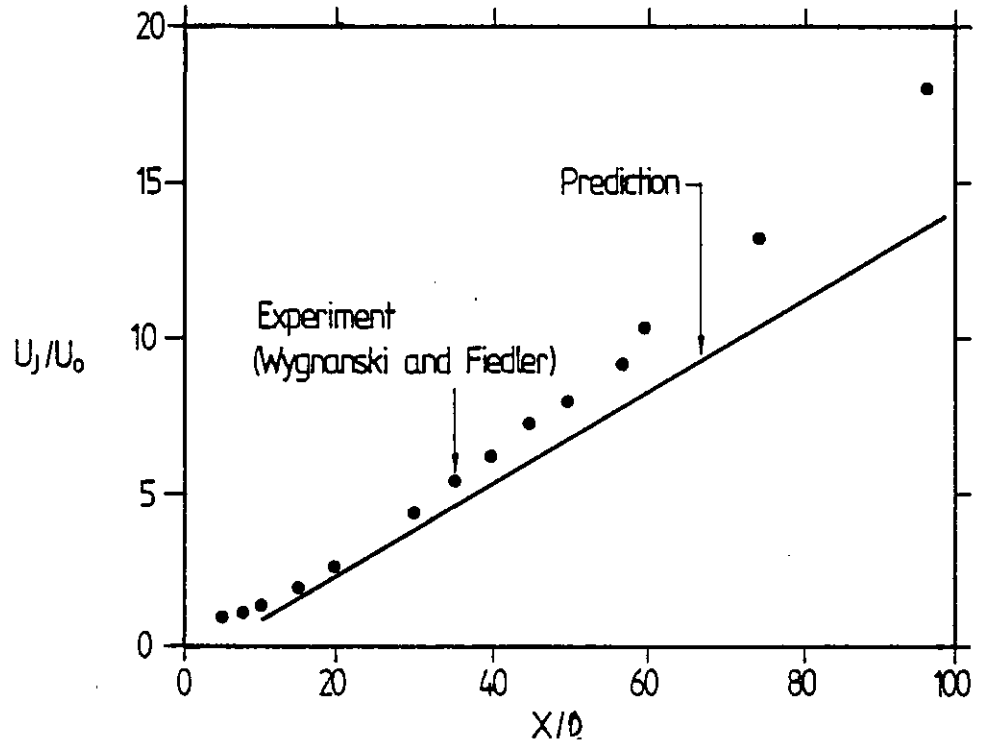

Fig. 7.45-1. Axial Variation of Centre-Line Mean Axial Velocity. U_o Round-Jet data of Wygnanski and Fiedler (1969).

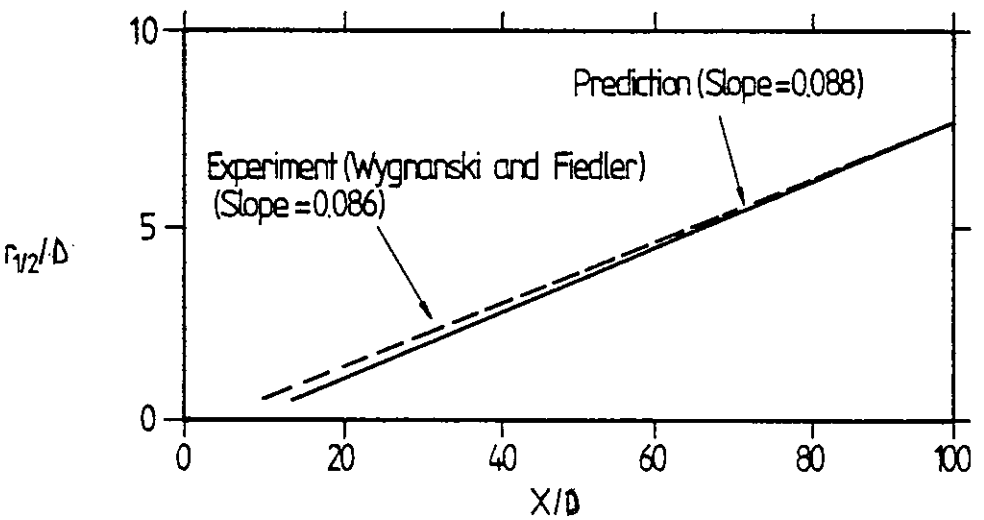

Fig. 7.45-2. Spread of Jet Half-Radius. Round-Jet data of Wygnanski and Fiedler (1969).

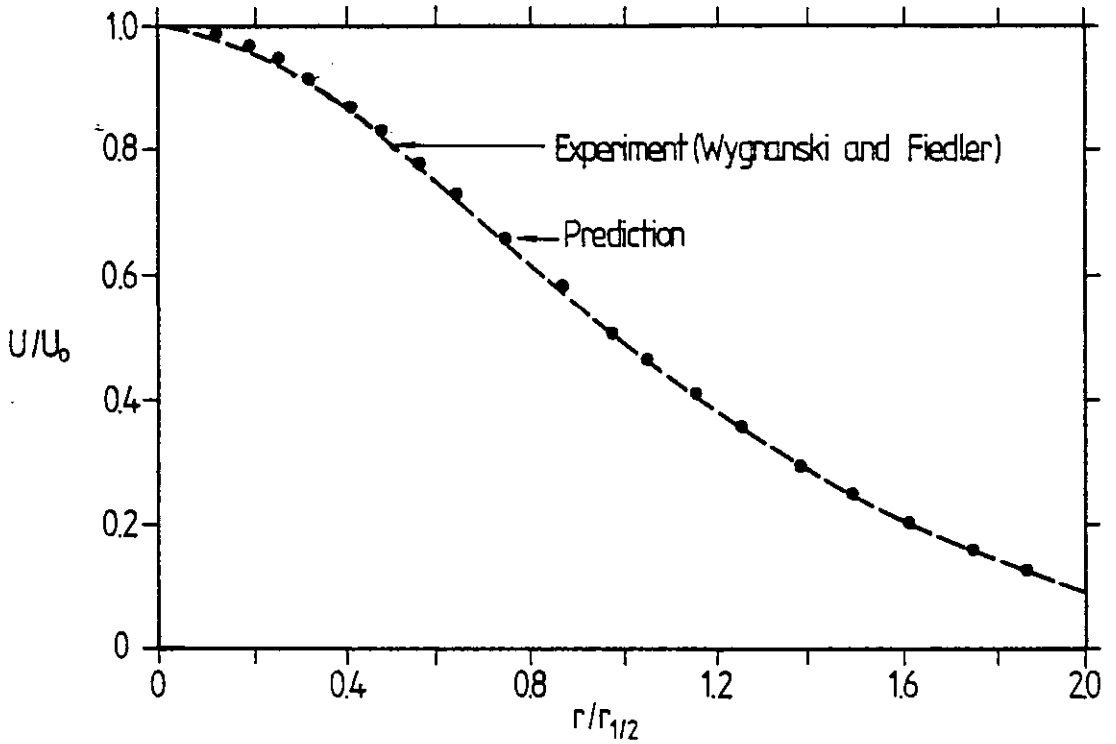

Fig. 7.45-3. Mean Axial Velocity Similarity Profile. Round-Jet data of Wygnanski and Fiedler (1969).

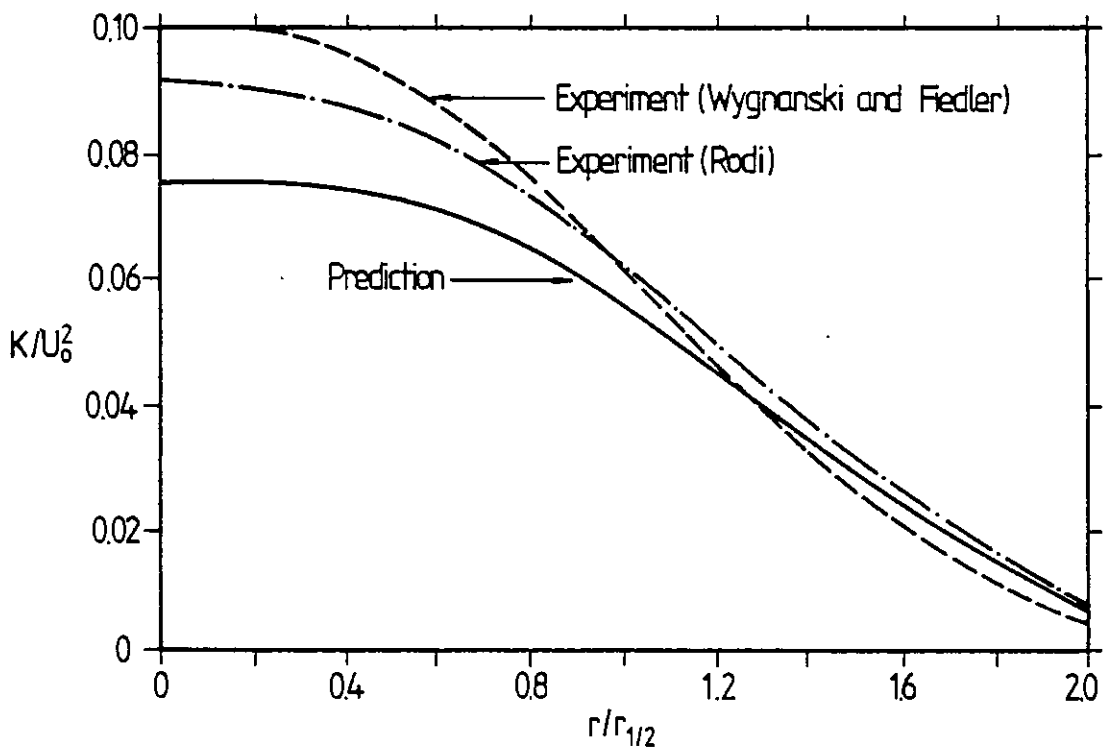

Fig. 7.45-4. Turbulence Kinetic Energy Similarity Profile. Round-Jet data of Wygnanski and Fiedler (1969); and Rodi (1972).

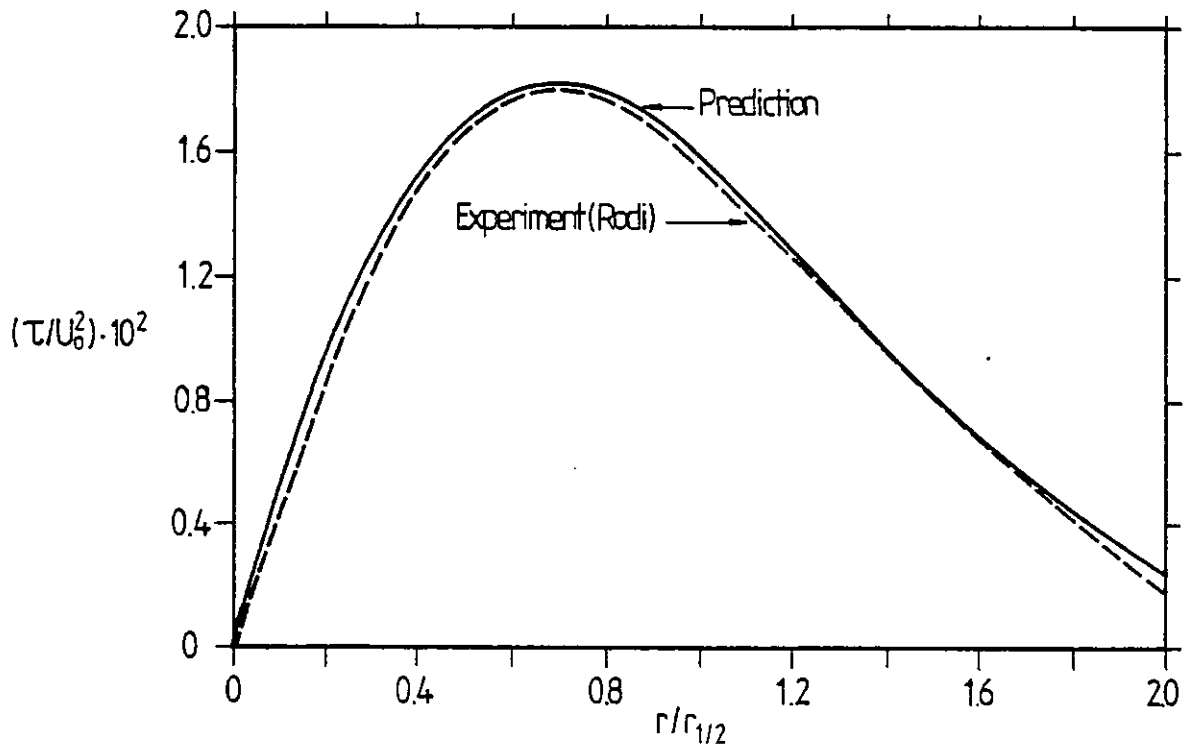

Fig. 7.45-5. Shear-Stress Similarity Profile. Round-Jet data of Rodi (1972).

7.46 Discussion

The agreement between the predicted and measured reciprocals of the mean velocity along the jet axis (Fig. 7.45-1), seems satisfactory up to about 50 nozzle diameters downstream, but then the predictions start to deviate. It should however be noted that the experimental accuracy is bound to diminish as the velocity excess tends to zero.

In Fig. 7.45-2, the predicted slope of 0.088 for the variation of the jet half-radius with the axial distance is in close agreement with the measured value of 0.086. Figure 7.45-3 shows that the predicted mean axial-velocity similarity-profile agrees well with the measurements.

Figure 7.45-4 shows that the predicted turbulence-energy is closer to the profile of Rodi. This is not surprising because in a review (Rodi, 1972), he reported that his measurements of turbulence energy and shear stress were more reliable than those of Wygnanski and Fiedler because of his more accurate method of analysing the hot-wire signals.

At the jet axis, however, the turbulence energy is still underpredicted by about 20%.

From Fig. 7.45-5, the predicted shear-stress profile appears satisfactorily in agreement with the measured profile. The maximum value of shear stress occurs at $r/r_{1/2} = 0.77$.

7.5 Closure

It has been demonstrated in this chapter that the new K-W model, despite its additional term which is directly relevant to wall flows, can still predict satisfactorily, a wide range of free flows.

The physical situations considered are turbulent flows in a plane jet issuing into slow-moving surrounding, a mixing layer with one stagnant free stream, and a round jet exhausting into still environment. The mean-flow and turbulence characteristics of each flow situation are predicted and compared with established experimental data.

The agreement appears generally satisfactory in all cases. However, as is true of all other two-equation turbulence models, it has been found that one of the turbulence-model "constants" has to be changed for the round jet to get acceptable results. Specifically, C_3 has been changed to 1.42.

This now completes the task of testing the universality of the new K-W model of turbulence and also the theoretical contribution of the present study. In the next chapter is presented the experimental investigation of flow in two-dimensional bodies of different geometries.

CHAPTER 8

THE EXPERIMENTAL INVESTIGATION: WAKE-FLOW VISUALIZATION

8.1 Introduction

This chapter is concerned with an experimental investigation of turbulent flows containing small regions of recirculation. In order to fascilitate this study, a flow-visualization technique which appears to be novel has been developed (Ilegbusi and Spalding, 1982a).

The insight into a physical process has been known to be improved if a pattern produced by or related to this process can be observed by visual inspection. However, most fluids, gaseous or liquid, are transparent media, and their motion remains invisible to the human eye during a direct observation. In order to be able to recognize the motion of the fluid, one must therefore provide a certain techinque by which the flow is made visible. Such methods are called flow-visualization techniques, and they have always played an important role in the understanding of fluid-mechanical problems.

However, besides such instructive applications the greater importance of many flow-visualization techniques is that one can derive quantitative data from the flow picture thus obtained. Such techniques provide information about the complete flow field under study without physically interfering with the fluid flow. In contrast, a single flow-measuring instrument, such as a certain pressure or temperature probe, provides data for only one point in the flow field, and in addition, the fluid flow is disturbed to a certain degree owing

to the presence of the measuring probe.

The purposes of this chapter can therefore be summarised thus:

(i) to describe the principle of the new flow-visualization technique developed;

(ii) to report on a preliminary embodiment of the principle; and

(iii) to present a few results from a study of the flow in the wake of a slender wedge, of a thin bar, and of a two-dimensional backward-facing step.

Further developments are also discussed.

The remainder of the chapter is divided into seven sections. Section 8.2 contains a brief review of existing flow-visualization techniques. In section 8.3, the new technique developed in this study is detailed. This includes a description of the principle on which it is based, the possible quantitative interpretation of the results from an improved version of it and a practical embodiment of the technique. Sections 8.4 to 8.6 respectively describe the application of the technique to flow in the wake of a slender wedge, of a thin bar, and of a backward-facing step.

A discussion of the results obtained with the new technique is contained in section 8.7. Section 8.8 contains the concluding remark on the major achievements of the chapter.

8.2 Review of Flow-visualization Techniques

The methods of flow visualization can be classified broadly into three groups namely;

(i) Those involving addition of foreign materials into gaseous and liquid fluid-flows;

(ii) Optical methods for compressible flows, and

(iii) Those employing flow-field marking by heat and energy addition.

A detailed description of each of these can be found in MerzKirch (1974) and those particularly applicable to wind tunnels in Hunter and Foughner (1982).

In the first group, Simpson (1972), Sarpkaya (1971), Maxworthy (1972), Martin and Lockwood (1964), Sullivan (1971) and many others used dye solutions to mark filament lines in their respective flow situations. Others who employed smokes are Zdravkovich (1968) and Dewey (1971). The hydrogen-bubble technique was used by Schraub et al (1965), Clutter and Smith (1961) and Davis and Fox (1967). Others visualized velocity profiles by electrolytic and photochemical dye-production. These include Buzyna and Veromis (1971) and Popovich and Hummel

(1967).

Optical methods (second group) have been employed variously by Larmore and Hall (1971), Corcoran (1967) and many others. These methods include the shadowgraph, Schlieren method, Mach-Zehnder interferometer and many others.

The methods of the third group could be considered partially as hybrids of the first two. They include methods employing artificially introduced density-changes (Schardin, 1942); velocity mapping with the spark-tracer technique (Frungell and Thorwart, 1970); electron-beam flow visualization (Grun et al 1953); and glow discharge and chemiluminescence (McCroskey et al, 1966; Horstmann and Kussoy, 1968).

In the next section, a detailed description of the new flow-visualization technique for the present study is given.

8.3 Description of the New Flow-visualization Technique

8.31 The Principle

Wind tunnels and water channels are expensive to build and to run. It is much cheaper, and can be very instructive, to pull the flow-creating body through fluid at rest, as is routinely performed in "towing tanks" for ship research.

The technique to be described below is of the pulling-through-fluid-at-rest kind; but it has the novel feature of using <u>two</u> fluids, one above the other, and making their flow-induced intermingling visible by the use of a dye.

The two fluids are at first kept separate by a small difference of density, sufficient to maintain a perfectly horizontal and well-defined interface, but not so great as to influence the flow generated by the movement of the test body. This latter condition simply requires the Froude number, U^2/gL, greatly to exceed the ratio $\Delta\rho/\rho$, where:

U ≡body velocity

L ≡body length

g ≡gravitational acceleration

$\Delta\rho$ ≡density difference between the two fluids

ρ ≡the density of one of them

The body is at first immersed at rest within the lower fluid, which is coloured with a dye. A steady upward force is then suddenly applied to it, so that it rises, steadied by suitable guides, attaining a uniform velocity before it breaks through the interface.

As the body emerges from the lower fluid, it is seen to carry with it, in its boundary layer and wake, significant quantities of the lower fluid. Entrainment of clear (upper) fluid into the boundary layer and wake progressively dilutes the dye, with obvious visible consequences.

A succession of photographs enables the various states of mixing to be recorded, and possibly, subsequently measured.

8.32 Quantitative Interpretation of the Results

Experiments are especially valuable if they yield quantitative results which may be compared with the predictions of a general theory. It is therefore necessary to ask whether such comparison is possible in the present case. The answer is affirmative, provided that sufficiently powerful computational procedures are available and the technique is fully established.

In a frame of reference which is fixed relative to the test body, the flow may be expected to be steady. A suitable method of prediction for the velocity and turbulence fields is therefore a steady-state one; the new experimental technique shares this requirement with conventional wind-tunnel techniques.

However, the equation for the dye concentration, if solved in the same reference frame (moving with the body) as is used for the velocity and turbulence fields, contains transient terms; this is a consequence of the movement towards and through the initially flat interface between dyed and undyed fluids. To solve this equation, therefore, more computational work must be done.

Fortunately, there is nowadays little difficulty about performing this extra work; for computer software and hardware are available. Thus, the only task will be to further develop the technique to the level at which the results can be

ouantitatively analysed.

8.33 A Practical Embodiment

Figure 8.33-1 illustrates the apparatus which has been built so as to test the practicability of this method for flow visualization. The apparatus consists of two water tanks, a metal framework, and system of smooth pulleys, rubber tube, steel wires, power-wound camera, water, dye, salt and weights. One of the tanks is made of 10mm-thick perspex with internal dimensions of 0.2 x 0.2 x 1.5m; and the other is a 15-litre glass jar.

The metal framework is an assembly of steel bars with provision for attaching two pairs of smooth pulleys each of 25mm radius. The dye consists of Nigrosine. The salt solution employed as the denser fluid has a concentration of 10g/litre.

The operational procedure is as follows. The perspex tank is mounted on the metal framework about 0.65m above the floor to avoid floor vibration. A graduated scale is attached to the tank so that the movement of the body at known time intervals could be recorded.

The two thin steel wires (each of which is attached to one side of the body) are used to suspend the body inside the tank. These wires are passed over the system of pulleys to known weights used to lift the test body.

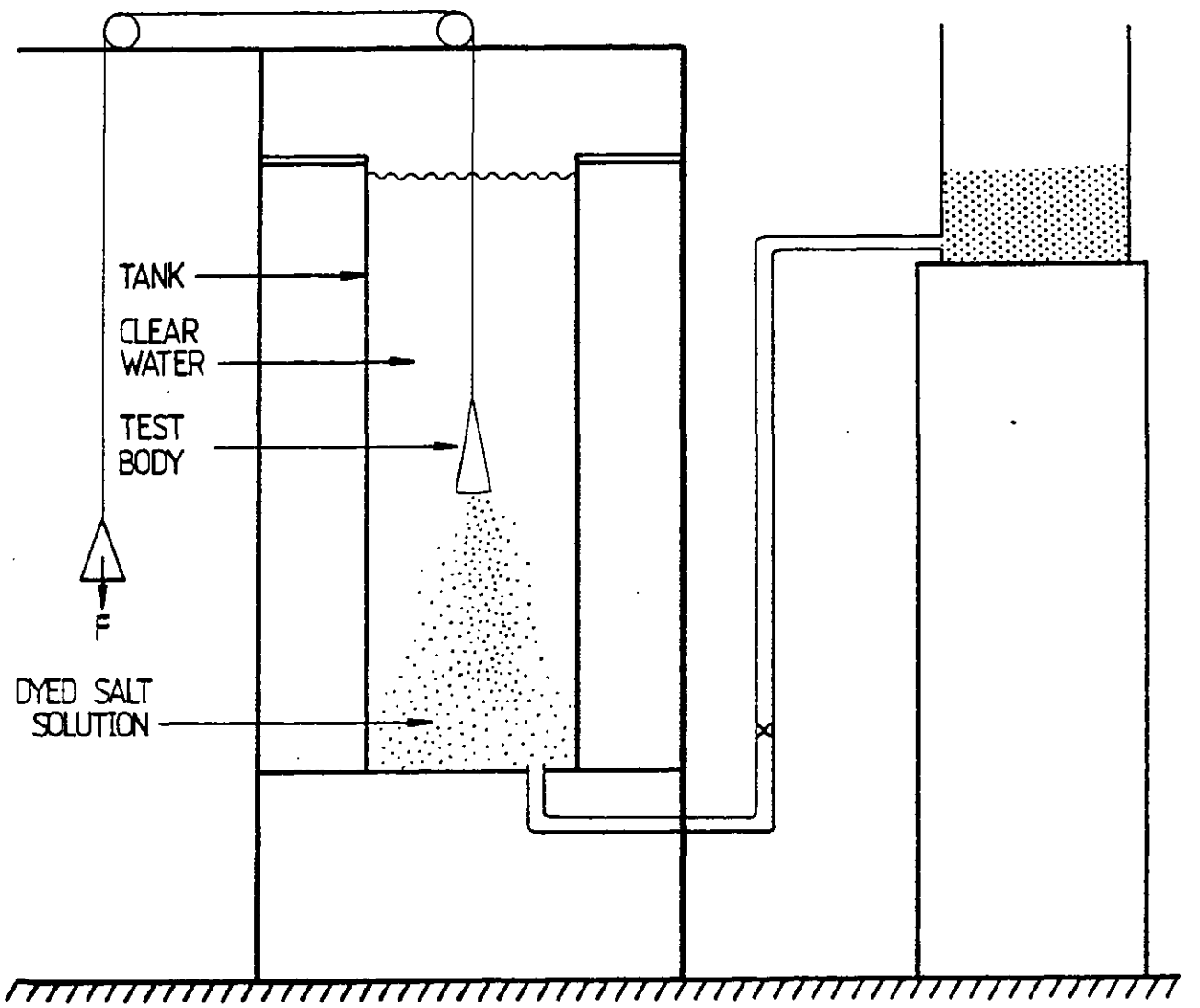

Fig. 8.33-1. The experimental set-up.

The above technique of suspending the body partly reduces any unnecessary lateral movement due to careless handling. A perfectly-straight movement is further ensured by two slots cut into the walls of the tank (one at each side) along which the body moves on soomthened guides.

The dyed fluid (salt solution of known concentration) is initially contained in the glass jar placed adjacent to the first tank. The fluid is introduced via a rubber tube connected to the bottom of the perspex tank. The flow rate is controlled by a valve on the connecting tube.

A translucent polythene paper is attached to the side of the perspex tank away from the camera so as to diffuse the light used to aid photography.

The perspex tank is first filled to about half height with clear water. The test body is then lowered into it and the dyed fluid is progressively introduced. The latter operation is performed slowly at first and later increased at a rate that will not disturb the interface.

The body is pulled upwards with known weights attached to the end of the suspension. Photographs of the boundary layer and wake formed behind the body are then progressively taken with the power-wound camera.

The time taken to perform the whole operation is typically half-an-hour, of which the movement of the test body

occupies about five seconds.

8.34 Auxiliary Information

Some additional precautions need also be taken to improve the technique. These are described below.

(a) Repeatability

A system by which the experiment can be made repeatable has been devised. This is done by starting the experiment with a relatively light dye concentration. At the end of the first set of tests, the mixed fluids can be stirred thouroughly to give a new homogeneous solution. This will now form the top light fluid for the next experiment during which a denser solution with thicker dye is introduced from the bottom.

(b) Two-dimensionality of Flow

This is ensured by making the body relatively thin and having a width almost equal to that of the tank. Thus the three-dimensional effects from the sides and guides are minimal.

(c) Steady Motion of Body

A preliminary investigation may be carried out to ascertain the height of interface required for the body to attain a fairly steady speed before breaking the interface. The speed is determined approximately by measuring the height of the body with time when drawn with known weights at the other end of the suspension.

However, the height of interface required may be limited

by that of the tank; the latter of course, also limited by consideration of photographic convenience.

(d) Distinction of Trailing Edge of Body

The sides of the body nearer the camera is covered with white polythene-paper. This allows the trailing edge of the body to be seen with sufficient clarity in the photographs when light dye-concentrations are used. However, this distinction becomes more and more difficult as the dye becomes thicker.

This problem has been solved by using the graduated scale on the tank to mark out the length of the body in the photographs. This approach is preferable to attaching a pin to the trailing edge of body as the pin will probably disturb the flow.

8.4 Application to Flows Near Blunt Trailing-Edges

The new flow-visualization technique just described has been employed in the researches on flow near blunt trailing-edges. The three different bodies considered as test cases are described below.

8.41 Flow Past a Wedge

(a) Laminar Separation

The first test body consists of an aluminium wedge (see Fig. 8.41-1) of which the cross-section is an isosceles triangle with an apex angle of 8.5 degrees and a base of 30mm. This wedge is pulled upward through the fluid layers at a speed of approximately 0.32m/s.

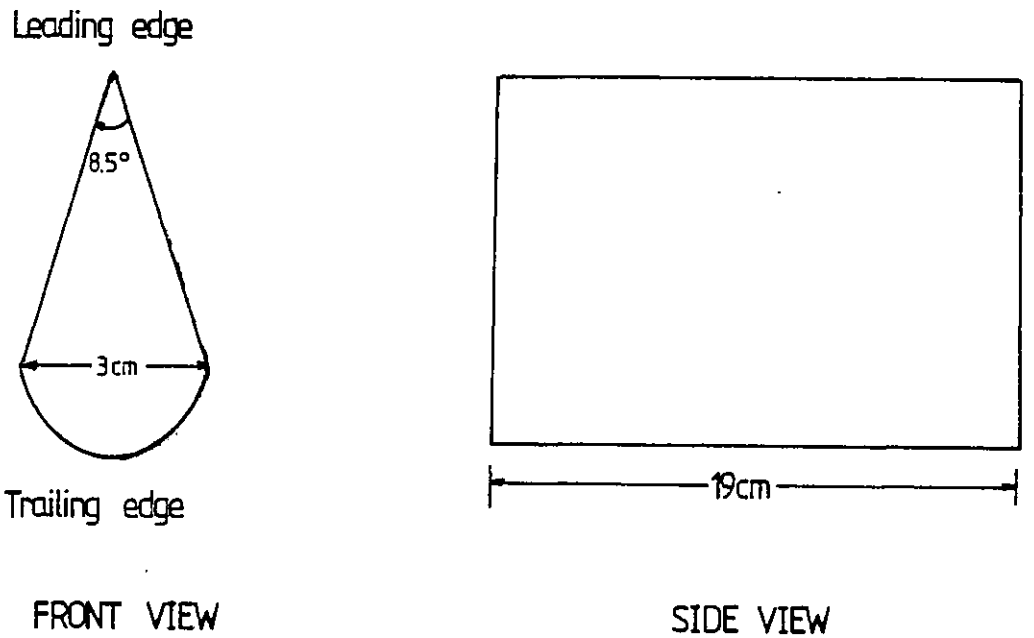

Fig. 8.41-1. Wedge dimensions used for the flow-visualization experiment.

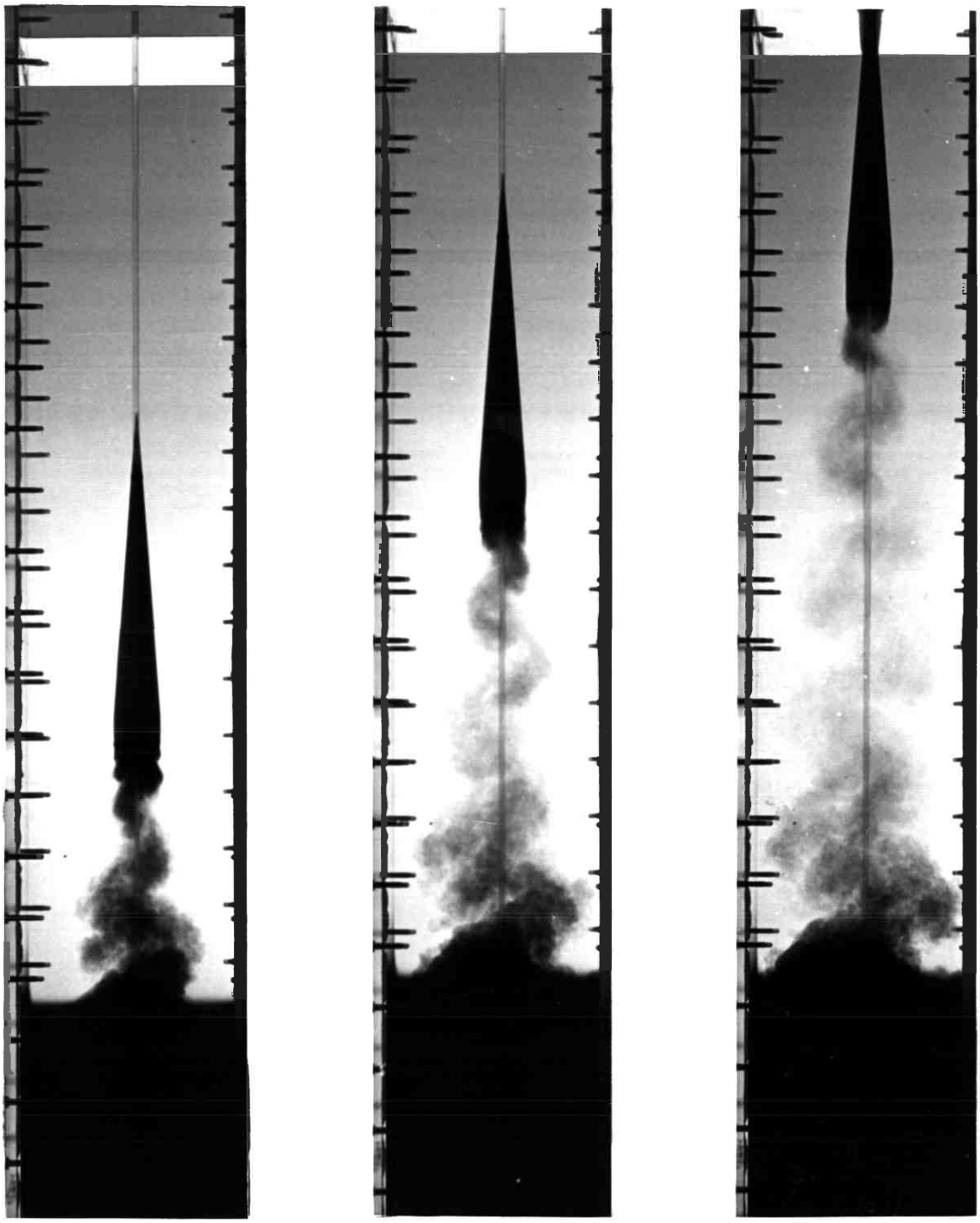

(a) (b) (c)

FIGURE 8.41-2: Photographs of Laminar Separation behind a Wedge

Figure 8.41-2 shows a succession of photographs taken during the rise of the wedge. The boundary layer and wake are clearly visible; and it is evident that the latter has a strongly oscillatory character.

(b) Turbulent Separation

In the experiment just described, the Reynolds number, based upon wedge height, is approximately 63400. This is too low to create a turbulent boundary-layer; and, even if it were not, the boundary layer would still be appreciably thinner than that to be investigated.

In a second experiment, therefore, two measures have been adopted which, together, ensure that the boundary layers on the surfaces of the wedge are both thick and turbulent: a wire gauze has been fixed to the wedge apex, with its plane at right angles to the motion; and the wedge surfaces have been roughened*. The geometrical details of these measures are as follows:

Grid size of wire gauze: 2 x 2mm
Mesh size of wire gauze: 25 grids/sq cm
Average roughness height: 0.6mm

Figure 8.41-3 presents a series of photographs taken with the rough wedge, fitted with the wire gauze. They show very

---

*The roughness element is a sand paper coded 127-2-36 ECL MD BC

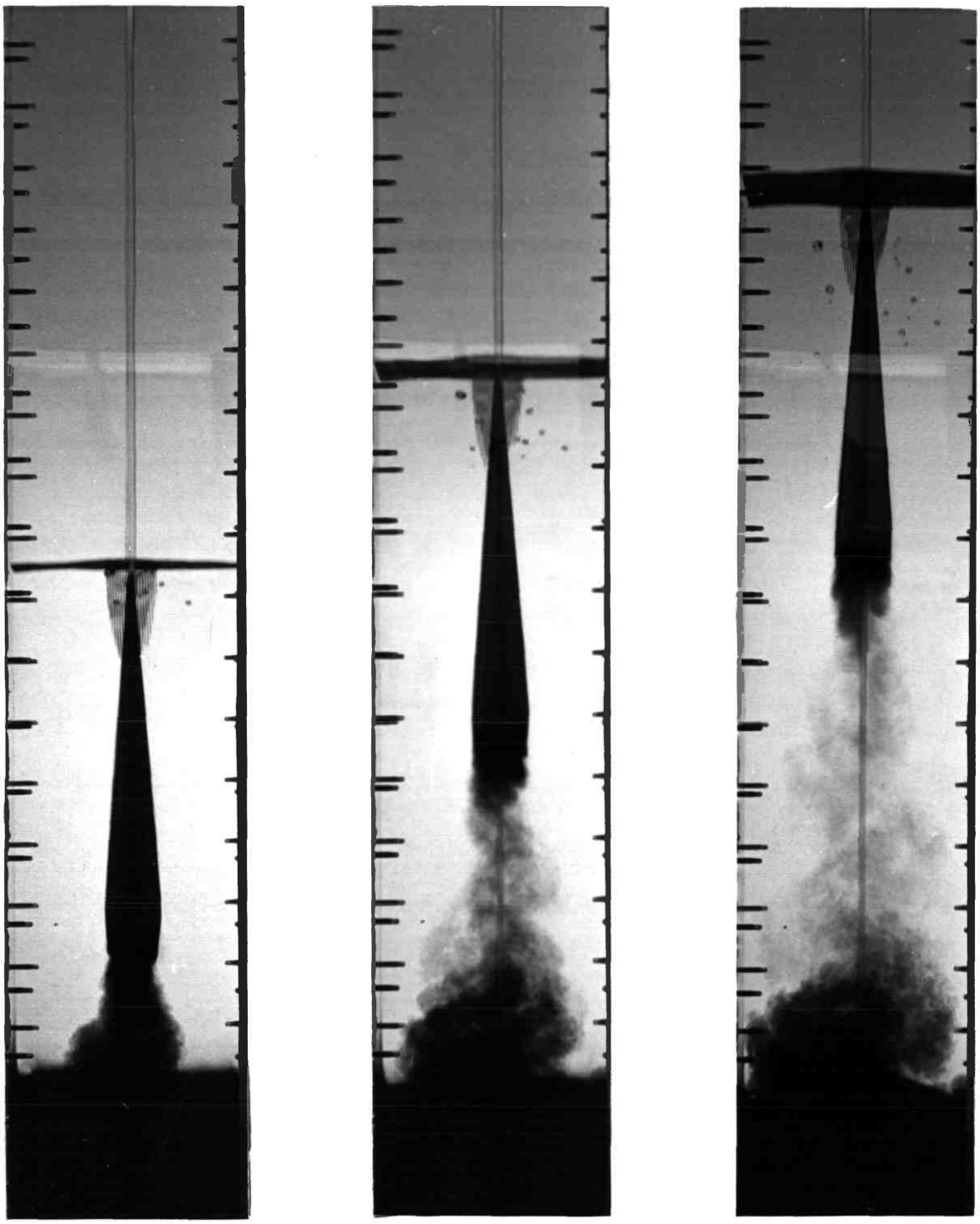

(a) (b) (c)

FIGURE 8.41-3: Photographs of Turbulent Separation behind a Wedge

clearly the boundary layer and wake behind the wedge and the strong oscillatory nature of the wake. Indeed, the generation and shedding of eddies very close to the wedge trailing-edge could be observed. This gives evidence of the vorticity fluctuations within the wake and of the intermittent nature of turbulence.

8.42 Flow Past a Thin Bar

(a) Laminar Separation

The second test body consits of a bar (Fig. 8.42-1) of which the cross-section is a rectangle. The leading edge is rounded to prevent premature separation there. The cross-section has a dimension of 18cm x 2.54cm and the body height measured from the base of the semi-circular leading-edge is 23 cm. The semi-circle has a radius of 1.2 cm.

The body is pulled upward through the fluid layers at a speed of approximately 0.35m/s.

Figures 8.42-2 shows a succesion of photographs taken as the body rises. The result is quite similar to that of the wedge.

(b) Turbulent Separation

In the above experiment, the Reynolds number, based upon body height, is approximately 80000. As in the case of the wedge, this Reynolds number is considered to be too low to either create a turbulent or thick enough boundary layer of interest. Thus, the bar surfaces have been similarly roughened and a wire screen is attached to the leading edge in a second

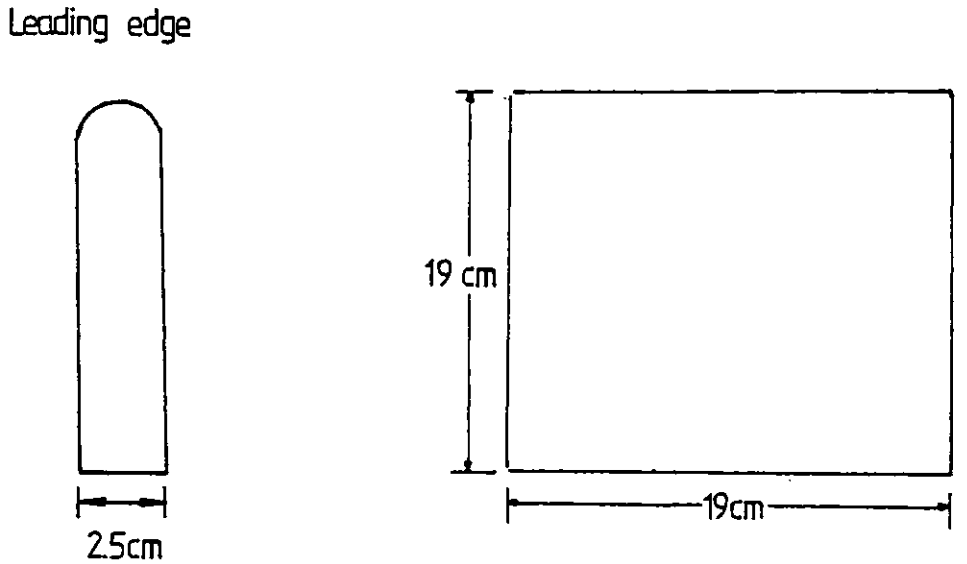

Fig. 8.42-1. Bar dimensions used for the flow-visualization experiment.

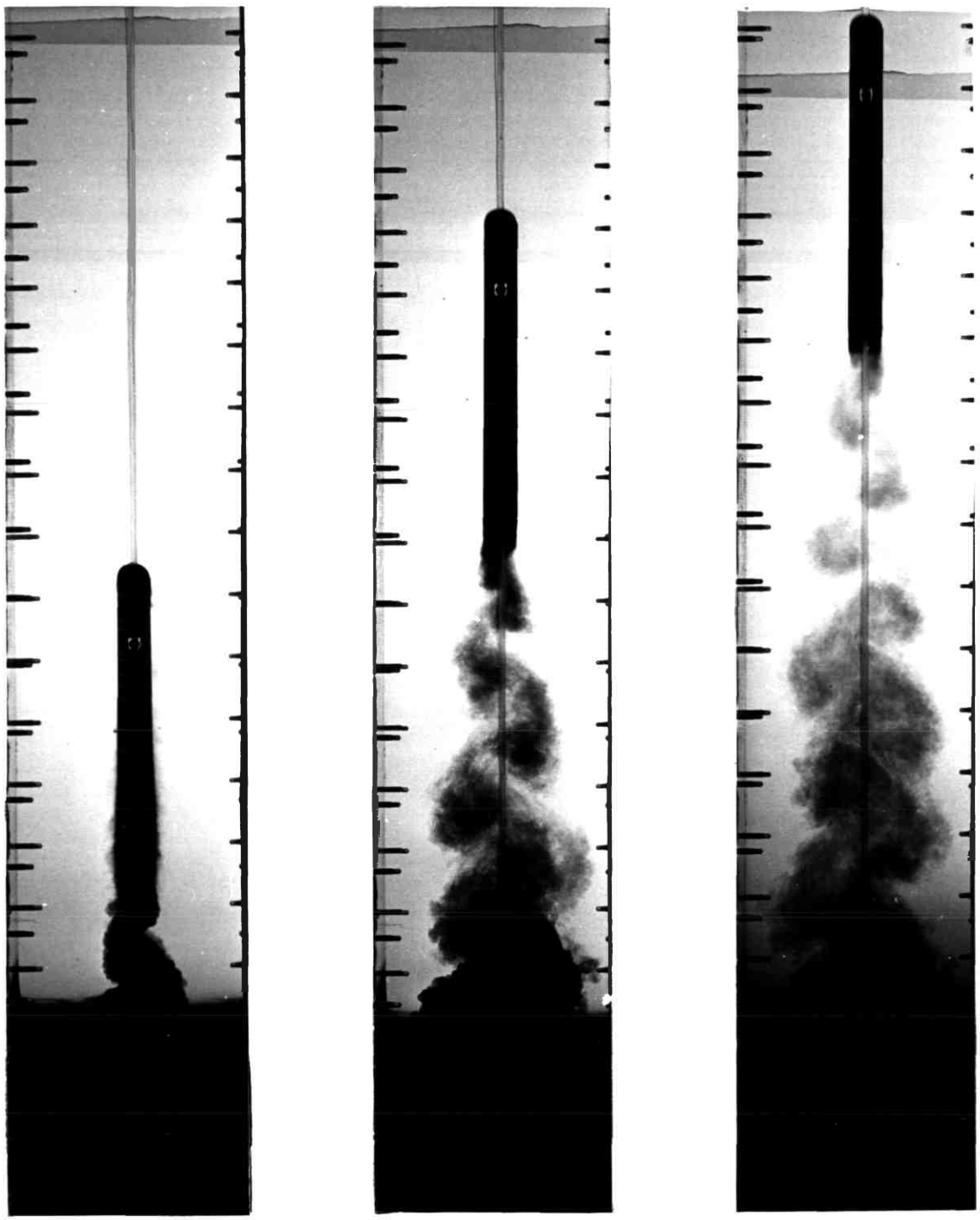

(a) (b) (c)

FIGURE 8.42-2: Photographs of Laminar Separation behind a Bar

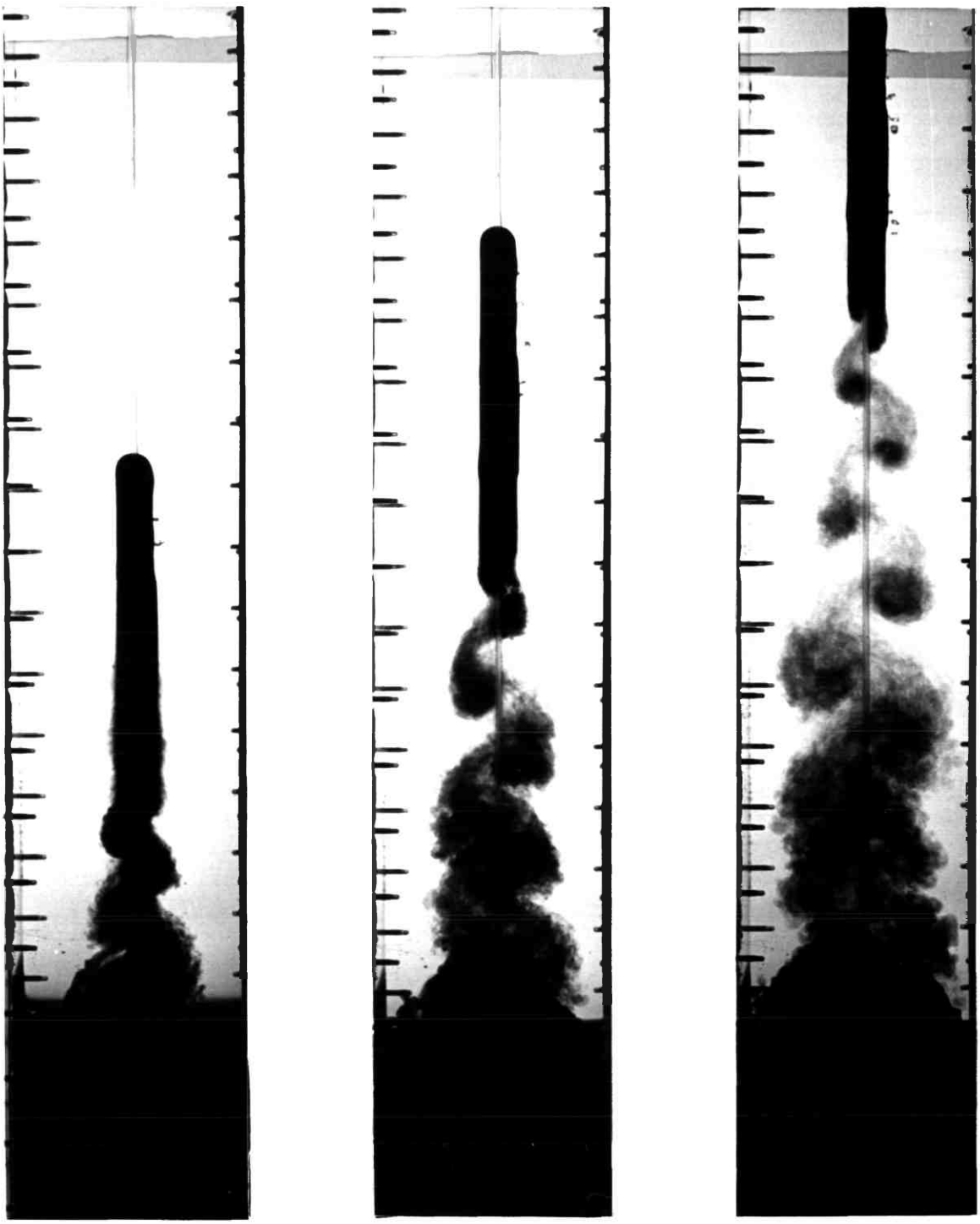

(a) (b) (c)

FIGURE 8.42-3: Photographs of Turbulent Separation behind a Bar (roughness-induced turbulence)

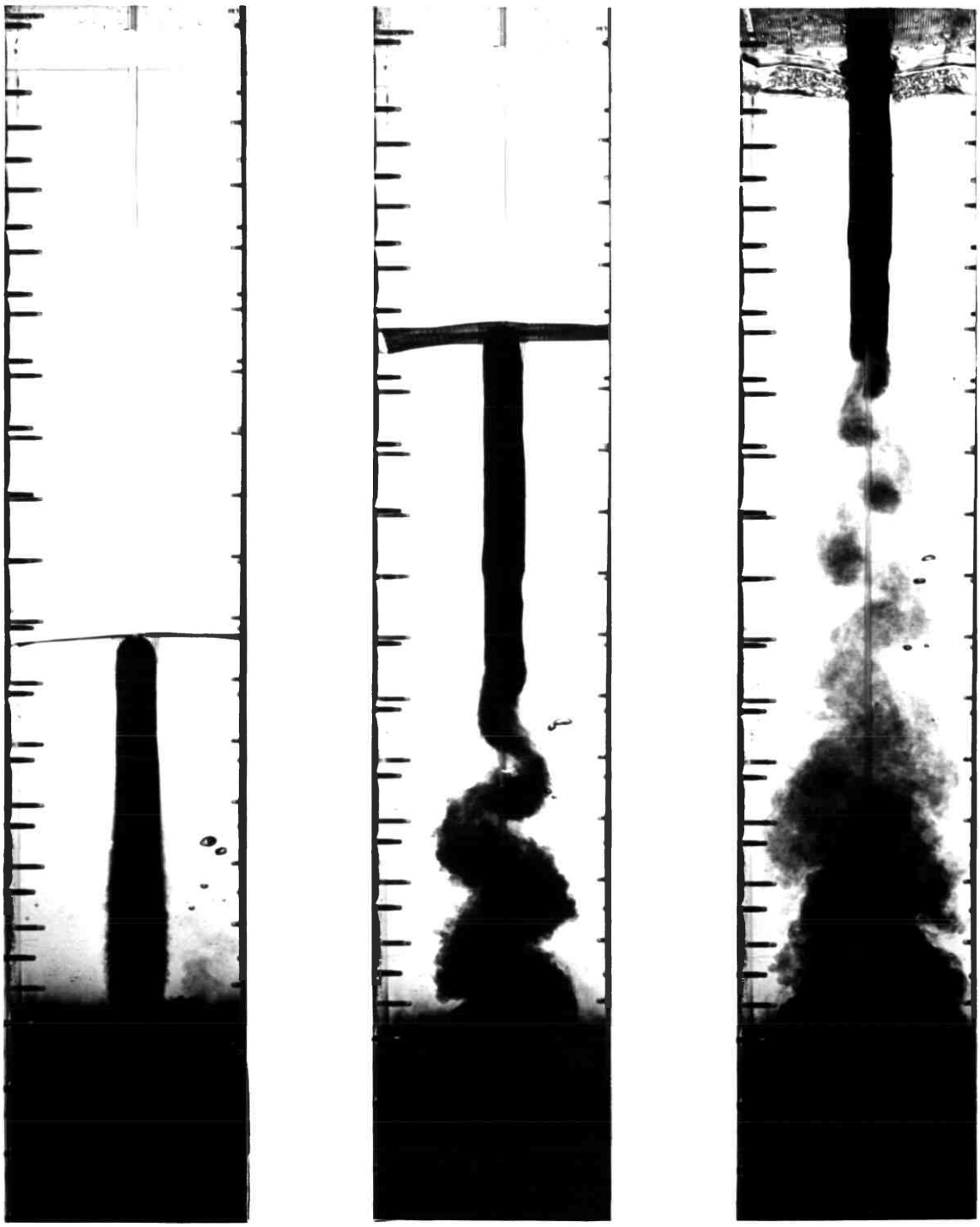

(a) (b) (c)

FIGURE 8.42-4: Photographs of Turbulent Separation behind a Bar (roughness-plus wire-screen-induced turbulence)

experiment.

Furthermore, an intermediate experiment has been carried out to investigate the effect of the roughness only. The results of these are shown in Figure 8.42-3. Figure 8.42-4 shows the photographs taken with a combination of roughness and wire screen. The oscillatory character of the wake behind the body is once again evident.

8.43 Flow Behind a Backward-facing Step

A "backward-facing step" model shown in figure 8.43-1 is used as the test body for the third investigation. The configuration has a test-section inlet height of 7.62cm with the step height of 2.54cm, thus giving an expansion ratio of 3:2. The step is formed from a perspex bar attached to a wall. The two walls are formed from sheets of stainless steel.

Like in the case of section 8.42, the leading edges of the bar and outer walls are rounded to avoid separation occuring there. The step is located some 8 step-heights downstream of the inlet to provide sufficient flow-development region. The reattachment wall is made to have a length of about 10 step-heights to ensure that the reattachment zone is adequately covered.

(a) Laminar Separation

The body is pulled upward through the fluid layers at a speed of approximately 0.4m/s.

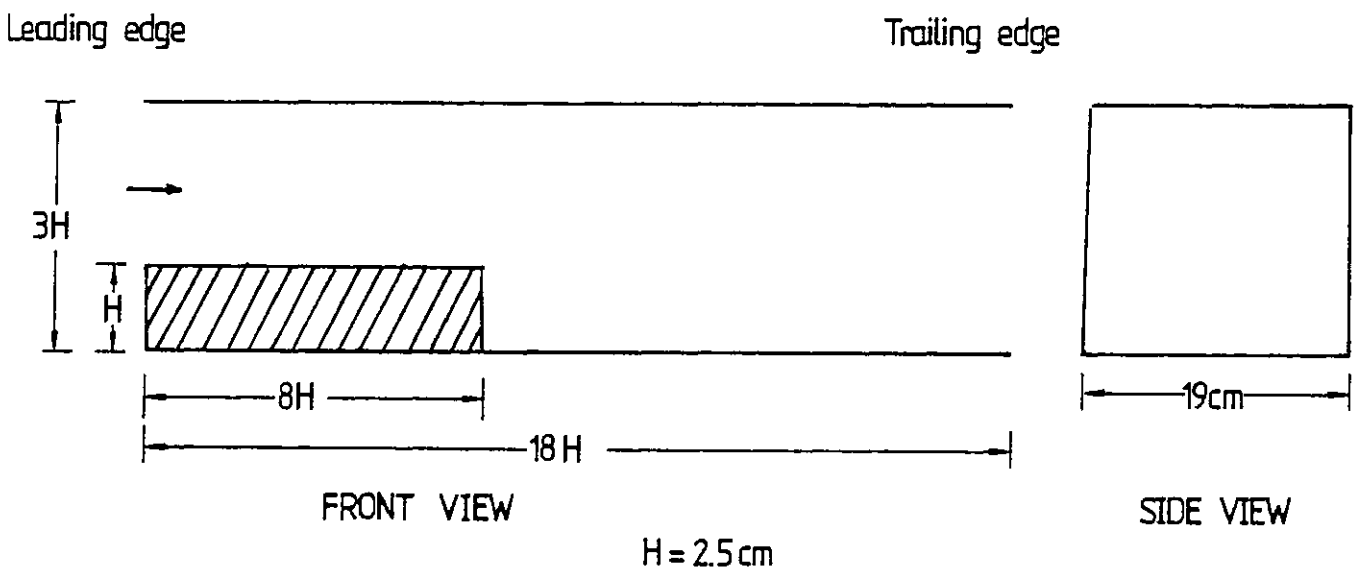

Fig. 8.43-1. Backward-facing step dimensions used for the flow visualization experiment.

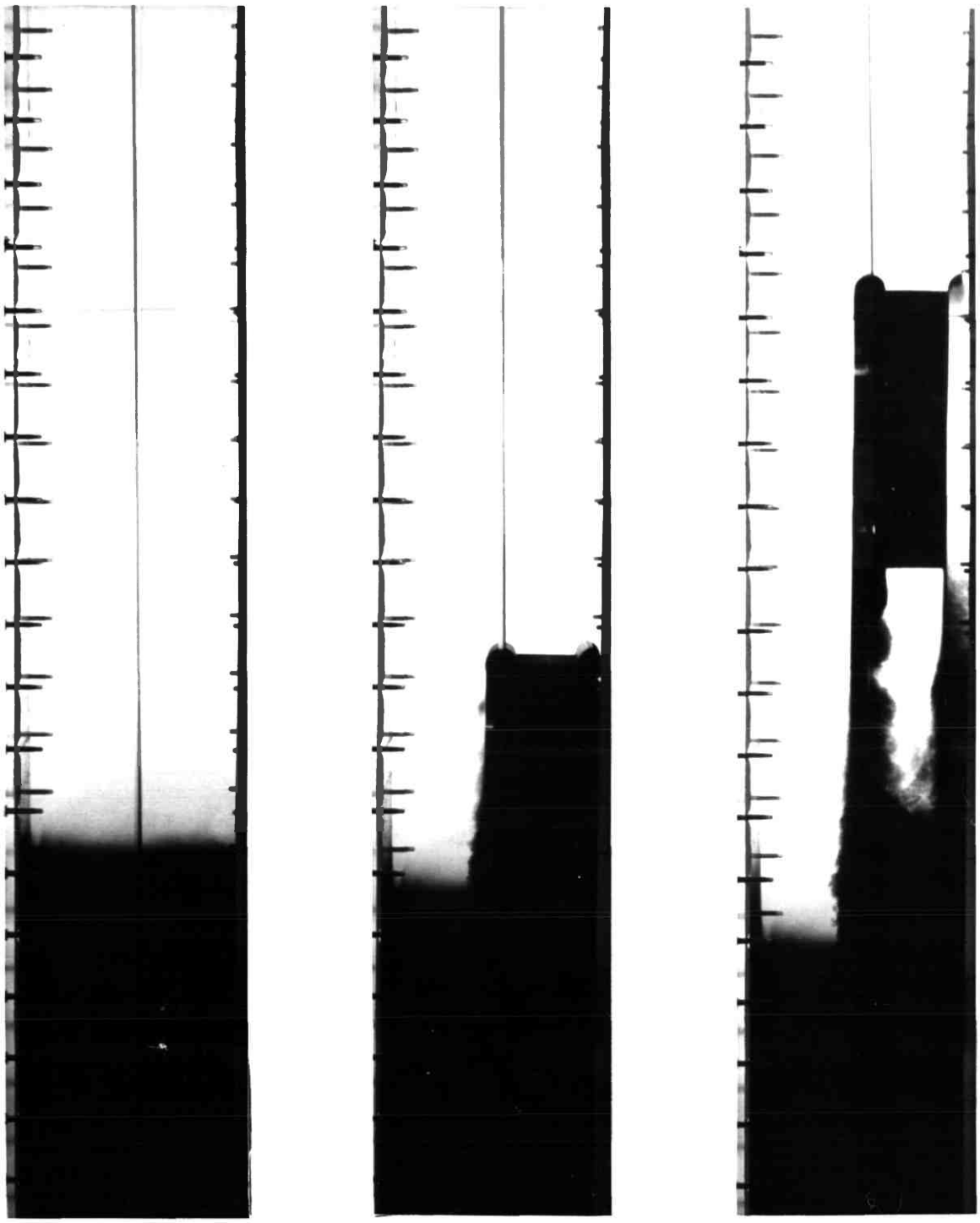

(a) (b) (c)

FIGURE 8.43-2: Photographs of Laminar Separation in a Backward-Facing Step

Figures 8.43-2 shows the succession of photographs taken as the body rises. The wake behind the step is clearly visible.

(b) Turbulent Separation

In the above experiment, the Reynolds number, based upon the development length (i.e. inlet to the step), is approximately 80790. Realising that this may be too low to create sufficient turbulence (if any) prior to separation, similar measures to those employed in the previous two cases have been introduced: the surface of the stepped wall in the development region has been roughened and a wire screen has been affixed to the leading edge. The geometrical details of these measures are exactly as those given earlier in section 8.41.

In figure 8.43-3 are presented the results of the investigation incorporating the above two measures. Once again, the wake behind the step can be seen clearly from the photographs. It appears as though the periodicity of the flow has indeed been reduced by the presence of the confining walls; but it is still present.

8.5 Discussion

8.51 Assessment of The Suitability of The Technique

The results achieved and described above appear to have justified the quite modest effort which has been expended. Certainly, the qualitative nature of the flows have been excellently revealed; and the presence of strong oscillation for both laminar and turbulent conditions might not have been so swiftly recognised had the technique not been used.

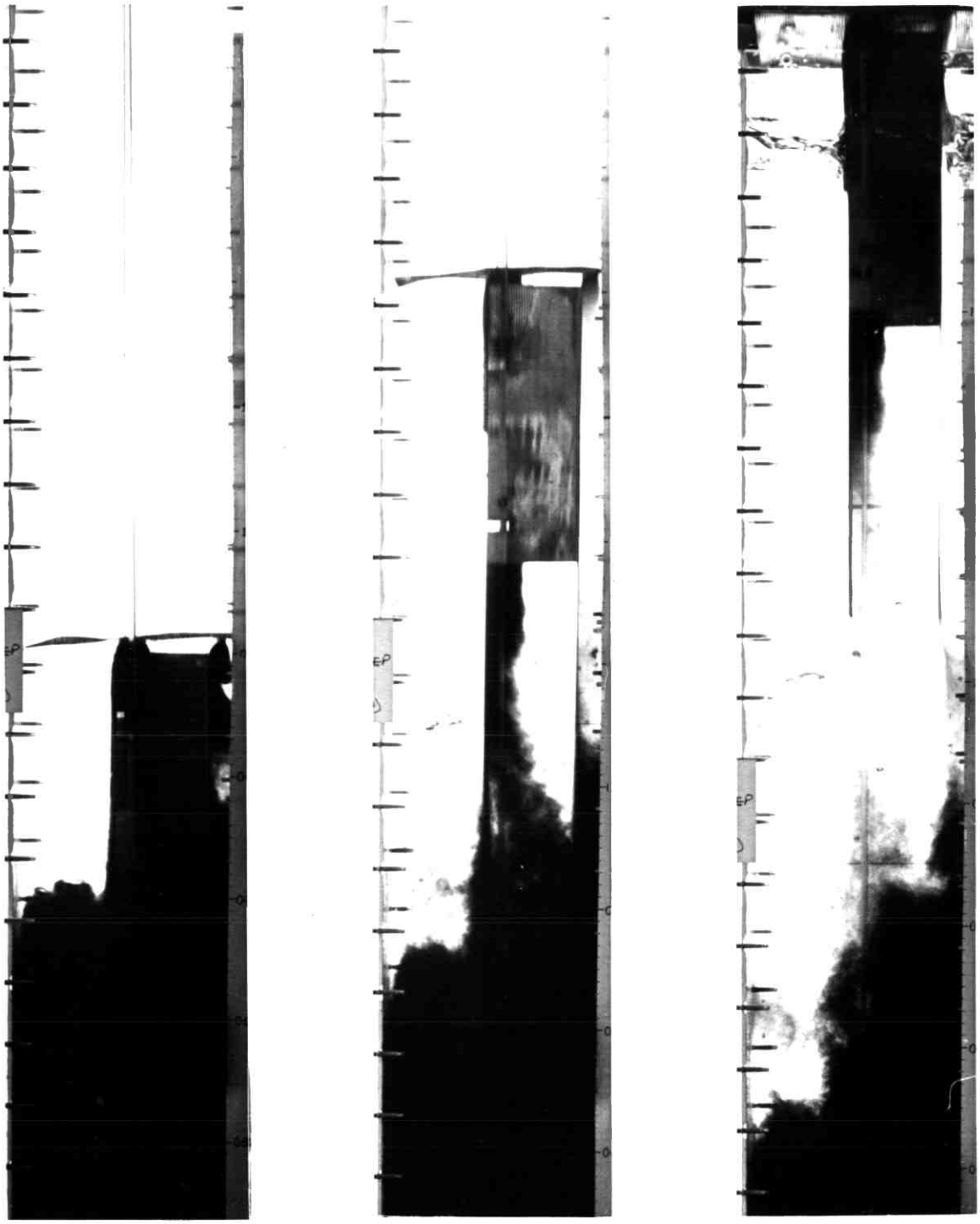

(a) (b) (c)

FIGURE 8.43-3: Photographs of Turbulent Separation
in a Backward-Facing Step

It could also be observed that the nature of the wake in the turbulent cases is similar to that in the accompanying laminar cases. The only major difference is that the test-body carries more fluid in the turbulent cases, the amount being larger the higher the degree of turbulence.

This observation shows that, despite the generally-held view of the diffusive nature of turbulence, it still has some concentrating characteristics and therefore, if looked at from this macro-scale view, its analysis would be highly simplified.

The low Reynolds numbers attainable with the present experimental technique are, of course, a disadvantage; but an increase of size can go a long way towards alleviating this.

For the purposes of the present investigation, the use of the gauze and the roughened surface will probably prove adequate.

8.52 Future Developments

The technique as described above is still at a preliminary stage. Two additional steps must be taken before it can be regarded as fully established: the photographs must be quantitatively evaluated; and the observations must be compared with numerical solutions of the equations.

It should be mentioned that there are other quantitative devices which can be applied. Thus, narrow light beams may be shone through the fluid to impinge on photocells of which the output can be recorded; and electrical-conductivity probes,

carried with the test body, can continuously register the local salt concentration.

The latter device, since it produces local and instantaneous information, can throw important light on the small-scale nature of the flow.

On the theoretical side, a suitable computer code may be used to solve first the steady-state hydrodynamic equations so as to generate a velocity field in body-fixed coordinates, and then to predict the behaviour of a "front" of dense fluid as it passes transiently over the body.

Two difficulties will have to be overcome in this computational work. First, "numerical diffusion" will of itself cause a blurring of the interface, quite apart from that which is physically produced, unless special devices of numerical analysis are adopted. One of these devices, namely that of particle tracking has been successfully used by Maxwell (1977) and Awn (1979); and has been demonstrated for the present application in appendix H.

The other difficulty arises from the fact that, even in body-fixed coordinates, the flow is not, as the experiments have revealed, truly steady; so even the hydrodynamic analysis requires a transient treatment. There is no essential difficulty about providing this; but it is still uncertain as to how the oscillation-triggering mechanism is to be properly introduced.

8.6 Closure

A new flow-visualization technique has been developed and used to study turbulent flows past a slender wedge, past a thin bar and in a backward-facing step.

The technique has provided insight into the flow around and behind the different bodies investigated; and, in doing so, it has provided a challenge to the computational-fluid dynamicist who wishes to predict the flows which it has revealed.

Developments are of course possible and desirable on both the experimental and the computational sides.

CHAPTER 9

CONCLUSIONS

9.1 Introductory Remarks

This, the final chapter of the thesis, provides a recapitulation of the successes and the failures of the present investigation, and proposes some guidelines for future research.

The remainder of the chapter comprises two sections. The first, (section 9.2) is devoted to a summary of the achievements of the study and the second (section 9.3) provides some recommendations for further work.

9.2 Achievements of The Present Work

The main achievements of the present work and the conclusions thereof can be summarised as follows:

9.21 The Theoretical Study

(a) A new version of the K-W model of turbulence has been developed. The modification consists of an additional-source term in the W-equation which is equal to:

$$\text{constant } X\rho W^{3/2}[|\text{grad}(k^{1/2}/W^{1/2})|]^2$$

Since $K^{1/2}/W^{1/2}$ is proportional to the length scale of turbulence, the term in brackets attains a fixed value near a wall, which is just what is required to ensure that the logarithmic velocity-profile is fitted; elsewhere the term may have less importance, although it is also significant in shear layers embedded in larger turbulent flows.

(b) The constants associated with the new term stated above have been determined. One of these was obtained directly from knowledge of the well-known logarithmic velocity-profile as 2.97 and a guess of the second as 2.0 (to make the term in bracket independent of sign) proved to be satisfactory.

(c) Near-wall boundary conditons for the new model have been prescribed. This was effected by devising formulae which fitted some well-known experimental conditions, and varied smoothly in between.

(d) The new model has been incorporated into a suitable computer program (the PHOENICS computer code of Spalding, 1982), with which tests could be made of the necessary grid-fineness requirements.

(e) Predictions of distributions of velocity, temperature, shear stress, turbulence energy etc., have been made by means of the computer program, for comparison with experimental data in various circumstances.

The physical situations considered are: turbulent pipe-flow; uniform - and non-uniform - pressure flow over a flat plate; flow over a flat plate with intense heat-transfer and with intense mass-transfer through the surface, flow and heat transfer downstream of an abrupt pipe-expansion; flow in a backward-facing step; flow in a plane jet; flow in a mixing layer and flow in a round jet.

(f) Grid-refineness tests have been done for all the calculations.

The new K-W model has been found to perform satisfactorily for all the above cases. However, like all other two-equation models, it has been found necessary to change one of the 'constants' of the turbulence model to give acceptable results for the round jet.

(g) A comparison of the present predicitons with those obtained with the old version of the K-W model showed the surperiority of the former. Comparisons were restricted to those cases in which performances of the two versions differ substantially.

(h) In addition, the new K-W model has been found to perform better than the K-ε model in predicting the flow downstream of a backward-facing step.

In general, the new version gives acceptable results with less arbitrariness of the model constants than ever before.

9.22 Experimental Study

(a) A new flow-visualization experimental technique has been devised for investigating turbulent flows containing small regions of recirculation.

This technique is the pulling-through-fluid-at-rest-kind; but it has the novel feature of using two fluids, one above the

other, and making their flow-induced intermingling visible by the use of a dye.

The experimental apparatus is relatively cheaper and faster to set up than conventional wind tunnels and water tunnels.

(b) The new flow-visualization technique has been used to study flows in the boundary layer and wakes of three different two-dimensional bodies namely: a wedge, a bar and a backward-facing step.

The body is at first immersed at rest within the lower fluid, which is coloured with a dye. A steady upward force is then suddenly applied to it; and as it emerges from the lower fluid, it is seen to carry with it, in its boundary layer and wake significant quantities of the lower fluid. Entrainment of clear (upper) fluid into the boundary layer and wake progressively dilutes the dye, with obvious visible consequences. A succession of photographs enables the various states of mixing to be recorded.

9.3 Suggestions for Future Work

The present investigation suggests a few areas where further research is needed. These are:

(a) Extension of Application of Model

The potential of the new K-W model seems much greater than that demonstrated in this thesis. Therefore, it may be

useful to extend the application of the model to:

(i) Flows with swirls like those in square ducts: This may involve the use of the so-called algebraic-stress model (Launder and Ying 1973; Tatchell, 1974) for simulating the secondary-flow driving terms.

(ii) Flows with chemical reaction: This will necessarily involve the incorporation of acceptable combustion models (e.g. the ESCIMO model of Spalding, 1976). However, having established the K-W model for the hydrodynamic and heat-transfer characteristics in the present investigation, it can satisfactorily serve as a standard in addition to which the effects of the combustion model can be tested.

(iii) Laminarizing boundary-layers: It will be interesting to develop a low Reynolds number version of the K-W model. This work may parallel that done by Jones and Launder (1972) in respect of the K-ε model.

(iv) Turbulent bouyant-flows: Some predictions have already been carried out by Malin and Spalding (1983) with a bouyancy-extended version of the K-W model described in the present study. The results appear encouraging with good agreement with experiment reported for both plane and axisymmetric turbulent plumes.

The model is however yet to be applied to cases in which gravity is not aligned with the main-flow direction e.g. a heated lake.

(v) Flows in curved and/or rotating surfaces: Other desirable flow situations are those in curved and/or rotating surfaces. A test may be carried out to check whether or not the new K-W model will require a similar treatment to the K-ε model, namely specifying one or more of the "constants" of the model as function(s) of the appropriate Richardson number(s).

(b) The Round-jet Problem

Agreement for the round jet could only be achieved by changing one of the 'constants' of the turbulence model from those used for the other flows. This entails changing the production term of the "vorticity" equation rather significantly.

Although this practice will probably meet the engineer's needs, it is unsatisfactory from a scientific point of view. The search for a model should therefore be continued which explains the different behaviour of the round jet.

In recent years, the discrepancy has been attributed to the dissipation equation or more generally, to the length-scale equation. For example, some successes have been achieved by the Launder group (Hanjalic and Launder, 1980) by sensitising the ε-equation to irrotational strain. However, this effects only a 50% improvement in predicted spreading-rate. It may be

desirable to see how this measure will affect the new K-W model.

In addition, it may be that future advances in simulating the pressure-strain term in the Reynolds stress equation will bring an answer. Or perhaps, other models that shift emphasis to the intermittent nature of turbulence (as revealed by the experimental investigation described in this Thesis) such as the "Two-Fluids Model" of Spalding (1983) will help to resolve the issue.

(c) The Eddy-viscosity Problem

Already, two-equation models employing a scalar eddy-viscosity like the present one have been applied to various flows. The eddy viscosity hypothesis is equivalent to retaining the leading term in an expansion of the (unknown) functional relation between Reynolds stress and mean-velocity distribution. So far, the success is partial, which may be attributed to the assumption of isotropic turbulence. Turbulence measurements have shown that in shear flows, the turbulence is very rarely even approximately isotropic (Champagne et al, 1970; Syred et al, 1971).

The relatively wide success of single-component effective viscosity models can be attributed to their use in flows where there is a single dominant velocity-gradient. The effective viscosity needs suit only the single turbulence-flux.

However, other more complex situations like the swirling flow or the bouyant flow mentioned above would probably require

a greater number of directional effective-viscosities to obtain accurate predictions.

This problem has been partially solved by using the so-called Reynolds stress models or their accompanying derivatives. These however, have proved expensive.

Therefore, it may be worthwhile to test the new l-Ω model of turbulence of Spalding (1981b) or the two-fluids model of Spalding (1983). The former may be regarded as an advanced form of the K-W model, in which, six equations are to be solved for the three components of length scale l, and the three components of vorticity, Ω. The equations are algebraic and are thus relatively easier to solve than the differential relations of the Reynolds stress models.

(d) Multiple-Scale Modelling

The K-ε model (which is currently the most popular two-equation model) like many others is a single-point model which adopts a single time scale proportional to the turbulence energy turnover time, namely K/ε (the ratio of the turbulence energy to the dissipation rate). However, it appears overly simplistic, at least conceptually, to assume that a single time scale can successfully characterize the rates of progress of different turbulence interractions. This realization has led to the development of the multiple-scale model (Hanjalic et al, 1979).

This approach is based on the realization that while the dissipation equation (or more generally, the length-scale

equation) and the turbulence kinetic-energy equation both contain production and dissipation terms, these processes occur in different spectral regions of the flow.

This model, despite its promise, is yet to be widely tested. It may be desirable to incorporate some of the features of it into the present K-W model.

(e) Improvement of the Experimental Technique

The flow-visualization technique as presented in the thesis, is still at its infancy. Further improvements are desirable to obtain reliable quantitative results from the experiment. For instance, narrow light beams may be shown through the fluid to impinge on photocells of which the output can be recorded; and electrical-conductivity probes, carried with the test body, can continuously register the local salt concentration. The latter device, since it produces local and instantaneous information, can throw important light on the small-scale nature of the flow.

In addition, it may be useful to drive the body upward with a motor to ensure steady motion through the fluid layers.

(f) Prediction of The Experimental Results

Having improved the experimental technique, it may be desirable to compare the results obtained from it with numerical solutions of the equations. A way of doing this may be to solve first the steady-state hydrodynamic equations so as to generate a velocity field in body-fixed coordinates and then to predict

the behaviour of a "front" of dense fluid as it passes transiently over the body.

However, two difficulties will have to be overcome in this computational task. These are the "numerical diffusion" which will of itself cause a blurring of the interface; and the large computer storage required for solving the transient equations.

The former problem may be solved by use of the particle-tracking method. There seems to be no essential difficulty about providing the necessary computer storage; but a means will need to be found to introduce the oscillation-triggering mechanism to simulate the observed periodicity of flows.

The particle-tracking technique has of course been used to predict qualitatively the flow in the backward-facing step of the present experimental investigation. However, further improvement of the technique is desirable to afford quantitative comparison with predictions.

REFERENCES

1 ABBOTT, D.E. and KLINE, S.J. (1962)
"Experimental Investigation of Subsonic Turbulent flow over Single and Double Backward-facing Steps". Trans. ASME J. Basic Engineering, 84D, Pp.317.

2 ABBOTT, I.H. and VON DOENHOFF, A.E. (1949)
Theory of Wing Sections. Mc Graw-Hill.

3 ABOELMEGUID, A.M., GOH, S.Y., ILEGBUSI, J.O. and SPALDING, D.B.(1981)
"Predictions of Complex Turbulent Flows using the PHOENICS Computer Code" Imperial College, Dept. of Mech. Eng. Report HTS/81/12.

4 ABRAMOVICH, G.N. (1963)
The Theory of Turbulent Jets. The MIT Press.

5 ALBERTSON, M.L., DAI, Y.B, JENSEN, R.A. and ROUSE, H. (1948)
"Diffusion of Submerged Jets". Proc. Am. Soc. Civil Engrs., 74, p.1751.

6 AL-SANEA, S. (1981)
"Numerical Modelling of Two-dimensional Shallow-water Flows". Ph.D. Thesis, University of London.

7 AWN, A.G.A. (1979)
"Numerical Modelling of Flows with Moving Interfaces". Ph.D. Thesis, University of London.

8 BOUSSINESQ, T.V. (1877)
Mem. pres. Acad. Sci. Third Edition, Paris XXII, p.46.

9 BRADBURY, L.J.S. (1965)
"The Structure of Self-preserving Turbulent Plane Jet". J. Fluid Mech., 23, pp. 31-64.

10 BRADSHAW, P. (1965)
"The Turbulence Structure of Equilibrium Boundary Layers". Nat. Phys. Labor. (NPL) Aero. Report No.1184.

11 BRADSHAW, P. (1965)
Turbulence 2nd Ed., Springer-Verlag, Heidelberg.

12 BRADSHAW, P. and HELLENS, G E (1966)
"The NPL 59in x 9in. Boundary-layer Tunnel" Aero. Res. Counc. Report, R & M No.3437.

13 BRADSHAW, P., FERRIS, D.H. and JOHNSON, R.F. (1964)
Turbulence In The Noise-producing Region Of A Circular Jet". J Fluid Mech., 19, pp. 591-624.

14 BRADSHAW, P., FERRISS, D.H. and ATWELL, N.P. (1967)
"Calculation of Boundary-layer Development using the Turbulent Energy Equation." J. Fluid Mechanics 28, p. 593.

15 BREMHORST, K. and WALKER, T.B. (1973)
"Spectral Measurements of Turbulent Momentum Transfer in Fully Developed Pipe Flow". J. Fluid Mech., 61 part 1, pp.173-186.

16 BREVOORT, M.J. and ARABIAN, B.D. (1958)
"Summary of Experimental Heat-transfer Measurements in Turbulent Flow for a Mach Number Range from 0.87 to 5.05". NACA TN 4248.

17 BROWN, G. and ROSHKO, A. (1971)
"The Effect of Density Difference on the Turbulent Mixing Layer". Paper delivered at AGARD Meeting, London, Sept. 1971.

18 BUZYNA, G and VERONIS, G (1971)
"Spin-up of a Stratified Fluid: Theory and Experiment". J. Fluid Mech. 50, pp. 579-608.

19 CARETTO, L S, GOSMAN, A D, PATANKAR, S V and SPALDING, D B (1973)
"Two Calculation Procedures for Steady, Three-dimensional Flows with Recirculation". Proc. 3rd Itern. Conf. on Numerical Methods in Fld. Mech., Vol. II, pp. 60-88.

20 CHATURVEDI, M.C. (1963)
"Flow Characteristics of Axisymmetric Expansions". ASCE, J. Hydraulics Division, 89, p. 61.

21 CHI, S.W. (1965)
"Friction and Heat Transfer in a Compressible Turbulent Boundary-layer on a Smooth Flat Plate". Ph.D. Thesis, University of London.

22 CHI, S.W. and SPALDING, D.B. (1966)
"Influence of Temperature Ratio on Heat Transfer to a Flat Plate Through a Turbulent Boundary-layer in Air". In Proc. 3rd International Heat Transfer Conference, Chicago.

23 CHIENG, C.C. and LAUNDER, B.E. (1980)
"On the Calculation of Turbulent Heat Transport Downstream from an Abrupt Pipe Expansion". Numerical Heat Transfer, Vol. 3, pp. 189-207.

24 CHOU, P.Y. (1945)
"On the Velocity Correlations and The Solution of the Equations of Turbulent Fluctuation". Quart. Applied Mathematics, Vol. 3, p. 38.

25 CLAUSER, F.H. (1954)
"Turbulent Boundary Layers in Adverse Pressure Gradients". J. Aero. Sci., Vol. 21, pp. 91-108.

26 CLUTTER, D.W. and SMITH, A.M.O. (1961)
"Flow Visualization by Electrolysis of Water". Aerosp. Eng., Vol. 20, pp. 24-27; 74-76.

27 COLES, D. and HIRST, E.A. (1969)
"Proceedings of the AFOSR-IFP Stanford Conference on Turbulent Boundary Layer Prediction-2; Compiled Data". Dept. of Mechanical Engineering, Stanford University.

28 CORCORAN, J.W. (1967)
"Application of the Isodensity-tracer in High-speed Photography". In Proc. 7th Int. Congress on High-speed Photography. (O Helwich, ed.) pp 466-471, O Helwich, Darmstadt, Germany.

29 CURRSIN, S. and KISTLER, A.L. (1954)
"The Free-stream Boundaries of Turbulent Flows". NACA, TN 3133.

30 DALY, B.J. and HARLOW, F.H. (1970)
"Transport Equations of Turbulence". Phys. Fluids, Vol. 13, p. 2634.

31 DAVIDOV, B.I., (1961)
"On the Statistical Dynamics of an Incompressible Turbulent Fluid". Dok. Akad. Nauk SSSR, 136, pp. 47-50 (Soviet Physics - Doklady, 6, p.10).

32 DAVIS, W. and FOX, R.W. (1967)
"An Evaluation of the Hydrogen Bubble Technique for the Quanlitative Determination of Fluid Velocities Within Clear Tubes". J. Basic Eng., 89, pp 771-781.

33 DATE, A.W. (1973)
"Prediction of Friction and Heat Transfer Characteristics of Flow in a Tube Containing a Twisted Tape". Imperial College, London, Mech. Eng. Dept. Report HTS/73/15.

34 DEARDORFF, J.W. (1970)
"A numerical Study of Three-dimensional Turbulent Channel Flow at Large Reynolds Numbers". J. Fluid. Mech., 41, p 453.

35 DEISSLER, R.G. (1955)
"Analysis of Turbulent Heat Transfer, Mass Transfer and Friction in Smooth Tubes at High Prandtl and Schmidt Numbers". NACA TR 1210.

36 DEWEY, J.M. (1971)
"The Properties of a Blast Wave Obtained From an Analysis of the Particle Trajectories". Proc. Roy. Soc. Ser A 324, pp. 275-299.

37 DURST, F. and RASTOGI, A.K. (1977)
"Turbulent Flow Over Two-dimensional Rences". First Symposium on Turbulent Shear Flows.

38 DURST, F. and RASTOGI, A.K. (1979)
"Turbulent Flow over 2-D Fences". Second Symposium on Turbulent Shear Flows.

39 EATON, J.K. and JOHNSTON, J.P. (1980)
"Turbulent Flow Reattachment: An Experimental Study of the Flow and Structure Behind a Backward-facing Step". Report MD-39 (Dept. Mech. Eng., Stanford University).

40 EATON, J.K. and JOHNSTON, J.P. (1981)
Comment on the Data for the 1981 AFOSR-IFP Stanford Conference on Complex Turbulent Flows, Stanford University.

41 EDE, A.J. (1959)
"Effect of an Abrupt Disturbance of the Flow on the Local Heat Transfer Coefficient in a Pipe". Heat 164, National Engineering Lab., East Kilbride, Glasgow.

42 EDE, A.J. HISLOP, C.I. and MOSSIR, R. (1956)
"Effect on the Local Heat-transfer Coefficient in a Pipe of an Abrupt Disturbance of the Fluid Flow: Abrupt Convergence and Divergence of Diameter Ratio 2:1". Proc. Inst. Mech. Eng. London, Vol. 170, p. 1113.

43 EDE, A.J., MORRIS, R. and BIRCH, E.S. (1962)
"The Effect of Abrupt Changes of Diameter on Heat Transfer in Pipes". NEL Report No. 73, National Engineering Laboratory, East Kilbride, Glasgow.

44 EMERSON, W.H. (1966)
"Heat Transfer in a Duct in Regions of Separated Flow". Proc. 3rd International Heat Transfer Conference, Paper No.26, pp. 267-275.

45 GIBSON, M.M. and SPALDING, D.B. (1972)
"Two-equation Model of Turbulence Applied to the Prediction of Heat and Mass Transfer in Wall Boundary Layers". ASME 72-HT-15, New York, pp. 1-8.

46 GOLDSTEIN, S. (ed., 1938)
Modern Developments In Fluid Dynamics. Clarendon Press, Oxford

47 GOLDSTEIN, S. (ed., 1965)
Modern Developments In Fluid Dynamics. Vol. 2, Dover.

48 GOSMAN, A. D., PUN, W.M., RUNCHAL, A.K., SPALDING, D.B., and WOLFSHTEIN, M. (1969)
Heat and Mass Transfer in Recirculating Flows
Academic Press.

49 GRUN, A.E., SCHOPPER, E and SCHUMACHER, B. (1953)
"Electron Shadowgraphs and Afterglow Pictures of Gas Jets at Low Densities". J. Appl. Phys. 24, pp. 1527-1528.

50 GUTMARK, E. (1970)
"The two-dimensional Turbulent Jet". MSc. Thesis, Thechnion-Isreal Institute of Technology.

51 HANJALIC, K. (1970)
"Two-dimensional asymmetric Turbulent Flow in Ducts". Ph.D. Thesis, University of London.

52 HANJALIC, K. and LAUNDER, B.E. (1972)
"A Reynolds-stress model of Turbulence and its Application to Asymmetric Shear Flows". J. Fluid Mechanics, Vol. 52, p. 609.

53 HANJALIC, K., LAUNDER, B.E. and SCHIESTEL, R.(1979)
"Multiple-Time Scale Concepts in Turbulent Transport Modelling". Second Symposium on Turbulent Shear Flows, Imperial College, London.

54 HARLOW, F.H. (ed., 1973)
"Turbulence Transport modelling". AIAA, New York.

55 HARLOW, F.H. and NAKAYAMA, P.I. (1967)
"Turbulent Transport Equations". The Physics of Fluids, Vol. 10, No.11, p. 323.

56 HARLOW, F.H. and NAKAYAMA, P.I. (1968)
"Transport of Turbulence Energy Decay Rate". Los Alamos Science Lab., University of California, Report LA-3854.

57 HARLOW, F.H. and WELCH J.E. (1965)
"Numerical Calculation of Time-Dependent Viscous Incompressible Flow of Fluid with Free Surface". The Physics of Fluids, Vol.8, No. 12, pp. 2182-2189.

58 HESKESTAD, G. (1965)
"Hot-wire measurements in a plane turbulent jet". J. of Appl. Mech., p. 1.

59 HILL, P.G. (1965)
"Turbulent Jets in Ducted Streams". J. Fluid Mech., Vol. 22, pp. 161-186.

60 HINZE, J.O. (1959)
Turbulence, McGraw Hill, New York.

61 HORSTMANN, C.C. and KUSSOY, M.I. (1968)
"Hypersonic Viscous Interaction on Slender Cones". AIAA J., 2, pp. 393-394.

62 HUNTER, W.W., Jr and FOUGHNER, J.T., Jr (1982)
"Flow Visualization and Laser Velocimetry for Wind Tunnels". NASA Conference Publication 2243, Proc. NASA workshop, Langley Research Centre, Hampton, Virginia.

63 ILEGBUSI, J.O. and SPALDING, D.B. (1982a)
"A Steady-unsteady Visualization Technique for Wake-flow Studies". CFDU, Imperial College, London, Report No. CFD/82/12

64 ILEGBUSI, J.O. and SPALDING, D.B. (1982b)
"Application of a new version of the K-W model of Turbulence to Equilibrium Boundary Layer Flow over a Flat Plate with (i) Intense Heat Transfer (ii) Streamwise Adverse Pressure Gradients". CFDU, Imperial College, London, Report No. CFD/82/14

65 ILEGBUSI, J.O. and SPALDING, D.B. (1982c)
"Application of a new version of the K-W model of Turbulence to a Boundary Layer with Mass Transfer". CFDU, Imperial College, London, Report No. CFD/82/15

66 ILEGBUSI, J.O. and SPALDING, D.B. (1983a)
"An improved version of the K-W model of Turbulence" CFDU, Imperial College, London, Report CFD/83/19 Also Paper to be presented at the National Heat Transfer Conference, Seattle, U.S.A., July 24-28, 1983.

67 ILEGBUSI, J.O. and SPALDING, D.B. (1983b)
"Steady Turbulent Flow in a Backward-facing Step" Paper at the 4th Symposium on Turbulent Shear Flows, University of Karlsruhe, F.R. Germany, September 12-14, 1983.

68 IRWIN, H.P.A.H. (1973)
"Measurements of a Self-preserving Plane wall Jet in a Positive Pressure Gradient". J. Fluid Mechanics, 16, pp. 33-63.

69 ISAKOFF, S.E. and DREW, T.B. (1957)
"Heat and Momentum Transfer in Turbulent Flow of Mercury". Inst. Mech. Engrs. General discussion of heat transfer. Proc. Amer. Soc. Mech. Engrs. 405, 479.

70 JENSEN, D.E. and WILSON, A.S. (1975)
"Prediction of Rocket Exhaust Flame Properties". Combustion and Flame, 25, pp 43-55.

71 JOHNSON, J.E. and MONAGHAN, R.J. (1951)
"Measurement of Heat Transfer and Skin Friction at Supersonic Speeds. Preliminary Results of Measurements on Flat Plate at Mach number of 2.5". ARC CP 59.

72 JONES, W.P. and LAUNDER, B.E. (1972)
"The Prediction of Laminarization with a 2-equation Model of Turbulence". Int. J. Heat and Mass Transfer, 15, p. 301.

73 KESTIN, J. and RICHARDSON, P.D. (1963)
"Heat Transfer Across Turbulent, Incompressible Boundary Layers". Int. J. Heat Mass Transfer,. Vol. 6, pp. 147-189.

74 KIM, J., KLINE, S.J. and JOHNSTON, J.P. (1978)
"Investigation of Separation and Reattachment of a Turbulent Shear Layer: Flow Over a Backward-facing Step". Report MD-37, Dept. of Mechanical Engineering, Stanford University.

75 KLEBANOFF, D.S. (1954)
"Characteristics of Turbulence in a Boundary Layer with Zero Pressure Gradient". NACA Report 1247, Washington.

76 KLEBANOFF, P.S. and DIEHL, F.W. (1951)
"Some Features of Artificially Thickened Fully Developed Turbulent Boundary Layers with Zero Pressure Gradient". NACA TN 3264.

77 KOLMOGOROV, A.N. (1942)
"Equations of Turbulent Motion in an Incompressible Fluid". Izv. Akad Nauk. SSSR. Seria Fizicheska VI, No. 1-2, pp 56-58 (English translation; Imperial College, London, Mech. Eng. Report ON/6, 1968).

78 KOLOVANDIN, B.A. and VATUTIN, I.A. (1969)
"On Statistical Theory of Non-uniform Turbulence". Paper presented at the Internantional Seminar on Heat and Mass Transfer, Herzeg Novi, Yugoslavia. Also, Int. J. Heat and Mass Transfer, Vol. 15 (1972), p. 2371.

79 KRALL, K.M. and SPARROW, E.M. (1966)
"Turbulent Heat Transfer in the Separated, Reattached and Redevelopment Regions of a Circular Tube". Trans. ASME, J Heat Transfer, Vol 88, No.1, pp 131-136.

80 LAUFER, J. (1954)
"The Structure of Turbulence in Fully-developed Pipe Flow". NACA, Report 1174, Washington.

81 LARMORE, L. and HALL, F.F. (1971)
"Optics for the Airborne Observer". SPIE J., Vol. 9, pp 87-94.

82 LAUNDER, B.E., MORSE, A., RODI, W. and SPALDING, D.B. (1972)
"The Prediction of Free Shear Flows - A Comparison of The Performance of Six Turbulence Models". Paaper presented at the NASA Conference on Free Shear Flows, Langley, Hampton, Virginia. Also: Imperial College, London, Dept. of Mech. Eng. Report TM/TN/A/19.

83 LAUNDER, B.E. and SPALDING, D.B. (1972a)
Mathematial models of turbulence. Academic Press, London.

84 LAUNDER, B.E. and SPALDING, D.B. (1972b)
"Turbulence Models and Their Application to The Prediction of Internal Flows". Heat and Fluid Flow, Vol.2.

85 LAWN, C.J. (1971)
"The Determination of the Rate of Dissipation in Turbulent Pipe Flow". J. Fluid Mech., 48, part 3, pp. 477-505.

86 LEFEUVRE, R. (1973)
"Laminar and Turbulent Forced Convection Processes Through in-line Tube Banks". Ph.D. Thesis, University of London.

87 LOGAN, E. and PHATARPHRUK, P. (1979)
"Turbulent Pipe Flow Past a Rectangular Roughness Element". ASME-CSME Applied Mechanics, Fluid Mechanics and Bioengineering Conference.

88 LUMLEY, J.L. (1975)
"Prediction Methods for Turbulent Flow - Introduction". Von Karman Institute for Fluid Dynamics, Lecture Series, No.76.

89 MALIN, M.R. and SPALDING, D.B. (1983)
"The Prediction of Vertical Plumes by Use of The K- and K-W Models of Turbulence". Unpublished work at Imperial College, London.

90 MALINA, J.A. and SPARROW, E.M. (1964)
"Variable-property, Constant-property, and Entrance-region Heat-transfer Results for Turbulent Flow of Water and Oil in a Circular Tube". Chemical Engineering Science, Vol.19, pp. 953-962.

91 MARTIN, B.W. and LOCKWOOD, F.C. (1964)
"Entry Effects in the Open Thermosyphon". J. Fluid Mech. Vol. 19, pp 246-256.

92 MATTHEWS, L. and WHITELAW, J.H. (1971)
"The Prediction of Film Cooling in the Presence of Recirculating Flows with a Two-equation Turbulence Model". Imperial College, London, Mech. Eng. Dept. Report HTS/71/31.

93 MAXWELL, T.T. (1977)
"Numerical Modelling of Free-surface Flows". Ph.D. Thesis, University of London.

94 MAXWORTHY, T. (1972)
"The Structure and Stability of Vortex Rings". J. Fluid Mech., Vol. 51, pp.15-32.

95 McCROSKEY, W. J., BOGDONOFF, S.M. and MCDOUGALL, J.G. (1966)
"An Experimental Model for the Sharp Flat Plate in Rarefied Hypersonic Flow". AIAA J., Vol. 4, pp. 1580-1587.

96 MAYDEW, R.C. and REED, J.F. (1963)
"Turbulent Mixing of Axisymmetric Compressible Jets (in the Half-jet Region) with Quiescent Air". SANDIA Corp. Aerothermodynamics, Sc-4764.

97 MELLOR, G.L. and GIBSON, D.M. (1966)
"Equilibrium Turbulent Boundary Layers". J. Fluid Mech., 24, part 2, pp. 225-253.

98 MELLOR, G.L. and HERRING, H.J. (1973)
"A Survey of Mean Turbulent Field Closure Models". AIAA Journal, 11, p. 590.

99 MERZKIRCH, W. (1974)
Flow Visualization. Academic Press, Inc.

100 MICKLEY, H.S., ROSS, R.C., SQUYERS, A.L. and STEWART, W.E. (1954)
"Heat, Mass and Momentum Transfer for Flow over a Flat Plate with Blowing and Suction". NACA TN 3208.

101 MILES, J.B. and SHIH, J.S. (1968)
"Similarity Parameter for Two-stream Turbulent Jet-mixing Region". AIAA J., 6, pp. 1429-1430.

102 MILLS, R.D. (1968)
"Numerical and Experimental Investigation of the Shear Layer Between Two Parallel Streams". J. Fluid Mech. 33, pp. 591-616.

103 MOFFAT, R.J. and KAYS, W.M. (1968)
"The Turbulent Boundary Layer on a Porous Plate: Experimental Heat Transfer with Uniform Blowing and Suction". Int J Heat Mass Transfer, Vol. 11, pp. 1547-1566.

104 MOON, L.F. and RUDINGER, G. (1977)
"Velocity Distributions in an Abruptly Expanding Circular Duct". ASME Journal of Fluids Engineering 99:2, pp. 226-230.

105 NEE, V.W. and LOVASZNAY, L.S.G. (1968)
"The Calculation of The Incompressible Turbulent Boundary Layer by A Simple Theory". Proc. of AFOSR/IFP Confernece on Computation of Turbulent Boundary Layers Vol.1, Stanford University. Also: Physics of Fluids, 12 (1969) p. 473.

106 NG , K.H. (1971)
"Predictions of Turbulent Boundary-Layer Developments Using a Two-equation Model of Turbulence". Imperial College, London, Mech. Eng. Dept. Report HTS/71/2.

107 NG , K.H. and SPALDING, D.B. (1970)
"Prediction of Two-dimensional Boundary Layers on Smooth Walls with a Two-equation Model of Turbulence". Imperial College, London, Mech. Eng. Dept. Report BL/TN/A/25.

108 NG ., K.H. and SPALDING, D.B. (1972)
"Some application of a Model of Turbulence to Boundary Layers near Walls". Phys. Fluids 15, p. 20.

109 PAPPAS, C.C. (1954)
"Measurement of Heat Transfer in the Turbulent Boundary Layer on FLat Plate in Supersonic Flow and Comparison with skin-friction Results". NACA TN 3222.

110 PAPPAS, C.C. and OKUNO, A.F. (1964)
"Measurement of Heat Transfer and Recovery Factor of A Compressible Turbulent Boundary Layer on a Sharp Cone with Foreign Gas Injection". NASA TN D-2230.

111 PATANKAR, S.V. and SPALDING, D.B. (1972)
"A Calculation Procedure for Heat, Mass and Momentum Transfer in Three-Dimensional Parabolic Flows". Int. J. Heat Mass Transfer, Vol. 15, pp. 1787-1806.

112 PATEL, R.P. (1970)
"A Study of Two-dimensional Symmetric and Asymmetric Turbulent Shear Flows". Ph.D. Thesis, McGill University.

113 PITZ, R.W. (1981)
"An Experimental Study of Combustion: The Turbulent Structure of a Reacting Shear Layer Formed at a Rearward-facing Step". NASA CR-165427.

114 POPOVICH, A.T. and HUMMEL, R.L. (1967)
"A New Method for Nondisturbing Turbulent Flow Measurements Very Close to a Wall". Chem. Eng. Sci., 22, pp. 21-25.

115 PRANDTL, L. (1925)
"Uber die ausgebildete Turbulenz". Zamm, 5, p. 136.

116 PRANDTL, L. (1945)
"Uber ein neues Formel-system fur die ausgebildete Turbulenz". Nachr Akad Wiss., Gottingen, Math.- Phys. KL 1945, p. 6 (with an appendix by K Wieghardt).

117 PRATAP, V.S. (1975)
"Flow and Heat Transfer in Curved Ducts". Ph.D. Thesis, University of London.

118 RANNIE, W.D. (1956)
"Heat Transfer in Turbulent Shear Flow". J. Aero Sci., Vol. 23, pp. 485-489.

119 REICHARDT, H. (1942)
"Gesetzmassigkeiten der freien Turbulenz". VDI Forshungsheft 414.

120 REICHARDT, H. (1957)
"Die Grundlagen des Turbulenten Warmeuberganges". Arch. Ges Warmetech. 2, pp. 129-142.

121 REYNOLDS, O. (1874)
"On The Extent and Action of The Heating Surface for Steam Boilers". Proc. Lit. Phil. Soc., Manchester, 14, pp. 7-12.

122 REYNOLDS, W.C.: KAYS, W.M. and KLINE, J.S. (1958)
"Heat Transfer in Turbulent Incompressible Boundary Layers - I Constant Wall Temperature". NASA Memo. 12-1-58W.

123 ROACHE, P.J. (1976)
Computational Fluid Dynamics. Hermosa Publications.

124 ROBERTS, L.W. (1972)
"Turbulent Swirling Flows with Recirculation". Ph.D. Thesis, University of London.

125 ROBINS, A.(1971)
"The Structure and Development of a Plane Turbulent Free Jet". Ph.D. Thesis, University of London.

126 ROQUEMORE, W.M. et al (1980)
"Velocity Measurement in a Bluff-body Diffusion Flame". AIAA Paper 80-1544.

127 RODI, W. (1972)
"The Prediction of Free Turbulent Boundary Layers by Use of a Two-equation Model of Turbulence". Ph.D. Thesis, University of London.

128 RODI, W. and SPALDING, D.B. (1970)
"A Two-parameter Model of Turbulence, and its Application to Free Jets". Warmeund Stoffubertragung, 3, p. 85.

129 ROTTA, J.C. (1951)
"Statistsckhe Theorie Nichthomogener Turbulenz". Zeitsch. f. Physik, Bd 129, pp. 547-572, and Bd 131, pp. 51-77 (English translation: Imperial College, Dept. Mech. Eng. Reports TWF/TN/38, 39 (1968)).

130 ROTTA, J.C. (1969)
"Uber eine Methode zur Berechnung Turbulenter Schertstromungen". Aerodynamische Versuchsanstalt Gottingen Report 69 A 14.

131 ROTTA, J.C. (1971)
"Recent Attempts to Develop a Generally Applicable Calculation Method for Turbulent Shear Flow Layers". AGARD Conference proceedings No. 93.

132 RUNCHAL, A.K. (1971)
"A Review of the Problems Associated with Numerical Instabilities". Imperial College, London, Dept. of Mech. Eng., Report EF/IN/10.

133 SABIN, C.M. (1965)
"An Analytical and Experimental Study of the Plane, Incompressible Turbulent Free-shear Layer with Arbitrary Velocity Ratio and Pressure Gradient". ASME Paper No. 64-WA/FE 19.

134 SAFFMAN, P.G. (1970)
"A Model of Inhomogeneous Turbulent Flow". Proc of the Roy. Soc., London, Ser. A, 317 pp. 417-433.

135 SAFFMAN, P.G. and WILCOX, D.C. (1974)
"Turbulence Model Predictions for Turbulent Boundary Layers". AIAA Journal, Vol. 12, No. 4.

136 SAMI, S., CARMODY, T. and ROUSE, H. (1967)
"Jet Diffusion in the Region of Flow Establishment". J. Fluid Mech., 27, pp. 231-252.

137 SAMUEL, A.E. and JOUBERT, P.H. (1974)
"A Boundary Layer Developing in an Increasingly Adverse Pressure Gradient". J. Fluid Mech., 66, Part 3, pp. 481-505.

138 SANDBURN, V.A. and SLOGAR, R.J. (1955)
"Study of the Momentum Distribution of Turbulent Boundary Layers in Adverse Pressure Gradients". NACA, TN 3264.

139 SARPKAYA, T. (1971)
"On Stationary and Travelling Vortex Breakdowns". J. Fluid Mech., 45, pp. 545-559.

140 SCHARDIN, H. (1942)
"Die Schlierenverfahren und ihre Anwendungen". Ergeb. Exakten Naturwiss. 20, pp. 303-439.

141 SCHLICHTING, H. (1968)
Boundary Layer Theory McGraw-Hill, New York.

142 SCHRAUB, F. A.; KLINE, S.J.; HENRY, J.; RUNSTADLER, P.W. and LITTELL, A. (1965)
"Use of Hydrogen Bubbles for Quantitative Determination of Time-dependent Velocity Fields in Low-speed Water Flows". J. Basic Eng. 87, pp. 429-444.

143 SEBAN, R.A. and BACK, L.H. (1962)
"Velocity and Temperature Profiles in Turbulent Boundary Layers With Tangential Injection". Trans ASME, J. Heat Trans., 84, Series C, pp. 45-54.

144 SIMPSON, J.E. (1972)
"Effects of the Lower Boundary on the Head of a Gravity Current". J. Fluid Mech., 53, pp. 759-768.

145 SLEICHER, C.A., Jr (1958)
"Experimental Velocity and Temperature Profiles for Air in Turbulent Pipe Flow". Trans. ASME, 80, p. 693.

146 SMITH, D.W. and WALKER, J.H. (1959)
"Skin Friction Measurements in Incompressible Flow". NASA TR R-26.

147 SPALDING, D.B. (1961)
"Heat Transfer to a Turbulent Stream From a Surface with Stepwise Discontinuity in Wall Temperature". Intern. Developments in Heat Transfer. ASME/Inst. Mech. Engrs. II, p. 439.

148 SPALDING, D.B. (1969)
"The Prediction of Two-dimensional, Steady Turbulent Flows". Imperial College, London, Heat Transfer Section Report EF/TN/A/16.

149 SPALDING, D.B. (1967)
"Heat Transfer from Turbulent Separated Flows". J. Fluid MEch., Vol. 27, P. 97.

150 SPALDING, D.B. (1971)
"Concentration Fluctuations in a Round Turbulent Free Jet". Chemical Engineering Science, Vol. 26, pp. 95-107.

151 SPALDING, D.B. (1972a)
"The K-W Model of Turbulence". Imperial College, London, Mechanical Engineering Dept. Report TM/TN/A/16.

152 SPALDING, D.B. (1972b)
"A Two-equation Model of Turbulence". VDI-Forsch Heft 549.

153 SPALDING, D.B. (1976)
"The ESCIMO Theory of Turbulent Combustion". Imperial College, London, Dept. of Mech. Eng. Report HTS/76/13.

154 SPALDING, D.B. (1977)
"GENMIX: A General Computer Program For Two-dimensional Parabolic Phenomena". Pergamon Press Ltd., Headington Hill Hall, Oxford.

155 SPALDING, D.B. (1981a)
"A General Purpose Computer Program for Multi-dimensional One and Two-phase Flow". Presented at Lehigh IMACS Conference, July; published in Mathematics and Computers in Simulation XIII 1981 pp. 267-276.

156 SPALDING, D.B. (1981b)
"Extract From the 1- Model of Turbulence". Unpublished work at Imperial College, London.

157 SPALDING, D.B. (1982a)
"A Modification to the K-W Model", Imperial College, London, CFDU File Note, February.

158 SPALDING, D.B. (1982b)
"Four Lectures on the PHOENICS Computer Code", CFDU, Imperial College, London, Report CFD/82/5.

159 SPALDING, D.B. (1983)
"Towards a Two-fluid Model of Turbulent Combusion in Gases with Reference to The Spark Ignition Engine". Paper presented at the Int. Conf. on Combustion in Engineering, Oxford, April.

160 SPENCER, B.W. (1970)
"Statistical Investigation of Turbulent Velocity and Pressure Fields in a Two-stream Mixing Layer". PhD Thesis, University of Illinois.

161 STRATFORD, B.S. (1959a)
"An Experimental Flow with Zero Skin Friction Throughout its Region of Pressure Rise". J Fluid, Mech., -, pp. 17-35.

162 SULLIVAN, P.J. (1971)
"Longitudinal Dispersion Within a Two-dimensional Turbulent Shear Flow". J. Fluid Mech., 49, pp. 551-576.

163 SUNYACH, M. and MATHIEU, J. (1969)
"Zone de Melang d'un Jet Plan; Fluctuations Induties Dans le Cone a Potentiel-intermittence". Int. J. Heat Mass Transfer, 12, pp. 1679-1697.

164 TATCHELL, D.G. (1975)
"Convection Processes in Confined, Three-dimensional Boundary Layers". Ph.D. Thesis, University of London.

165 TORII, K., NISHIWAKI, N. and HIRATA, M. (1966)
"Heat Transfer and Skin Friction in Turbulent Boundary Layer (sic) With Mass Injection". In: Proceedings of the Third International Heat Transfer Conference, AIChE-ASME, New York.

166 TENEKES, H. and LUMLEY, J.L. (1972)
A First Course in Turbulence. The MIT Press.

167 TOLLMIEN, W. (1926)
"Berechnung Turbulenter Ausbreitungsvorgange". ZAMM, Vol. 6, pp. 468-478, also translated as NACA TM 1085, 1945.

168 TOWNSEND, A.A. (1956)
The Structure of Turbulent Shear Flow. Cambridge University Press.

169 TOWNSEND, A.A. (1961)
"Equilibrium Layers and Wall Turbulence". J. Fluid Mech., 48, part 3, pp. 477-505.

170 TROPEA, C. and DURST, F. (1981)
Evaluators' comment, 1981 AFOSR-IFP Stanford Conference on Complex Turbulent Flows.

171 VAN DRIEST, E.R. (1956)
"On Turbulent Flow Near Wall". J. Aero Sci 23, pp. 1007.

172 VON KARMAN, TH (1939)
"The Analogy Between Fluid Friction and Heat Transfer". Trans. ASME, 61, pp. 705-710.

173 WILCOX, D.C. and ALBER, I.E. (1972)
"A Turbulence Model for High Speed Flows". Proceedings of the 23rd Heat Transfer and Fluid Mechanics Institute, Northridge, Califo, June 14-16, pp. 231-252.

174 WILCOX, D.C. and RUBESIN, M.W. (1980)
"Progress in Turbulence Modelling for Complex Flow Fields Including Effects of Compressibility". NASA Technical Paper 1517.

175 WILCOX, D.C. and TRACI, R.M. (1976)
"A Complete Model of Turbulence". AIAA Paper 76-351.

176 WINKLER, E.M. (1961)
"Investigation of Flat Plate Hypersonic Turbulent Boundary Layer with Heat Transfer". Trans. ASME Vol. 28, pp. 323-329.

177 WYGNANSKI, I. and FIEDLER, H. (1969)
"Some Measurements in the Self-preserving Jet". J. Fluid Mech., Vol. 38, part 3, pp. 577-612.

178 WYGNANSKI, I. and FIEDLER, H. (1970)
"The Two-dimensional Mixing Region". J. Fluid Mech., Vol 41, Part 2, pp. 327-362.

179 ZDRAVKOVICH, M.M. (1968)
"Smoke Observations of the Wake of a Group of Three Cylinders at Low Reynolds Numbers". J. Fluid Mech., Vol 32, pp. 339-351.

180 ZEMANICK, P.P. and DOUGALL, R.S. (1970)
"Local Heat Transfer Downstream of Abrupt Circular Channel Expansion". ASME, J. Heat Transfer, Vol. 92, p. 53.

NOMENCLATURE

Symbol	Meaning	Location of first Appearance
A	Area of cell surface	Eon. 4.22-1
a	Coefficient in the discretized equation	Eon. 4.23-1
B	Constant in chapter 3	Table 3.51
	Nozzle slot width elsewhere	Table 7.32-2
C	Convection coefficients in the discretized equation	Table 4.23-1
C_1, C_2, C_3, C_4, C_5 C_D, C_ω	Constants in the turbulence model	Eon. 3.42-6 to Eon. 3.43-6
C_f	Skin friction coefficient	Fig. 5.25-1
C_p	Specific heat	Eon. 3.52-1
$C_{p,wall}$	Wall static-pressure coefficient	Eon. 6.45-1
C_ϕ	General expression for coefficient of the finite-domain equations for variable ϕ	Eon. 4.51-1
D	Diffusion coeffieicnts of the discretised equations in chapter 4	Table 4.23-1
	Diameter	Table 7.32-2
	Diameter of **large** pipe	Fig. 6.34-1
d	Diameter of **small** pipe	Fig. 6.34-1

NOMENCLATURE

Symbol	Meaning	Location of first Appearance
E	Constant in log-law of the wall	Eqn. 3.51-1
$\widetilde{E}_{ij}$	Rate of Strain	Eqn. A3-2
F	Constant of proportionality in expanding grid formula	Eqn. 5.24-1
G_k	Generation of turbulence energy	Eqn. 3.43-4
g	Gravitational acceleration	Chapter 8
H	Step height	Fig. 6.41-1
H_{12}	Boundary-layer shape-factor	Fig 5.25-1
h	Nozzle-slot height	Table 7.22-1
J_Φ	Flux of Φ	Eqn. 4.22-1
K	Kinetic energy of turbulence	Eqn. 2.5-3
L	Body length	Chapter 8
L_R	Separation length	Table 6.35-1
l	Length scale	Eqn. 3.42-1
l_m	Mixing length	Eqn. 3.22-2
l_{ij}	length scale associated with cell node ij	Eqn. 4.43-3
M	Mass transfer number	Eqn. C1-1

NOMENCLATURE

Symbol	Meaning	Location of first Appearance
M_i	Theoretical momentum-excess flux	Eqn. G-1
M_e	Experimental momentum-excess flux	Eqn. G-1
$\dot{m}$	Mass transfer rate per unit area through surface	Eqn. 3.54-1
$\dot{m}_b$	Mass flow across boundary (inflow or outflow)	Eqn. 4.51-1
Nu	Nusselt number	Fig. 6.35-1
P	Mean pressure	Eqn. 2.2-6
$\tilde{P}$	Instantaneous pressure	Eqn. 2.2-2
$\overline{P}$	Average pressure field used in parabolic procedure	Sectn. 2.4
p	Fluctuating pressure component	Eqn. 2.2-6
P_J	Jayatillaka P-function	Eqn. 3.52-1
P_o	Free-stream pressure at inlet of calculation domain	Eqn. 6.45-1
P_{wall}	Wall-static pressure	Eqn. 6.45-1
P'	Pressure correction	Eqn. 4.25-2
P'_{pnew}	New value of the pressure correction at node P	Eqn. 4.52-4

NOMENCLATURE

Symbol	Meaning	Location of first Appearance
$\dot{q}$	Heat transfer rate per unit area at surface	Eqn. 3.52-1
R	Pipe radius	Fig. 6.25-1
R_1	Small pipe radius	Fig. 6.31-1
R_2	Large pipe radius	Fig. 6.31-1
Re	Reynolds number	Fig. 6.25-1
Re_2	Reynolds number based on the momentum thickness	Fig. 5.35-3
Re_x	Reynolds number based on axial length	Table 5.44-1
R_f	Under-relaxation factor	Eqn. 4.52-4
R_ϕ	Residual of the finite-domain equation for Φ	Eqn. 4.52-1
R_*	Residual	Eqn. 4.25-1
r	Radial coordinate measured from pipe centre	Fig. 6.24-1
r'	Radial coordinate measured from pipe wall ($\equiv$ R-r)	Fig. 6.25-1
r_o	Outer boundary of grid used for round jet calculation	Eqn. 7.44-1

NOMENCLATURE

Symbol	Meaning	Location of first Appearance
$r_{o_{in}}$	Value of r_o at inlet of calculation domain	Eqn. 7.44-1
$r_{1/2}$	Half-radius of round jet	Fig. 7.44-2
S	New function to be included in W equation	Eqn. 3.42-1
s	Skin-friction coefficient based on wall-layer quantities	Eqn. C1-1
S_k	Source for the K equation	Eqn. 3.43-1
S_p	Implicit part of a linearised source	Eqn. 4.43-1
S_u	Explicit part of a linearised source	Eqn. 4.43-1
S_w	Source for the W equation	Eqn. 3.43-2
S_ϕ	Source of the equation for ϕ	Eqn. 4.22-3
$S_{\phi r}$	Term added to the finite-domain equation for ϕ when inertial under-relaxation is applied	Eqn. 4.52-3
St	Stanton number	Fig. 5.45-1
T	Temperature (°K)	Eqn. 3.52-1
T_G	Temperature in the main stream (°K)	Fig. 5.45-1

NOMENCLATURE

Symbol	Meaning	Location of first Appearance
T_s	Temperature at the surface (wall)	Eqn. 3.52-1
t	Time (seconds)	Eqn. 2.2-1
t_o	Time large compared with largest turbulence time-scale	Eqn. 2.2-4
U	Mean velocity component along the stream direction	Eqn. 3.22-2
U_i	Mean velocity component along i-th direction	Eqn. 2.2-3
$\widetilde{U_i}$	Instantaneous velocity component along i-th direction	Eqn. 2.2-1
U	Generalised velocity vector	Eqn. 4.22-1
U_o	Maximum velocity excess	Fig. 7.1-3
U_{ij}	Streamwise velocity associated with cell node i,j	Eqn. 4.43-1
U_*	Friction velocity	Fig. 6.25-4
u_i	Fluctuating velocity component along i-th direction	Eqn. 2.2-3
U^+	Velocity normalised with friction velocity	Table 3.5l
$\overline{u_i u_j}$	Reynolds stress tensor	Eqn. 2.2-11

NOMENCLATURE

Symbol	Meaning	Location of first Appearance
$\overline{u_i\phi'}$	Turbulent flux of ϕ	Eqn. 2.3-4
V	Mean-velocity component along the cross-stream direction	Fig. 4.21-2
V_m	"Value" for mass in the finite-domain equation	Eqn. 4.51-1
V_o	Volume of control cell	Eqn. 4.22-1
V_{ij}	Cross-stream velocity associated with cell node ij	Eqn. 4.43-2
V	General expression for "Value" of the finite-domain equations for	Eqn. 4.51-1
W	Time-mean square vorticity fluctuations	Eqn. 3.42-1
X	Coordinate along main-flow direction	Section 2.4
X_i	Generalised cartesian tensor coordinate	Eqn. 2.2-1
y	Coordinate across the main stream direction	Eqn. 3.22-1
y^+	Non-dimensional distance from wall ($\equiv yU_*/\nu$)	Table 3.51

NOMENCLATURE

Symbol	Meaning	Location of first Appearance
y_G	Boundary-layer thickness (where $U = 0.99\ U_G$)	Fig. 5.24-1
y_L	Cross-stream height of the free stream grid-line	Eqn. 5.24-1
$y_{1/2}$	Half-width of jet	Table 7.22-1
Z	Generalised dependent variable	Section 3.22

Greek Symbols

δ	Boundary layer thickness	Eqn. G-3
δ_o	Characteristic width of free flows	Fig. 7.1-3
δ_1	Displacement thickness	Eqn. 5.31-1
δ_2	Momentum thickness	Fig. 5.25-1
δ_{ij}	Kronecker delta	Eqn. 2.5-1
ε	Rate of dissipation of turbulence energy	Eqn. 4.42-1
Γ	Exchange Coefficient	Eqn. 4.22-9
κ	Von-Karman constant in the logarithmic law ($\equiv 0.435$)	Eqn. 3.44-1
η	Non-dimensional cross-stream distance ($\equiv y/y_G$)	Eqn. 5.24-4

NOMENCLATURE

Greek Symbol	Meaning	Location of first Appearance
η^+	Reciprocal of velocity gradient in universal coordinates ($\equiv dy^+/du^+$)	Table 3.51
ϕ	Time-mean value of a scalar quantity	Eqn. 2.3-1
Φ	Instantaneous value of a scalar quantity	Eqn. 2.3-1
ϕ'	Fluctuating component of a scalar quantity	Eqn. 2.3-1
$\phi_{P,old}$	Previously-existing value of at node P	Eqn. 4.52-3
ϕ_t	Typical value of ϕ	Eqn. 4.52-2
ρ	Density	Eqn. 2.2-1
τ	Local shear-stress	Eqn. 3.51-1
$\bar{\tau}$	Average shear-stress	Eqn. 3.53-1
τ_s	Local shear-stress at the wall	Eqn. 3.53-1
μ	Dynamic viscosity	Eqn. 2.2-2
ν	Kinematic viscosity	Eqn. A2-3
ω, w	Fluctuating component of vorticity	Eqn. A3-4
$\bar{\omega}, \overline{w}$	Instantaneous component of vorticity	Eqn. A3-1
Ω	Major component of vorticity	Eqn. 3.43-6

NOMENCLATURE

Greek Symbol	Meaning	Location of first Appearance
λ	Inertial under-relaxation factor	Eqn. 4.52-3
σ	Prandtl number	Eqn. 2.3-4
Subscripts		
C, $\mathbb{C}$	Centre-line value	Fig. 6.31-1
ct	Edge of Couette-flow layer	Eqn. C1-2
E, W, N, S, P	In chapter 4, for east, west, north south and central nodes respectively of the finite-domain grid	Fig. 4.21-1
E	External (outer) stream (chapter 7)	Fig 7.1-1
e, w, n, s	East, west, north and south interfaces of the control volume respectively	Fig. 7.1-1
eff	Effective (Laminar + turbulent)	Eqn. 2.5-4
G,∞	Free stream	Eqn. 5.24-2 Fig. 5.24-1
Symbol		
h	Enthalpy (turbulent component)	Eqn. 3.52-2
h,l	Enthalpy (laminar component)	Eqn. 3.52-2

NOMENCLATURE

Symbol	Meaning	Location of first Appearance
I	Generalised node in chapter 4	Eqn. 4.22-7
	Internal (inner) stream in chapter 7	Fig. 7.1-1
Subscripts		
i	Component in the main-flow (x) direction	Eqn. 4.22-7
ij	Cell at the i-th and j-th locations of the finite-domain grid	Eqn. 4.43-1
J	Jet	Fig. 7.44-1
j	Component in the y-direction	Eqn. 2.5-1
K	Turbulence kinetic energy	Eqn. 3.43-1
m	Mass	Eqn. 4.51-2
max	Maximum	Table 7.22-1
ref	Reference	Fig. 6.45-2
Symbol		
t	Typical value	Eqn. 4.52-3
up	Upstream value	Eqn. 4.32-1
W	Time-mean square vorticity	Eqn. 3.43-2
ϕ	A Scalar quantity	Eqn. 4.22-1

NOMENCLATURE

Superscripts	Meaning	Location of first Appearance
a	Exponent for the similarity condition for equilibrium boundary layer with longitudinal pressure gradient	Eqn. 5.31-3
e	Exponent of expanding-grid formula	Eqn. 5.24-1
'	Fluctuating component	Eqn. 2.3-1

APPENDIX A

DERIVATION OF THE EQUATIONS FOR K AND W

A.1 Introduction

The purpose of this appendix is to present the derivation of the equations for K, the turbulence energy, and W, the time-mean square of the vorticity fluctuation employed in the turbulence model of chapter three.

The equations for K have been reported widely in the literature (see for example Hinze, 1959; Harlow and Nakayama, 1968, Townsend, 1980, and Tennekes and Lumley 1972). Thus, only the outlines of the derivation will be presented here for the sake of completeness.

The full derivation of the W-equation will however be presented as it has not been fully documented in the literature.

These derivations will be presented in tensor notations for the sake of simplicity.

A2 The K-equation

The equations of motion in the absence of external force fields take the following tensorial form for uniform-density Newtonian fluids:

$$\frac{\partial U_i}{\partial t} + \frac{\partial}{\partial x_j} U_i U_j = - \frac{1}{\rho} \frac{\partial P}{\partial x_i} + \frac{\partial}{\partial x_j} \left[\frac{\mu}{\rho} \left(\frac{\partial U_i}{\partial x_j} + \frac{\partial U_j}{\partial x_i} \right) \right] \qquad \text{(A2-1)}$$

where U_i is the component of instantaneous velocity in the x_i direction, P is the static pressure, and ρ and μ are the fluid density and dynamic viscosity, respectively.

An equation governing the transport of Reynolds stress, $\overline{u_i u_j}$, can be derived from the Navier-Stokes equation by multiplying equation (A2-1) by u_j and adding to it the same equation with suffixes i and j interchanged. Time averaging the resultant gives:

$$\frac{\partial}{\partial t}(\overline{u_i u_j}) + U_K \frac{\partial}{\partial x_K}(\overline{u_i u_j}) = -\{\overline{u_i u_K}\frac{\partial U_j}{\partial x_K} + \overline{u_j u_K}\frac{\partial U_i}{\partial x_K}\}$$

$$- 2\nu \overline{\frac{\partial u_i}{\partial x_K}\frac{\partial u_j}{\partial x_K}} - \nu\left(\overline{\frac{\partial u_i}{\partial x_K}\frac{\partial u_K}{\partial x_j}} + \overline{\frac{\partial u_j}{\partial x_K}\frac{\partial u_K}{\partial x_i}}\right) + \overline{\frac{p}{\rho}\left(\frac{\partial u_i}{\partial x_j} + \frac{\partial u_j}{\partial x_i}\right)}$$

$$- \frac{\partial}{\partial x_K}\{\overline{u_i u_j u_K} + \delta_{jK}\frac{\overline{u_i p}}{\rho} + \delta_{iK}\frac{\overline{u_j p}}{\rho}$$

$$-\nu\left(\frac{\partial}{\partial x_K}\overline{u_i u_j} + u_j\frac{\partial u_K}{\partial x_i} + u_i\frac{\partial u_K}{\partial x_j}\right)\} \qquad ,(A2\text{-}2)$$

where p is the fluctuating component of the static pressure P and the δ's are Kronecker deltas.

The turbulent kinetic energy equation can be obtained from equation (A2-2), by setting i = j and dividing by 2 giving:

$$\frac{\partial K}{\partial t} + U_K\frac{\partial K}{\partial x_K} = -\overline{u_i u_K}\frac{\partial U_i}{\partial x_K} - \nu\overline{\frac{\partial u_i}{\partial x_K}\frac{\partial u_i}{\partial x_K}} - \nu\overline{\frac{\partial u_i}{\partial x_K}\frac{\partial u_k}{\partial x_i}}$$

$$+ \frac{\partial}{\partial x_K}\{\nu\left(\frac{\partial K}{\partial x_K} + \frac{\partial\overline{u_i u_k}}{\partial x_i}\right) - \frac{\overline{u_i^2 u_K}}{2} - \frac{1}{\rho}\overline{\rho u_i}\,\delta_{iK}\}$$

in which K is defined as:

$$K \equiv \tfrac{1}{2}\,\overline{u_i^2} \qquad .(A2\text{-}4)$$

This equation when modelled and reduced to its high Reynolds number form becomes:

$$\frac{\partial K}{\partial t} + U_K \frac{\partial K}{\partial x_K} = - \overline{u_i u_K} \frac{\partial U_i}{\partial x_K} - \varepsilon + \frac{\partial}{\partial x_K} \left(\nu \frac{\partial K}{\partial x_K} + G_K \overline{u_i u_K} \frac{K}{\varepsilon} \frac{\partial K}{\partial x_i} \right) \qquad ,(A2\text{-}5)$$

where within the high Reynolds number approximation, ε, the rate of dissipation of K, is represented by $\nu \overline{\frac{\partial u_i}{\partial x_K} \frac{\partial u_i}{\partial x_K}}$; and $\frac{\overline{u_i^2 u_k}}{2}$ has been taken as $C_K \overline{u_i u_K} \frac{K}{\varepsilon} \frac{\partial K}{\partial x_K}$,

the form proposed by Daly and Harlow (1970).

The term $\nu \overline{\frac{\partial u_i \partial u_K}{\partial x_K \partial x_i}}$ which represents diffusive transport through the moleculer motion is neglected because it is insignificant at high Reynolds numbers. Diffusive transport through the pressure-fluctuating-velocity correlations, is also assumed negligble as a result of Irwin's (1973) study of self-preserving jets in adverse pressure gradients, and Hanjalic and Launder's (1972) work on asymmetric plane-channel flow. Even though Lumley (1975) has made suggestions for modelling this term, no proven models are as yet available.

The form of the K transport equation above can be further simplified by introducing the additional postulate $\overrightarrow{u_i u_k} = 2/3\, \delta_{ik} K$ into the diffusion term to yield:

$$\frac{\partial K}{\partial t} + U_K \frac{\partial K}{\partial x_K} = - \overline{u_i u_K} \frac{\partial U_i}{\partial x_K} - \varepsilon + \frac{\partial}{\partial x_K} \left(\nu \frac{\partial K}{\partial x_K} + \frac{\nu_t}{\sigma_K} \frac{\partial K}{\partial x_K} \right) \qquad ,(A2\text{-}6)$$

where σ_K is the turbulent kinetic energy Prandtl number.

By using the relation,

$$\varepsilon = C_D \rho K W^{1/2} \qquad ,(A2\text{-}7)$$

and equation (3.42-4) for the 'generation' term, the above equation in vector form reduces to equation (3.42-1) presented in section 3.42.

A3 The W-equation (i.e. equation for the time-mean-square vorticity fluctuations)

The instantaneous vorticity equation (see Tennekes and Lumley, 1972) reads:

$$\frac{\partial \tilde{w}_i}{\partial t} + \tilde{U}_j \frac{\partial \tilde{w}_i}{\partial x_j} = \tilde{w}_j \tilde{E}_{ij} + \frac{\nu \partial^2 \tilde{w}_i}{\partial x_j \partial x_j} \qquad ,(A3\text{-}1)$$

in which

$$\tilde{E}_{ij} = \tfrac{1}{2}\left(\frac{\partial \tilde{U}_i}{\partial x_j} + \frac{\partial \tilde{U}_j}{\partial x_i}\right) \qquad ,(A3\text{-}2)$$

and $\tilde{w}_i$ is the instantaneous vorticity component.

Multiplying through (A3-1) by $\tilde{w}_i$ gives

$$\underset{I}{\tilde{w}_i \frac{\partial \tilde{w}_i}{\partial t}} + \underset{II}{\tilde{w}_i \tilde{u}_j \frac{\partial \tilde{w}_i}{\partial x_j}} = \underset{III}{\tilde{w}_j \tilde{E}_{ij} \tilde{w}_i} + \underset{IV}{w_i \frac{\nu \partial^2 \tilde{w}_i}{\partial x_j \partial x_j}} \qquad .(A3\text{-}3)$$

Now, substitute for instantaneous quantities term by term and time average using the following notations:

$$\Omega_i = \tilde{w}_i - w_i \qquad ,(A3\text{-}4)$$

$$E_{ij} = \tilde{E}_{ij} - e_{ij} \qquad ,(A3\text{-}5)$$

$$U_j = \tilde{u}_j - u_j \qquad .(A3\text{-}6)$$

The terms crossed out in the following expressions are equal to zero. Thus:

Term I

$$(\Omega_i + w_i)\frac{\partial(\Omega_i + w_i)}{\partial t} = \Omega_i \frac{\partial \Omega_i}{\partial t} + \cancel{\Omega_i \frac{\partial \bar{w}_i}{\partial t}} + \cancel{\bar{w}_i \frac{\partial \Omega_i}{\partial t}} + \overline{w_i \frac{\partial w_i}{\partial t}}$$

thus:

TERM II Term I $= \frac{\partial}{\partial t}\{\tfrac{1}{2}\Omega_i^2\} + \frac{\partial}{\partial t}\{\tfrac{1}{2}w_i^2\}$ $\qquad .(A3\text{-}7)$

$$(\Omega_i + w_i)(U_j + u_j)\frac{\partial \tilde{w}_i}{\partial x_j} = \{\Omega_i U_j + \Omega_i u_j + w_i U_j + w_i u_j\}\frac{\partial(\Omega_i + w_i)}{\partial x_j}$$

$$= \overline{\Omega_i U_j \frac{\partial \Omega_i}{\partial x_j}} + \overline{\cancel{\Omega_i u_j \frac{\partial \Omega_i}{\partial x_j}}} + \overline{\cancel{w_i U_j \frac{\partial \Omega_i}{\partial x_j}}} + \overline{w_i u_j \frac{\partial \Omega_i}{\partial x_j}}$$

$$+ \overline{\cancel{\Omega_i U_j \frac{\partial w_i}{\partial x_j}}} + \overline{\Omega_i u_j \frac{\partial w_i}{\partial x_j}} + \overline{w_i U_j \frac{\partial w_i}{\partial x_j}} + \overline{w_i u_j \frac{\partial w_i}{\partial x_j}}$$

Therefore,

$$\text{Term II} = U_j \frac{\partial}{\partial x_j}\{\tfrac{1}{2}\Omega_i^2\} + U_j \frac{\partial}{\partial x_j}\{\tfrac{1}{2}w_i^2\} + \overline{w_i u_j}\frac{\partial \Omega_i}{\partial x_j} + \Omega_i u_j \frac{\overline{\partial w_i}}{\partial x_j} + \overline{w_i u_j}\frac{\overline{\partial w_i}}{\partial x_j} \qquad .(A3\text{-}8)$$

Term III

$$[\Omega_j + w_j][E_{ij} + e_{ij}][\Omega_i + w_i] = \{\Omega_j E_{ij} + \Omega_j e_{ij} + w_j E_{ij} + w_j e_{ij}\}[\Omega_i + w_i],$$

$$= \Omega_j E_{ij}\Omega_i + \cancel{\Omega_j \overline{E_{ij}} w_j} + \cancel{\Omega_j \overline{e_{ij}}\Omega_i} + \Omega_j \overline{e_{ij} w_i}$$

$$+ \overline{w_j E_{ij} w_i} + \overline{w_j} E_{ij}\Omega_i + \overline{w_j e_{ij}}\Omega_i + \overline{w_j e_{ij} w_i}$$

Thus,

$$\text{Term III} = \Omega_i \Omega_j E_{ij} + \overline{w_i w_j} E_{ij} + \Omega_i \overline{w_j e_{ij}} + \overline{w_i e_{ij}}\Omega_j + \overline{w_i w_j e_{ij}} \qquad .(A3\text{-}9)$$

Term IV

$$\nu \frac{\tilde{w}_i \partial^2 \tilde{w}_i}{\partial x_j \partial x_j} = \nu (\Omega_i + w_i) \frac{\partial^2}{\partial x_j \partial x_j}(\Omega_i + w_i)$$

$$= \nu \frac{\Omega_i \partial^2 \Omega_i}{\partial x_j \partial x_j} + \nu \cancel{\left| \frac{\partial^2 \overline{w_i}}{\partial x_j \partial x_j} \right| \Omega_i} + \nu \overline{w_i} \cancel{\frac{\partial^2 \Omega_i}{\partial x_j \partial x_j}} + \nu \overline{w_i} \frac{\partial^2 \overline{w_i}}{\partial x_j \partial x_j}$$

Expanding, therefore,

$$\text{Term IV} = \frac{\nu \partial^2}{\partial x_j \partial x_j}\left[\tfrac{1}{2}\Omega_i^2\right] - \nu \frac{\partial \Omega_i}{\partial x_j}\frac{\partial \Omega_i}{\partial x_j} + \frac{\nu \partial^2}{\partial x_j \partial x_j}\left[\overline{\tfrac{1}{2}w_i^2}\right] - \nu \frac{\partial \overline{w_i}}{\partial x_j}\frac{\partial \overline{w_i}}{\partial x_j} \qquad .(A3\text{-}10)$$

Hence, from equations (A3-3) to (A3-10), we have:

$$\frac{\partial}{\partial t}\{\tfrac{1}{2}\Omega_i^2\}+\frac{\partial}{\partial t}\{\tfrac{1}{2}\overline{w_i^2}\}+U_j\frac{\partial}{\partial x_j}\{\tfrac{1}{2}\Omega_i^2\}+U_j\frac{\partial}{\partial x_j}\{\tfrac{1}{2}\overline{w_i^2}\}$$

$$=-\overline{w_iu_j}\frac{\partial\Omega_i}{\partial x_j}-\Omega_i\overline{u_j\frac{\partial w_i}{\partial x_j}}-\overline{w_iu_j}\frac{\partial\overline{w_i}}{\partial x_j}+\Omega_i\Omega_jE_{ij}+\overline{w_iw_j}E_{ij}$$

$$+\Omega_i\overline{w_je_{ij}}+\overline{w_ie_{ij}}\Omega_j+\overline{w_iw_je_{ij}}+\frac{\nu\partial^2}{\partial x_j\partial x_j}\{\tfrac{1}{2}\Omega_i^2\}$$

$$-\nu\frac{\partial\Omega_i}{\partial x_j}\frac{\partial\Omega_i}{\partial x_j}+\frac{\nu\partial^2}{\partial x_j\partial x_j}\{\tfrac{1}{2}\overline{w_i^2}\}-\nu\frac{\partial\overline{w_i}}{\partial x_j}\frac{\partial\overline{w_i}}{\partial x_j}$$

.(A3-11)

Now, subtracting from equation (A3-11) the following equation for the square of the mean-vorticity (see Tennekes and Lumley, 1972),

$$\frac{\partial}{\partial t}\{\tfrac{1}{2}\Omega_i^2\}+U_j\frac{\partial}{\partial x_j}\{\tfrac{1}{2}\Omega_i^2\}=-\frac{\partial}{\partial x_j}\{\Omega_i\overline{U_jw_i}\}+\overline{U_jw_i}\frac{\partial\Omega_i}{\partial x_j}$$

$$+\Omega_i\Omega_jE_{ij}+\overline{w_je_{ij}}\,\Omega_i+\frac{\nu\partial^2}{\partial x_j\partial x_j}\{\tfrac{1}{2}\Omega_i^2\}-\nu\frac{\partial\Omega_i}{\partial x_j}\frac{\partial\Omega_i}{\partial x_j}$$

,(A3-12)

gives: $\frac{\partial}{\partial t}\{\tfrac{1}{2}\overline{w_i^2}\}+U_j\frac{\partial}{\partial x_j}\{\tfrac{1}{2}\overline{w_i^2}\}=\frac{\partial}{\partial x_j}\{\Omega_i\overline{u_jw_i}\}-2\overline{w_iu_j}\frac{\partial\Omega_i}{\partial x_j}$

$$-\overline{w_je_{ij}}\Omega_i+\overline{w_iw_j}E_{ij}+\Omega_i\overline{w_je_{ij}}+\overline{w_ie_{ij}}\Omega_j+\overline{w_iw_je_{ij}}$$

$$-\Omega_i\overline{u_j\frac{\partial w_i}{\partial x_j}}-\overline{w_iu_j}\frac{\partial\overline{w_i}}{\partial x_j}+\frac{\nu\partial^2}{\partial x_j\partial x_j}\{\tfrac{1}{2}\overline{w_i^2}\}-\nu\frac{\partial\overline{w_i}}{\partial x_j}\frac{\partial\overline{w_i}}{\partial x_j}$$

Therefore,

$$\frac{D}{Dt}\{\tfrac{1}{2}w_i^2\} = \frac{\partial}{\partial x_j}\{\Omega_i\overline{U_j w_i}\} + \overline{w_i w_j e_{ij}} + \overline{w_i w_j}E_{ij} + \Omega_j\overline{w_i e_{ij}}$$

$$+ \frac{\nu\partial^2}{\partial x_j \partial x_j}\{\tfrac{1}{2}w_i^2\} - \nu\overline{\frac{\partial w_i}{\partial x_j}\frac{\partial w_i}{\partial x_j}} - 2\overline{w_i u_j}\frac{\partial \Omega_i}{\partial x_j}$$

$$- \frac{\partial\{\overline{\Omega_i u_j w_i}\}}{\partial x_j} - \overline{u_j w_i}\frac{\partial \Omega_i}{\partial x_j} - \tfrac{1}{2}\frac{\partial}{\partial x_j}\{\overline{U_j w_i^2}\}$$

The relation $\frac{\partial}{\partial x_j}\{\overline{U_j w_i^2}\} \equiv \overline{\frac{u_j \partial w_i^2}{\partial x_j}}$ ..... has been

used for the last expression in the above equation.

Hence,

$$\frac{\partial}{\partial t}\{\tfrac{1}{2}\overline{w_i^2}\} + U_j\frac{\partial}{\partial x_j}\{\tfrac{1}{2}\overline{w_i^2}\} = -\overline{u_j w_i}\frac{\partial \Omega_i}{\partial x_j} - \tfrac{1}{2}\frac{\partial}{\partial x_j}(\overline{U_j w_i^2}$$

$$+ \overline{w_i w_j e_{ij}} + \overline{w_i w_j}E_{ij} + \Omega_j\overline{w_i e_{ij}} + \frac{\nu\partial^2}{\partial x_j \partial x_j}\{\tfrac{1}{2}w_i^2\} - \nu\overline{\frac{\partial w_i}{\partial x_j}\frac{\partial w_i}{\partial x_j}}$$

.(A3-13)

substituting,

$$W \equiv \overline{w_i^2} \qquad \text{(A3-14)}$$

and multiplying through equation A3-13 by 2 gives:

$$\frac{\partial W}{\partial t} + U_j \frac{\partial W}{\partial x_j} = \underbrace{- 2 \overline{u_j w_i} \frac{\partial \Omega_i}{\partial x_j}}_{\text{I}} \underbrace{- \frac{\partial}{\partial x_j} (\overline{u_j w_i^2})}_{\text{II}} + \underbrace{2 \overline{w_i w_j e_{ij}}}_{\text{III}}$$

$$+ \underbrace{2 E_{ij} \overline{w_i w_j}}_{\text{IV}} + \underbrace{2 \Omega_j \overline{w_i e_{ij}}}_{\text{V}} + \underbrace{\frac{\nu \partial^2 W}{\partial x_j \partial x_j}}_{\text{VI}} \underbrace{- 2\nu (\overline{\frac{\partial w_i}{\partial x_j}^2})}_{\text{VII}} \qquad \text{.(A3-15)}$$

This is as far as rigorous derivation can take us. We now therefore introduce certain hypothesis about the correlations appearing on the right-hand side. These hypothesis have been employed by many workers, for example Kolmogorov (1942) and in Hinze (1959) and already employed in the derivation of K above. They are:

(i) Transport hypothesis:

$$-\overline{u_j w_i^2} \equiv \frac{\nu_t}{\sigma_W} \frac{\partial W}{\partial x_j} \qquad \text{,(A3-16)}$$

where ν_t stands for the kinematic viscosity of the turbulent motion and σ_W is a corresponding Prandtl number for W of the order of unity. Substituting (A3-16) into Term II of (A3-15) and combining the latter with the molecular diffusion Term VI leads to:

$$- \frac{\partial}{\partial x_j} (\overline{u_i w_i^2}) + \frac{\nu \partial^2 W}{\partial x_j \partial x_j} = \frac{\nu_{eff}}{\sigma_W} \frac{\partial^2 W}{\partial x_j \partial x_j} \qquad \text{,(A3-17)}$$

in which ν_{eff} stands for the effective kinematic viscosity of the turbulent motion.

(ii) Dissipation hypothesis:

The disipation term VII of equation (A3-15) is modelled thus:

$$-2\nu\,\overline{\left(\frac{\partial w_i}{\partial x_j}\right)^2} \equiv -C_2 W^{3/2} f^* \qquad ,(A3\text{-}18)$$

where C_2 is a "dissipation constant" appropriate to W, and f^* is a function here defined as:

$$f^* = 1 + C_4\,(\partial l/\partial x_i)^{2C_5} \qquad ,(A3\text{-}19)$$

the term in the gradient of the length scale l being of course a development of the present investigation.

The remaining four terms of equation (A3-15) are the generation terms of the W equation modelled thus:

$$\underset{(a)}{-2\,\overline{u_j w_i}\,\frac{\partial \Omega_i}{\partial x_j}} + \underset{(b)}{2\,\overline{w_i w_j e_{ij}}} + \underset{(c)}{2\,\Omega_j \overline{w_i e_{ij}}} + \underset{(d)}{2\,E_{ij}\overline{w_i w_j}}$$

$$\equiv C_1 \nu_t\,(\mathrm{grad}\Omega)^2 + C_3\,\frac{W}{K}\,G_K \qquad .(A3\text{-}20)$$

Terms (a), (b) and (c) are sources. In particular, term (a) extracts vorticity from the mean-vorticity equation and is thus a source. Term (d) can be either a source or sink of W as the strain rate E_{ij} can be either positive or negative.

In the above equation (A3-20), G_k is the production rate of turbulent energy expressed in equation 3.43-4 and Ω is the major component of vorticity.

APPENDIX B

DETAILS OF THE RELATION BETWEEN THE TURBULENT-MODEL CONSTANTS

In the fully turbulent region close to a wall, the approximate balance between energy generation and decay, and the assumption that the convection terms in the W equation are negligble, lead to the following relation between the model "constants":

$$\left(\frac{4}{\sigma_W} + C_1 C_D\right) \kappa^2 - \frac{C_2' C_\mu}{C_D^{\frac{1}{2}}} + \frac{C_3 C_D^{\frac{1}{2}}}{C_\mu^{\frac{1}{2}}} = 0 \qquad ,(B\text{-}1)$$

where,

$$C_2' = C_2 + C_4 \left| |\text{grad}1|^2 \right|^{C_5} \qquad .(B\text{-}2)$$

The relation in equation (B-1) is consistent with the well-established "law of the wall" and the use of C_2' (given by relation in B-2) rather than C_2 is required to make it satisfied by values of the constants suggested by free shear-flows or the outer region of a wall boundary-layer.

If C_2 is substituted in place of C_2', a residual, R_*, is got at the right-hand side of the equation thus:

$$\left(\frac{4}{\sigma_W} + C_1 C_D\right) \kappa^2 - \frac{C_2 C_\mu}{C_D^{\frac{1}{2}}} + \frac{C_3 C_D^{\frac{1}{2}}}{C_\mu^{\frac{1}{2}}} = R_* \qquad .(B\text{-}3)$$

From equations (B-1) and (B-3),

$$C_2' = C_2 + \frac{R_* C_D^{\frac{1}{2}}}{C_\mu} \qquad .(B-4)$$

From equations (B-2) and (B-4),

$$C_4 = \frac{R_* C_D^{\frac{1}{2}}}{C_\mu \left[|\text{grad} l|^2 \right] C_5} \qquad .(B-5)$$

Grad l is shown to have a fixed value near a wall as follows:

$$\mu_t = \rho l K^{\frac{1}{2}} = \kappa y \sqrt{\tau \rho} \qquad .(B-6)$$

$$\text{Thus} \quad l = \kappa y \sqrt{\frac{\tau}{\rho K}} \qquad .(B-7)$$

Now, experimental data in boundary layers of various kinds (e.g. Laufer, 1954; and Klebanoff, 1954) have shown that $\tau/\rho K$ in such circumstances takes up a value of about $C_D^{1/2}$, where C_D=0.09.

Thus,

$$l = \kappa C_D^{1/4} y \qquad ,(B-8)$$

and,

$$\text{grad} l = \kappa C_D^{1/4} \qquad .(B-9)$$

From equations (B-5) and (B-9),

$$C_4 = \frac{R_* C_D^{\frac{1}{2}}}{C_\mu \left[\kappa^2 C_D^{\frac{1}{2}}\right] C_5} \qquad .(B\text{-}10)$$

Taking C_5 to be equal to 1 as a first guess (which indeed proved to be adequate), and substituting for R_* from equation (B-10) into equation (B-3), gives the expression in equation (3.43-1), i.e

$$(4\sigma_W^{-1} + C_1 C_D - C_\mu C_4)\kappa^2 - C_2 C_\mu C_D^{-\frac{1}{2}} + C_3 C_D^{\frac{1}{2}} C_\mu^{-\frac{1}{2}} = 0 \qquad .(B\text{-}11)$$

Substituting the asymptotic, high Reynolds number values of the constants as given in Table 3.43-1 gives:

$$C_4 = 2.97 \qquad .(B\text{-}12)$$

APPENDIX C

Details of The Wall Functions

In this appendix, the details of the wall functions used to account for the effects of mass transfer through the wall and turbulence diffusion are presented.

C1. Effect of Mass Transfer Through The Wall

The solution for the shear-stress coefficient, s for the couette-flow region near the wall when there is mass transfer is:

$$s = \left[\frac{\kappa}{\ln(ER_a s^{\frac{1}{2}})}\left\{1 - \frac{M}{4}\left[\frac{\ln(ER_a s^{\frac{1}{2}})}{\kappa}\right]^2\right\}\right] \qquad ,(C1\text{-}1)$$

in which,

$$M \equiv \dot{m}/(\rho U)_{ct} \qquad \text{(the mass transfer number)}, \qquad ,(C1\text{-}2)$$

$$R_a \equiv \left(\frac{\rho U y}{\nu}\right)_{ct} \qquad ,(C1\text{-}3)$$

and the subscript 'ct' denotes "edge of couette-flow layer". Unfortunately, the value of E is not a constant; but it depends upon the value of $Ms^{-1/2}$ in ways not yet agreed upon universally by theoreticians and experimenters; so the value of the closed-form solution is limited.

Therefore, following the procedure of Spalding (1975), an 'average' value of shear stress is postulated within the region. Now, the shear stress equation can be solved to yield:

$$\tau = \tau_s + \dot{m}U \qquad ;(C1\text{-}4)$$

in which τ_s is the shear stress at the wall.

The U-y profile is usually such that the velocity rises quickly to near its maximum value, thus:

$$\frac{U}{U_{ct}} = \left(\frac{y}{y_{ct}}\right)^n \qquad ,(C1\text{-}5)$$

where:

$$n \approx s^{\frac{1}{2}}/\kappa \qquad .(C1\text{-}6)$$

Therefore, it is reasonable as an approximation, to define an average shear stress $\bar{\tau}$ by:

$$\bar{\tau} = \tau_s + \frac{\dot{m}U_{ct}}{1+n} \qquad ,(C1\text{-}7)$$

and correspondingly,

$$\bar{s} = s + \frac{M}{(1+n)} \qquad .(C1\text{-}8)$$

It is thus assumed that the following relation (equation C1-9) for the simple flow without mass transfer is still valid but with $(\bar{s})^{1/2}$ inserted on the right-hand side of the equation in place of $s^{1/2}$.

From this, the shear stress $\bar{\tau}$ is obtained as given in equation (3.54-1).

For strong suction, the heat-transfer resistance of the near-wall region is known to have no influence. In order to account for this, and to accord with experimental evidence, the practice adopted in the present study has been to take as the value of $(T-T_s)/\dot{q}$ the <u>smaller</u> of that given by the shear stress obtained from the above formulae, on the one hand, and $(c_p\dot{m})^{-1}$ on the other; c_p being the specific heat at constant pressure.

C2. <u>Effect of Turbulence Diffusion</u>

The log-law wall functions based on equilibrium-boundary layer theory do not hold in the separation region because large-scaled turbulence diffusion appears to be the main mechanism bringing energy to the wall rather than the production.

A wall function suitable for these cases has been proposed by Launder and Spalding (1974) as follows.

The fluxes of momentum and heat to the wall are supposed to obey the relations:

$$\frac{U_P}{(\tau/\rho)_s} C_D^{1/4} K_P^{1/2} = \frac{1}{\kappa} \ln \left[\frac{E y_P (C_D^{\frac{1}{2}} K_P)^{\frac{1}{2}}}{} \right] \qquad ,(C2\text{-}1)$$

$$\frac{(T_p-T_s)}{\dot{q}_s} C_p\rho C_D^{\frac{1}{2}} K_p^{\frac{1}{2}} = \frac{\sigma_h}{\kappa} \ln\left[E y_p (C_D^{\frac{1}{2}} K_p)^{\frac{1}{2}}\right]$$

$$+ \frac{\sigma_h \pi/4}{\sin\pi/4} \left(\frac{A}{\kappa}\right)^{\frac{1}{2}} \left(\frac{\sigma_{h1}}{\sigma_h} - 1\right) \left(\frac{\sigma_h}{\sigma_{h1}}\right)^{1/4} \qquad .(C2\text{-}2)$$

In the above, U_p, τ_s, T_p, $\dot{q}_s$ and y_p are respectively the average velocity of the fluid at the near-wall node P, the shear stress on the wall in the direction of U_p, the time-average temperatures of the fluid at point P and the wall respectively, the heat flux to the wall and the distance of point P from the wall.

The quantity K_p, the value of K at P, is calculated from the budget of the turbulence energy over the wall-adjacent cell. The convection terms (which are small) are handled in such a way that assume all fluid leaving the cell has the energy at node P. The diffusional flux to the wall is set equal to zero.

The evaluation of the mean production and dissipation rates of K require special treatment. Figure C2-1 shows typical near-wall scalar cell (bounded on the west by a wall). The grid is so arranged that node P lies outside the viscous sublayer in the fully-turbulent region. The viscous sublayer thickness y_v is assumed to adjust itself according to the external turbulence energy such that the sublayer Reynolds number $Re_v \equiv y_v k_v^{1/2}/\nu$ (where K_v is the turbulence energy at the edge of the viscous sublayer) is a universal constant equal

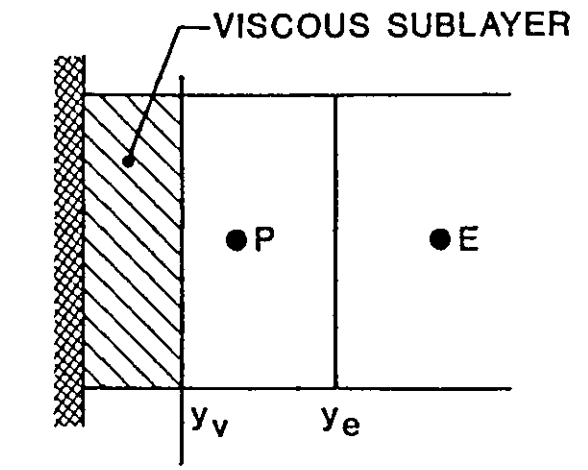

(a) Wall Adjacent Cell

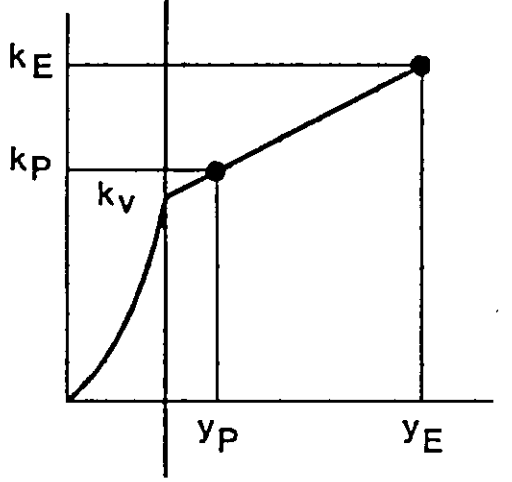

(b) Assumed Distribution of Turbulent Kinetic Energy

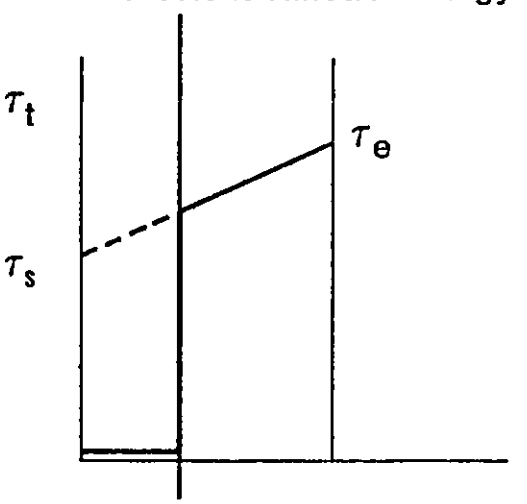

(c) Assumed Distribution of Turbulent Shear Stress

FIGURE C2-1: Near-Wall Physical Model.

to 20. The assumed kinetic energy distribution is also shown in figure C2-1.

As shown in this same figure, a piece-wise shear stress variation is assumed thus

$$\tau_t = \begin{cases} 0 & 0 \leq y < y_v \\ \tau_s + (\tau_e - \tau_s) y/y_e & y_v \leq y \leq y_e \end{cases} \quad .(C2\text{-}3)$$

The mean production rate of K per unit volume is evaluated by integrating $\tau_t \frac{\partial U}{\partial y}$ over the surface of the cell.

$$\text{Mean production rate} = \frac{1}{y_e} \int_{y_v}^{y_e} \tau_t \frac{\partial U}{\partial y} \, dy.$$

Substituting equation C2-3 for τ_t and equation C2-1 for U and integrating, gives;

$$\frac{\tau_s (U_e - U_v)}{y_e} + \frac{\tau_s (\tau_e - \tau_s)}{\kappa^* \rho K_v^{\frac{1}{2}} y_e} \left(1 - \frac{y_v}{y_e}\right) \quad ,(C2\text{-}4)$$

where $\kappa^* = \kappa C_D^{1/4}$.(C2-5)

The mean dissipation rate of kinetic energy is evaluated by integrating the ε distribution over the volume of the cell. In the viscous sublayer the dissipation rate has been shown to be equal to $2\nu \left(\partial k^{1/2} / \partial y \right)^2$ by Pope and Whitelaw (1976) and coupling this with the assumed parabolic variation of K($= K_v (y/y_v)^2$) in this same region gives:

$$\varepsilon = 2\,K_v/y_v^{\,2} \qquad .(C2\text{-}6)$$

In the fully-turbulent region, following Spalding (1967), ε is taken to vary as

$$\varepsilon = K^{3/2}/C_t Y \qquad ,(C2\text{-}7)$$

where C_t is a universal constant taken as 2.55. The mean dissipation rate is then evaluated by integrating equation (C2-6) over the viscous sublayer and equation (C2-7) over the fully turbulent region (assuming a linear K variation as shown in Figure C2-2) and averaging the resultant to obtain:

$$\bar{\varepsilon} = \frac{1}{y_e}\,2\,\frac{K_v^{\,3/2}}{Re_v} + \frac{1}{y_e c_t}\left[\frac{2}{3}\,(K_e^{\,3/2}-K_v^{\,3/2})+2a(K_e^{\,\frac{1}{2}}-K_v^{\,\frac{1}{2}})+\lambda_\varepsilon\right] \qquad ,(C2\text{-}8)$$

where

$$\lambda_\varepsilon = a^{3/2}\log\left[\frac{(K_e^{\,\frac{1}{2}}-\sqrt{a})}{(K_e^{\,\frac{1}{2}}+\sqrt{a})}\Big/\frac{(K_v^{\,\frac{1}{2}}-\sqrt{a})}{(K_v^{\,\frac{1}{2}}+\sqrt{a})}\right] \qquad \text{if } a \geq o \qquad ,(C2\text{-}9)$$

$$\lambda_\varepsilon = 2(-a)^{3/2}\left[\tan^{-1}\frac{K_e^{\,\frac{1}{2}}}{\sqrt{-a}} - \tan^{-1}\frac{K_v^{\,\frac{1}{2}}}{\sqrt{-a}}\right] \qquad \text{if } a < o \qquad ,(C2\text{-}10)$$

and

$$a = K_p - (K_p - K_E)y_p/(y_p - y_E) \qquad .(C2\text{-}11)$$

K_v is obtained by extrapolating the line through K_p and K_E to $y = y_v$, thus

$$K_v = K_p + (y_p - y_v)(K_E - K_p)/(y_E - y_p) \qquad .(C2\text{-}12)$$

The thickness of the viscous sublayer y_v and the mean velocity at the location U_v are then expressed as

$$y_v = \nu \, Re_v / K_v^{1/2} \qquad ,(C2\text{-}13)$$

and

$$U_v = Re_v(\tau_S/\rho)/K_v^{1/2} \qquad .(C2\text{-}14)$$

An iterative scheme is employed in which the previous iteration level of y_v in (C2-13) is used to evaluate the current K_v vlaues.

APPENDIX D

The PHOENICS Program

PHOENICS (which is an acronym for Parabolic Hyperbolic Or Elliptic Numerical Code Series) is a single flow-simulating computer code developed for the solution of fluid-flow and heat and mass-transfer problems in circumstances ranging in complexity from one-dimensional single-phase and steady, to three-dimensional multi-phase and transient.

The program utitlises three layers of modularity. At the basic level, the "EARTH" program provides the fascilities for solving the equations representing the laws of conservation of mass, momentum and energy and related entities. It sets up the grid dividing the problem into cells for which the equations are solved in turn, allocates computer storage, sets up the balance equations for each cell and each variable, obtains solutions and arranges for printing of the required output. As the key to the whole PHOENICS program, EARTH is protected from corruption by being inaccessible to the user.

In order to harness the fascilities within EARTH to the solution of a particular problem, one of the range of Satellite programs (see Fig D1-1) is used to effectively tell EARTH what it is being asked to simulate. Specific to each application or range of applications, the Satellites are Ground Station subroutines. In contrast to the Satellites, the shape and size of the domain of interest, how fine a grid is to be used, the

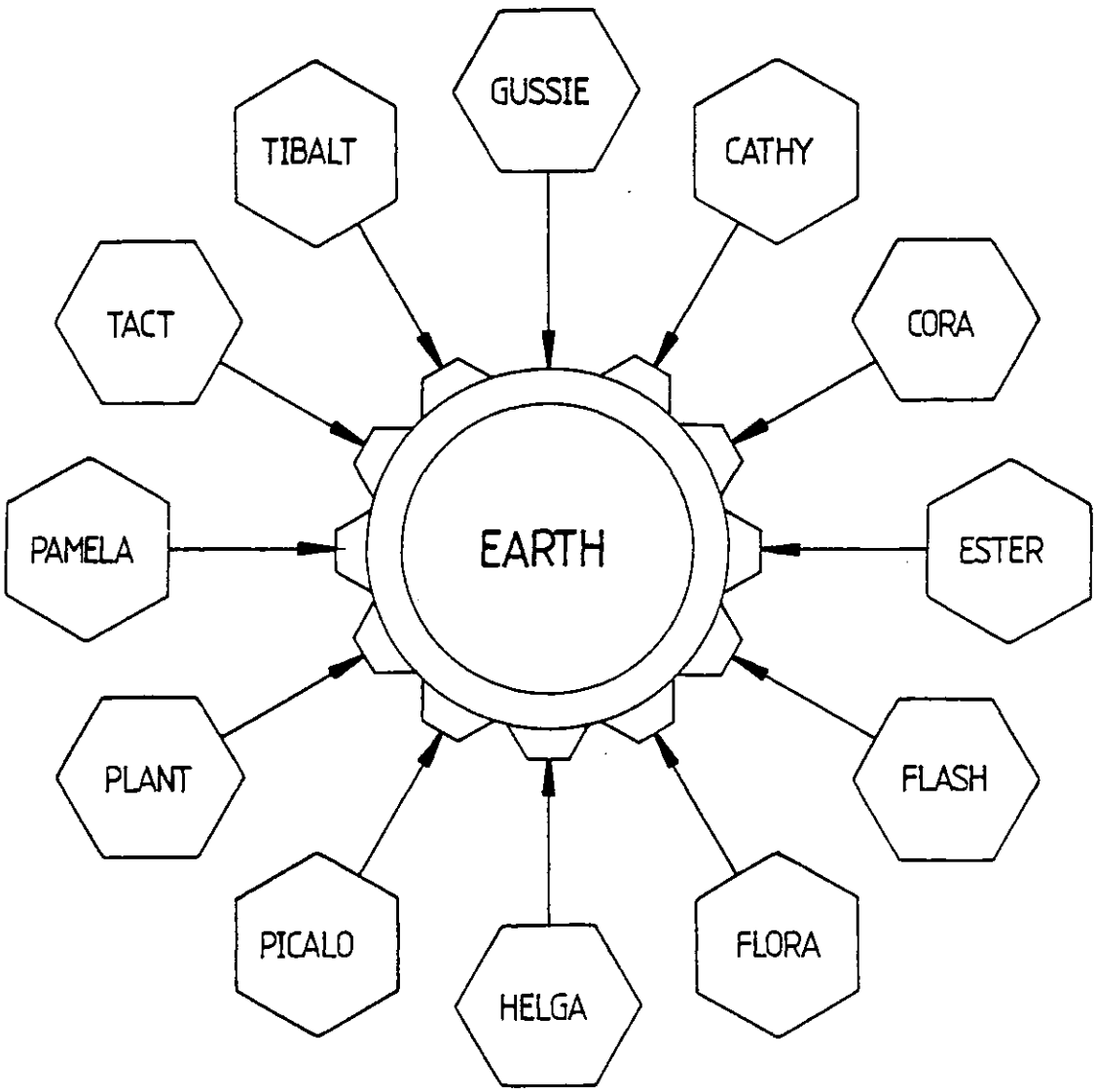

Fig. D1-1. Structure of the PHOENICS computer code.

degree of accuracy required and the type of output.

At the intermediate level between EARTH and the Satellites are Ground Station subroutines. In contrast to the Satellites which deliver data to EARTH and have no further role to play, Ground Station subroutines actually participate in EARTH computations, providing features specific to the problem to be solved. An example is the introduction of the new K-W model into PHOENICS as described in Chapter 4. This is done through the Ground-station subroutine GROUND.

At an appropriate stage of the solution, GROUND is called by EARTH so as to compute and add the necessary sources to the W-equation, compute the necessary output etc. Other subsidiary subroutines e.g user-generated WALL subroutine for computing the wall functions may be conveniently attached to and called from GROUND when required.

APPENDIX E

```
      SUBROUTINE GROUND(IRN,ICHAP,ISTP,ISWP,IZED,INDVAR)
C-----------------------------------------------------------------
C
C       THIS IS THE GROUND-STATION SUBROUTINE FOR THE CODING OF THE
C       W EQUATION. NOTE: THE ESSENTIAL PARTS ARE CONTAINED IN
C       CHAPTER 5 WHERE THE SOURCES ARE CALCULATED AND ADDED
C
C       BY: J.O.ILEGBUSI
C
C-----------------------------------------------------------------
$LIST
$INCLUDE 9,CMNGUSSI.FTN/G
$INCLUDE 9,GUSSEQUI.FTN/G
$INCLUDE 9,USER.CMN
$NLIST
$LIST
C-----------------------------------------------------------------
C                           CHAPTER 0
C
C-----------------------------------------------------------------
C     NON-USER DIMENSION STATEMENTS, & TYPE DECLARATIONS, HERE...
      LOGICAL EXISTS
C
      LOGICAL INLET
      LOGICAL STEP
C
      DIMENSION SPTAPE(3)
C-----------------------------------------------------------------
C------ENTER REQUIRED NON-EXECUTABLE (DATA,DIMENSION...ETC)
C       STATEMENTS HERE:
      DIMENSION LSPDA(1),ISPDA(1),RSPDA(1)
      DIMENSION CPHI(5,5),VPHI(5,5),CM(5,5),VM(5,5),CVZERO(5,5)
      DIMENSION SORC1(5,5),SORC2(5,5),SORC3(5,5),TKEP(5),OUT(5)
      DIMENSION GK(5,5)
      DATA CPHI,VPHI,CVZERO/75*0.0/
      DATA CD,CAPPA/0.09,0.435/
      DATA TINY/1.E-10/
      DATA IGN/3/
      DATA IVISIT,EXISTS,SPTAPE/0,.FALSE.,4HSPDA,4HTA.D,2HTA/
          IF(IVISIT.EQ.IRN) GO TO 5
C
      CDCA=1./(SQRT(CD)*CAPPA**2)
      SQRTCD=SQRT(CD)
      NXM1=NX-1
      NYM1=NY-1
      IXSTP=2
      IYSTP=2
      IXSTP1=IXSTP+1
      IYSTP1=IYSTP+1
      INLET=.FALSE.
      STEP=.TRUE.
      KOUNT=0
      IVISIT=IRN
```

```
      CALL LEGEND(8H07.10.81,4HG001)
          IF(.NOT.SPDATA) GO TO 5
          IF(EXISTS) GO TO 1
      CALL TAPES(11,SPTAPE,3,2,0)
      EXISTS=.TRUE.
    1 READ(11) LSPDA,ISPDA,RSPDA
          IF(IRN.EQ.NRUN) CALL TAPES(11,SPTAPE,3,3,0)
    5 CONTINUE
C*** HIR 03/09/81 NEXT STATEMENT...
      INTGR(54)=ICHAP
      CALL AMEND(ICHAP,INDVAR)
      IF(ICHAP.EQ.12.AND.INDVAR.EQ.-1) INTGR(54)=-2718
C*** HIR 28/08/91 CALL STRIDE WHEN ICHAP=-1...
      IF(PARAB.AND.ICHAP.EQ.-1) CALL STRIDE(IZED,INDVAR,IRN)
          IF(ICHAP.GT.0) GO TO 2
C      LOCATION FOR SETTING DISTORTED GEOMETRY READ IN AS SPECIAL
C      DATA...
      RETURN
    2 GO TO (100,200,300,400,500,600,700,800,900,1000,1100,1200,
     &1300,1400,1500,1600),ICHAP
      RETURN
C-------------------------------------------------------------
C                        CHAPTER 2
C     GROUND CALLED AT THE START OF EACH SWEEP LOOP
C-------------------------------------------------------------
  200 CONTINUE
C
C      DEACTIVATE SOLUTION OF EPSILON EQUATION AT BEGINING
C      OF THE CALCULATION
C
      SOLVAR(13)=.FALSE.
      STOVAR(13)=.TRUE.
      RETURN
C-------------------------------------------------------------
C                        CHAPTER 4
C     GROUND CALLED AT THE START OF EACH HYDRODYNAMIC LOOP
C     NOTE : INDVAR GIVES ITERATION COUNTER FOR CURRENT Z SLAB.
C-------------------------------------------------------------
  400 CONTINUE
C---- SET DISTANCES OF NEAR-WALL NODES
      IF(INDVAR.GT.1.OR.KOUNT.GT.0) GO TO 499
      CALL GET1D(122,XG,NX)
      CALL GET1D(123,XU,NX)
      CALL GET1D(126,YG,NY)
      CALL GET1D(127,YV,NY)
      YP1=YG(IYSTP1)-YV(IYSTP)
      YP2=XG(IXSTP1)-XU(IXSTP)
      KOUNT=1
  499 CONTINUE
      RETURN
```

```
C-------------------------------------------------------
C                        CHAPTER 5
C     GROUND CALLED WHEN SOURCE TERM IS COMPUTED
C     NOTE : INDVAR SPECIFIES DEPENDENT VARIABLE INDEX 1 TO 25
C
C*****PLEASE NOTE: IF YOU HAVE MASS FLOW BOUNDARY CONDITIONS AT THE
C     CURRENT SLAB, YOU MUST (REPEAT: MUST) CALL ADD FOR INDVAR=9
C     USING CM & VM TO SET THE TOTAL BOUNDARY MASS FLOW FOR THE
C     FIRST PHASE. SIMILARLY, IN A TWO-PHASE CASE, ADD MUST BE
C     CALLED FOR INDVAR=10 TO SET THE FLOWS FOR THE SECOND PHASE.
C     NOTE: FOR INDVAR=9, OR 10, CPHI & VPHI HAVE NO SIGNIFCANCE,
C     BUT THE ARGUMENT LIST OF ADD MUST BE COMPLETE.
C-------------------------------------------------------
  500 CONTINUE
      IF(INLET) CALL BDRYIN(IRN)
C---- INLUDE CALL GETS HERE
      CALL GET(3,U,NY,NX)
      CALL GET(5,V,NY,NX)
      CALL GET(12,TKE,NY,NX)
      CALL GET(17,W,NX,NY)
      CALL GET(101,VOL,NY,NX)
      CALL GET(103,AE,NY,NX)
      CALL GET(104,AN,NY,NX)
      CALL GET(106,DIFE,NY,NX)
      CALL GET(107,DIFN,NY,NX)
      CALL GET(112,EMUEF,NY,NX)
      IF(INDVAR.NE.17) GO TO 565
C---- CALCULATE LENGTH SCALE (AL)
      DO 510 IX=1,NX
      DO 510 IY=1,NY
      AL(IY,IX)=SQRT(TKE(IY,IX)/(W(IY,IX)+TINY))
  510 CONTINUE
C---- CALCULATE TURBULENT VISCOSITY (EMUT)
      DO 520 IX=1,NX
      DO 520 IY=1,NY
      EMUT(IY,IX)=EMUEF(IY,IX)-EMULAM
  520 CONTINUE
C---- CALCULATE GRADIENTS OF VELOCITIES AND LENGTH SCALE
      CALL GRAD(IRN)
C---- CALCULATE GENERATION OF TURBULENT ENERGY
      CALL PRODK(IRN,GK)
C---- CALCULATE VORTICITY AND ITS 1ST.& 2ND. DERIVATIVES
      CALL VORTI(IRN)
C---- CALCULATE LINEARISED SOURCES FOR THE W-EQUATION
      CALL SORCW(IRN,SORC1,SORC2,SORC3,GK)
C---- ADD SOURCES TO W-EQUTION
C---- NOTE: CPHI & VPHI MUST BE SET TO ZERO FOR NEAR-WALL NODES
C----       OTHER THAN THOSE AT IY=1,IY=IYSTP1,IY=NY & IX=IXSTP1
```

```
C----1: PRODUCTION SOURCE TERMS
      DO 530 IX=2,NXM1
      DO 530 IY=2,NYM1
      CPHI(IY,IX)=0.0
      VPHI(IY,IX)=0.0
      IF(IY.EQ.IYSTP1.AND.IX.LE.IXSTP) GO TO 530
      IF(IX.EQ.IXSTP1.AND.IY.LE.IYSTP) GO TO 530
      CPHI(IY,IX)=1.E-10
      VPHI(IY,IX)=(SORC1(IY,IX)+SORC2(IY,IX))*1.E10
  530 CONTINUE
      CALL ADD(17,2,NXM1,2,NYM1,7.,CVZERO,CVZERO,CPHI,VPHI,NY,NX)
C----2: DISSIPATION SOURCE-TERMS
      DO 540 IX=2,NXM1
      DO 540 IY=2,NYM1
      CPHI(IY,IX)=0.0
      VPHI(IY,IX)=0.0
      IF(IY.EQ.IYSTP1.AND.IX.LE.IXSTP) GO TO 540
      IF(IX.EQ.IXSTP1.AND.IY.LE.IYSTP) GO TO 540
      CPHI(IY,IX)=-SORC3(IY,IX)
  540 CONTINUE
      CALL ADD(17,2,NXM1,2,NYM1,7.,CVZERO,CVZERO,CPHI,VPHI,NY,NX)
C---- WALL-BOUNDARY CONDITION ON W
C---- NOTE: CPHI & VPHI MUST BE SET APPROPRIATELY FOR OTHER WALLS
      DO 560 IX=1,NX
      DO 560 IY=1,NY
      IF(IY.EQ.1.OR.IY.EQ.NY) GO TO 550
      IF(IY.EQ.IYSTP1.AND.IX.LE.IXSTP) GO TO 552
      IF(IX.EQ.IXSTP1.AND.IY.LE.IYSTP) GO TO 554
      CPHI(IY,IX)=0.0
      VPHI(IY,IX)=0.0
      GO TO 560
  550 YP=YV(IY)-YG(IY)
C---- NOTE: FOR IY=1, THE ABOVE IMPLIES YP=YG(1)
      GO TO 556
  552 YP=YP1
      GO TO 556
  554 YP=YP2
  556 CPHI(IY,IX)=1.E10
      VPHI(IY,IX)=TKE(IY,IX)*CDCA/YP**2
  560 CONTINUE
      CALL ADD(17,1,NX,1,NY,0.,CVZERO,CVZERO,CPHI,VPHI,NY,NX)
      GO TO 599
  565 CONTINUE
      IF(INDVAR.EQ.3.OR.INDVAR.EQ.12) GO TO 566
      GO TO 599
  566 CONTINUE
      YP=YG(1)
      IF(.NOT.STEP) GO TO 599
      CALL WALFUN(IRN,OUT,TKEP,IXSTP,YP)
```

```
C---- RE-INITIALISE CPHI & VPHI ARRAYS
      DO 568 IX=1,NX
      DO 568 IY=1,NY
      CPHI(IY,IX)=0.0
  568 VPHI(IY,IX)=0.0
      IF(INDVAR.EQ.3) GO TO 570
      IF(INDVAR.EQ.12) GO TO 580
      GO TO 599
  570 CONTINUE
      DO 575 IX=IXSTP1,NX
      VPHI(IY,IX)=0.0
      YPLUS=SQRT((AMAX1(TKEP(IX),TINY))*SQRTCD)*YP/EMULAM
      IF(YPLUS.GT.11.5) GO TO 575
      OUT(IX)=EMULAM/YP
  575 CPHI(IY,IX)=OUT(IX)
      CALL ADD(3,IXSTP1,NX,1,1,4.,CVZERO,CVZERO,CPHI,VPHI,NY,NX)
      GO TO 599
  580 CONTINUE
      DO 585 IX=IXSTP1,NX
      CPHI(1,IX)=1.E10
  585 VPHI(1,IX)=TKEP(IX)
      CALL ADD(12,IXSTP1,NX,1,1,0.,CVZERO,CVZERO,CPHI,VPHI,NY,NX)
  599 CONTINUE
      RETURN
C-------------------------------------------------------------
C                        CHAPTER 6
C     GROUND CALLED AT THE END OF EACH HYDRODYNAMIC LOOP
C     NOTE : INDVAR GIVES ITERATION COUNTER FOR CURRENT Z SLAB.
C-------------------------------------------------------------
  600 CONTINUE
C---- SET EPSILON FROM VALUES OF W
      CALL GET(12,TKE,NY,NX)
      CALL GET(17,W,NY,NX)
      DO 610 IX=1,NX
      DO 610 IY=1,NY
      EPS(IY,IX)=AMAX1(TINY,CD*TKE(IY,IX)*SQRT(W(IY,IX)))
  610 CONTINUE
      CALL SET(13,1,NX,1,NY,EPS,NY,NX)
      RETURN
      END
```

```
C-------------------------------------------------------------
C
C       USER.CMN
C
C       THE FOLLOWING ARE THE SPECIAL COMMON BLOCKS PROVIDED
C       FOR THE W-EQUATION CODING IN GROUND AND THE ADDITIONAL
C       SUBROUTINES
C
C       BY: J.O.ILEGBUSI
C
C-------------------------------------------------------------
      COMMON/GRAD1/DUDY(5,5),DVDY(5,5),DLDY(5,5)
      COMMON/GRAD2/DUDX(5,5),DLDX(5,5)
      COMMON/VAR1/U(5,5),V(5,5),TKE(5,5),EPS(5,5),W(5,5)
      COMMON/VAR2/EMUT(5,5),EMUEF(5,5),AL(5,5)
      COMMON/VAR3/XG(5),XU(5),YG(5),YV(5),VOL(5,5)
      COMMON/VAR4/AE(5,5),AN(5,5),DIFE(5,5),DIFN(5,5)
      COMMON/VORTI/VORT(5,5),DVORDY(5,5),GRVOR2(5,5)
```

```
      COMMON/WALL1/UW(5),UE(5),US(5),UN(5)
      COMMON/WALL2/EMUW(5),EMUE(5),EMUS(5),EMUN(5)
      COMMON/WALL3/CW(5),CE(5),CS(5),CN(5)
      COMMON/WALL4/DW(5),DE(5),DS(5),DN(5)
      COMMON/WALL5/AKW(5),AKE(5),AKS(5),AKN(5)
      COMMON/WALL6/TKEW(5),TKEE(5),TKES(5),TKEN(5)
      COMMON/WALL7/DISSK(5),PRODK(5),DUDDY(5)
      COMMON/WALL8/YLAM(5),ULAM(5),TAUW(5),UPN(5)
      COMMON/WALL9/SRTKV(5),SRTKN(5),TAUPN(5)
      COMMON/WALL10/UWN(5),UEN(5),UMID(5),UMIDN(5)
```

APPENDIX F1

```
      SUBROUTINE GRAD(IRN)
C
C       THE PURPOSE OF THIS SUBROUTINE IS TO CALCULATE
C       GRADIENTS OF VELOCITIES AND OF LENGTH SCALE
C
C       BY :  J.O.ILEGBUSI
C
$INCLUDE 9,CMNGUSSI.FTN/G
$INCLUDE 9,GUSSEQUI.FTN/G
$INCLUDE 9,USER.CMN
C
CHAPTER 0  PRELIMINARIES
      DATA IVISIT,TINY/0,1.E-10/
      IF(IVISIT.EQ.IRN) GO TO 5
      NYM1=NY-1
      NXM1=NX-1
      IVISIT=IRN
    5 CONTINUE
C
CHAPTER 1 Y-DIRECTION GRADIENTS (DUDY,DVDY,DLDY)
      DO 199 IX=1,NX
      DO 199 IY=1,NY
      IF(IY.EQ.1) GO TO 140
      IF(IY.EQ.NY) GO TO 170
      DYN=YG(IY+1)-YG(IY)
      DYS=YG(IY)-YG(IY-1)
      DYP=YV(IY)-YV(IY-1)
      IF(IX.EQ.1) GO TO 110
      IF(IX.EQ.NX) GO TO 120
      DUN=0.5*(U(IY+1,IX)+U(IY+1,IX-1)-U(IY,IX)-U(IY,IX-1))/DYN
      DUS=0.5*(U(IY,IX)+U(IY,IX-1)-U(IY-1,IX)-U(IY-1,IX-1))/DYS
      GO TO 130
  110 DUN=(U(IY+1,IX)-U(IY,IX))/DYN
      DUS=(U(IY,IX)-U(IY-1,IX))/DYS
      GO TO 130
  120 DUN=(U(IY+1,IX-1)-U(IY,IX-1))/DYN
      DUS=(U(IY,IX-1)-U(IY-1,IX-1))/DYS
  130 DUDY(IY,IX)=0.5*(DUN+DUS)
      DLN=(AL(IY+1,IX)-AL(IY,IX))/DYN
      DLS=(AL(IY,IX)-AL(IY-1,IX))/DYS
      DLDY(IY,IX)=0.5*(DLN+DLS)
      DVDY(IY,IX)=(V(IY,IX)-V(IY-1,IX))/DYP
      GO TO 199
  140 DYN=YG(IY+1)-YG(IY)
      DLDY(IY,IX)=(AL(IY+1,IX)-AL(IY,IX))/DYN
      DVDY(IY,IX)=V(IY,IX)/YV(IY)
```

```
      IF(IX.EQ.1) GO TO 150
      IF(IX.EQ.NX) GO TO 160
      DUDY(IY,IX)=0.5*(U(IY+1,IX)+U(IY+1,IX-1)-U(IY,IX)-U(IY,IX-1))
     1/DYN
      GO TO 199
  150 DUDY(IY,IX)=(U(IY+1,IX)-U(IY,IX))/DYN
      GO TO 199
  160 DUDY(IY,IX)=(U(IY+1,IX-1)-U(IY,IX-1))/DYN
      GO TO 199
  170 DYS=YG(IY)-YG(IY-1)
      DLDY(IY,IX)=(AL(IY,IX)-AL(IY-1,IX))/DYS
      DVDY(IY,IX)=DVDY(IY-1,IX)
      IF(IX.EQ.1) GO TO 180
      IF(IX.EQ.NX) GO TO 190
      DUDY(IY,IX)=0.5*(U(IY,IX)+U(IY,IX-1)-U(IY-1,IX)-U(IY-1,IX-1))
     1/DYS
      GO TO 199
  180 DUDY(IY,IX)=(U(IY,IX)-U(IY-1,IX))/DYS
      GO TO 199
  190 DUDY(IY,IX)=(U(IY,IX-1)-U(IY-1,IX-1))/DYS
  199 CONTINUE
C
CHAPTER 2 X-DIRECTION GRADIENTS (DUDX,DLDX)
      DO 230 IX=1,NX
      DO 230 IY=1,NY
      IF(IX.EQ.1) GO TO 210
      IF(IX.EQ.NX) GO TO 220
      DXP=XU(IX)-XU(IX-1)
      DXE=XG(IX+1)-XG(IX)
      DXW=XG(IX)-XG(IX-1)
      DUDX(IY,IX)=(U(IY,IX)-U(IY,IX-1))/DXP
      DLE=(AL(IY,IX+1)-AL(IY,IX))/DXE
      DLW=(AL(IY,IX)-AL(IY,IX-1))/DXW
      DLDX(IY,IX)=0.5*(DLE+DLW)
      GO TO 230
  210 DUDX(IY,IX)=U(IY,IX)/XU(IX)
      DLDX(IY,IX)=(AL(IY,IX+1)-AL(IY,IX))/(XG(IX+1)-XG(IX))
      GO TO 230
  220 DUDX(IY,IX)=DUDX(IY,IX-1)
      DLDX(IY,IX)=(AL(IY,IX)-AL(IY,IX-1))/(XG(IX)-XG(IX-1))
  230 CONTINUE
      RETURN
      END
```

APPENDIX F2

```
      SUBROUTINE PRODK(IRN,GK)
C-------------------------------------------------------------C
C                                                             C
C     THE PURPOSE OF THIS SUBROUTINE IS TO CALCULATE THE
C     GENERATION RATE OF TURBULENCE ENERGY
C
C     J.O.ILEGBUSI
C
C-------------------------------------------------------------
$INCLUDE 9,CMNGUSSI.FTN/G
$INCLUDE 9,GUSSEQUI.FTN/G
$INCLUDE 9,USER.CMN
C
      DIMENSION GK(5,5)
C
CHAPTER 0 PRELIMINARIES
      DATA IVISIT,TINY/0,1.E-10/
      IF(IVISIT.EQ.IRN) GO TO 5
      IVISIT=IRN
   5  CONTINUE
C
CHAPTER 1 CALCULATE GENK
      DO 100 IX=1,NX
      DO 100 IY=1,NY
      TERM1=2.*DUDX(IY,IX)*DUDX(IY,IX)
      TERM2=DVDY(IY,IX)*DVDY(IY,IX)
      TERM3=DUDY(IY,IX)*DUDY(IY,IX)
      GK(IY,IX)=EMUT(IY,IX)*(TERM1+TERM2+TERM3)
 100  CONTINUE
      RETURN
      END
```

APPENDIX F3

```
      SUBROUTINE VORTI(IRN)
C
C     THE PURPOSE OF THIS SUBROUTINE IS TO CALCULATE
C     VORTICITY AND ITS 1ST.& 2ND. DERIVATIVES
C
C      J.O.ILEGBUSI
C
$INCLUDE 9,CMNGUSSI.FTN/G
$INCLUDE 9,GUSSEQUI.FTN/G
$INCLUDE 9,USER.CMN
C
CHAPTER 0 PRELIMINARIES
      DATA IVISIT,TINY/0,1.E-10/
      IF(IVISIT.EQ.IRN) GO TO 5
      IVISIT=IRN
   5  CONTINUE
C
CHAPTER 1 CALCULATE VORTICITY
      DO 100 IX=1,NX
      DO 100 IY=1,NY
      VORT(IY,IX)=ABS(DUDY(IY,IX))
  100 CONTINUE
C
CHAPTER 2: CALCULATE GRADIENT OF VORTICITY AND ITS SQUARE
      DO 240 IX=1,NX
      DO 240 IY=1,NY
      IF(IY.EQ.1) GO TO 210
      IF(IY.EQ.NY) GO TO 220
      DYN=YG(IY+1)-YG(IY)
      DYS=YG(IY)-YG(IY-1)
      DVORN=(VORT(IY+1,IX)-VORT(IY,IX))/DYN
      DVORS=(VORT(IY,IX)-VORT(IY-1,IX))/DYS
      DVORDY(IY,IX)=0.5*(DVORN+DVORS)
      GRVOR2(IY,IX)=0.5*(DVORN*DVORN+DVORS*DVORS)
      GO TO 240
  210 DVORDY(IY,IX)=(VORT(IY+1,IX)-VORT(IY,IX))/(YG(IY+1)-YG(IY))
      GO TO 230
  220 DVORDY(IY,IX)=(VORT(IY,IX)-VORT(IY-1,IX))/(YG(IY)-YG(IY-1))
  230 GRVOR2(IY,IX)=0.5*DVORDY(IY,IX)*DVORDY(IY,IX)
  240 CONTINUE
      RETURN
      END
```

APPENDIX F4

```
      SUBROUTINE SORCW(IRN,SORC1,SORC2,SORC3,GK)
C
C     THE PURPOSE OF THIS SUBROUTINE IS TO COMPUTE
C     LINEARISED SOURCES OF THE W-EQUATION
C     NOTE: SW=SU+SP*W   ; SP=-AP
C
C     J.O. ILEGBUSI
C
$INCLUDE 9,CMNGUSSI.FTN/G
$INCLUDE 9,GUSSEQUI.FTN/G
$INCLUDE 9,USER.CMN
C
      DIMENSION SORC1(5,5),SORC2(5,5),SORC3(5,5),GK(5,5)
C
CHAPTER 0 PRELIMINARIES
      DATA CW1,CW2,CW3,CW4,CW5/3.5,0.17,1.04,2.97,1.0/
      DATA IVISIT,TINY/0,1.E-10/
      IF(IVISIT.EQ.IRN) GO TO 5
C---- INITIALISE SOURCE ARRAYS
      DO 5 IX=1,NX
      DO 5 IY=1,NY
      SORC1(IY,IX)=0.0
      SORC2(IY,IX)=0.0
      SORC3(IY,IX)=0.0
    5 CONTINUE
      NXM1=NX-1
      NYM1=NY-1
      IVISIT=IRN
   10 CONTINUE
C
CHAPTER 1: EXPLICITLY-FORMULATED PART (PRODUCTION TERMS)
      DO 100 IX=1,NX
      DO 100 IY=1,NY
      SORC1(IY,IX)=CW1*EMUT(IY,IX)*GRVOR2(IY,IX)
      SORC2(IY,IX)=CW3*SQRT(AMAX1(W(IY,IX),TINY))*GK(IY,IX)
     1/(EMUT(IY,IX)+TINY)
  100 CONTINUE
C
CHAPTER 2: IMPLICITLY-FORMULATED PART (DISSIPATION TERM)
C----- NOTE: THIS PART CONTAINS THE NEW TERM
      DO 200 IX=1,NX
      DO 200 IY=1,NY
      GRADLSQ=(DLDY(IY,IX)+DLDX(IY,IX))**2
      CONSTC=CW2+CW4*GRADLSQ**CW5
      SORC3(IY,IX)=-CONST*SQRT(AMAX1(W(IY,IX),TINY))
  200 CONTINUE
      RETURN
      END
```

APPENDIX F5

```
      SUBROUTINE WALFUN(IRN,OUT,TKEP,IXSTP)
C-----------------------------------------------------------------
C
C       THE PURPOSE OF THIS SUBROUTINE IS TO CALCULATE
C       THE WALL FUNCTION FOR FLOWS WITH SIGNIFICANT
C       TURBULENT DIFFUSION AS IN SEPARATED FLOWS
C
C       BY : J.O.ILEGBUSI
C
C-----------------------------------------------------------------
$INCLUDE 9,CMNGUSSI.FTN/G
$INCLUDE 9,GUSSEQUI.FTN/G
$INCLUDE 9,USER.CMN
$INCLUDE 9,WAL.CMN
      DIMENSION TKEP(5),OUT(5)
      DATA CD,CAPPA,EE/0.09,0.435,9.0/
      DATA TINY,ITOT/1.E-10,11/
      DATA TKINTE,UREF/0.003,1.0/
      DATA CCL,REV/2.55,20.0/
      DATA IVISIT/0/
C-----------------------------------------------------------------
C---- CHAPTER 0  PRELIMINARIES
      IF(IVISIT.EQ.IRN) GO TO 40
      DYN=YG(2)-YG(1)
      YP=YG(1)
      YPN=2.*YP
      NXM1=NX-1
      IXSTP1=IXSTP+1
      IXSTP2=IXSTP+2
      SQRTCD=SQRT(CD)
C---- INITIALISE TKEP & OUT ARRAYS
      DO 10 IX=1,NX
      YLAM(IX)=TINY
      ULAM(IX)=TINY
      TAUW(IX)=TINY
      SRTKV(IX)=TINY
      SRTKN(IX)=TINY
      TKEP(IX)=TINY
   10 OUT(IX)=TINY
C---- INITIALISE TKE AT WALL FOR FIRST VISITATION
      DO 20 IX=IXSTP1,NX
      TERM=1.5*(TKINTE*UREF)**2
   20 TKEP(IX)=AMAX1(TINY,TERM)
C---- INITIALISE VALUES OF LAMINAR-SUBLAYER THICKNESS
      DO 30 IX=IXSTP1,NX
      TAU=SQRTCD*TKEP(IX)
      UTAU=SQRT(TAU)
      YLAM1=5.0*EMULAM/(UTAU+TINY)
   30 YLAM(IX)=AMIN1(YLAM1,YP)
      IVISIT=IRN
   40 CONTINUE
      ITER=0
   50 ITER=ITER+1
```

```
C-----------------------------------------------------------------
CHAPTER 1 VELOCITIES AT CELL BOUNDARIES
      DO 110 IX=IXSTP2,NXM1
      UW(IX)=U(1,IX-1)
      UWN(IX)=U(2,IX-1)
      UE(IX)=U(1,IX)
  110 UEN(IX)=0.0
      UW(IXSTP1)=0.0
      UWN(IXSTP1)=0.0
      UW(NX)=U(1,NXM1)
      UWN(NX)=U(2,NXM1)
      UE(IXSTP1)=U(1,IXSTP1)
      UEN(IXSTP1)=U(2,IXTP1)
      UE(NX)=0.0
      UEN(IX)=0.0
      DO 120 IX=IXSTP1,NX
      US(IX)=0.0
  120 UN(IX)=V(1,IX)
C-----------------------------------------------------------------
CHAPTER 2 CELL-FACE AREAS
      AREAW=AE(1,1)
      AREAE=AREAW
      AREAS=AN(1,1)
      AREAN=AREAS
C-----------------------------------------------------------------
CHAPTER 3 VISCOSITIES BETWEEN CELLS
      DO 310 IX=IXSTP2,NXM1
      EMUW(IX)=0.5*(EMUEF(1,IX)+EMUEF(1,IX-1))
  310 EMUE(IX)=0.5*(EMUEF(1,IX)+EMUEF(1,IX+1))
      EMUW(IXSTP1)=0.0
      EMUW(NX)=0.5*(EMUEF(1,NX)+EMUEF(1,NXM1))
      EMUE(IXSTP1)=0.5*(EMUEF(1,IXSTP1)+EMUEF(1,IXSTP2))
      DO 320 IX=IXSTP1,NX
      EMUS(IX)=0.0
  320 EMUN(IX)=0.5*(EMUEF(1,IX)+EMUEF(2,IX))
C-----------------------------------------------------------------
CHAPTER 4 CALCULATE CONVECTION COEFFICIENTS
      DO 410 IX=IXSTP1,NX
      CW(IX)=UW(IX)*AREAW
      CE(IX)=UE(IX)*AREAE
      CS(IX)=US(IX)*AREAS
  410 CN(IX)=UN(IX)*AREAN
C-----------------------------------------------------------------
CHAPTER 5 CALCULATE DIFFUSION COEFFICIENTS
      DO 510 IX=IXSTP2,NXM1
      DW(IX)=EMUW(IX)*DIFE(1,IX)
  510 DE(IX)=EMUE(IX)*DIFE(1,IX)
      DW(IXSTP1)=0.0
      DW(NX)=EMUW(NX)*DIFE(1,NXM1)
      DE(IXSTP1)=EMUE(IXSTP1)*DIFE(1,IXSTP1)
      DE(NX)=0.0
      DO 520 IX=IXSTP1,NX
      DS(IX)=0.0
  520 DN(IX)=EMUN(IX)*DIFN(IY,IX)
```

```
C-----------------------------------------------------------------
CHAPTER 6 F-D COEFFICIENTS OF THE K-BALANCE
      DO 610 IX=IXSTP1,NX
      AKW(IX)=AMAX1(DW(IX),DW(IX)+CW(IX))
      AKE(IX)=AMAX1(DE(IX),DE(IX)-CE(IX))
      AKS(IX)=AMAX1(DS(IX),DS(IX)+CS(IX))
      AKN(IX)=AMAX1(DN(IX),DN(IX)-CN(IX))
  610 CONTINUE
C-----------------------------------------------------------------
CHAPTER 7 GENERATION OF TURBULENT ENERGY
C
C----7:1 TKE AT EDGE OF LAMINAR SUBLAYER
      DO 710 IX=IXSTP1,NX
      YINT=(YP-YLAM(IX))/DYN
      TKV1=TKEP(IX)+YINT*(TKE(2,IX)-TKEP(IX))
      TKV=AMAX1(TKV1,TINY)
  710 SRTKV(IX)=SQRT(TKV)
C----7:2 WALL-SHEAR STRESS
      DO 720 IX=IXSTP1,NX
      UMID(IX)=0.5*(UW(IX)+UE(IX))
      ARG=EEW*YP*SRTKV(IX)
  720 TAUW(IX)=CAP*UMID(IX)*SRTKV(IX)/ALOG(ARG)
C----7:3 VELOCITIES AT EDGE OF LAMINAR SUBLAYER
      DO 730 IX=IXSTP1,NX
  730 ULAM(IX)=REV*TAUW(IX)/(SRTKV(IX)+TINY)
C----7:4 VELOCITIES & SHEAR STRESS AT NORTH FACES OF CELLS
      DO 740 IX=IXSTP1,NX
      UMIDN(IX)=0.5*(UWN(IX)+UEN(IX))
      UPN(IX)=UMID(IX)+(YPN-YP)*(UMIDN(IX)-UMID(IX))/DYN
      EMUTN=0.5*(EMUEF(2,IX)+EMUEF(1,IX))-EMULAM
      DUDYN=(UMIDN(IX)-UMID(IX))/DYN
  740 TAUPN(IX)=EMUTN*DUDYN
C----7:5 CALCULATE GENK
      DO 750 IX=IXSTP1,NX
      TERM1=TAUW(IX)*(UPN(IX)-ULAM(IX))/YPN
      TERM2=TAUW(IX)*(TAUPN(IX)-TAUW(IX))*(1.0-YLAM(IX)/YPN)
     1/(CAP*SRTKV(IX)*YPN+TINY)
  750 PRODK(IX)=(TERM1+TERM2)*VOL(1,IX)
C-----------------------------------------------------------------
CHAPTER 8 DISSIPATION OF TKE
      DO 830 IX=IXSTP1,NX
      TKPN=0.5*(TKEP(IX)+TKE(2,IX))
      SRTKN(IX)=SQRT(TKPN)
      A=TKEP(IX)+(TKEP(IX)-TKE(2,IX))*YP/DYN
      IF(A.GE.0.0) GO TO 810
      AA=-A
      SQRTA=SQRT(AA)
      DENOM=SQRTA+TINY
      ARG1=SRTKN(IX)/DENOM
      ARG2=SRTKV(IX)/DENOM
      FAC1=ATAN(ARG1)
      FAC2=ATAN(ARG2)
      GO TO 820
```

```
  810 SQRTA=SQRT(A)
      FAC1=(SRTKN(IX)-SQRTA)/(SRTKN(IX)*SQRTA+TINY)
      FAC2=(SRTKV(IX)-SQRTA)/(SRTKV(IX)+SQRTA+TINY)
      FAC=FAC1/(FAC2+TINY)
      FACTOR=(SQRTA**3)*ALOG(FAC)
  820 CONTINUE
      TERM1=2.*(SRTKV(IX)**3)/(YPN*REV)
      TERM2=2.*(SRTKN(IX)**3-SRTKV(IX)**3)/3.
      TERM3=2.*A*(SRTKN(IX)-SRTKV(IX))
      EPSAV=TERM1+(TERM2+TERM3+FACTOR)/(YPN*CCL)
      DISSK(IX)=EPSAV*VOL(1,IX)
  830 CONTINUE
C-----------------------------------------------------------------
CHAPTER 9: DEDUCE YLAM FROM K
      DO 910 IX=IXSTP1,NX
      YLAM1=EMULAM*REV/(SRTKV(IX)+TINY)
      YLAM(IX)=AMIN1(YLAM1,YP)
  910 CONTINUE
C-----------------------------------------------------------------
CHAPTER 10 CALCULATE K AT NEAR-WALL NODE
      DO 1010 IX=IXSTP2,NXM1
      TKEW(IX)=TKE(1,IX-1)
 1010 TKEE(IX)=TKE(1,IX+1)
      TKEW(IXSTP1)=0.0
      TKEW(NX)=TKE(1,NXM1)
      TKEE(IXSTP1)=TKE(1,IXSTP2)
      TKEE(NX)=0.0
      DO 1020 IX=IXSTP1,NX
      TKES(IX)=0.0
 1020 TKEN(IX)=TKE(2,IX)
      DO 1030 IX=IXSTP1,NX
      TERM1=TKEW(IX)*AKW(IX)+TKEE(IX)*AKE(IX)+TKES(IX)*AKS(IX)
     1+TKEN(IX)*AKN(IX)+PRODK(IX)-DISSK(IX)
      TERM2=AKW(IX)+AKE(IX)+AKS(IX)+AKN(IX)+TINY
 1030 TKEP(IX)=AMAX1(TERM1/TERM2,TINY)
      IF(ITER.LT.ITOT) GO TO 50
C-----------------------------------------------------------------
CHAPTER 11 CALCULATE RATIO OF SHEAR STRESS TO VELOCITY
      DO 1110 IX=IXSTP1,NX
      TERM3=SQRT(AMAX1(SQRTCD*TKEP(IX),TINY))
      ARGM=EE*YP*TERM3/EMULAM
C---- NOTE: OUT STORES (SHEAR STRESS)/VELOCITY
 1110 OUT(IX)=CAPPA*TERM3/ALOG(ARGM)
C-----------------------------------------------------------------
      CONTINUE
      RETURN
      END
```

APPENDIX G

Nozzle-wall Boundary-Layer Approximation for Plane Jet of Bradbury (1965)

The ideal momentum excess flux is given by:

$$M_i = \rho U_J (U_J - U_E) h \qquad .(G\text{-}1)$$

Bradbury's measured excess momentum flux is given by:

$$M_e = \rho \int_{-\infty}^{\infty} U\,(U - U_E)\,dy \qquad .(G\text{-}2)$$

The excess momentum flux is constant so that the loss occurs in the nozzle-wall boundary-layers. So, assuming symmetry,

$$U_J^2 \delta_2 = \int_0^{\delta} U\,(U_J - U)\,dy \equiv 1/2\,(M_i - M_e) \qquad ,(G\text{-}3)$$

in which,

δ $\equiv$ boundary-layer thickness, and

δ_2 $\equiv$ momentum thickness.

Assuming a 1/7th power-law velocity-profile,

$$\delta = 72/7\ \delta_2 \qquad .(G\text{-}4)$$

With $M_i = 7.2009$ and $M_e = 6.9129$,

$$\frac{\delta}{h} \approx 0.17 \qquad .(G-5)$$

For the cells within the boundary-layer,

$$U = U_J(y/\delta)^{1/7} \qquad .(G-6)$$

Therefore, in order to match the experimental excess momentum flux, the mean streamwise velocity, U, within the boundary layer is suitably scaled, thus,

$$\frac{\delta}{h} \approx 0.15 \qquad .(G-7)$$

APPENDIX H

Prediction of flow in Backward facing step of present experimental Investigations

H1 Principle of the experiment

The details of the experimental investigation are contained in Chapter 8. These include the principle of the technique used and the results of its application to three different two-dimensional bodies. Therefore, only a brief explanation of its application to one of these bodies - the backward-facing step will be given here. This is the case chosen for comparison with the results deduced from the new K-W model.

The experimental technique involves pulling the body upwards through two fluid layers which were at first kept separate by a small difference of density . As the body emerges from the lower (coloured) fluid, it is observed to carry with it, in its boundary layer and wake, significant quantities of the lower fluid. A succession of photographs enables the various states of mixing of the two fluids to be recorded.

H2 Resolving the interface with the Particle-Tracking Technique

The interface between dyed and undyed fluid as the body moves through the fluid layers has been resolved in the present study by means of the "particle-tracking technique". This technique has been employed and described by Maxwell (1977) and Awn (1979) for other similar situations.

In principle, the interface is marked by a series of massless particles at an initial time (here taken as the time when the body breaks the interface between the two fluid layers). The momentum and turbulence equations are solved in the transient mode so as to obtain the velocity field. Then the coordinates X_p and Y_p characterising the position of the particles are calculated using the following relations:

$$X_p = X_{p,o} + U_p \Delta t \qquad ,(H2\text{-}1)$$

$$Y_p = Y_{p,o} + V_p \Delta t \qquad ,(H2\text{-}2)$$

where $(X_{p,o}, Y_{p,o})$ is the old location of the particle and U_p and V_p are the instantaneous velocity components of the

particle. U_p and V_p are evaluated at $(X_{p,o}, Y_{p,o})$ by linear interpolation of the four nearest velocities in the appropriate direction.

H3 Results

Figure H3-1 shows a series of photographs obtained for the flow in a backward-facing step at the given times after the body breaks the initial interface between the two fluid layers. Figure H3-2 shows the results obtained with the K-W model incorporating the particle-tracking features just mentioned. It should be mentioned that the interface actually represents that between the colourless fluid moving into the dyed fluid due to the orientation of the movement of the body.

H4 Discussion

It appears from Figures H3-1 and H3-2 that the qualitative features of the flow in the step have been fairly predicted. The separated flow which appear as the dark regions beyond the step in Figure H3-1 are predicted in Figure H3-2 as regions with little or no colourless fluid.

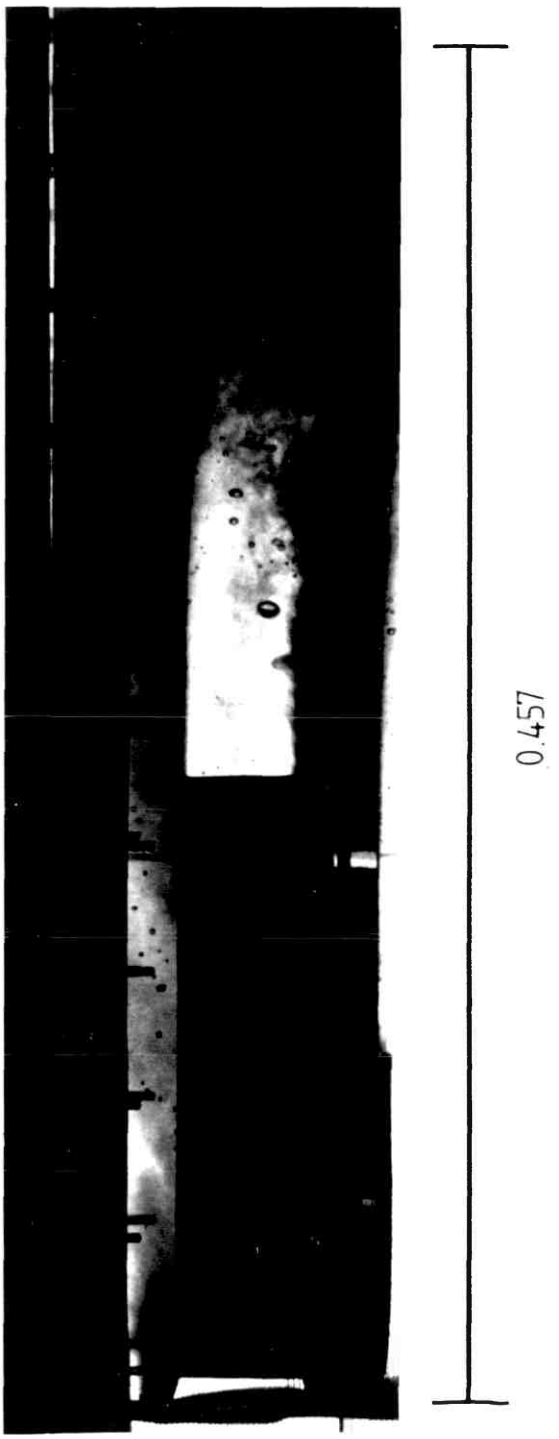

Fig. H3-1a. Experimental result for flow in a backward-facing step at time = 0.6 sec. from when the body breaks the interface.

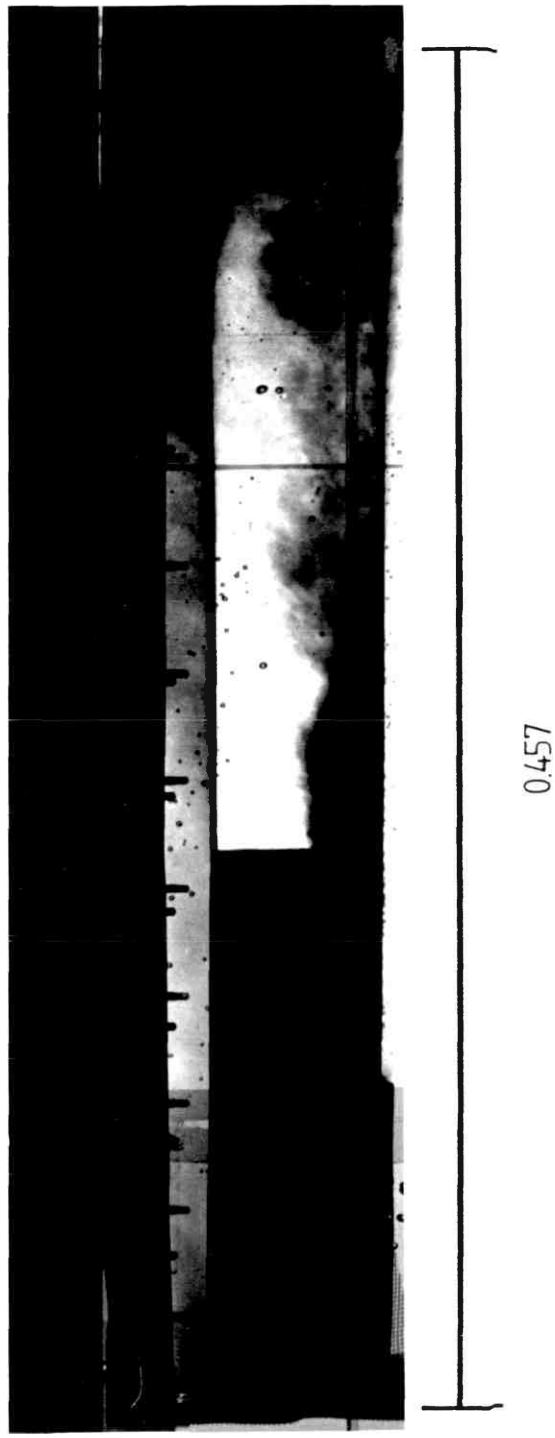

Fig. H3.1b. Experimental result at time = 0.8 second.

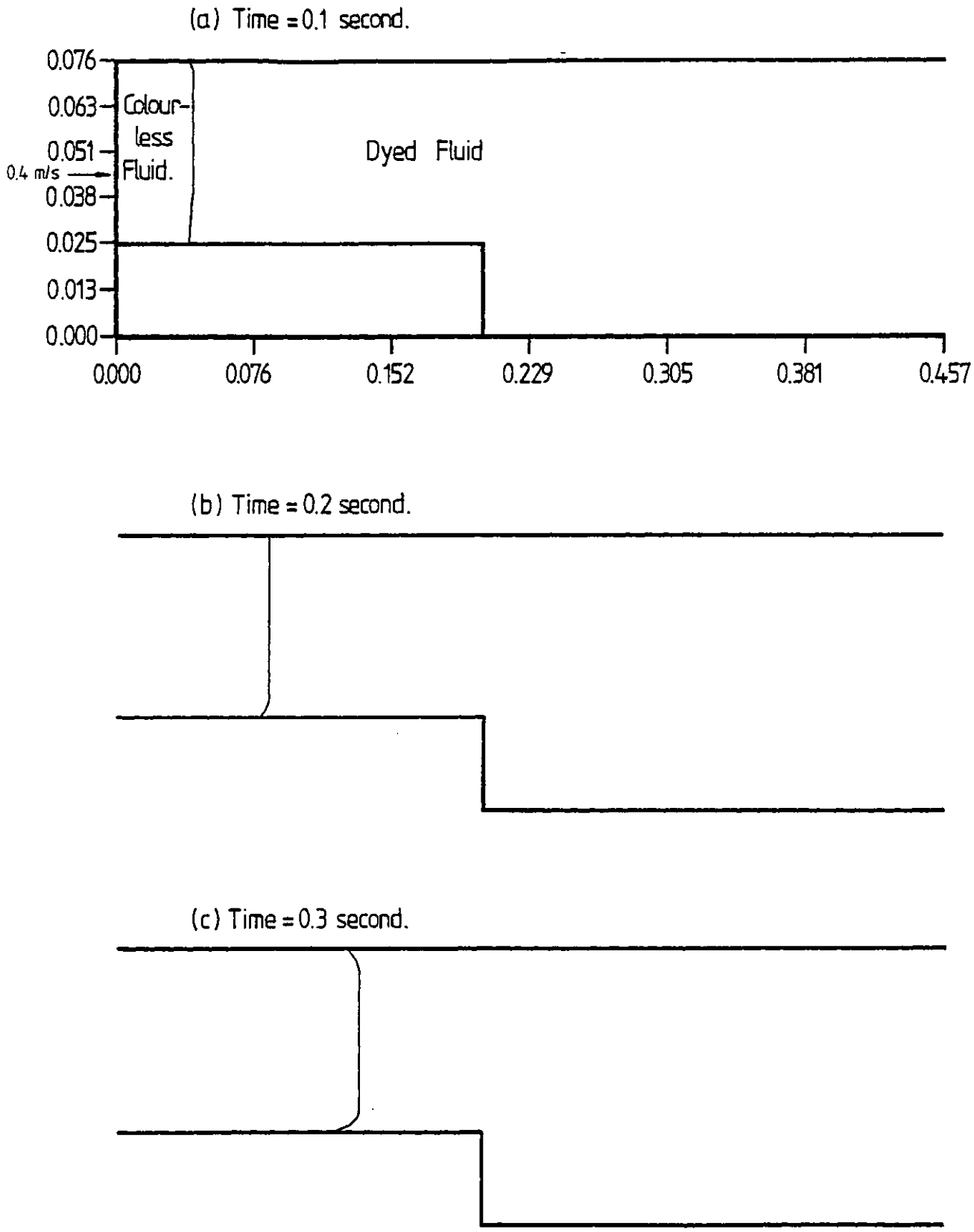

Fig. H3-2. Predicted plot of interface at various time intervals for flow in backward facing step of present experimental investigation.

(d) Time = 0.4 second.

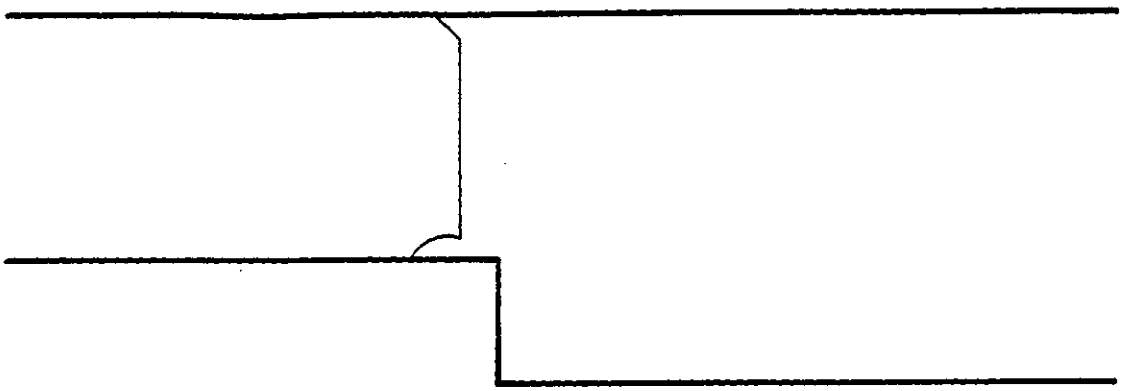

(e) Time = 0.5 second.

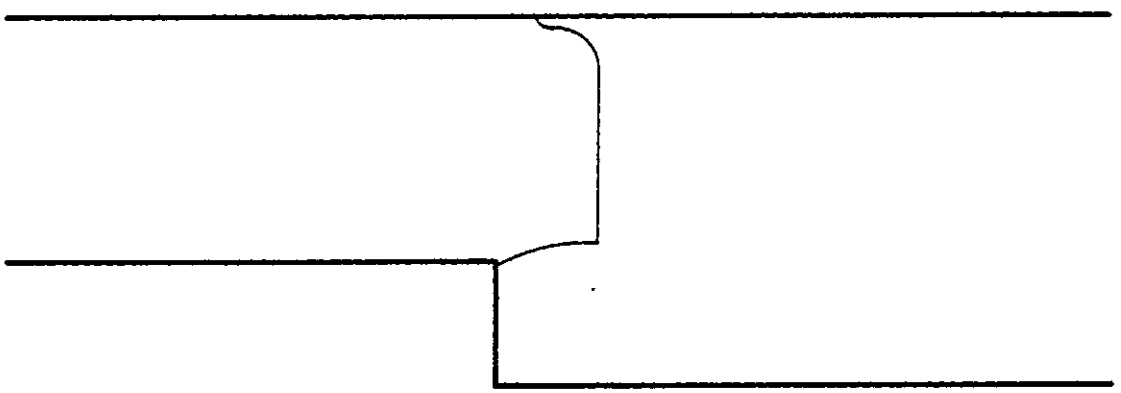

(f) Time = 0.55 second.

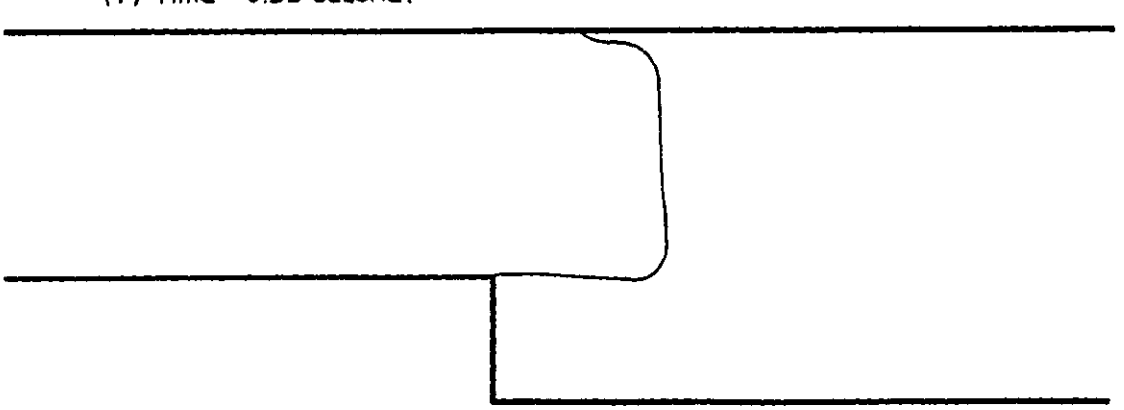

Fig. H3-2. (continued)

(g) Time = 0.6 second.

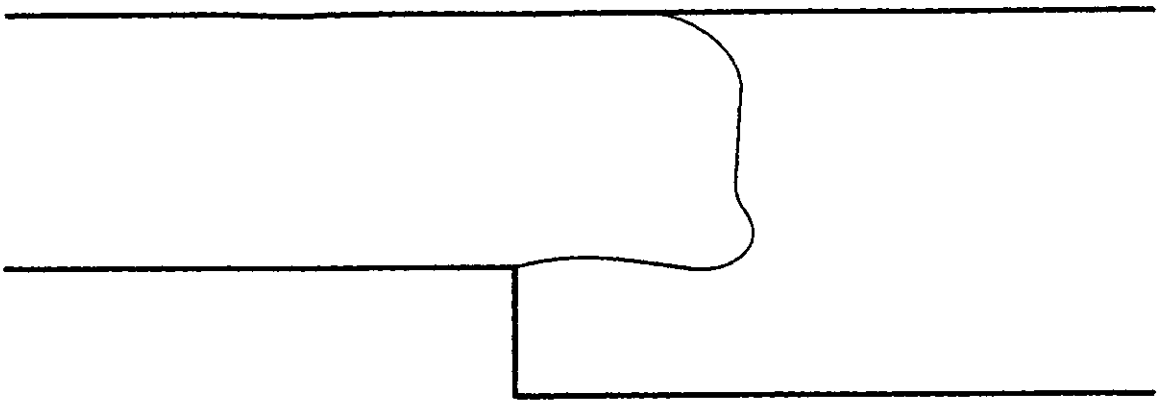

(h) Time = 0.65 second.

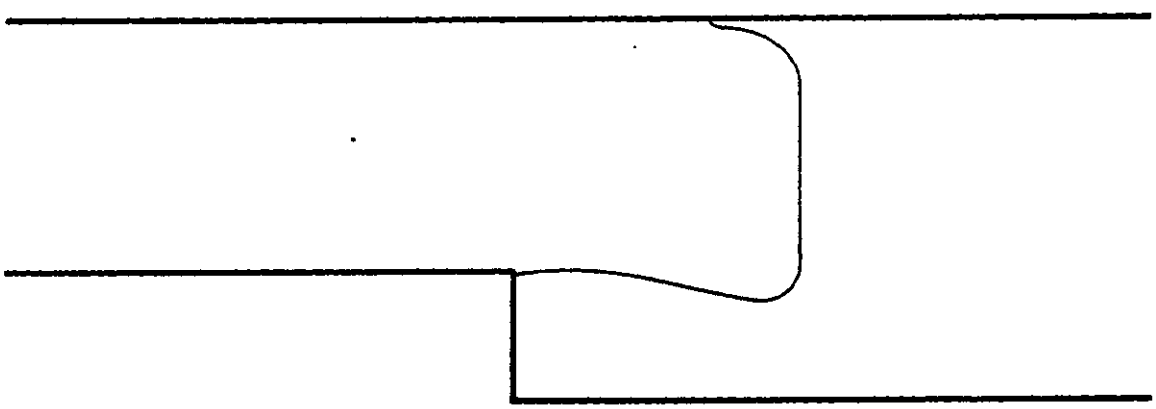

(i) Time = 0.7 second.

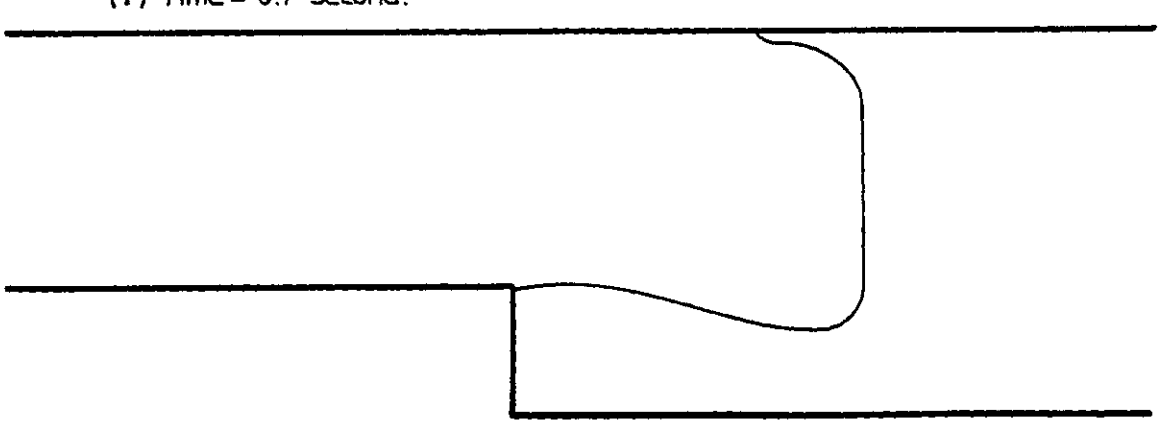

Fig. H3-2. (continued)

(j) Time = 0.8 second.

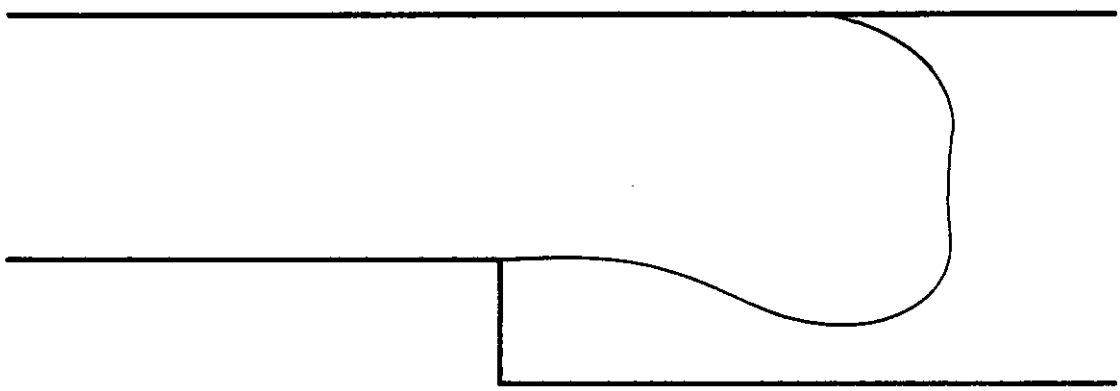

(k) Time = 0.9 second.

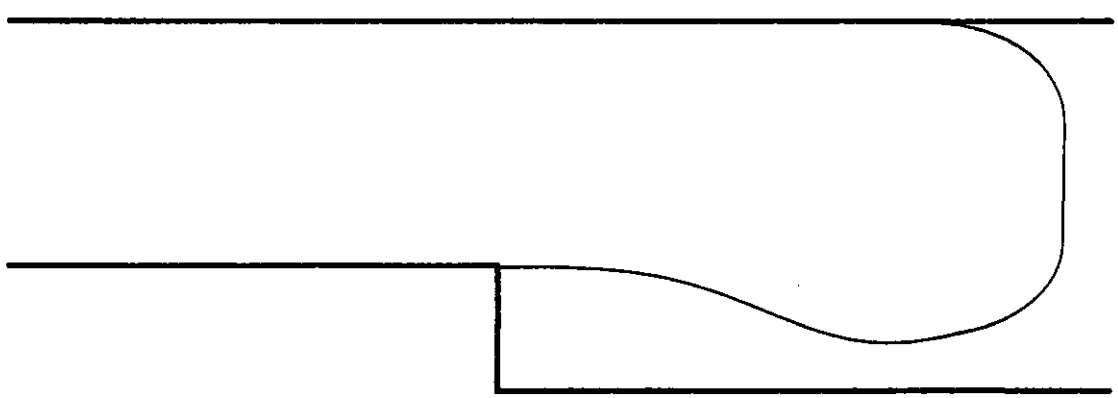

Fig. H3-2. (continued)